FABRICATION AND CHARACTERIZATION OF NOVEL IRON OXIDE/ ALUMINA NANOMATERIALS FOR ENVIRONMENTAL APPLICATIONS

Thesis submitted in partial fulfillment of the requirements for the degree of

Doctor of Philosophy

By

Abhipsa Mahapatra

Under the guidance of

Dr. Garudadhwaj Hota

&

Dr. Braja Gopal Mishra

DEPARTMENT OF CHEMISTRY
NATIONAL INSTITUTE OF TECHNOLOGY, ROURKELA
ROURKELA-769008, ODISHA, INDIA

July 2013

CERTIFICATE

This is to certify that the thesis entitled "**Fabrication and Characterization of Novel Iron Oxide/ Alumina Nanomaterials for Environmental Applications**" being submitted by Abhipsa Mahapatra to the National Institute of Technology, Rourkela, India, for the award of the degree of **Doctor of Philosophy** is a record of bonafide research work carried out by her under my supervision and guidance. I am satisfied that the thesis has reached the standard fulfilling the requirements of the regulations relating to the nature of the degree. To the best of my knowledge, the matter embodied in the thesis has not been submitted to any other University / Institute for the award of any Degree or Diploma.

Supervisor

Place: Rourkela
Date:

Dr. Garudadhawaj Hota,

Department of Chemistry,
National Institute of Technology,
Rourkela-769008

Co-Supervisor

Dr. Braja Gopal Mishra
Department of Chemistry
National Institute of Technology
Rourkela- 769008

Acknowledgement

I take this opportunity to express my deep sense of gratitude and indebtedness to my research mentor **Prof Garudadhawaj Hota**, for providing his excellent guidance, support, encouragement, and inspiration throughout my doctoral work. It has been a great opportunity to work with him with his vast scientific knowledge and analytical approach. Many discussions I had with him have made me to think logically and have helped me to improve my knowledge. I greatly feel fortunate enough for his patience to assist me, which he devoted from his busy schedule. Without his expertise and guidance, this work would not have been accomplished. I am also very much thankful to his family members for their hospitality, love and encouragement during my stay.

I would also like to acknowledge **Prof. B.G. Mishra**, my co-supervisor for providing his excellent technical support and valuable time, which helped me making this research work a success.

I am thankful to all my Doctoral Scrutiny Committee members **Prof. R. K. Patel**, (Chairman DSC), **Prof. M. Kundu**, **Prof. S. Mahapatra** and **Prof. A. Mondal** for their valuable suggestions throughout my research career.

I would also like to express my deep sense of gratitude to Head of the Chemistry Department, NIT Rourkela for allowing me to avail the facilities of the department.

I wish to express my sincere thanks to **Dr. K. M. Purohit** (Ex-HOD), **Prof S. Patel** and **Prof U. Subbudhi**, Department of Chemistry, NIT, Rourkela for good suggestions and useful discussions during my research work.

I am also very much thankful to **Prof B. P. Nayak**, Department of Biotechnology and Medical Engineering, NIT Rourkela, for carrying out the related biological work with the help of Nidhi Garg, his M.Tech student.

I would like to thank all the faculty members and staff members, Department of Chemistry, NIT Rourkela for their constructive suggestions and inspirations.

I convey my heartfelt thanks to Dr. S. K. Swain, BIT Mesra, for his support in characterization of samples. I am also grateful to Department of Chemical, Ceramic and

Metallurgical Engineering, NIT Rourkela, for acquiring various characterization techniques presented in this thesis.

I wish to thank my labmates Jyoti Prakash, Shabna, Tapaswini, Priyadarshini didi and Saswati Madam for their immense help, timeless effort and cooperation throughout my work in laboratory. My special thanks to T. Deepthi, Subhraseema and Nagachaitanya for their companionship, emotional support and entertainment, which helped me a lot to get through the difficult times during my work.

My earnest thanks to my dear juniors and friends Prakash, Smruti Snigdha, Smruti Ranjan, Sandip, Vijayalaxmi, Sagarika didi and Biswajit Bhai for their unconditional love, affection and care during my stay.

No words can convey my gratitude to my parents, for their constant inspiration and mental support, without which it would have never been possible for me to complete my thesis. My husband, Subodh K. Panigrahi, was a gem in the ring for being more friend than family and providing absolutely necessary inputs in every little bit of time. I must thank my elder sisters, Archana nani and Amrita nani who have stood beside me in every trajectory of my life and made it pretty exciting and lovely.

My immense thanks are due to the members of my in-laws' family for their love, blessing and good wishes. I would like to add a special note of thanks for my grandfather Dr B. Mahapatra for his motivation in carrying out the research work.

July 2013 Abhipsa Mahapatra

CONTENT

CERTIFICATE ii

ACKNOWLEDGEMENTS iii

CONTENTS v

LIST OF TABLES xi

LIST OF FIGURES xvi

ABBREVIATIONS xvii

NOTATIONS xviii

ABSTRACT xix

CHAPTER 1- INTRODUCTION 01

1. Introduction to nanomaterials 01

1.1 Nanofibers/nanowires 02

1.2 Composite nanomaterials 04

1.3 Methods of preparation of nanomaterials 04

1.3.1 Physical methods 04

1.3.1.1 Laser ablation method 04

1.3.1.2 Inert gas condensation 05

1.3.1.3 High energy ball milling 05

1.3.1.4 Chemical vapour deposition 06

1.3.1.5 Electro-deposition method 06

1.3.2 Chemical methods 07

1.3.2.1 Hydrothermal method 07

1.3.2.2 Sol-gel method 08
1.3.2.3 Sonochemical method 09
1.3.2.4 Co-precipitation method 09
1.3.2.5 Electrospinning method 10
1.4 Importance of alumina and iron oxide nanomaterials 11
1.4.1 Alumina 11
1.4.2 Iron oxide 12
1.5 Application of nanomaterials 13
1.5.1 Chemical applications 14
1.5.2 Optical and Electronic applications 15
1.5.3 Magnetic applications 15
1.5.4 Metal and Ceramics applications 16
1.5.5 Biological applications 17
1.5.6 Environmental applications 18
1.6 Objective of this study 20
1.7 Organization of the thesis 20
CHAPTER 2 LITERATURE REVIEW 21
2.1. Sol-gel method 21
2.1.1 Iron oxide nanomaterial by sol gel method 22
2.1.2 Alumina nanomaterial by sol-gel method 23
2.1.3 Mixed metal oxide nanocomposite by sol gel method 26
2.2. Hydrothermal method 29
2.2.1 Iron oxide nanomaterials by hydrothermal method 29
2.2.2 Alumina nanomaterials by hydrothermal method 34
2.2.3 Mixed metal oxide nanocomposite by hydrothermal method 45
2.3. Electrospinning method 46
2.3.1 Iron oxide nanomaterial by electrospinning method 48

2.3.2 Alumina nanomaterial by electrospinning method 52

2.3.3 Mixed metal oxide nanocomposite by electrospinning method 55

2.4. Characterization techniques 58

2.4.1 UV-Vis spectroscopy 58

2.4.2 Fourier transforms infrared spectroscopy 59

2.4.3 X-Ray Diffraction 59

2.4.4 Scanning electron microscope 61

2.4.5 Transmission electron microscopy 61

2.4.6 Brunauer, Emmett Teller (BET) 62

2.4.7 Thermogravimetric analysis (TGA-DTA) 63

2.4.8 Atomic absorption spectrometry (AAS) 65

2.5. Concluding remarks 66

CHAPTER 3 SOL-GEL MEDIATED SYNTHESIS OF BOEHMITE (ALOOH) NANOMATERIALS FOR REMOVAL OF CONGO RED DYE FROM AQUEOUS SOLUTIONS 67

3.1 Introduction 67

3.2 Experimental section 69

3.2.1 Materials and methods 69

3.2.2 Characterizations techniques 69

3.2.3 Adsorption experiments 69

3.3 Results and discussion 70

3.3.1 Structural properties 70

3.3.2 Morphology 71

3.4 Adsorption studies 72

3.4.1 Effect of pH on adsorption of Congo red 72

3.4.2 Effect of contact time on adsorption of Congo red 73

3.4.3 Effect of adsorbent dosage on adsorption of Congo red 75

3.4.4 Effect of change in initial concentration on adsorption of Congo red dye 76

3.4.5 Adsorption isotherms 77

3.4.6 Adsorption kinetics 79

3.5 Conclusions 80

CHAPTER 4 STUDIES ON ELECTROSPUN ALUMINA NANOFIBERS FOR REMOVAL OF Cr (VI) & F^- TOXIC IONS FROM AQUEOUS SYSTEM 81

4.1 Introduction 81

4.2 Experimental procedure 85

4.2.1 Materials 85

4.2.2 Fabrication of Alumina nanofibers 86

4.2.3 Adsorbent characterization techniques 86

4.2.4 Adsorption experiments 87

4.3 Results and discussion 88

4.4 Adsorption studies 94

4.4.1 Effect of pH on adsorption of Cr (VI) and fluoride ions 94

4.4.2 Effect of contact time on adsorption of Cr (VI) and fluoride ions 96

4.4.3 Adsorption kinetics study 96

4.4.4 Effect of initial concentration on adsorption of Cr (VI) and fluoride ions 98

4.4.5 Adsorption Isotherm study 99

4.4.6 Effect of adsorbent dosage on adsorption of Cr (VI) and fluoride ions 100

4.5 Conclusions 101

CHAPTER 5 SYNTHESIS OF MIXED Fe_2O_3-Al_2O_3 NANOCOMPOSITES FOR ADSORPTIVE REMOVAL OF CONGO RED DYE 103

5.1 Introduction 103

5.2 Experimental procedure 105

5.2.1 Materials 105

5.2.2 Synthesis of Fe_2O_3 –Al_2O_3 nanocomposites 106

5.2.3 Characterization techniques 106

5.2.4 Adsorption experiments for Congo red dye by batch process 106

5.3 Results and discussion 107

5.3.1 Structural properties 107

5.3.2 UV-Vis adsorption spectroscopy analysis 109

5.4 Adsorption study of Congo red by mixed nanocomposites 111

5.4.1 Effect of pH on adsorption of Congo red dye 112

5.4.2. Effect of contact time on adsorption study on Congo red dye 113

5.4.3. Effect of initial concentration on adsorption study of Congo red dye 114

5.4.4. Adsorption isotherm study of Congo red dye 115

5.4.5. Adsorption kinetics study 117

5.5 Conclusion 118

CHAPTER 6 ELECTROSPUN Fe_2O_3-Al_2O_3 NANOCOMPOSITE FIBERS AS EFFICIENT ADSORBENT FOR REMOVAL OF HEAVY METAL IONS FROM AQUEOUS SOLUTION **119**

6.1 Introduction 119

6.2 Experimental section 121

6.2.1 Materials and methods 121

6.2.2 Fabrication of iron oxide and mixed nanocomposite fibers 121

6.2.3 Adsorbent characterization technique 122

6.2.4 Adsorption experiments of mixed oxide nanocomposite fibers 123

6.3 Result and discussion 123

6.3.1 Structural properties of iron oxide-alumina mixed oxide 123

6.3.2 Thermal behaviour by TGA-DTA studies 124

6.3.3 N_2 adsorption-desorption isotherm graph 125

6.3.4 Morphology studies by SEM and TEM analysis 126

6.4 Adsorption studies of mixed oxide nanocomposite fibers 128

6.4.1 Effect of pH on adsorption study of metal ions 128

6.4.2 Effect of time on adsorption study of metal ions 129

6.4.3 Effect of initial concentration of adsorbate on adsorption study 130
6.4.4 Adsorption isotherm study of metal ions 131
6.4.5 Adsorption kinetic study of metal ions 133
6.4.6 Desorption studies and reusability study 134
6.5 Conclusion 136
CHAPTER 7 SYNTHESIS OF ELECTROSPUN PAN-AG COMPOSITE NANOFIBER FOR ANTIBACTERIAL APPLICATION **137**
7.1 Introduction 137
7.2 Experimental section 140
7.2.1 Materials and methods 140
7.2.2 Fabrication of PAN nanofiber containing silver nanoparticle 140
7.2.3 Characterization techniques 141
7.2.4 Antimicrobial test 142
7.3 Results and discussions 142
7.3.1 Antibacterial activity 147
7.4 Conclusion 150
CONCLUSIONS 151
REFERENCES 153
BIODATA 179
LIST OF PUBLICATIONS 179

List of figures

Figure	Title	Page No
2.1	TEM images of nanoscale alumina particles hydrolyzed for 20 min (a), 4 h (b) and 24h (c), (Teoh et al., 2007).	24
2.2	TEM images of alumina nanofibers calcined at (a) 580°C and (b) 800°C (Wang et al., 2007).	25
2.3	TEM images of silica-coated magnetite particles using different amount of TEOS: (a) 1ml, (b) 3ml, (c) 5ml and (d) 7 ml as precursor (Deng et al., 2005).	27
2.4	(a, b) SEM images and (c, d) TEM images of Fe_2O_3 hollow sphere (Li et al., 2007).	31
2.5	(a, b) SEM images of the α-Fe_2O_3 nanorods, and (c) TEM image and the inset is the SAED pattern of the α-Fe_2O_3 nanorods (Li et al., 2009).	32
2.6	Bright field TEM images of the α-Fe_2O_3 nanorods at different temperature (a) 120 °C,(b) 140°C, (c) 180°C, (d) 200 °C (e) 220 °C and (f) 240°C (Almeida et al., 2009).	32
2.7	TEM images of the products obtained after (a) 1.5, (b) 3, (c) 6 and (d) 12 h. (Wu et al., 2010).	33
2.8	FeSEM and TEM images of α-FeOOH (Wang et al., 2012).	34
2.9	SEM images of γ-AlOOH bundles (a, b), EDS pattern (inset) of the products (c) and representative SEM image of irregular nanowires (d) (Zhang et al., 2006).	36
2.10	TEM images of boehmite nanowire, hydrothermally treated (a) at 120°C, 6 days and (b) at 100°C, 30 days (Zhao et al., 2007).	36
2.11	Effect of AlF_3 concentration on morphology of α-Al_2O_3: (a) 2%, (b) 10% and (c) 20% (Feng et al., 2008).	37
2.12	(a) SEM images of boehmite nanoleaves; (b) TEM image of boehmite nanoleaves with the inset SAED, and (c) SEM images of 3-D flower-like boehmite (Liu et al., 2008).	38
2.13	TEM images of boehmite nanomaterials in the presence of 0 (a), 0.0054 (b), 0.011 (c), 0.021 (d), 0.032 (e), 0.043 (f), 0.054 (g), 0.064 (h), and 0.086 (i) mol L^{-1} H_2SO_4 240 °C for16.0 h (He et al., 2008).	39
2.14	TEM images of ((a), (b)) as-prepared boehmite and ((c), (d)) calcined γ-Al_2O_3 (Lu et al., 2009).	40
2.15	TEM images of γ-AlOOH at different pH value of reaction solution: (a) pH 4, (b) pH 5, (c) pH 6, (d) pH 7 and (e) pH 10 (Deng et al., 2010).	42

2.16	SEM image of boehmite nanorod synthesized by hydrothermal method for (a) 24 h, (b) obtained without buffer solution and (c) TEM image of boehmite (Liu et al., 2010).	43
2.17	Typical SEM images of $(CH_3COO)_2Al(OH)$ obtained at 120°C for 12 h; (a) nanoleaf, (b) nanofibers (c) microflowers, (d) The TEM images of γ-Al_2O_3 at 600°C and (e) schematic illustration for the growth process of the precursor aluminum acetate hydroxide (Kim et al., 2010).	44
2.18	SEM images of CuO-Fe_2O_3 (a) hollow microspheres and (b) mixed oxides nanorods (Liu et al., 2009).	46
2.19	SEM images of as-calcined α-Fe_2O_3 nanofibers with 40 wt. % $FeAc_2$ at different calcination temperature for 4 h (a) 400; (c) 600; (d) 800°C (Zhu et al., 2006).	49
2.20	SEM images of the α-Fe hollow fibers (a, b), maghemite (γ-Fe_2O_3) hollow fibers (c), and short maghemite hollow fibers (d) (Zhan et al., 2007).	49
2.21	SEM images of electrospun nanofibers: (a) PVA/$Fe(NO_3)_3.9H_2O$ composite nanofibers, (b) magnified composite nanofibers, (c) calcined at 800°C and (d) TEM image of electrospun nanofibers calcined at 800°C (Zheng et al., 2009).	50
2.22	(a) SEM image of electrospun PVA/Fe $(NO_3)_3$ composite nanofibers; (b, c) SEM image of Fe nanofibers; and (d) SAED pattern of Fe nanofiber (Shao et al., 2011).	51
2.23	FESEM images of (a) $Fe(acac)_3$–PVP composite fibers, (b) α-Fe_2O_3 hollow fibers and (c) TEM of α-Fe_2O_3 hollow fibers (Chaudhari et al., 2012).	52
2.24	SEM images of alumina-borate/PVA composite fibers (a) as-spun composite fiber, and calcined at (b) 1000°C, (c) 1200°C and (d) 1400°C (Dai et al., 2002).	53
2.25	SEM images of alumina nanofibers (a) as-spun composite fibers, (b) after calcinations at 1200°C and (c) TEM images of after calcination (Yu et al., 2012).	54
2.26	SEM images of ceramic fibers, (a) as-spun and (b) calcined at 1100°C (Milanovic´ et al., 2013).	55
2.27	(a) TEM image of TiO_2/ZnO nanofibers, inset is SAED image of TiO_2/ZnO and (b) HR0TEM image of TiO_2/ZnO nanofibers (Liu et al., 2010).	56
2.28	SEM images of (a) ZnO nanofiber, (b) 67Zn33In nanofibers, (c) 50Zn50In nanofiber, (d) 33Zn67In nanofibers and (e) In_2O_3 nanofibers after heat treatment at 600°C (Lee et al., 2013).	57
3.1	XRD pattern of (a) γ-AlOOH and (b) α-Al_2O_3 (Calcined at 1000^0 C).	70
3.2	Nitrogen adsorption–desorption isotherm graph of AlOOH.	71
3.3	SEM images of AlOOH powder and (b) EDAX analysis.	71
3.4	TEM images of (a) AlOOH and (b) Electron diffraction pattern of AlOOH.	72

3.5	(a) Percentage removal with change in pH, (b) absorption spectra of Congo red dye (100mgL^{-1}, 30 min) and (c) Zeta potential of boehmite nanoparticle as a function of solution pH.	73
3.6	Percentage removal of Congo red using boehmite with change in Time (min).	74
3.7	Percentage removal graph of (a) Al_2O_3 nanoparticle and (b) γ-AlOOH nanoparticle as a function of time (min) at two different concentration of 100 mg/L and 1000 mg/L	75
3.8	Percentage removal graph of Congo red as a function of dosage (g/L) by boehmite nanoparticles.	76
3.9	(a) Percentage removal of Congo red by boehmite nanomaterials as a function of initial concentration (mgL^{-1}) and (b) The sorption capacity of boehmite nanomaterials as a function of time.	77
3.10	Langmuir and Freundlich isotherm for the adsorption of Congo red onto boehmite nanoparticle at room temperature.	79
3.11	Pseudo-second-order kinetic plots for Congo red adsorption onto boehmite nanoparticle.	80
4.1	Schematic diagram of electrospinning setup.	89
4.2	XRD pattern of Alumina nanofiber (a) PVP-Alac-aspun nanofiber (b) Al_2O_3 nanofiber obtained after sintering at 1000° C.	90
4.3	FTIR of (a) as-spun composite fiber and (b) fiber sintered at 1000^0 C**.**	91
4.4	TGA/DTA curve of the PVP-Aluminium acetate as-spun nanofiber membrane.	92
4.5	SEM images of (a, b) as-spun nanofibers of PVP-aluminum acetate precursor and (c, d) sintered at 1000^0 C.	92
4.6	SEM images of alumina nanofibers (a) before adsorption, (b) EDX spectrum before adsorption, (c) alumina nanofiber after adsorption and (d) EDX spectrum after adsorption.	93
4.7	(a) TEM images and (b) Electron diffraction pattern of alumina nanofibers.	94
4.8	Percentage removal of Cr (VI) and fluoride by alumina nanofibers with variation in pH.	95
4.9	(a) Percentage removal of Cr (VI) and fluoride ions as a function of time (min) by alumina nanofibers and (b) sorption capacity of alumina with time.	96
4.10	Pseudosecond-order plot for Cr (VI) and Fluoride ion removal by alumina nanofiber.	97
4.11	Percentage adsorption graph of Cr (VI) and fluoride ions with variation in concentration of metal ion by alumina nanofibers.	98
4.12	Freundlich isotherms for the adsorption of Cr (VI) and fluoride ion on alumina nanofiber.	100
4.13	Percentage removal graphs of Cr (VI) and fluoride ions with variation in dosage (g/L) by electrospun alumina nanofibers.	101
5.1	XRD data of (a) unsintered mixed oxy-hydroxide nanocomposite, (b) mixed oxide sintered at 500°C, (c) mixed oxide sintered at 1000°C.	107

5.2	SEM image of (a) mixed FeOOH and AlOOH nanocomposite, (b) mixed γ-Fe_2O_3 and γ-Al_2O_3 nanocomposite sintered at 500°C, (c) mixed α-Fe_2O_3 and α-Al_2O_3 sintered at 1000°C, (d) EDAX image of mixed iron oxide and alumina nanocomposites.	108
5.3	HRTEM image of (a) mixed γ-Fe_2O_3 and γ-Al_2O_3 nanocomposite sintered at 500°C, and (b) SAED image of mixed oxide nanocomposite.	109
5.4	UV-Vis analysis of (a) mixed FeOOH and AlOOH nanocomposite, mixed γ-Fe_2O_3 and γ-Al_2O_3 nanocomposite sintered at 500°C, mixed α-Fe_2O_3 and α-Al_2O_3 sintered at 1000°C, (b) Optical property of all the samples.	110
5.5	UV-Vis absorption spectra of Congo red solution and after being treated by three different samples, the initial concentration of Congo red are 100 mg/L. (a) Before adsorption, after adsorption by 0.1gm (b) un-sintered, (c) sintered at 500°C and (d) sintered at 1000°C mixed Iron oxide and alumina nanocomposite, in 15mins at pH 7.	111
5.6	Effect of pH on percentage removal of the Congo red dye.	112
5.7	Effect of contact time on removal of the Congo red dye.	113
5.8	Effect of initial concentration on percentage removal of the Congo red dye.	114
5.9	(a) Adsorption rate and (b) adsorption capacities of mixed nanocomposite for Congo red (100 mg L^{-1}, 10 ml) where mass of the sample were 0.002 g.	115
5.10	Langmuir and Freundlich isotherm as obeyed of all the three different phases (a) FeOOH-AlOOH, (b) γ-Fe_2O_3-Al_2O_3 and (c) α-Fe_2O_3-Al_2O_3 of mixed oxide nanocomposite.	116
5.11	Kinetic study of mixed oxide nanocomposite of three different phases.	118
6.1	XRD pattern of Fe_2O_3-Al_2O_3 mixed nanocomposite sintered at 1000°C where (a) Al_2O_3, (b) Fe_2O_3 and (c) Fe_2O_3-Al_2O_3 nanomaterials.	124
6.2	TGA/DTA profile of as-spun AlOOH–PVP–$Fe(acac)_3$ mixed nanocomposite fiber.	125
6.3	Nitrogen adsorption–desorption isotherm and pore size distribution curve (inset) of Fe_2O_3–Al_2O_3 nanofibers.	126
6.4	SEM images of Fe_2O_3 nanofiber (a) as-spun fiber, (b) sintered at 1000°C and (c) EDAX pattern of sintered fiber.	126
6.5	SEM images of Fe_2O_3-Al_2O_3mixed nanocomposite sintered at (a) 500°C (b) 700°C, (c) 1000°C, and (d) EDAX analysis of 1000°C sintered fiber.	127
6.6	Electron microscopic study of Fe_2O_3-Al_2O_3 mixed nanocomposite fiber (a) TEM images (b) electron diffraction pattern.	128
6.7	(a) Percentage removal of metal ions with variation in pH and (b) zeta potential of Fe_2O_3-Al_2O_3 nanocomposites as a function of pH.	129
6.8	(a) Percentage removal of metal ions with a function of time (min) and (b) sorption capacity versus variation in time (min).	130
6.9	Percentage removal of different ions with a function of initial concentration (mg/L).	131
6.10	Langmuir adsorption isotherm of Fe_2O_3–Al_2O_3 mixed oxide nanocomposite using (a) Cu(II) and (b) Pb(II). Freundlich adsorption	132

	isotherm of Fe_2O_3–Al_2O_3 mixed oxide nanocomposite using (c) Ni (II) and (b) Hg (II) at room temperature.	
6.11	Kinetic study of all of the four ions (a) psuedo-first order model and (b) psuedo-second order model.	134
6.12	Desorption of metal ions (Cu^{2+}, Pb^{2+}, Ni^{2+} and Hg^{2+}) from Al_2O_3-Fe_2O_3 mixed nanocomposite using 0.05 M HCl solution.	135
6.13	Reusability of Al_2O_3-Fe_2O_3 mixed nanocomposite adsorbent for adsorption/desorption of metal ions during four cycles.	136
7.1	Flow chat of the formation PAN-Ag composite nanofibers via e lectrospinning methods.	141
7.2	UV-Vis spectra of PAN-Ag nanocomposites prepared by (a) refluxed method, (b) $NaBH_4$ reduction method and (c) heat treatment method.	143
7.3	SEM images of PAN-Ag nanofiber prepared by $NaBH_4$ reduction method (a) lower magnification, (b) higher magnification and (c) EDAX spectrum.	144
7.4	SEM images of PAN-Ag composite nanofiber prepared by refluxed method; (a, b) different magnification and (c) EDAX spectrum.	145
7.5	SEM images of PAN-Ag composite nanofibers prepared by heat treatment method; (a, b) different magnification and (c) EDAX spectrum.	146
7.6	TEM images of PAN-Ag composite nanofibers prepared by refluxing method; (a. b) different magnification images.	146
7.7	TEM imagesof PAN-Ag composite nanofibers, prepared by $NaBH_4$ reduction; (a, b) different magnification images.	147
7.8	Photographs showing zone of inhibition of the PAN-Ag composite membrane prepared by (a) $NaBH_4$ treated (i) *B. Subtilis (ii) S. aureus* (b) Refluxed (i) *E. Coli* (ii) *S. aureus,* and (c) Heat treatment *(i) S. aureus* and (ii) *B. Subtilis*.	148

List of Tables

Table No	Title	Page No
3.1	Adsorption isotherm parameters of boehmite nanoparticle.	78
4.1	Values of pseudosecond-order kinetics parameters for removal of Cr (VI) and fluoride ions by alumina nanofiber.	97
4.2	Values of Langmuir and Freundlich constants for adsorption of Cr (VI) and fluoride by alumina nanofiber.	100
5.1	Adsorption isotherm parameter of mixed oxide nanocomposite.	117
6.1	Langmuir and Freundlich parameters for adsorption of cations on mixed oxide nanocomposites.	133
6.2	Kinetics parameters for adsorption of various cations on mixed oxide nanocomposites.	134
7.1	Antibacterial activity of PAN-Ag composite fibers prepared by different synthetic strategies.	149

Abbreviations

UV-Vis	:	Ultra-visible spectroscopy
FTIR	:	Fourier- transform infrared spectroscopy
SEM	:	Scanning electron microscopy
TEM	:	Transmission electron microscopy
XRD	:	X-ray diffraction
BET	:	Brunauer-Emmett-Teller
BJH	:	Barrett-Joyner-Halenda
AAS	:	Atomic absorption spectroscopy
TGA-DTA	:	Thermal gravimetric analysis-differential thermal analysis
AlOOH	:	Boehmite
IUPAC	:	International union of pure and applied chemistry
JCPDS	:	Joint committee for powder diffraction standards
CR	:	Congo red dye

Notation

eV	:	Electronvolt
m^2/g	:	Square meter per gram
g	:	Gram
nm	:	Nanometer
Hz	:	Hertz
Å	:	Angstrom
cm	:	Centimetre
KJ	:	Kilo Joule
h	:	Hour
θ	:	Bragg angle
ν	:	Frequency
KHz	:	Kilo Hertz
min	:	Minute
L/g	:	Litre per gram
M	:	Molar
mg L^{-1}	:	Milligram per litre

Abstract

One-dimensional (1D) nanomaterials such as nanowires, nanotubes, nanorods, nanofibers and nanobelts have drawn a lot of attention because of their novel and unique properties and a wide range of applications. In particular, ceramics and polymers with 1D nano-architectures have received increasing interest since it provide a good material system to investigate the shape, size and dimensionality dependent electrical, optical, thermal and mechanical properties. 1D ceramic nanomaterials with their large surface-to-volume ratio shows the tremendous application potential in various fields. Recent research focused on the applications of nanomaterials for environmental clean-up and preventing environmental pollution. Using nanomaterials to solve environmental issues will become an inexorable trend in the future. Developing simpler and versatile approach to synthesize one dimensional nanostructure still remains a technical challenge. In the past few decades a large number of synthesis techniques have been adopted world wide by many researchers.

In the present study we have chosen three convenient bottom-up methods such as sol-gel, hydrothermal and electrospinning method for synthesis of boehmite (AlOOH), alumina (Al_2O_3) and Fe_2O_3-Al_2O_3 mixed oxide composite nanomaterials. The synthesized boehmite, alumina and their mixed oxides nanocomposite were characterized by UV-Vis, FT-IR spectroscopy, SEM, TEM, XRD, BET surface area, TGA-DTA, and AAS analytical techniques.

The SEM and TEM images of the synthesized nanomaterials confirm the formation of 1D nanostructures. The XRD studies indicate the formation of different crystalline phases of aluminum and iron oxides nanomaterials. The obtained nanomaterials and nanocomposites were used as adsorbents for environmental applications, especially decontamination of toxic metal ions like Cr (VI), Pb (II), Hg (II), Ni (II), fluoride ions and organic dye from aqueous solution. Batch experiments were carried out for adsorption studies by varying pH, contact time, adsorbent dose and initial concentration. Furthermore, the kinetics and isotherm studies have also been investigated. The needle shaped boehmite nanomaterials synthesized by sol-

gel method have been used for removal of Congo red. It shows 99% removal of Congo red within a short contact time of 10 min and removal capacity of 198 mg/g. Similarly, alumina nanofibers of diameters in the range of 100-500 nm were synthesized by electrospinning method and have been used for adsorption of Cr (VI) and fluoride ion from aqueous solution.

We have also synthesized iron oxide-alumina mixed oxide nanocomposite in two different methods such as hydrothermal and electrospinning. These as prepared materials have been sintered in air at different temperatures to obtain alpha and gamma crystalline phases. The gamma phase mixed oxide nanocomposite synthesized by hydrothermal method has been found to be very efficient adsorbent for removal of Congo red and adsorption capacity was found to be 498 mg/g. However, electrospun mixed oxide nanocomposite shows better result for removal of toxic metal ions such as Cu^{2+}, Pb^{2+}, Ni^{2+} and Hg^{2+}. The removal percentage was found to be in the order of $Cu^{2+} < Pb^{2+} < Ni^{2+} < Hg^{2+}$.

Furthermore, we have also synthesized PAN-Ag composite nanofibers by electrospinning method. Here, the surface of PAN nanofiber was functionalized with 5-15 nm sized spherical silver nanoparticles. From the TEM studies it was observed that, nano-sized silver particle were uniformly distributed on the surface of PAN nanofibers. These composite nanofibers membrane has been used for antibacterial studies which show promising anti-bacterial properties against *E.coli*, *S.aures* and *S.bacillus* microorganisms.

Key words: Nanomaterials, Nanofiber, Nanocomposite, Boehmite, Toxic metal ions, Adsorption, Organic dye, Electrospinning, sol-gel, Hydrothermal, Antibacterial activity.

CHAPTER-1

INTRODUCTION

1. Introduction to Nanomaterials

The increasing interest in nanotechnology is due to the nanostructured material with dimensions i.e. grain size, layer thickness or shapes below 100 nm (Hornyak et al., 2009). The unusual properties of nanomaterials are specific to the nano-dimensions. Nanomaterials are the materials having at least one dimension under 100 nm (Chattopadhyay et al., 2009). In the past two decades, worldwide efforts in both the theory and the experimental investigation of growth, characterization and applications of inorganic nanostructures including metal oxides, ceramics and composites have resulted in a mature, multidisciplinary field. Nanostructured materials are noted for their stability, green chemistry and find diverse technical application (Bhushan et al., 2010). Arising out of their high value addition and surface dominated properties, nanostructure metal oxides could virtually replace all bulk metal oxides in applications such as catalysis, solar cell, hydrogen storage batteries, membrane and separation technology, structural application requiring high strength, sensors, optical, electronics, tissue engineering and so on (Wang et al., 2009, Kim et al., 2010). Beside this one dimensional (1D) nanostructures including nanowires, nanotubes, nanorods, and nanofibers, have received steadily growing interest as a result of their peculiar and fascinating properties superior to their bulk and particle counterpart (Tiwari et al., 2012, Zhang et al., 2008). In this study, we have focused on iron oxide and alumina 1D nanomaterials and also about iron oxide-alumina mixed nanocomposite. Alumina and iron oxide are the most important ceramic materials. Alumina shows a large number of promising chemical and physical properties. It is widely used as an electrical insulator, presenting exceptionally high resistance to chemical agents, as well as giving excellent performance as a catalyst for many chemical reactions, in microelectronics, membrane applications, and wastewater treatment. Moreover, iron oxide plays an important role in environmental and biological processes and is also widely used in different technological applications. It is an n-type semiconductor and

has unique antiferromagnetic properties. It is known to catalyse a number of chemical reactions and due to its low toxicity can be successfully employed in many environmental and biochemical applications. However, the main purpose of nanocomposite preparation is to obtain the synergic effect of both of the metal oxide compounds. Furthermore, composite nanomaterials offer advantage over the individual material due to tuning of optical band gap and control of inter-particle electron transfer (Zhang et al., 2009).

To achieve different morphologies such as rods, wires, thin films, or fibers at the nanoscale, novel fabrication techniques need to be adopted. In our study, we have chosen the simple and widely used synthetic techniques such as sol-gel, hydrothermal and electrospinning method for the synthesis of 1D alumina, iron oxides and their mixed oxides nanostructures. Application of nanomaterials in the field of environmental science and engineering are of great interest. Clean environment is essential to human health. The modern world is facing formidable challenges in meeting rising requirements to clean the environment (Zhang et al., 2010). Nanomaterials provide a powerful tool for detection and treatment of pollutants from the environment. Recent research focused on the use of nanomaterials to solve environmental problems and to clean the environment for the future. Nano-sized materials are new functional materials, which offer high specific surface area to volume ratio and surface active sites, therefore, can be used as effective adsorbents. Furthermore, nanomaterials have been used in various environmental applications such as in green chemistry, photo-catalytic degradation of organic dye, remediation of polluted water, pollutant sensing and detection, antibacterial activity and so on.

In this thesis we have presented on the synthesis and characterization of nano-sized one dimensional polymer and ceramic materials such as alumina, iron oxide and their composite oxides. The obtained nanomaterials and their composites have been used in environmental applications, such as adsorption studies of toxic metal ions, removal of organic dye from aqueous solution and antibacterial applications.

1.1 Nanofibers/nanowires

One-dimensional nanostructures, such as nanorods, nanowires, nanotubes, nanowhiskers, nanofibers have received increasing attention due to their special physical and chemical properties (Li et al., 2012). 1D nanostructures have also become the focus of intensive research owing to their unique applications in mesoscopic physics and fabrication of nanoscale devices (Xia et al., 2003). The 1D nanomaterial have been used as active components or interconnects in fabricating nano-scaled electronic, optical, optoelectronic,

electrochemical, and electromechanical devices, for example, photo detectors, single-electron transistors, electron emitters, light-emitting diodes (LEDs), biological and chemical sensors, and ultraviolet nanolasers. One-dimensional materials possess two confined and one unconfined directions. This allows free movement of electron and holes along the unconfined direction. Hence it shows unique optical and electrical properties as compared to other dimensional nanomaterials. Fabrication of architectural one-dimensional (1D) nanostructures is still a challenging and important research subject in nanoscience and nanotechnology arising out of their unique size- and shape-dependent properties. Geometrical configuration and elemental composition of this 1D nanostructure is very useful for different applications. To date, various research groups have successfully synthesized 1-D nanostructures from a large number of inorganic and polymeric precursors. Such 1D nanostructures possess a highly anisotropic morphology and preferentially grow in one particular crystalline direction. One dimensional single crystalline TiO_2 based nanostructures including nanotubes, nanobelts, nanowires, and nanorods were reviewed and also its recent advances in the properties, synthesis, modifications and applications were studied by Zhou et al. (2010). 1D metal-oxide nanostructures have attracted much attention because metal oxides are the most fascinating functional materials. The 1D morphology can easily enhance the unique properties of the metal-oxide nanostructures, which make them suitable for a wide variety of applications. Devan at el. (2012) have reported a comprehensive review on recent developments in novel synthesis, exceptional characterization and prominent applications of 1D nanostructures of a number of metal oxides. 1D nanostructure has a profound impact in nanoelectronics, nanodevices and systems, nanocomposite materials, alternative energy resources and national security.

Nanofibers are an important class of nanomaterials which have attracted much research attention in last few decades, because of their large surface to mass ratio, porosity and special characteristic attractive for advanced applications. One-dimensional (1D) nanofiber materials have attracted great interest over the past decade because they can potentially address many advanced applications involving dimensionality and size-confined quantum phenomena. Functionalization of nanofiber surface by chemical compounds and nanomaterials have attracted much attention. The removal efficiency of nanofiber adsorbent for heavy metal ions, various organic dyes increases remarkably after the surface modification with different functional molecules, which can remove these contaminants either by electrostatic interaction or by chelation (Feng et al., 2013).

1.2 Composite nanomaterials

In the recent years, the emergence of multifunctional nanomaterials have yielded substantial advances in development and application of nanoparticles architectures for quantitative measurements (Chan et al., 1998). Composite materials are distinct, interspersed domains of different materials. The combination of multiple materials often minimizes or masks the disadvantageous properties of individual component materials to yield a better result. Furthermore, compartmentalization of different nanoparticles allows multiple components to be combined within one particle by providing suitable environments for each individual component (Janczak et al., 2012). Multiphase solid materials in which the average crystallite size of at least one of the phases lies in the nanometer range are considered composite nanomaterials. The composites nanomaterials can considerably show better sorption, catalytic, optical, electrical, and other special properties (Novoselova, 2012). As compared to their single component counterpart these nanocomposites are high performance materials that exhibit unusual properties in combinations and are thought of as the materials of the 21st century.

1.3 Methods of preparation of nanomaterials

The preparation of nanomaterials with well defined size and morphology is an important challenge. A variety of techniques have been used for the synthesis of nanomaterials which depends on the material of interest and the size range involved. The basic principle for the synthesis of nanomaterials is to produce a large number of nuclei and to inhibit the growth and aggregation of grains. Different metals, metal oxides, sulfides, polymers and composite nanomaterials can be prepared using a number of synthetic techniques, which are broadly classified into two categories, namely, physical methods and chemical methods.

1.3.1. Physical methods

Since past few decades, various methods have been used for the synthesis and commercial production of various nanomaterials, thin films and nanocomposite. Brief and concise descriptions of most of the physical pathway used for the synthesis of nanomaterial are as follows.

1.3.1.1 Laser ablation method

In the laser ablation technique, a high power laser pulse was used to vaporize carbon from a target at high temperature. This method is useful for depositing nanocrystalline thin films and powder. As a result, a supersonic jet of particles (plume) is ejected normal to the target

surface. The plume expands away from the target with a strong forward directed velocity distribution of different particles. This ablation process takes place in a vacuum or in presence of some background gases. The substrate temperature has to be sufficiently large (700-800°C). This method is applicable to high melting point elements and transition metals. Iron, gold, palladium and compounds of sulphides have been prepared by this method. This method is also suitable for highly toxic and radioactive materials, often in trace amounts. The advantage of this method is that the rate of production of materials is high usually 2-3 gm/min. Nanocrystalline NiO thin-film electrodes were prepared by reactive pulsed laser ablation of a metallic Ni target in oxygen ambient (Wang et al., 2002). Laser ablation of gold dipped in liquid alkanes from n-pentane to n-decane produced Au sol with varying results (Compagnini et al., 2003, Dahl et al., 2007).

1.3.1.2 Inert gas condensation method

Gas condensation was the first technique used to synthesize nanocrystalline metals and alloys. In this technique, the evaporation of a material takes place in presence of a cool inert gas, usually He or Ar, at low pressure condition, in the order of 1mbar. This method is also called as 'inert gas evaporation' process. The evaporated atoms or molecules undergo a homogeneous condensation to form nanoclusters via collisions with gas atoms or molecules. In this technique, a metallic or inorganic material is vaporized using thermal evaporation sources such as Joule heated refractory crucibles, electron beam evaporation device in an atmosphere of 1-50 m bar. According to researchers' gold/ palladium nanoparticles were fabricated by inert-gas condensation on a sputtering reactor, where they found the particle are icosahedral in shape and there is no evidence of a core-shell structure (Pérez-Tijerina et al., 2008).

1.3.1.3 High energy ball milling method (Mechanical alloying method)

This is a top-down approach for nanomaterial synthesis. This method has been used for the generation of magnetic and catalytic nanoparticles. Ball milling and subsequent annealing is a simple method for the large production of various nanopowders. Here elemental blends, prealloyed powders and ceramics are milled to achieve alloying at the atomic level. This method consists of placing graphite powder into a stainless steel container along with four hardened steel balls. Argon is purged into the container (Shah and Ahmad, 2010). The milling is done for longer period of time, which is followed by annealing in inert atmosphere at 1400°C. The mechanism of this process is still not known. It is suggested that the alloy

generated due to collision of balls resulting in continuous fragmentation, coalescence events of the alloy at the collision site are the procedure of mechanical alloying. Recently, Mg_2Ni was synthesized by a solid state reaction from the constituent elemental powder mixtures via mechanical alloying (Iturbe-García et al., 2010).

1.3.1.4 Chemical vapor deposition method

Chemical vapor deposition (CVD) is a widely used materials-processing technology. It is a process in which a substrate is exposed to one or more volatile precursors, which react and/or decompose on the substrate surface to produce a non-volatile solid deposit or thin film. The majority of its applications involve formation of solid thin-film coatings to surfaces, but it is also used to produce high- purity nano materials and powders, as well as fabricating composite materials via infiltration techniques (Creighton et al., 2001). Because of versatile nature of CVD, the chemistry is very rich and various types of chemical reactions are involved. General experience is that low temperature CVD (600-900°C) yields MWNTs, whereas higher temperature (900-1200°C) reaction favours SWNT growth. Sometimes carbon nanofibers and nano beads are also formed depending upon the nature of the source materials (Bhattacharjee et al., 2012). Recently, a group found that single-walled carbon nanotubes (SWNTs) with highly graphitized structure were synthesized by thermal chemical vapor deposition method using an improved nitrogen-pretreatment Fe-Mo/MgO catalyst. From the whole observation they inferred that nitrogen pretreatment enhances the catalytic activity and promotes the growth mechanism to yield longer SWNTs. It also produced long length, highly graphitized SWNTs (Patil et al., 2012).

1.3.1.5 Electro-deposition method

Template-assisted electrodepositing is an important technique for synthesizing metallic nanomaterials with controlled shape and size. The development of materials science has brought great momentum to applied electrochemical fields. Arrays of nanostructured materials with specific arrangements can be prepared by this method, employing either an active or restrictive template as a cathode in an electrochemical cell. Preparation of oxide films by electro deposition from aqueous solution presents several advantages over other techniques; this method presents interesting characteristics for large-area, low-cost, and generally low-temperature and soft processing of materials. The electro deposition process involves the formation of either an instantaneous or a progressive nucleation. Synthesis of ZnO nanoparticles and electrodeposition of polypyrrole/ZnO nanocomposite film is studied

by Moghaddam et al. (2009). Li et al. (2013) also developed a new facile synthesis method of polyaniline nanoparticles (PANI) by an in-situ electro deposition technique. The morphology of PANI nanoparticle was controlled by the growth time during the electro deposition process.

1.3.2. Chemical methods

Although the bottom up approach is nothing new it plays an important role in the fabrication and processing of nanostructures and nanomaterials. This approach refers to the building-up of materials from the bottom: atom by atom, molecule by molecule or cluster by cluster. Nanoparticles of various oxides can also be synthesized by confining chemical reaction, nucleation and growth process. Various synthesis methods can be grouped into two categories: thermodynamic approach or kinetic approach.

In the thermodynamic approach, synthesis process consists of (i) generation of super saturation, (ii) nucleation, and (iii) subsequent growth. In kinetic approach, formation of nanoparticles is achieved by either limiting the amount of precursors available for the growth or confining the process in a limited space.

A brief and concise description of most of the chemical methods for nanomaterial synthesis is as follows:

1.3.2.1 Hydrothermal method

Hydrothermal method can be defined as a method of synthesis of single crystals which depends on the solubility of minerals in hot water under high pressure. Since ionic product of water (K_w) has a maximum value of around 250-300°C, hydrothermal synthesis is usually carried out below 300°C. The crystal growth is performed in an apparatus consisting of a steel pressure vessel called autoclave, in which a nutrient is supplied along with water. The contribution of the dielectric constant to the reaction rates becomes remarkable based on the electrostatic theory. The dielectric constant of water is 78 at room temperature, in which polar inorganic salts can be soluble in water. The dielectric constant of water decreases with increasing temperature and decreasing pressure (Hayashi et al., 2010). This method has the capability to create crystalline phases which are not stable at the melting point and is also suitable for the growth of large good- quality crystals while maintaining good control over their composition. The formation mechanism of metal oxide particles from metal salt solution is as follows: first hydrated metal ions are hydrolyzed to metal hydroxide. Then, metal hydroxides proceed to precipitate as metal oxides through dehydration. Hydrolysis is

regarded as an electrostatic reaction between metal ions and hydroxyl ions. This method has proved to be efficient both in search of new compounds with specific physical properties and in the systematic physicochemical investigation of intricate multicomponent systems at elevated temperature and pressure. Crystalline nanotubes of γ-AlOOH and γ-Al_2O_3 have been synthesized by hydrothermal method and its formation mechanism and catalytic performance has been studied (Lu et al., 2009). Similarly, synthesis of alpha alumina by hydrothermal method and its surface characterization with controlled chemical composition has been observed by Suchanek et al. (2010).

Solvothermal synthesis is also a similar type of synthesis, where different organic solvents are used in place of aqueous medium (Li et al., 2010). Recently, ultra small Tungsten Oxide nanoparticles were synthesized by solvothermal method. Here a one-pot, two precursor synthesis route was adopted in which a polyoxometalate salt is decomposed thermally in a high boiling organic solvent oleylamine. These findings provide a new method to control the size and shape of transition metal oxide nanoparticles, which will be especially useful in catalysis (Soultanidis et al., 2012).

1.3.2.2 Sol-gel method

Sol-gel method involves the formation of a concentrated suspension of a metallic oxide or hydroxide (sol), which is subsequently dehydrated by evaporation or solvent extraction, resulting in a semi-rigid mass (gel). This method is carried out in solution, tailoring of certain desired structural characteristic such as compositional homogeneity, grain size, particle morphology and porosity is possible. A uniform distribution of the particles is important for optimal control of grain size and micro structure to maintain high reliability (Shah and Ahmad, 2010). A wide range of pure and mixed oxides can be produced on controlled heating of this gellated material. In a typical sol-gel method, a colloidal suspension or a sol is formed from hydrolysis and polymerization reactions of precursors, which are usually inorganic metal salts or metal organic compounds such as metal alkoxide. The characteristics and properties of a particular sol-gel network are related to a number of factors that affect the rate of hydrolysis and condensation reactions, such as: pH, temperature and time of reaction, reagent concentration, nature and concentration of catalyst, H_2O/M^+ molar ratio, aging temperature and time and drying. Nickel oxide was prepared by modified sol-gel method and spherical NiO nanoparticls were obtained by Wu et al. (2007). In this paper, influence of some parameters on the synthesis of nanosized NiO materials has produced spherical

nanoparticle. Similarly, many more metal oxides like SnO_2 (Aziz et al., 2013), TiO_2 nanoparticle (Hema et al., 2013) were also synthesized by sol-gel method.

1.3.2.3 Sonochemical method

Sonochemistry is a process in which molecules undergo a chemical reaction due to the application of powerful ultrasound radiation having frequency in the range of 20 KHz-10MHz. The ultrasonic vibrations are intensified and focused through an ultrasonic probe in a very intense flow. The stream passes through the liquid causing alternatively a compression and a relaxation of the liquid. This change in pressure leads to the emergence of microscopic bubbles (cavities) that expand during the decompression phase and implode violently during the compression phase. The cavitations are a quenching process, and hence the composition of the particles formed is identical to the composition of the vapour in the bubbles, without phase separation (Shafi et al., 2001). Sonochemistry has been used to prepare various kinds of nanostructured materials magnetic which include materials of metal alloy, metal oxide, ferrite, nitride and so on (Nguyen et al., 2012, Ziylan et al., 2013). Synthesis of silver nanoparticles by sonochemical method was studied by Manoiu et al. (2010), where they found spherical shape and uniform size. A novel method for sonochemical preparation of nanosized hollow iron oxide using carbon nanoparticles as template has been demonstrated by Bang et al. (2007). Nano-sized metal-organic lead (II) polymer is used as precursor for the preparation of nano-structured lead (II) iodide and lead (II) oxide by sonochemical method was studied by Aslani et al. (2009).

1.3.2.4 Co-precipitation method

Coprecipitation synthesis involves dissolution of compound salt precursor in aqueous media and subsequent precipitation from the solution by pH adjustment. The co-precipitation technique is a useful method for the preparation of ceramics and metal oxide powders. Apart from its simplicity, atomic mixing of the constituents by chemical co precipitation yields a final product of near-perfect stoichiometry without high-temperature treatment. Wang et al. (2009) have synthesized highly photocatlytic ZnO/In_2O_3 heteronanostructures by co precipitation method. Jadhav et al. (2009) have studied on effect of different surfactants on the size and optical properties of Y_2O_3: Eu^{3+} nanoparticles prepared by co-precipitation method. A cost effective co precipitation method has also been used by Wang et al. (2010) for the synthesis of indium tin oxide nanoparticle without chlorine contamination. Recently,

Kim et al. (2013) have investigated on characterization of as- synthesized FeCo magnetic nanoparticles by using co precipitation method.

1.3.2.5 Electrospinning method

A large number of advanced techniques have been employed to fabricate 1-D nanostructure, but electrospinning seems to be the simplest and most versatile method. Electrospinning is a broadly used technique for electrostatic fiber formation. In this method electrical force is utilized to produce polymer fibers with diameters ranging from few nanometers to several micrometers using polymer solutions of both natural and synthetic polymers (Bhardwaj et al., 2010). It is the process by which continuous nanofibers are produced with high surface area-to-volume ratio. Basically, an electrospinning system consists of three major components: a high voltage power supply, a spinneret (e.g., a pipette tip) and a grounded collector (usually a metal screen, plate, or rotating mandrel) and utilizes a high voltage source to inject charge of a certain polarity into a polymer solution or melt, which is then accelerated towards a collector of opposite polarity (Liang et al., 2007). In this process, a polymer solution is injected from a needle in the presence of electric field. A DC voltage in the range of several tens of kVs is necessary to generate electric field during the electrospinning. When the applied electric field overcomes the surface tension of the liquid a continuous jet is ejected which upon subsequent solvent evaporation and bending produces nanofibers on the collector surface (Greiner et al., 2007). This method has following advantages: (i) the ability to produce thin fibers with diameters in the micrometer and nanometer ranges; (ii) one-step forming of the two-or three dimensional nanofiber network assemblies and (iii) applicability for a broad spectrum of molecules, such as synthetic and biological polymers (Matsumoto et al., 2011). Recently, various applications of electrospun fibers are being carried out, as these fibers have high surface to volume ratio, very high porosity and enhanced physico-mechanical properties. Thavasi et al. (2008) have reviewed on electrospun nanofibers in energy and environmental applications. Applications of electrospun nanofibers in drug delivery and tissue engineering have also been investigated by Sill et al. (2008). Agarwal et al. (2008) have investigated on the use of electrospinning technique for biomedical applications. Similarly, Dong et al. (2011) have studied on the use of electrospinning to create materials suited for four major energy-related applications i.e. fuel cells, dye-sensitized solar cell, Li-ion batteries and super capacitors. Teo et al. (2009) have reviewed on electrospun nanofibers as a platform for multifunctional, hierarchically organized nanocomposite. Ceramic nanofibers have great potential in various applications such as

photonics, nanoelectronics, data storage, catalysis, adsorption studies and many more (Formo et al., 2009, Biswas et al., 2012). These ceramic nanofibers can be amorphous, polycrystalline, dense, porous, or hollow (Sigmund et al., 2006). Recently, electrospinning technique has been used to prepare various ceramic nanofibers (Dai et al., 2011, Wu et al., 2012). In a review article Ramaseshan et al. (2007) have reported the fabrication and usefulness of various nanostructured ceramics by electrospinning method. They have also highlighted some important applications and the physicochemical properties of nanostructured ceramics material.

1.4 Importance of alumina and iron oxide nanomaterials

Synthesis of various functional nanomaterials such as metals, semiconductors, magnetic materials and so forth has been of immense scientific and technological interest (Ge et al., 2009). Among them aluminium and iron oxide nanomaterial are well-known and widely used materials in ceramics manufacturing. These compounds have both cationic and anionic chemisorption properties and this can possibly be used to remove metal ions from the aqueous phase. While the sorption capabilities of these aluminum and iron compounds are known, they have not found wide usage in this capacity because their sorption capacities have been limited compared to other materials already commercially available. However, the nano-material form of this aluminum and iron is anticipated to be more catalytically active than its bulk form and if indeed sorption is the key mechanism, then the substantial increase in surface area of the nano form would increase capacities very significantly.

1.4.1 Alumina

Alumina has many appealing properties which makes the material interesting for applications in many different areas. Alumina especially has a high melting point, high strength, corrosion resistance, chemical stability, low thermal conductivity and good electrical insulation properties. As a type of important structural ceramic material, alumina has applications in absorbent, catalyst, carrier and reinforcement of ceramic composites. Alumina occurs in nature as the minerals, corundum (Al_2O_3); diaspore ($Al_2O_3.H_2O$); gibbsite ($Al_2O_3.3H_2O$); and most commonly as bauxite, which is an impure form of gibbsite. Alumina exists in a number of crystalline phases (polymorphs), three of the most important being γ, θ, and α. The α-alumina structure is thermodynamically stable at all temperatures up to its melting point at 2051°C, but the metastable phases (e.g., γ and θ) still appear frequently in alumina growth studies. Transition aluminas are high surface area oxides formed by

controlled calcination of aluminum oxy-hydroxide. The structures of aluminium oxide are of two types, hexagonal and octahedral in which it holds the atoms. Hexagonal sites are the corner atoms in the cell while the octahedral sites are present between two layers of vertical stacking. The oxygen present in octahedral sites permits strong bonding and therefore, gives rise to the characteristics properties of alumina. The basic unit cell structure of corundum i.e., α-alumina has a hexagonal structure but the γ-alumina has a spinel structure. The γ-alumina phase is an unstable phase and it is transformed to the θ-alumina phase at a temperature of 700-800°C. This phase of alumina is used as catalyst and catalyst support because of it shows high surface area. The lattice structure of gamma alumina has two different lattices, the first lattice is comprised of aluminium ions and it is formed from octahedral and tetrahedral interstitial locations and the oxygen lattice is formed with the face centre cubic structure. Boehmite (γ-AlOOH) is an aluminium oxyhydroxide, which is used as a precursor for many aluminium oxide materials, especially for the preparation of catalysts, membrane, coating, adsorbents etc. Upon heating at temperatures between 400 and 700°C, boehmite undergoes an isomorphous transformation to nanocrystalline γ-Al_2O_3 without altering the morphology of the parent material (Cai et al., 2010).

Among one-dimensional nanostructures, nanofibers show broad application and properties. So, alumina nanofibre has a large number of applications including high-temperature insulation, catalyst support in high temperature reactions, fire protection and as reinforcement for resins, metal and ceramic (Yu et al., 2012). Its importance is due to its high strength and modulus, resistance to attack by molten metal's and non-oxide materials, chemical inertness in both oxidizing and reducing atmospheres up to 1000°C, low thermal conductivity and good electrical insulation (Ma et al., 2007, Wakihara et al., 2009, Liu et al., 2012).

1.4.2 Iron oxides

Research on iron oxide nanomaterials has experienced a surge in the recent decade or two. This is likely due to new synthetic techniques as well as interest in new applications of iron oxides nanomaterials (Vincent et al., 2012). Iron oxides have been extensively studied in diverse fields. Recently, functionalized iron oxide nanoparticles have also been used in many advanced nano-technological applications. The most important advantage of nano-sized iron oxides among other nanomaterials are due to its relatively low toxicity and biodegradability. It is observed that generally, amorphous metal oxides show great industrial potential in many advanced applications such as solar energy transformation, electronics,

electrochemistry, manufacture of magnetic storage media, sorption and purification processes and catalysis (Perkas et al., 2001). In above all, the applications, amorphous iron (III) oxide plays a vital role, especially because of its superior catalytic activity, super paramagnetic behavior, and the large specific surface area of the nanoparticle (Machala et al., 2007). Iron oxides are one of the most important metal oxides of technological importance. It has sixteen pure phases i.e., oxides, hydroxides or oxy-hydoxides, which are known till date. These are

$Fe(OH)_3$, $Fe(OH)_2$, $Fe_5HO_8{\cdot}4H_2O$, Fe_3O_4, FeO, five polymorphs of FeOOH and four of Fe_2O_3. Characteristics of these oxide compounds include mostly the trivalent state of the iron, low solubility and brilliant colors. Among them mostly are crystalline except few (Mohapatra et al., 2010). Further, the oxy hydroxide compounds like goethite, α-FeO(OH) exhibits an orthorhombic symmetry. Similarly, akaganeite, β- FeOOH, has a large tunnel-type structure where iron atoms are strongly bonded to the framework. Lepidocrocite, γ-FeOOH, crystal structure is built by double layers of Fe-octahedral, with the hydroxyl groups being located on their external surfaces and hydrogen bonding between the layers. The basic morphology of lepidocrocite are lath-like or tabular (Cornell et al., 2003, Huber et al., 2005). Moreover, hematite exhibits a rhombohedral structure which is antiferromagnetic in nature. α- Fe_2O_3 (hematite) is a semiconductor (E_g = 2.1 eV) which is environmentally friendly-nontoxic, corrosion- resistant- and easily obtainable (Wen et al., 2005). Hematite (α-Fe_2O_3), the most stable iron oxide, is widely used in catalysts, pigments, magnetic devices, ferrofluid, sensors, especially in biomedical field and as the raw material for the synthesis of maghemite (γ-Fe_2O_3) (Jia et al., 2005). Whereas, magnetite and maghemite are ferrimagnetic and both crystallize in the inverse spinel cubic structure. At ambient conditions, these phases are thermodynamically less stable than hematite. Inspite that, maghemite is used in large number of applications viz., magnetic resonance imaging, magnetic recording media, fabrication of biocompatible magnetic fluids and elctrochromic devices (Martinez et al., 2009).

1.5 Application of nanomaterials

Nanotechnology is moving into the centre of world-wide public attention because of its broad range of applications which could dramatically impact both the scientific community and the commercial market place. Generally speaking, nanotechnology can be defined as the application of scientific and engineering principles to make and utilize very small things (Mu et al., 2010). Nanotechnology applications have been applied across biomedical, optical, electronic, mechanical and chemical fields as well as in consumer goods

such as foods and cosmetics. Nanotechnology is merging with information technology, biology and social sciences and is expected to reinvigorate discoveries and innovations in many areas of the economy. A complete list of the potential applications of nanomaterials is too vast and diverse. Few of these applications are described briefly as follows.

1.5.1 Chemical applications

1.5.1.1 Catalysis

Catalysis is of vital importance in our society and constitutes a cornerstone of life from biological processes to large-scale production of bulk chemicals. Nanomaterials having small size and large surface area exihibit unique catalytic properties. For example, gold is a poor catalyst in the bulk form whereas nanosized gold is not. Nanomaterial-based catalysts are usually heterogeneous catalyst. The extremely small size of the particles maximizes surface area exposed to the reactant, allowing more reactions to occur on the surface. However, thermal stability of these nanomaterials is limited by their critical sizes; the smaller the crystallite size, the lower thermal stability (Viswanathan, 2009). The two types of catalyst that carry out chemical reactions with high rates and selectivity are (1) Enzymes (nature's catalysts) and (2) Synthetic catalysts. There are three parameters, which are main key to determining the suitability of activity, selectivity and stability. Zhong et al., 2007 have synthesized three dimensional flowers like ceria micro/nanocomposite which is used as a support for gold nanoparticles to remove CO by catalytic oxidation. Similarly, Polshettiwar et al., 2009 have studied on a number of metal oxides (Fe, Co, Mn, Cr, and Mo) three dimensional nanostructures which were observed to show a novel support for various catalytic organic transformations. Nanoferrites was functionalized and coated with Pd metal, which was catalyzing various C-C coupling and hydrogenation reactions with high yields. Positively-charged gold nanoparticles possess intrinsic peroxidase-like activity, and can catalyze oxidation of the peroxidase substrate 3, 3, 5, 5-tetramethylbenzidine (TMB) by H_2O_2 (Jv et al., 2010).

1.5.1.2 Paints, pigments and coating

Nanomaterials are defined by its sizes of less than 100nm. Since a fairly long time they are part of the innovative materials for industry and research. In formulations of paints, coatings, inks and varnishes increases the use of nanomaterials rapidly. Color and gloss characteristics are numbered among the decorative aspects; conductivity, microbial inactivation or antistatic properties are numbered to the functional aspects. By addition of nanoparticles, also the

protective functions of paints and coatings, such as scratch resistance and UV stability can be improved. When changing the size of these materials, also the material properties are changing, such as the color, the interaction with other substances and the chemical reactivity. This change in material properties results from a change in the electronic properties. Zinc phosphate nanomaterials is found to be the widest application in paints, since it provides excellenmt corrosion resistance and is non-toxic (Grzmil et al., 2007). Mathiazhagan et al. (2011) have reviewed on nanomaterials used in a new prospective in organic coating. They have emphasized mainly on different types of coatings, pigments used in paint formulation and a special focus is set on the uses of nanomaterials/fillers in coating application.

1.5.2 Optical and electronic applications

Semiconductor nanomaterials possess unique and interesting optical properties and functionalities that find important applications in emerging technologies (Li et al., 2009). In case of semiconductor materials, the reduction in particle size, results in increase in the band gap which results in shift of the absorption light towards in the high-energy region. In addition, the band edge position of valence and the conduction bands are stabilized and destabilized respectively (Viswanathan, 2009). This leads to an increase in the oxidation and reduction ability of the semiconductor. Certainly, the rate of recombination of photo excited electron-hole pair is also reduced greatly. Recently, Li et al. (2010) have reviewed on nanocomposites composed of inorganic nanoparticles and the polymer matrix for optical applications. Polymer-inorganic nanocomposite are found to be promising new lines of exploration which can show new bi-functional applications i.e. optoelectronic and magneto-optic.

1.5.3 Magnetic applications

Magnetism is an intrinsic façade of existence of living creatures, from iron in blood to the capability of magneto tactic bacteria, birds and other creatures to navigate by the Earth's magnetic field. Diverse applications in data storage, security/sensors to biomedical applications led to noteworthy advances in development of variety of multifunctional magnetic nanoparticles.

Polymer inorganic nanocomposite is basically used in optical application, magnetic applications, mechanical applications, catalysis, electrochemical applications, electrical and thermal applications and biomedical applications (Li et al., 2010). For magnetic applications, metal and metal alloys such as Fe or CoPt, oxides such as ferric oxide and ferrite are always

used as inorganic nanofillers. Sharma et al. (2011) have presented a review which recapitulates the development of state-of-the-art multifunctional magnetic nanoparticles and the foremost applications of these multifunctional magnetic nanoparticles in magnetic targeting, drug delivery, separation, and contrast agents in magnetic resonance imaging, hyperthermia and sensors.

Super-paramagnetic iron oxide nanoparticles with appropriate surface chemistry can be used for numerous in vitro applications such as MRI contrast enhancement tissue immunoassay, detoxification of biological fluids, hyperthermia, drug delivery, and cell separation (Laurent et al., 2008). Liang et al. (2010) have successfully fabricated free-standing graphene/Fe_3O_4 hybrid papers, which exhibit good flexibility, electrical conductivity, and mechanical strength, and also superparamagnetism. These hybrid papers can also show potential applications in fields such as magnetic controlling devices, data storage, magnetic detection, electromagnetism shielding materials, electrochemical devices, batteries and so on.

1.5.4 Metal and ceramics applications

Metallic nanomaterials (nanoparticles, nanowires and nanorods) have gained a large interest in industry because of their unique physicochemical properties resulting from nanoconfinement effects. Abdullayev et al. (2011) have reported on the selective formation of silver nanorods within the inner lumen of halloysites. Halloysite tube templates have a potential for scalable manufacturing of ceramic encapsulated metal nanorods for composite materials. In particular, ceramic with one dimensional nanostructure received increasing interest since it provides a good material system to investigate the dependence of electrical, optical, thermal and mechanical properties on dimensionality and size reduction (Lu et al., 2009). For practical application of one-dimensional ceramic nanomaterials scalable materials production and convenient devices integration are extremely important (Wu et al., 2012). An important class of fiber nanomaterials appeared encompassing simple, binary and ternary oxide ceramics. Moreover, since the oxide ceramics are also biocompatible, novel electrospun fibrous materials have been synthesized for medical application (Starbova et al., 2012). The fiber immobilization has been found very important for the development of various functional ceramic materials synthesis of many ferroelectric oxides ceramics of different structural families are reported by various group. For example, lead zirconate titanate ceramics, lead gadolinium zirconate (Panigrahi et al., 2013). It is also observed that porous ceramics are widely used as filters, catalyst carriers, separation membrane and bio-

ceramics. Isobe et al. (2007) have synthesized porous alumina ceramics with unidirectional – oriented pores to study the gas permeability and mechanical property. The gas permeability is higher than that of conventional sample; it is due to increasing porosity and pore size. Similarly, Kritikaki et al. (2009) have fabricated porous alumina ceramics by sol-gel method. Thus, ceramics prepared by employing nanomaterials in powder form exhibits less uniform microstructure. Very recently, Fung and coworkers, (2013) have investigated on reinforcement of porous alumina by nickel aluminate spinel for its use as ceramic membrane.

1.5.5 Biological applications

Nanomaterials have number of potential applications in medical and biological fields. From nanotechnology there is only one step to nanomedicine, which may be defined as the monitoring, repair, construction, and control of human biological systems at the molecular level, using engineered nanodevices and nanostructures. Nanomedicine is dominated by nanoparticulate drug delivery system because of their ability to cross biological barriers, accumulate at tumour sites and /or increase the solubility of drugs. Sahoo et al. (2007) have investigated on the present and future of nanotechnology in human health care. According to them applications of nanotechnology to medicine and physiology imply materials and devices designed to interact with the body at subcellular scales with a high degree of specificity. Recently, M. P. Marszałł, (2011) has studied on the application of magnetic nanoparticles in pharmaceutical sciences. The use of magnetic nanoparticles as drug carriers in targeted therapy provides huge opportunities in cancer treatment. Similarly, Shao et al. (2012) have reviewed on magnetic nanoparticles and micro NMR for diagnostic applications. They investigated that biosensing strategies using magnetic nanoparticles offer unique advantages over traditional detection methods.

Microorganisms such as bacteria, molds, and viruses are a big problem for human being. Thus, novel antibiotics and antimicrobial agents have been synthesized and developed for preventing disease in public health settings and for antifouling treatment in the biomedical industries. Chae and co-workers, (2011) have synthesized electrospun nanofiber composite with functionalized silver nanoparticle on it. A mixture of PAN and β-cyclodextrin solution was used for synthesizing electrospun composite nanofiber. Here β-cyclodextrin acted as a stabilizing and reducing agent for the formation of silver nanoparticle. The antimicrobial activities of nanocomposite fibers containing silver nanoparticles (Ag/NFs) against *Escherichia coli* (*E. coli*) and *Staphylococcus epidermidis* (*S. epidermidis*) were evaluated by optical density testing. Silver is known for its antimicrobial properties and has been used in

medical field for antimicrobial applications and are also used in water and air filtration to eliminate microorganisms (Sharma et al., 2009). Magnetic nanocomposite can be transported purposely to a certain location in the human body and may thus act as effective drug carriers. Combining magnetic iron oxide nanoparticle and silver nanoparticle shows a unique property (Prucek et al., 2011). They have studied two types of magnetic nanocomposite exhibiting high antimicrobial activities–Ag@Fe_3O_4 and γ-Fe_2O_3@Ag. Both synthesized nanocomposites exhibited very significant antibacterial and antifungal activities against ten tested bacterial strains (minimum inhibition concentrations (MIC) from 15.6 mg/L to 125 mg/L) and four candida species (MIC from 1.9 mg/L to 31.3 mg/L).

1.5.6 Environmental application

Presently, nano-environmental concerns are starting to be taken seriously around the globe. Direct applications of nanotechnology for environmental cleanup relate to the removal of some toxic elements or compounds from the environment, through, the use of nanofiltration, nanoporous sorbents, and catalysis by filtering, separating, and destroying environmental contaminants. Vaseashta et al. (2007) have investigated on nanostructures which are used in environmental pollution detection, monitoring and remediation. They have also presented the sorption studies using nanomaterials based sorbents that are effective in the removal of cadmium and arsenic from water streams. Pollution in water system impairs or destroys aquatic life, threatens human health and simply fouls the water such that recreational and aesthetic potential are lost. The waste water is not properly treated prior to discharge, and then highly toxic metal ions may leak into ground water. Conventional water treatment methods are such as activated charcoal, coagulation-flocculation, reverse osmosis, distillation, and adsorptive filtration through ion exchange resins. Activated alumina, or iron oxide can effectively remove only certain heavy metal ions (Hu et al., 2008). Mauter et al. (2008) have studied on environmental application of carbon based nanomaterials. Carbon-based nanomaterials have a broad range of environmental applications: sorbents, high-flux membranes, depth filters, antimicrobial agents, environmental sensors, renewable energy technologies and pollution prevention strategies.

1.5.6.1 Adsorptive removal of metal ions

Removal of inorganic and organic pollutants from waters has been one of the major investigations in the last few decades. A large number of nanoadsorbents such as nanosized metal oxides like ferric oxide, manganese oxides, aluminium oxides, titanium oxides, magnesium oxides and cerium oxides are classified as the promising ones for heavy metal removal from aqueous system (Hua et al., 2012). This is partly because of their large surface

areas and high activities caused by the size quantization effect. Chen et al. (2010) have studied on synthesis of Goethite and hematite nanomaterials using co-precipitation method, which was used for adsorption studies of copper. The maximum Cu (II) adsorption capacity is 149.25 and 84.46 mg/g for nano-goethite and nano-hematite, respectively. Recently, Parham et al. (2012) have synthesized magnetic iron oxide nanoparticles modified with 2-mercaptobenzothiazole for fast and efficient removal of mercury. With a very short equilibrium time of 4 min, the adsorbent was able to remove 98.6% of mercury. Very recently, Ferrate (VI)-induced Arsenite and Arsenate removal by in situ structural incorporation into magnetic iron (III) oxide nanoparticles was studied by Prucek et al. (2013). At pH 6.6 efficiency of arsenic removal was found to be 100%. Activated form of alumina is also considered as one of the commonly used adsorbent for heavy metal removal. Surface developed alumina adsorbent with immobilized 1-nitroso-2-naphthol was used for removal and pre-concentration of lead (II), copper (II), chromium (II) and iron (III) from wastewater. High metal up-take was found providing this order: Cu (II) > Cr (III) > Pb (II) owing to the strong contribution of surface loaded 1-nitroso-2-naphthol (Mahmoud et al., 2010).

1.5.6.2 Adsorptive removal of organic dyes

Clean water, free of toxic chemicals, is important to human beings. Over the past few years, many research groups have tried to use functional metal oxide nanomaterials to remove toxic ions and organic pollutants from water. Different industries such as textiles, rubber, paper and plastics contain wastewater effluents which have several kinds of synthetic dye-stuffs. A very small amount of dye in water is highly visible (Chatterjee et al., 2009). Adsorption technique is quite popular due to simplicity and high efficiency, as well as the availability of a wide range of adsorbents. It has proved to be an effective method for removal of dye from wastewater. Mahmoodi et al. (2012) have studied on synthesis of amine functionalization and dye removal ability of titania/silica nanohybrid. A comparison between titania/silica nano-hybrid (TSNH) and amine-functionalized titania/silica nano-hybrid (AFTSNH) i.e., (LAFTSNH: low amine-functionalized titania/silica nano-hybrid and HAFTSNH: high amine functionalized titania/silica nano-hybrid) were carried out for removal of two textile dyes i.e., Reactive Red 198 (RR198) and Acid Red 14 (AR14). The dye removal ability of HAFTSNH was higher than that of LAFTSNH due to higher amine functionalization onto TSNH. Very recently, carbon–incorporated ZnO nanostructure synthesized by solvothermal method shows high adsorption of Congo red dye (Zhou et al., 2013). The maximum adsorption capacity of Congo red was found to be 162 mg g^{-1} calculated by Langmuir equation while commercially available ZnO nanoparticle shows 18.8 mg/g. Afkhami et al. (2010) have studied on

adsorptive removal of Congo red, from aqueous solution by maghemite nanoparticles. The maximum adsorption occurs at pH 5.9, with a maximum adsorption capacity of 208.33 mg/g of the adsorbent.

1.6 Objective of this study

The objectives of the work describes in this thesis were to:

1. To synthesize alumina, iron oxide and their mixed composite 1D nanomaterials (nanofiber / nanorods) using different soft chemical synthetic methods such as sol-gel, hydrothermal and electrospinning method.
2. Detailed characterization of the nanomaterials by spectroscopic, microscopic, sorptometric and scattering analytical techniques to obtain the information on the surface morphology, dimension, porosity, crystalline structure and surface active sites.
3. To investigate the feasibility of using 1D Fe_2O_3/Al_2O_3 nanomaterials for removal of toxic metal ions such as Cr, Pb, Ni, Cu, As, Hg and also organic dyes from aqueous solution by chemisorption / adsorption process.
4. To obtain an overall correlation between surface properties of the synthesized nanomaterial and their sorption activities.

1.7 Organization of the thesis

This thesis is organized into eight chapters. Chapter 1 represents the introduction to nanomaterials, their synthesis and applications. The next chapter (Chapter 2) is a review of the literatures investigating three different methods i.e. sol-gel, hydrothermal and electrospinning for synthesis and applications of alumina, iron oxide and mixed oxide composite nanomaterials. Chapter 3 describes about the synthesis of boehmite nanomaterials by sol-gel method and its adsorptive studies for removal of Congo red dye. Chapter 4 shows the synthesis and characterization of α-alumina nanofiber via electrospinning method and its studies on removal of Cr (VI) and F^- toxic ions from an aqueous system. Chapter 5 represents the adsorptive removal of Congo red dye from wastewater by mixed iron oxide-alumina nanocomposites. In chapter 6, synthesis and characterization of electrospun Fe_2O_3-Al_2O_3 nanocomposite fibers has been studied. In the same time its application as efficient adsorbent for removal of heavy metal ions from aqueous solution is also investigated. In the following chapter 7, studies on the synthesis of electrospun PAN-Ag composite nanofibers for antibacterial application were evaluated. The final chapter 8 concludes our works and highlighted the contributions.

CHAPTER 2

LITERATURE REVIEWED

This chapter comprises the literature reviewed on the current developments in the area of synthesis and characterisation of alumina, iron oxide and their mixed nanocomposites. Literature reported on these metal oxide and their composites using especially sol-gel, hydrothermal and electrospinning synthetic methods have been highlighted here. Apart from this the basic principles of formation along with the advantages using these synthetic techniques have been briefly presented. Furthermore, the applications of these materials specifically in the area of adsorption of toxic metal ions, dyes removal and antibacterial activity have also focused in this chapter.

2.1 Sol-gel method

The sol-gel process is a versatile soft chemical process, widely used for synthesizing metal oxides, ceramic and glass materials. Sol-gel chemistry has opened a new opportunity in the field of materials science. Sol-gel method normally involves the use of metal alkoxides or organometallic inorganic salts as precursors. In this process, the precursor's undergoes a series of hydrolysis and polycondensation reaction to form a colloidal suspension or a sol. The sol-gel process involves the transition of a system from a liquid "sol" (mostly colloidal) into a solid "gel" phase (Chaudhury et al., 2007; Mourad et al., 2009). Then drying of the gel followed by calcination at different temperatures to obtain the metal oxide nanopowder. In sol-gel method it is possible to control the shape, morphology and textual properties of the final materials. That shows the versatility of the sol gel process. In contrast to high-temperature processes, Sol-gel method has large advantages such as possibility of obtaining metastable materials, achieving superior purity and compositional homogeneity of the products at moderate temperature. Furthermore, this process also influences the particle morphology during the chemical transformation of the molecular precursor to the final oxidic network. Various research groups have reported previously on synthesis of iron oxide and alumina nanomaterials using sol-gel method.

2.1.1 Iron oxide nanomaterial by sol gel method

Metal oxides prepared by sol-gel chemistry have high surface area, and porosity because of which they are attractive in various applications. Among various metal oxides, hematite (α-Fe_2O_3) is one of the most stable iron oxide. Being a strategic industrial material and one of the most used metal oxides, hematite has been extensively studied. Over the past years, on the synthesis of iron oxide particles by the sol-gel method, a lot of work has been done.

Nanorods as one-dimensional nanomaterials have attracted much attention due to their peculiar properties, which is due to their high surface area and low dimensionality. Among them, metal oxide nanorods have shown to possess interesting properties viz. catalysts, electrochromic devices, magnetic storages, lasers and sensors. Woo et al. (2003) have reported on a novel and easy route to Fe_2O_3 nanorods by a sol-gel mediated reaction of Fe^{+3} ions in reverse micelles. The diameter and length of the iron oxide nanorods could be controlled by the H_2O/oleic acid ratio in the gelation process and the phase of the nanorods could be controlled by temperature and hydrous state of the gels during crystallization. With increasing H_2O/oleic-acid ratio, the average diameters and lengths of the nanorods increased. The synthesis of discrete and phase-controlled Fe_2O_3 nanorods is challenging and of important issue in relation with magnetic properties derived from shape anisotropy. Synthesis of rod-shaped hematite and maghemite nanoparticles with diameter of 5nm and length of 16 and 17 nm was reported by Woo et al. (2004). They have studied for magnetic properties, and observed that this nanorod exhibits superparamagnetic behaviour.

Synthesis of iron oxide particles, tubes and fibrils were done by sol-gel method using metalloorganic compounds within the pores of nanoporous polycarbonate and alumina membranes. By hydrolysis and polymerization of iron salts, particles were formed in pores, building iron oxide nanowires. Magnetic nanowires have mean diameters of 9 nm (Suber et al., 2005). Crystalline hematite tubes were obtained after heat treatment of the amorphous phase at 600°C.

Similarly, Chuanbo et al. (2010) have synthesized Fe_2O_3 microtubules by sol-gel template method. Fe_2O_3 microtubules were synthesized after the process of self-propagation or calcinations. Its external diameter ranged between 8 and 13 μm, and the thickness ranged between 0.5 and 2 μm. It shows high magnetic properties after calcination at 400°C for 2 hrs. The different calcination temperature plays a very important part in developing the Fe_2O_3 phase and the variation in the magnetic properties.

Recently, uniform α-Fe_2O_3 nanoparticles have been prepared by sol-gel method using three different carboxylic acids i.e. citric acid, tartaric acid and succinic acid as chelating agents. The particle size was found to be 18-25nm. Among the prepared samples, the tartaric acid stabilized Fe_2O_3 nanoparticles shows the best thermal stability and the smallest particle size. Arising out of their high scattering and reflection efficiency these iron oxide nanoparticle were used in pigments applications (Fouda et al., 2013).

Iron oxide nanoparticles with different structures (α-Fe_2O_3, γ-$Fe_2O_3$and Fe_3O_4) constitute an outstanding category of functional materials that can be applied in various fields. Herein, an epoxide assisted sol-gel route is carried out to synthesize mono-dispersed iron oxide nanoparticles on large scale (Cui et al., 2013). They have reported that the formation of monodispersed different iron oxide i.e. α-Fe_2O_3, γ-Fe_2O_3 and Fe_3O_4 nanoparticles at low temperature (78°C) heat treatment. The strategy developed in this study offers important advantages over the conventional routes, showing potential for its application in industrial production of iron oxides. The structure of iron oxide nanoparticles were tuned by the changing of drying conditions of the sol.

2.1.2 Alumina nanomaterial by sol-gel method

Nano alumina is one of the most important ceramic materials. It has large number of applications such as unique catalyst for many chemical reactions, in microelectronics, membrane applications, waste water treatment and many more. Pure alumina nanoparticles have been synthesized by a variety of techniques. Among them sol gel method is simple, cost effective and the size and morphology of the nanoparticle can also be controlled (Srivastava et al., 2011).

Li et al. (2006) have synthesized ultrafine α-Al_2O_3 nano powder by a modified sol-gel method. A citrate polymeric precursor was derived from aluminium nitrate and citric acid, which plays an important role in phase transition and morphology of alumina. When the molar ratio of citric acid to metal nitrate (C/N) =1, a yield of well dispersed ultrafine α-Al_2O_3 powder with a particle size of ~200nm was observed. The evolution in the alumina precursor involves decomposition followed phase transformation from amorphous to γ-Al_2O_3 and γ- to α-Al_2O_3. At 800°C, γ-Al_2O_3 phase appears with a crystallite size of about 15nm. However, with increase in calcination temperature the crystallite size rapidly grew up to ~75nm at 1000°C.

In the year 2007, Teoh et al. have synthesized alumina nanofiber of high aspect ratio and high surface area (>300 m^2/g) in bulk quantities by using sol-gel method. They have used aluminium isopropoxide (AIP) as the precursors for alumina. The hydrolysis and condensation reaction of AIP plays an important role in the size and morphology of the alumina fibers. The authors have controlled the hydrolysis reaction by using the mixed solvent water and alcohol. They have reported that by varying the AIP hydrolysis time period, the morphology of alumina were changed from spherical nanosize particles to continuous nanofibers as shown in TEM figure 2.1. Figure 2.1(a) depicts the TEM micrographs of alumina nanostructures after hydrolysis times of 20 min. With increase in hydrolysis time from 4 h to 24 h, the morphology changed from fibril to fibers as shown in figure 2.1 (b, c).

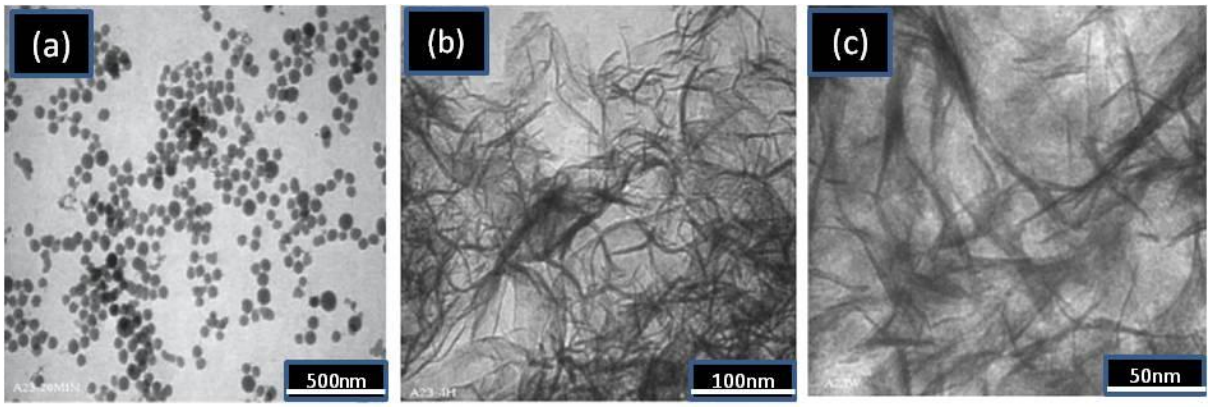

Figure 2.1 TEM image of nanoscale alumina particles hydrolyzed for 20 min (a), 4 h (b) and 24 h (c), (Teoh et al., 2007).

Alumina nanofibers were also prepared by Wang et al. (2007) using aluminium nitrate and hexamethylenetetramine by sol-gel synthetic route. The synthesis was carried out in presence of hexamethylenetetramine (HMTA) followed by the supercritical fluid drying (SCFD) process. In this reaction HMTA is a suitable hydrolyser and coagulant for the preparation of alumina gel. Alumina nanofibers were obtained after drying the gel followed by heat treatment. TEM data reveals the formations of alumina fibers synthesized in this way are shown in figure 2.2. Sample calcined at 580°C, the dimension of δ-Al_2O_3 fiber is 2nm in diameter and 50nm in length. However, some aggregation of the alumina fiber was observed at elevated temperature from 580°C to 1200°C.

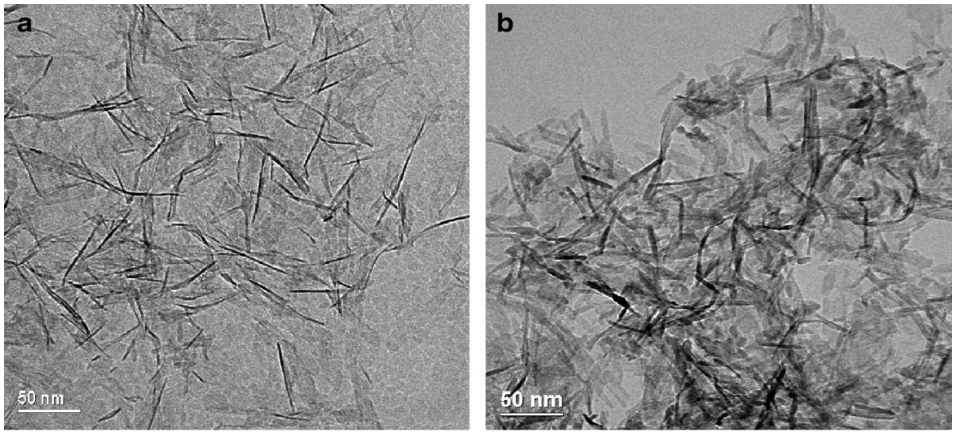

Figure 2.2: TEM images of alumina nanofibers calcined at (a) 580°C and (b) 800°C (Wang et al., 2007).

Shojaie-Bahaabad et al. (2008) reported a simple aqueous sol-gel method for the economical synthesis of nano-sized alumina powder. They have used $AlCl_3$ and commercially available aluminium powder in order to synthesize Al_2O_3 nanopowder. To the acidic solution of $AlCl_3$, aluminium powder was added with stirring to obtain a gel. After that the gel was dried and calcined at high temperature to form 32-100 nm Al_2O_3, spherical shaped particle.

Sharma et al. (2008) reported on the sol-gel mediated synthesis of alumina nanoparticles and the obtained nanomaterials were further used as adsorbents for the removal of Ni (II) ions from aqueous solutions. The nanoalumina was synthesized using aluminium sulphate and ammonia solution. To get pure alumina powder, dried gel was calcined for 1h at 1100°C. The average particle size of the powder was in the range of 15-20 nm. From the adsorption experiment it was found that nanoalumina is an effective adsorbent for the removal of Ni (II) from aqueous solution. The removal of Ni (II) is pH dependent and gives maximum removal of 25mg/L at pH 8.0. A 100% removal was achieved at 20 g/L adsorbent within 120 min.

Chandradass et al. (2008) have synthesized alumina fibers by sol-gel method using α-Al_2O_3 seeded boehmite sol. The starting material used for the synthesis of boehmite sol was aluminium-tri-isopropoxide. Here extended ball milling was used to introduce α-Al_2O_3 seed particles to boehmite sol. It was also observed from differential thermal analysis that the phase transition to α-Al_2O_3 takes place at a much lower temperature by seeding α-Al_2O_3. This method is suitable to reduce the transformation temperature, as well as the sintering temperature.

Sol-gel methods are commonly used for the synthesis of such oxides involving the formation of an amorphous gel from a precursor solution (Farag et al., 2009). In the present study, alumina, titania and mixed alumina-titania with a molar ratio of 1:1 were synthesized by sol-gel method in trifluoromethylsulphonyl amide (TFSA) using aluminium isopropoxide and titanium isopropoxide as precursors. After hydrolysis, the boehmite powder obtained was having an average pore diameter of 3.8 nm. Further the boehmite powder was calcined at 800 and 1000°C for the phase transformation into γ-Al_2O_3 and δ-Al_2O_3. In fact the presence of alumina in mixed oxide results in stabilization of the anatase phase of titanium oxide and elevation of the temperature at which rutile phase occurs.

Sharma et al. (2010) again synthesized nano-Al_2O_3 powder by sol-gel method for the removal of hexavalent Chromium from aqueous solutions. The average crystallite size was found to be in the range of 15-20 nm. The adsorption of Cr (VI) on nano-Al_2O_3 was found to be exothermic in nature and its maximum removal was achieved in the acidic range of pH 2.0. The process of removal was governed by pseudosecond–order kinetics. The adsorption capacity of nano-Al_2O_3 was found to be 8.56 mg g^{-1}.

A rapid, facile, one-pot and organic-solvent free strategy for the synthesis of Fe_2O_3 and Al_2O_3 nanoparticles has been explored by Low et al. (2013). The pre-formation of colloidal particles provides higher surface area than attained for sacrificial templating of solutions of metal salt precursors. The role of the supporting dextran template was investigated and found to be crucial in tuning surface area and morphological shape. A high surface area iron oxide and alumina nanoclusters has been used for gas adsorption/ desorption analysis.

2.1.3 Mixed metal oxide nanocomposite by sol gel method

Synthesis of mixed metal oxides is also possible in sol-gel chemistry. Here mixing of two or more metal oxide phases can be controlled on both the molecular and the nanoscale. These metal oxides are attractive with respect to applications in catalysis, sensing, energy storage, electronics and many more. Many research works is being carried out for synthesis of mixed metal oxide nanocomposite since past few years.

Cannas et al. (2004) synthesized ferrite-silica nanocomposites by a sol-gel mediated autocombustion method for the first time. The combustion involves a thermally induced autocatalytic oxidation-reduction reaction between the nitrate and the citrate ions. Gel obtained by mixing citric acid; metal nitrates, ammonia and tetraethylorthosilicate were

converted in ferrite silica composites through rapid autocombustion reactions. The mean particle size was found to be 3.5 and 5 nm.

The carbon nanotube/alumina nanocomposite with enhanced hardness and fracture toughness was successfully fabricated by sol-gel process by Mo et al. (2005). Homogeneous distribution of carbon nanotubes within alumina matrix can be obtained by mixing both of them and followed by condensation into gel. The composite powders were further sintered by spark plasma process, which forms carbon nanotube reinforced alumina matrix nanocomposite.

A systematic investigation for the formation of silica-coated magnetite nanoparticles via sol-gel approach was also conducted (Kim et al., 2005, Deng et al., 2005). Figure 2.3 shows the TEM images of silica-coated magnetite nanoparticles with different amount of tetraethylorthosilicate (TEOS) as silica precursor. With increase in amount of precursor TEOS larger silica-coated magnetite particles were obtained with more regular shape and monodispersed in size. This result shows that the reaction parameters such as type of alcohol, of alcohol/water volume ratio, the amount of ammonia solution and amount of TEOS plays an important role on the formation of silica-coated magnetite nanoparticles. These coated nanoparticles show supermaganetic properties.

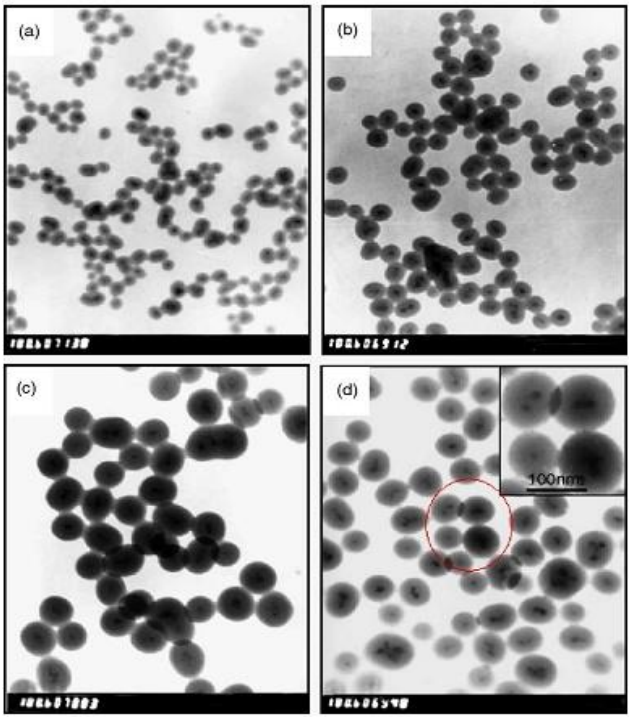

Figure 2.3: TEM images of silica-coated magnetite particles using different amount of TEOS: (a) 1ml, (b) 3ml, (c) 5ml and (d) 7 ml as precursor (Deng et al., 2005).

Tadic et al. (2007) have synthesized, α-Fe_2O_3/SiO_2 nanocomposite by sol-gel method containing 30 wt. % of α-Fe_2O_3. For synthesis of α-Fe_2O_3/SiO_2 nanocomposite hematite nanoparticles was put in a silica matrix. (Niederberger et al., 2007).

Nanocrystalline iron oxide particles have attracted an increasing interest in the field of nanoscience and nanotechnology based on their unique and novel physical and chemical properties (Raileanu et al., 2007). Iron oxide nanomaterials have many properties and applications in domains as: environmental protection, biomedical, catalysis, information displays and electronics. They have proposed an alternative use of sol-gel process, the colloidal route, which is less toxic and less expensive, in order to obtain a Fe_3O_4-SiO_2 nanocomposite. For the synthesis procedure aqueous colloidal silica sol is used, instead of tetraethyorthosilicate (TEOS), as SiO_2 source. Although the prepared nanocomposite had a low content of Fe related to SiO_2 (3 wt. %), it was proved to be suitable for water decontamination, being tested in arsenic removal.

Chromium-iron bulk mixed oxides with different Cr/Fe ratios were successfully prepared by a sol-gel method using propylene oxide as a gelation promoter at 75°C. This mixed oxide shows better results as compared to the corresponding pure oxides, α-Fe_2O_3 and Cr_2O_3. The catalytic activities were also compared with the corresponding pure oxides (Khaleel et al., 2010). The mixed oxides shows better catalytic activity as compared to their single component counters parts.

Chen et al. (2011) have studied on a novel foaming esterification sol-gel route for the synthesis of Magnesia-Yttria (MgO-Y_2O_3) nanocomposite. This process utilizes ethylene glycol, citric acid and corresponding metal nitrate salt followed by heat treatment at 200°C, resulting organometalic precursors and organic foam. Upon further heat treatment at higher treatment the Mg-Y containing organic form was converted into MgO-Y_2O_3 mixed composite materials. This novel method can also be utilized for formation of other mixed oxide nanocomposites.

Recently, Mohanmmadi et al. (2012) have prepared crystalline TiO_2-Fe_2O_3 mixed oxide nanostructures by a new aqueous particulate sol-gel route. In the reaction, titanium (IV) isopropoxide and iron (III) chloride were used as precursors, and hydroxypropyl cellulose (HPC) was used as a polymeric fugitive agent in order to increase the specific surface area. First the authors have prepared TiO_2 solution using titanium isopropoxide. Then iron chloride and HPC solution was prepared with stirring. After that this solution was mixed with titania sol followed by drying at room temperature to obtain mixed TiO_2- Fe_2O_3 powder. This

nanocomposite was showing the promising properties towards gas sensing and thin film applications.

2.2 Hydrothermal method

Hydrothermal chemistry involves chemical reactions in water above ambient temperature and pressure. Under hydrothermal conditions a broad range of nanostructured materials have been synthesized. It is a liquid-solid-solution reaction (Lu et al., 2007). Hydrothermal reaction is defined as "any heterogeneous chemical reaction in the presence of a solvent (whether aqueous or non-aqueous) above room temperature and at pressure greater than 1 atm in a closed system" (Byrappa et al., 2001). Under autogenous conditions, water functions both as a pressure-transmitting medium and as a solvent. The vapour pressure of water increases inside the sealed vessel, as the temperature is raised above its normal boiling temperature, but below its critical temperature. The selected reaction temperature and the degree of free volume to be filled with water at room temperature, determines the prevailing experimental pressure. When water is used as solvent, dielectric constant and viscosity are also important. With the variation of dielectric constant and viscosity of water, the increase in temperature has a prominent effect on the speciation, solubility, and transport of solids (Sheets et al., 2006).

Major advantages of hydrothermal process are preparing homogeneous, fine crystalline oxide materials with controlled particle size and morphology. The hydrothermal method is cost-effective and easy route for preparing various metal hydroxides and oxy hydroxides at low temperature and in a short reaction time (Durrani S. et al., 2012). Reaction parameters such as reaction temperature, reaction times, pH values, solvent choice, solute concentration and the presence of additives, can influenced the particle formation homogeneity, size and morphology in hydrothermal process (Mao et al., 2007).

2.2.1 Iron oxide nanomaterial by hydrothermal method

Properties of inorganic nanomaterials extensively depend on their size and shape. As a consequence, synthesis of inorganic nanomaterials has attracted the present researchers. For synthesis of these inorganic nanomaterials new controlled methodologies were developed. Among them hydrothermal method have some advantages including mild synthetic conditions, simple, cost effective, green technology and good crystallization of the products. Hydrothermal method is one of the attractive and promising methods for the preparation of

nanomaterials with high quality. The powders prepared by hydrothermal method have good crystallinity, good dispersity, and do not show macroscopic agglomeration.

In view of the above, Yin et al. (2009) have suggested that hydrothermal process without surfactant is a convenient and effective approach to controllable synthesis of variety of metal oxides and hydrates nanostructures. They successfully synthesized α-Fe_2O_3 nanocrystals with different morphology by a facile 5-sulfosalicylic acid dehydrate assisted hydrothermal process. In addition to that synthesis of honeycomb-like Ni $(OH)_2$ structure and Co_3O_4 microspheres was also reported.

Large scale synthesis of single-crystal dendritic micro-pines of magnetic α-Fe_2O_3 is found out by Cao et al. (2005). The method is based on the weak dissociation of $[Fe(CN)_6]^{3-}$ ions under hydrothermal conditions. Formation of such structures requires a suitable iron complex precursor that slowly dissociates to yield Fe^{3+} ions under the hydrothermal conditions. It can be further used for biomedical science due to the biodegradability of iron oxide.

Liu et al. (2006) have reported on preparation of γ-FeOOH, by hydrothermal process. Upon sintering at high temperature, γ-FeOOH, transform into crystalline Fe_2O_3. The authors have investigated effect of iron oxide and oxalate on the photo degradation of 2-mercaptobenzothiazole (MBT). The photodegradation of MBT strongly depend on the crystal structure, the dosage of iron oxide and the initial concentration of oxalate.

Again using hydrothermal method economical and large scale synthesis of iron oxide was reported via one-step solution-based route. Li et al. (2007) have fabricated Fe_2O_3 hollow spheres, which show better photocatalytic performance. Hydrothermal method has a control on morphology of the product. Through controlling the concentration of $H_2PO^{4-}$to adjust the different speeds of $Fe(CN)_6^{4-}$ ionization, author got dendritic and hollow Fe_2O_3 spheres. Figure 2.4 is the SEM images of hollow Fe_2O_3 spheres with a diameter of 150-200 nm. Figure 2.4(b) shows the entire hollow sphere shell which is built up of numerous Fe_2O_3 nanoparticles with 15-20 nm diameters. In this reaction, surfactant CTAB is used not as template but as dispersant. Replacing CTAB by other surfactants has no effect on the morphology of the product.

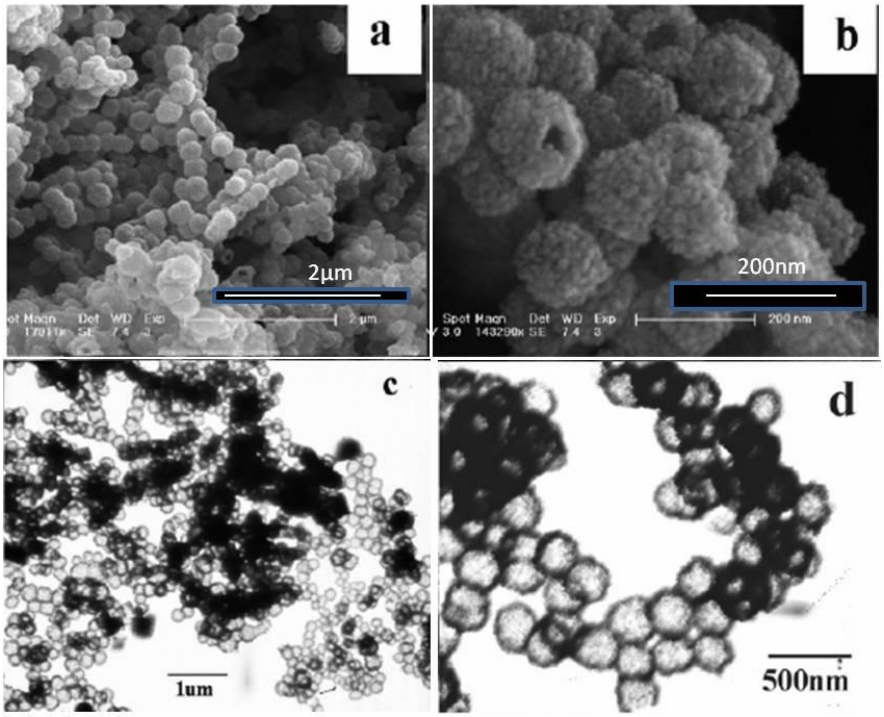

Figure 2.4: (a, b) SEM images and (c, d) TEM images of Fe_2O_3 hollow sphere (Li et al., 2007).

Li et al. (2009) have also reported synthesis of uniform α-Fe_2O_3 nanorods in a large scale by a simple and direct 1.2-propanediamine-assisted hydrothermal method. In the formation process of α-Fe_2O_3 nanorods, the 1, 2-propanediamine not only provides OH^- but also plays a role for retaining the rod-like morphology of hematite. Figure 2.5 (a, b) represents the SEM images of the α-Fe_2O_3 nanorods. Figure 2.5 (c) shows the TEM image of α-Fe_2O_3 nanorods with diameters of 30-40 nm and lengths of 400-600 nm, which are consistent with SEM images. The SAED pattern confirms Fe_2O_3 are crystalline in nature and the spots correspond to the orthorhombic phase of α-Fe_2O_3.

At the same time, Almeida et al. (2009) have demonstrated a process map for hydrothermal synthesis of the formation of lenticular single crystal α-Fe_2O_3 nanorods from $FeCl_3$ precursor solution. It was observed that at lower hydrothermal synthesis temperature (120°C) and short reaction time intermediate β-FeOOH nanorods were formed. However with increase in hydrothermal process temperature (120-240°C) and in the absence of surfactant, rhombohedral α-Fe_2O_3 nanoparticles with sharp edge were formed. Furthermore, at higher processing temperature and in presence of a phosphate surfactant, well crystallized lenticular α-Fe_2O_3 nanorods were obtained. Therefore, it was observed that the surfactant PO_4^{3-} ions plays an important role in mediating the shape and crystallinity of α-Fe_2O_3 nanoparticles prepared by a comprehensive hydrothermal route. Fig 2.6 illustrates the bright

field TEM images of the Fe_2O_3 nanrods where the effect of increasing hydrothermal synthesis temperature from 120-240°C.

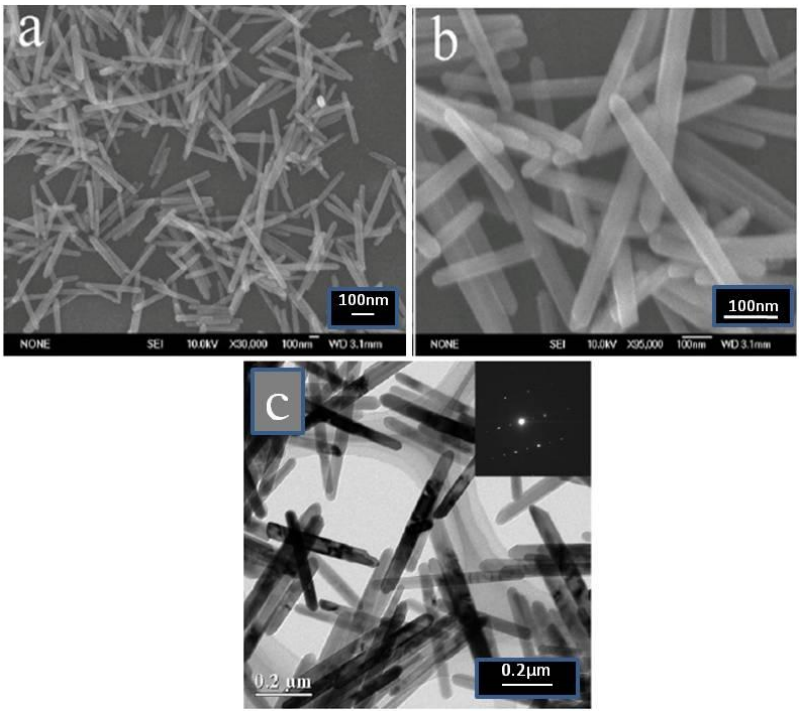

Figure 2.5: (a, b) SEM images of the α-Fe_2O_3 nanorods, and (c) TEM image and the inset is the SAED pattern of the α-Fe_2O_3 nanorods (Li et al., 2009).

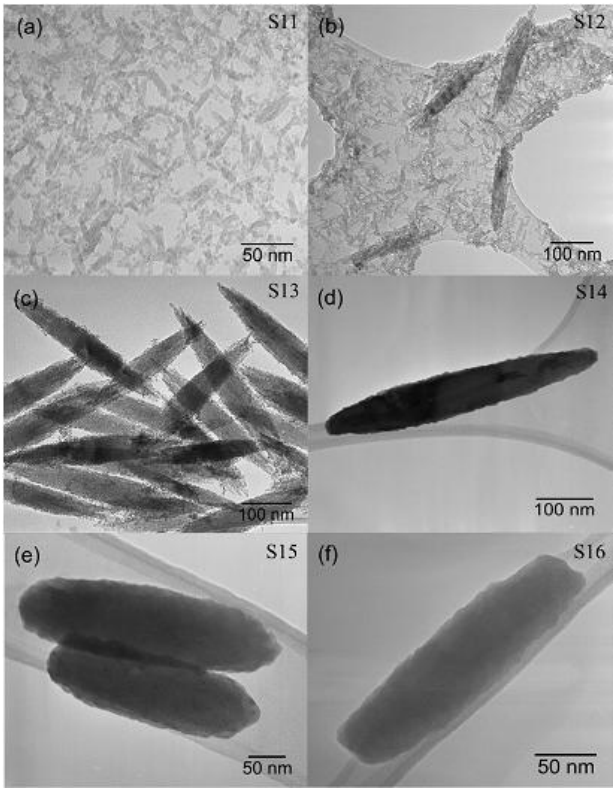

Figure 2.6: Bright field TEM images of the α-Fe_2O_3 nanorods at different temperature (a) 120 °C,(b) 140°C, (c) 180°C, (d) 200°C (e) 220°C and (f) 240°C (Almeida et al., 2009).

Meanwhile, Wu et al. (2010) presented a facile approach on the production of magnetic iron oxide short nanotubes employing an anion-assisted hydrothermal route by using both phosphate and sulphate additive. From the mechanism of formation of nanotubes, it was revealed that the ferric ions concentrations, the amount of salt additive, and the reaction time make significant contributions to short nanotubes growth. Figure 2.7 (a-d) shows the morphological change in hematite short nanotubes with increase in reaction time. In 1.5 h, capsule like nanoparticles with a thickness of 51.5nm was observed. When the reaction proceeds to 3h, capsule like nanoparticle begins to appear hollow like structure with a thickness of 28.4nm. However, further increase in reaction time to 6 h and 12h, the tube like morphology remains unchanged but the thickness decreases to 16 nm. Effect of phosphate and sulphate ions also play an important role in formation of short nanotubes. By adjusting the ratios of the above three precursors, serials of solid or hollow nanostructures with a tunable size and morphology can be formed.

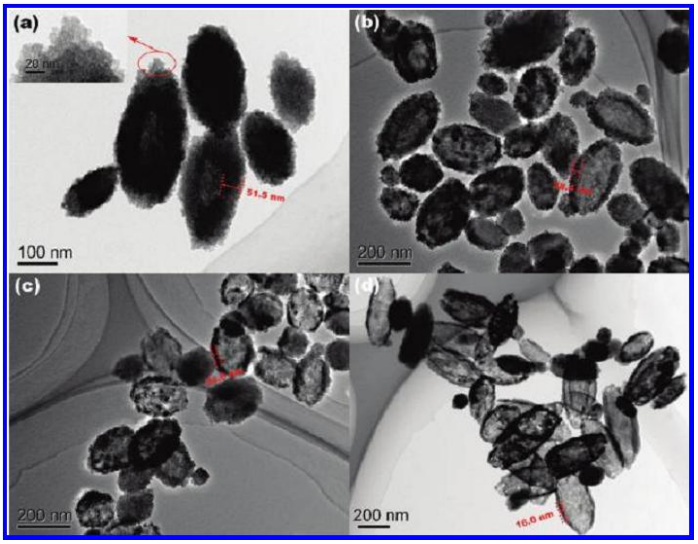

Figure 2.7: TEM images of the products obtained after (a) 1.5, (b) 3, (c) 6 and (d) 12 h. (Wu et al., 2010)

Pradhan et al. (2011) reported on hydrothermal synthesis of one-dimensional α-Fe_2O_3 nanorods, nanosphere and nanohexagon using $(NH_4)_2HPO_4$ as the structure directing agent. The authors have also reported the synthesis of pt-doped Fe_2O_3 nanorods using hydrothermal method. The Fe_2O_3 nanomaterials having different morphologies and pt-doped Fe_2O_3 nanorods were used as catalyst for solar light driven photo catalytic degradation of methylene blue, Congo red and phenol organic pollutants. Among all other morphological samples, nanorod-shaped α-Fe_2O_3 shows highest photocatalytic activity for degradation of phenol and other dyes. However, Pt-doped hematite further enhances the catalytic activity.

Fei et al. (2011) reported large scale synthesis of three dimensional hierarchical ferric hydroxide and oxide nanostructures at a low-temperature hydrothermal process assisted by two-way phase transition under sonication. The as-prepared α-FeOOH and α-Fe_2O_3 nanomaterials were used as adsorbents in waste-water treatment, and showed very good ability to remove organic pollutants. The maximum adsorption capacities of the α-FeOOH and α- Fe_2O_3 samples were found to be about 239 mg g^{-1} and 66 mg g^{-1} respectively.

Recently Wang et al. (2012) reported on template-free formation of uniform urchin like α-FeOOH hollow spheres. It was synthesized via a glycerol-assisted one-pot reaction. A ratio between glycerol and water was maintained and three different samples were studied. Figure 2.8 shows α-FeOOH, which consist of urchin like hollow spheres with a size of about 500 nm in diameter. It also exhibit excellent water treatment performance with high removal capacities towards organic dyes and heavy metal ions.

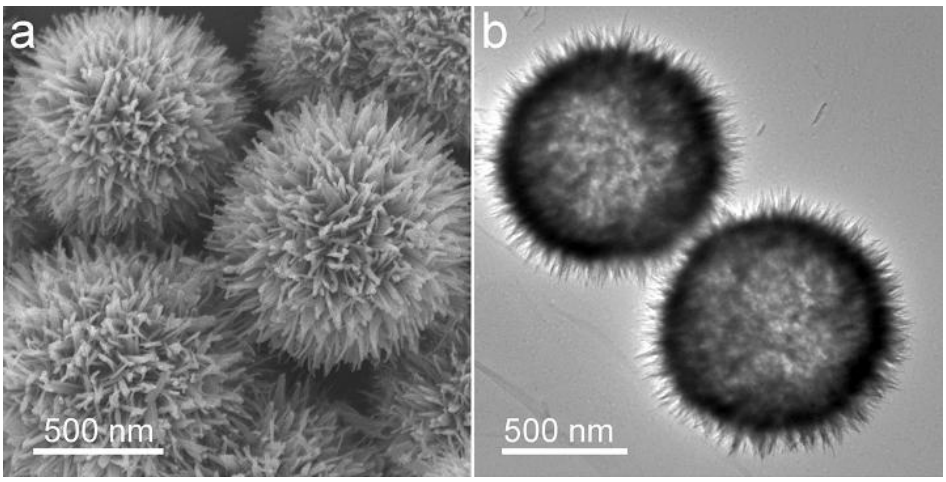

Figure 2.8: FeSEM and TEM images of α-FeOOH (Wang et al., 2012).

More recently, α-Fe_2O_3 nanofibers were synthesized via a simple hydrothermal route followed by calcinations (Ren et al., 2013). Very thin and porous α-Fe_2O_3 nanofibers have been synthesized, which were used for investigation of removal of Cr (VI) from wastewater. Maximum adsorption capacity was found to be 16 mg g^{-1}. Further recycling and ability of adsorbents shows no change in the adsorption capacity.

2.2.2 Alumina/Boehmite nanomaterial by hydrothermal method

Alumina nanostructures have a large number of applications viz. in adsorbents, catalysts and catalyst supports. However, the synthesis of these nanostructures is still a challenge owing to their extremely small size and their anisotropy. The control of nucleation and growth of nanostructured materials is therefore becoming crucial. Alumina nanomaterials

with different size and morphologies have been synthesized and reported earlier by hydrothermal method.

Tang et al. (2005) have synthesized Boehmite (AlOOH) nanoneedles, nanorods and nanotubes by a facile sol-hydrothermal method without using surfactant. Further, it was calcined at 700°C to obtain γ-Al_2O_3 nanoneedle, nanorods and nanotubes. It was also observed that the produced sol and the pH of solution play an important role on the nucleation and growth of nanostructured materials.

As per experimental data and theoretical analysis, the mechanism of $Al(OH)_3$ dehydration and α-Al_2O_3 formation under hydrothermal condition depends strongly on pressure. Al'myasheva et al. (2005) have studied on preparation of nanocrystalline alumina under hydrothermal condition, both theoretically and experimentally. Results indicate that reducing the pressure in hydrothermal system increases the percentage of α-Al_2O_3 particles less than 100 nm in size. It also depends on the structure of the parent aluminium hydroxide.

In the year 2006, Zhang et al. have reported a facile hydrothermal method used to synthesize orthorhombic γ-AlOOH bundles in presence of alkali salt $Na_2B_4O_7$. In this experiment, the morphology and size of the AlOOH was found to depend strongly on the alkali salts $Na_2B_4O_7$. At constant pH, when $Na_2B_4O_7$ is replaced by NaOH solution, irregular nanowires were observed. Figure 2.9 shows the images of nanowires with sodium borohydroxide and with NaOH solution in. One effect of the $Na_2B_4O_7$ salts is to increase the chemical potential of the solution, and higher chemical potential conditions would be advantageous for nanowire growth. Addition of $Na_2B_4O_7$ salt also decreases the inter nanowire repulsion by increasing the ionic strength, and offering the anion adsorption on the surface of nanowires. These γ-AlOOH bundles are further used for technical applications in the areas of catalysts, adsorbents, ceramics and optical nanodevice.

Li et al. (2006) presented the synthesis of AlOOH nanofibers by hydrothermal method. In aqueous solution of cetyltrimethyl ammonium bromide (CTAB) surfactant at 200°C the hydrothermal reaction was carried out. Aluminium chloride ($AlCl_4.6H_2O$) and ammonia solution, together with CTAB as surfactant were used as precursors during hydrothermal reaction. It was observed that at pH= 8 and Al^{3+}/ CTAB = 80, the obtained fibers are uniform in size and pure. The obtained nanofibers were polycrystalline in nature with average diameter of 10 nm and length of 150-250 nm. Furthermore, the AlOOH nanofibers might have potential applications in ceramic industry and other fields.

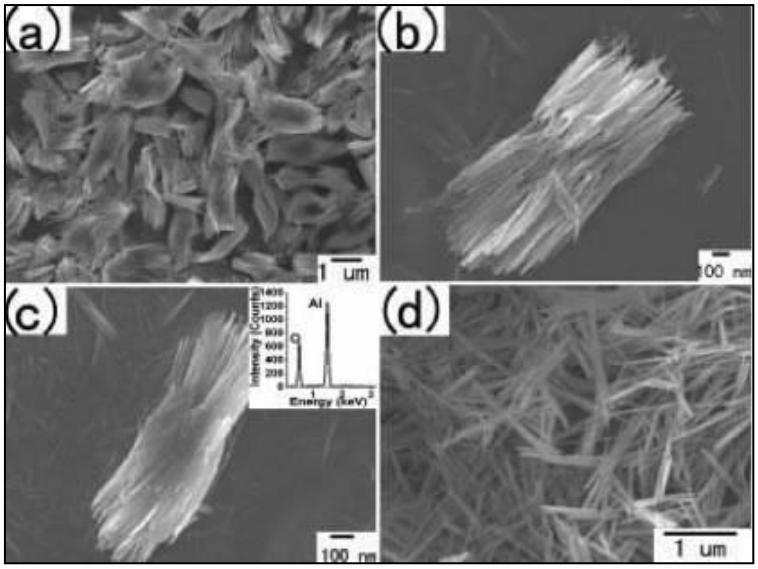

Figure 2.9 SEM images of γ-AlOOH bundles (a, b), EDS pattern (inset) of the products (c) and representative SEM image of irregular nanowires (d)(Zhang et al., 2006).

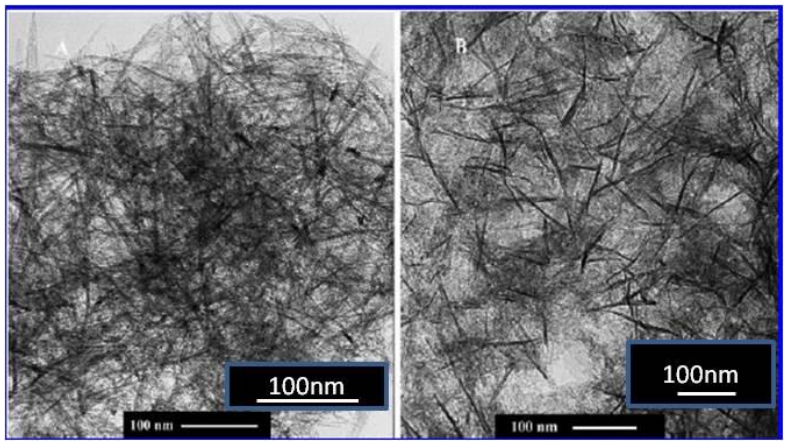

Figure 2.10 TEM images of boehmite nanowire, hydrothermally treated (a) at 120°C, 6 days and (b) at 100°C, 30 days (Zhao et al., 2007).

Similarly, boehmite nanofibers and nanotubes using hydrothermal synthesis route at low temperatures were studied by Zhao et al. (2007). This methodology depends upon the use of surfactants as directing agents. Non-ionic PEO surfactant, aluminium hydroxide gel which was synthesized from aluminium nitrate and water at 80°C, were mixed and kept in hydrothermal pot at 100°C for 6 days. The surfactants form longer micelles, enabling longer boehmite nanotubes. Figure 2.10 shows the morphology of boehmite nanowires prepared by hydrothermal treatment at 120°C for 6 days. From the figure it is clear that nanotubes and lath-like nanofibers with a length of 300 nm were formed. Whereas figure 2.10 (b) shows the image of the boehmite, which is treated at 100°C for 30 days. There was no remarkable change in the morphology but more uniform nanotubes were formed with the length ranging

from 90 to 170 nm. The external diameter of most of the nanotubes was around 4.5 nm. Higher Al/PEO ratio resulted in the formation of shorter nanotubes.

Feng et al. (2008) have reported on the synthesis of α-Al_2O_3 platelets using aluminium isopropoxide precursors by hydrothermal method. They have introduced aluminium fluoride additives to aluminium isopropoxide precursors and studies on the effect of AlF_3 additive on the phase transformation and morphologies of α-Al_2O_3 particles. Fig 2.11 shows the effect of AlF_3 concentration on morphology of α-Al_2O_3. It was observed that with increase in AlF_3 concentration, the morphology of α-Al_2O_3 was changed from irregular platelets to flat hexagonal shape. Furthermore, with increase in hydrothermal reaction temperature from 120-240°C, the morphology of α-Al_2O_3 changes from polyhedron to platelet and finally to vermicular shape.

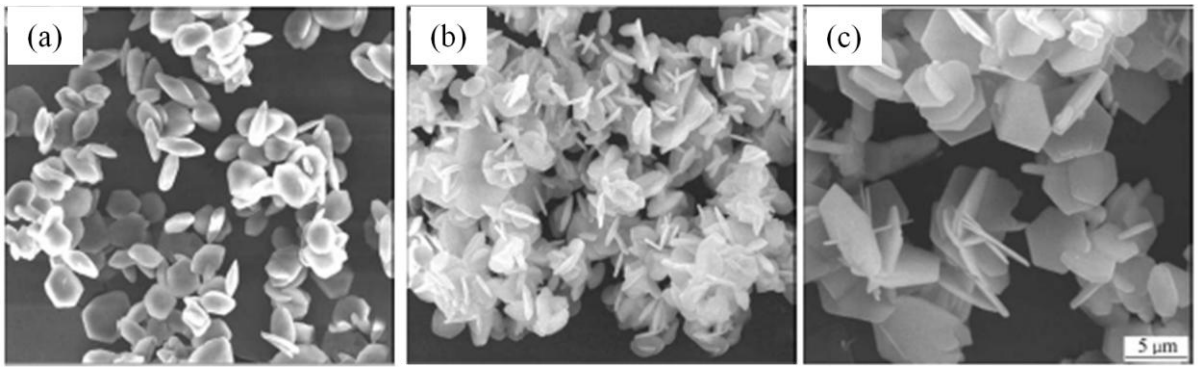

Figure 2.11: Effect of AlF_3 concentration on morphology of α-Al_2O_3: (a) 2%, (b) 10% and (c) 20% (Feng et al., 2008).

Liu et al. (2008) have synthesized microscale boehmite and gamma alumina nanoleaves by hydrothermal method. In this work, novel single-crystal leaf-like boehmite nanostructures (thickness under 100 nm) with high anisotropy and boehmite flowers with single-crystal petals were obtained for the first time. Solution of NaOH, $AlCl_3$ were mixed together, with a subsequent addition of CTAB solution in ethanol. Further, it was reacted in hydrothermal pot for 12 h at 160°C. Fig 2.12 shows the SEM and TEM images of boehmite nanostructures. 3D flower-like superstructures with an average diameter of 10μm (Fig 2.12C) were obtained, which were resulted of an in situ assembly of the nanoleaves during crystallization process.

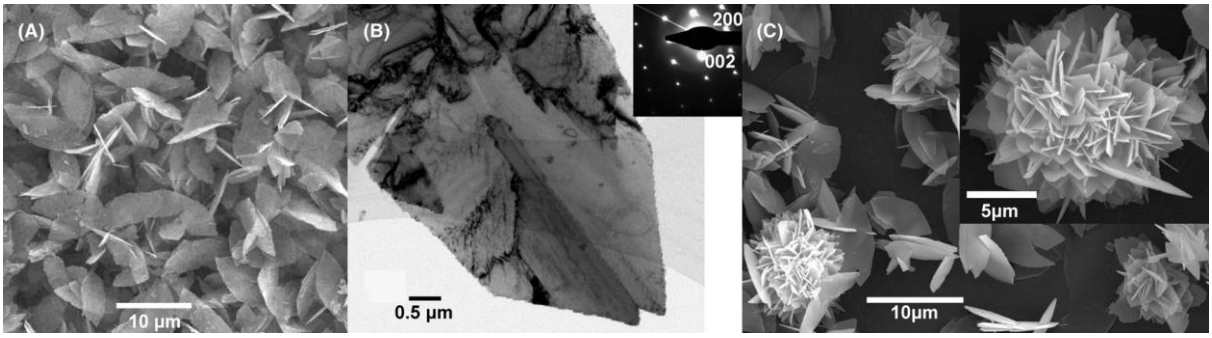

Figure 2.12: (a) SEM images of boehmite nanoleaves; (b) TEM image of boehmite nanoleaves with the inset SAED, and (c) SEM images of 3-D flower-like boehmite (Liu et al., 2008).

Synthesis of one-dimensional nanostructures with various morphologies such as nanotubes, nanowires, nanorods, nanofibers, lace-like nanoribbons and plate-like nanostructures have been reported recently. Arami et al. (2008) have synthesized boehmite nanostrips with average diameter of about 19.5 nm and crystalline size of 4.5 nm. It was prepared through a surfactant free hydrothermal route. Self-assembled bundles were formed from different numbers of nanostrips due to lateral hydrogen interactions. In this experiment, ethanolic solution of $AlCl_3.6H_2O$ was refluxed and the resultant colourless solution was put in hydrothermal pressure pot at 200°C for 24 h. Addition of ethanol inhibits the fast growth of the crystallites and subsequent addition of water culminates in occurrence of hydroxylation process on the surface and forms Al $(OH)_3$ colloidal crystallites. In hydrothermal condition, these one-dimensional $Al(OH)_3$ clusters transform to boehmite (AlOOH) nanostrips.

The, one dimensional boehmite nanostructure is in a large demand. There are a large number of synthesis procedures to produce these boehmite nanostructures. Sometimes surfactant–assisted hydrothermal route becomes expensive or the product becomes impure. Thus, He et al. (2008) have developed a facile hydrothermal method to synthesize boehmite nanorods in acidified media, using sulfate as the morphology–directing agent. Figure 2.13 shows the typical TEM images of the boehmite prepared by hydrothermal route at different initial H_2SO_4 concentrations. In the absence of H_2SO_4, platelike boehmite with a length of 50-200 nm and a width of 40-70 nm were formed. Nanorods were formed in the presence of H_2SO_4, and an increase of the initial H_2SO_4 concentration from 0.0054 to 0.054 mol L^{-1} led to an increase of the length from about 150 to 2000 nm and a decrease of the diameter from around 13 to 6 nm. A mixture of cube- and the rod-shaped particles was formed in the initial H_2SO_4 range of 0.054-0.086 mol $\cdot L^{-1}$. The morphology of the nanorods remained unchanged once the cube-shaped particles occurred. Boehmite nanoflakes with a width of about 50 nm were formed under alkaline conditions (initial pH 10.5), irrespective of the existence of

sulfate. Sulfate adsorbed on boehmite surfaces via the H-bond interaction under acidic conditions.

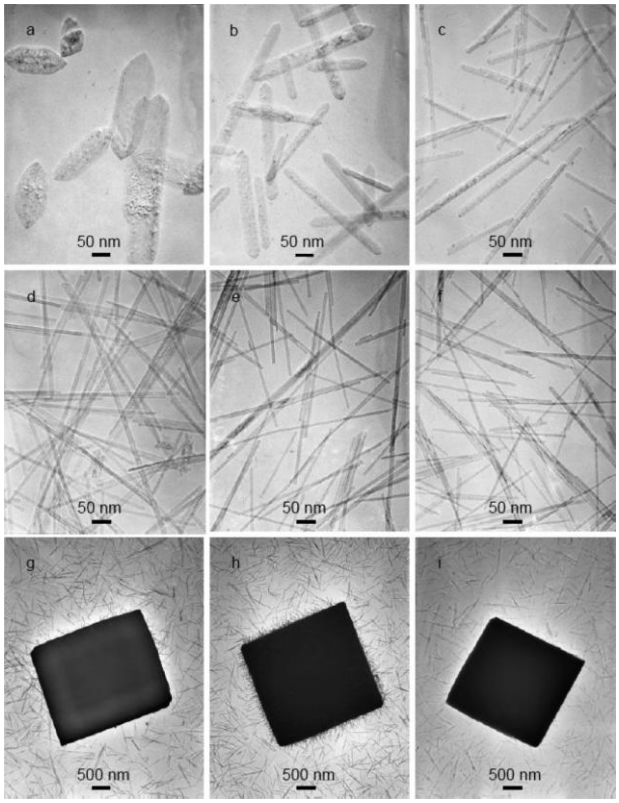

Figure 2.13: TEM images of boehmite nanomaterials in the presence of 0 (a), 0.0054 (b), 0.011 (c), 0.021 (d), 0.032 (e), 0.043 (f), 0.054 (g), 0.064 (h), and 0.086 (i) mol · L^{-1} H_2SO_4 240 °C for16.0 h (He et al., 2008).

Lu et al. (2009) have studied on synthesis of γ-AlOOH and γ-Al_2O_3 nanotubes using hydrothermal method. An anionic surfactant-assisted hydrothermal process yields γ-AlOOH nanotubes, which on further calcinations yields γ-Al_2O_3. Here camphorsulfonic acid (CSA) was used as an anionic surfactant and aluminium nitrate (Al $(NO_3)_3.9H_2O$) as an inorganic reagent. This mixture was mixed in aqueous medium and pH 5.4 was maintained and kept in an autoclave at 160°C for 24h. The obtained *γ* -AlOOH nanotubes were mesoporous materials with an average pore diameter of 24.3 nm. In order to investigate the morphology, TEM studies were performed and were shown in figure 2.14. The as-prepared boehmite exhibits a tubular like structure with sizes of ~500nm in length and 20-40nm in diameter. The tubular like morphology was also retained after calcination 2.14 (c, d) which indicates the formation of γ-Al_2O_3 nanotubes with high temperature heat treatment also the nanotubes does not collapse. The nanotube sample shows a higher catalytic activity than the nanoparticles for the reaction of dehydration of ethanol to ethylene. This kind of γ-Al_2O_3 nanotube may find potential application in catalysis and separation.

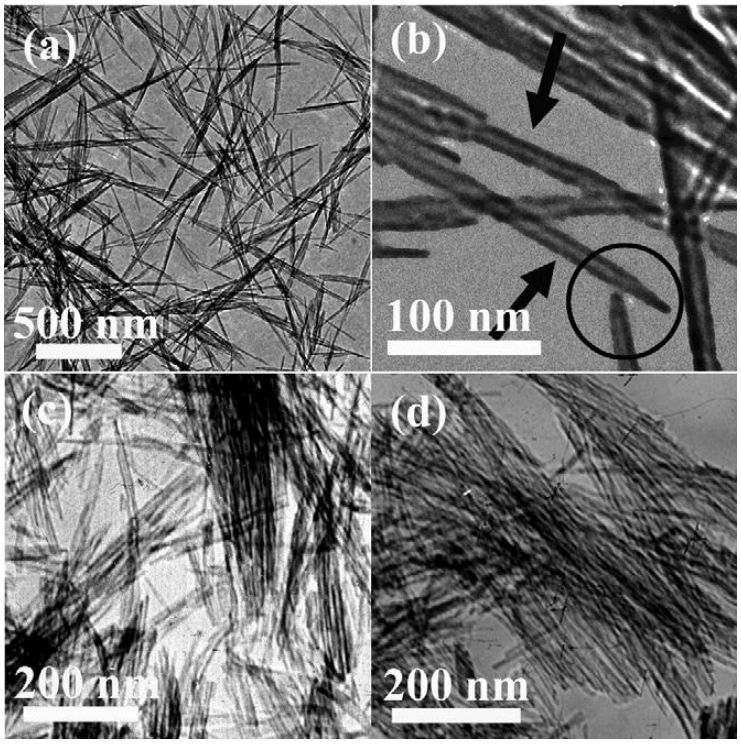

Figure 2.14: TEM images of ((a), (b)) as-prepared boehmite and ((c), (d)) calcined γ-Al_2O_3 (Lu et al., 2009).

Solid-based hydrothermal synthesis of alumina nanofibers with controllable aspect ratios were investigated by Shen et al. (2009). The morphology and aspect ratios of resulting AlOOH nanofibers were significantly influenced by the alkaline medium used in the preparation of solid precipitates obtained from $Al(NO_3)_3$ solution. Four samples were prepared using four different tetra-alkylated ammonium hydroxides such as tetramethylammonium hydroxide (TMAOH), tetraethylammonium hydroxides (TEAOH), tetrapropylammonium hydroxide (TPAOH), and tetrabutylammonium hydroxide (TBAOH). When TMAOH was used for precipitation, short rod-like nanofibers were obtained but in other three cases led to the formation of long wire-like nanofibers with larger aspect ratios. After thermal treatment, γ-Al_2O_3 nanofibers with different aspect ratios have been obtained. Compared with alumina micropowder, the nanofibers of alumina exhibited high thermal stability and crystal structure transformation at high temperature above 1000°C. This experimental process may have the potential in large-scale production of 1D nanostructured materials for high-temperature applications such as catalysis, gas-turbines, boilers and jet engines.

An interesting morphological evolution from boehmite nanoflakes, their assemblies, flower-like structures and hollow boehmite microspheres was reported by Cai et al. (2010) for the first time. It was prepared from Al $(NO_3)_3.9H_2O$ with addition of urea and different

amounts of $KAl(SO_4)_2.12H_2O$ under hydrothermal conditions. This unprecedented evolution of boehmite structures from nanoflakes to hollow microspheres was achieved by simply varying the concentration of sulfate ions in the aluminum nitrate/aluminum chloride-urea hydrothermal system. A number of sulfate such as $AlNH_4(SO_4)_2.12H_2O$, $Al_2(SO_4)_3.18H_2O$, Na_2SO_4, $(NH_4)_2SO_4$, and $MgSO_4.7H_2O$ were used in the aqueous phase of aluminum nitrate and urea. This study shows that sulfate mediated transformation strategy can be extended for other metal oxide systems which can be used for catalysis, adsorption and separation applications.

The boehmite (γ-AlOOH) nanowires and nanoflakes were successfully synthesized by regulating the pH of the reaction solution with a simple hydrothermal route by Deng et al. (2010). The starting material used here were anhydrous $AlCl_3$, NaOH and Ammonia solution. This solution mixture was maintained at different pH and kept in autoclave at 200°C for 12 h. The pH of the solution plays an important role in the formation of γ-AlOOH nanowires. The γ-Al_2O_3 nanowires with linear structure were obtained by using γ-AlOOH nanowires as the precursor. Figure 2.15 shows the TEM images of γ-AlOOH obtained by change in pH of the solution from pH- 4 to 10. As shown in figure, the samples exhibit distinct morphologies with change in pH from 4 to 10. At pH 4, the nanowires obtained were larger in size (figure 2.15a) but in a minimal amount. However, boehmite synthesized at pH 5 (figure 2.15b), a large quantity of nanowires with diameters of 10-30 nm and lengths of several hundreds of nanometer were obtained. At pH 6, the sample has needle-like morphology with diameters of 10-30 nm and lengths of 100-200 nm, and their surface exhibit zigzag patterns (figure 2.15c). Whereas with increase in pH to 7, figure 2.15d, the morphology of the sample changes dramatically to nanoflakes, with very few rod-like structures. At pH 10 total formations of nanoflakes takes place with the width of tens of nanometers. This indicates that the γ-AlOOH nanowires are significantly sensitive to the pH value. The size and morphology of γ-Al_2O_3 can be well preserved during the transformation from γ-AlOOH to γ-Al_2O_3.

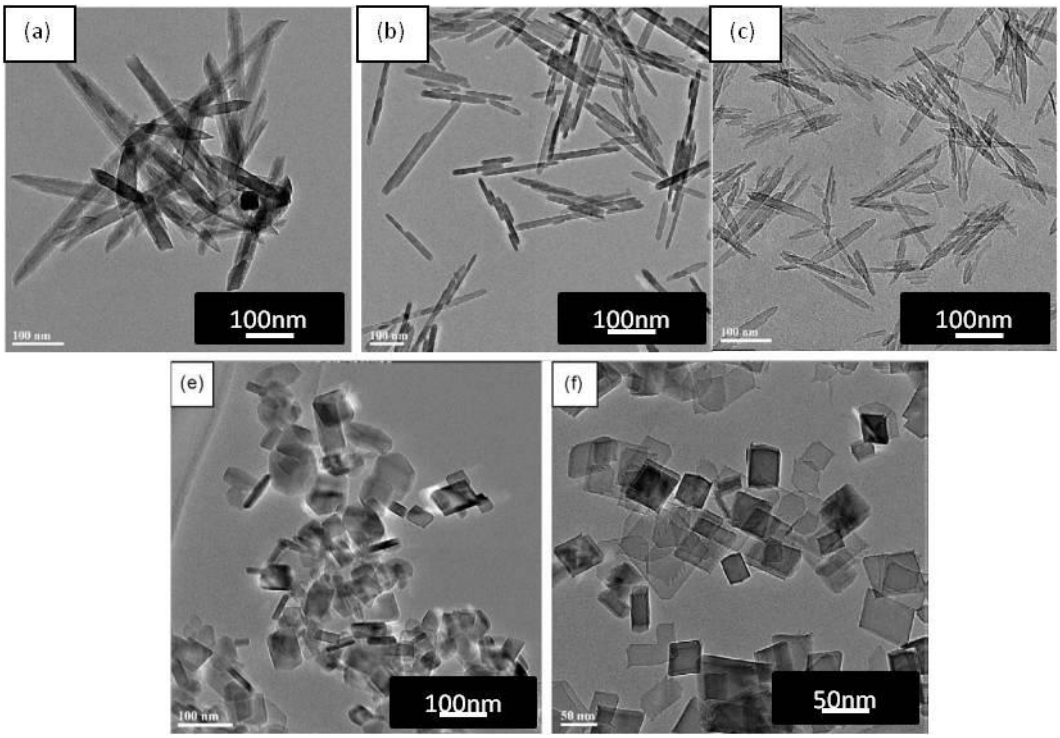

Figure 2.15: TEM images of γ-AlOOH at different pH value of reaction solution: (a) pH 4, (b) pH 5, (c) pH 6, (d) pH 7 and (e) pH 10 (Deng et al., 2010).

Liu et al. (2010) have studied on preparation of flower-like and rod-like boehmite via a hydrothermal route in presence of a buffer solution. In the present study poly-styrene-gradient-poly-2-hydroxyethyl methacrylate surfactant was used as structure-directing reagent for synthesizing boehmite in the acetic acid-sodium buffer solution. Under such synthetic conditions, rod-like structure was formed as shown in figure 2.16(a), when the reaction time was kept for 24h at 150°C. On the other hand, some flower-like assemblies were observed as shown in figure 2.16 b, when the reaction was carried out without using the buffer solution. In the above case, when the reaction time was extended to 48 h, the product totally transform to the nanorods. With the prolonged reaction time, acetate in the buffer solution began to corrode the surface of the boehmite, resulting porous structure. From the above study it was clear that the buffer solution plays an important role in controlling the morphology of the crystalline boehmite.

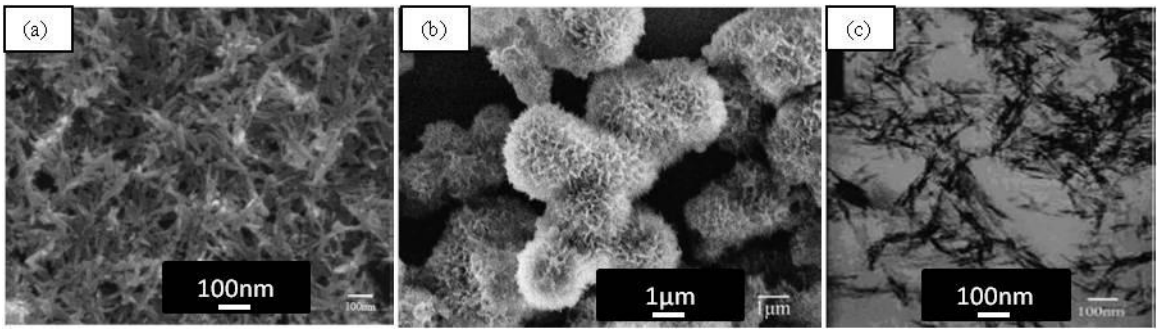

Figure 2.16: SEM image of boehmite nanorod synthesized by hydrothermal method for (a) 24 h, (b) obtained without buffer solution and (c) TEM image of boehmite (Liu et al., 2010).

Kim et al. (2010) investigated on morphology controllable synthesis of γ-Alumina nanostructures via an ionic liquid-assisted hydrothermal route. The precursor, aluminum acetate hydroxide was used to synthesize various morphologies of boehmite including nanoleave, nanofibers and microflowers. The ionic liquid 1-butyl-2, 3-dimethylimidazolium chloride ([bdmim][Cl]) is used as template in the reaction. The corresponding AlOOH and γ-Al_2O_3 nanostructures have been obtained by calcining precursors at 300°C and 600°C for 2 h, respectively. The morphology of nanostructures was well preserved during the thermal transformation process. These nanostructures can be used in some applications, such as adsorbents, catalysts, catalyst supports, and ceramics, etc. Detailed morphology studies of the samples obtained with variation of ionic liquid [bdmim][Cl] have been shown in figure 2.17. In the synthesis procedure, 2.1 mmol of $AlCl_3.6H_2O$ was mixed with 2.1, 5.3 and 10.6 mmol of ionic liquid [bdmim][Cl] in aqueous solution, which was named as S-1, S-2 and S-3 respectively. Figure 2.17 shows the high-magnification SEM images of S-1, which is nanoleaf- like structure. Similarly figure 2.17 b shows SEM images of high magnification, which is composed of highly dispersed nanofiber, with an average length and diameter of approximately 1.5µm and 90 nm, respectively. The flowerlike nanoarchitectures is visible in figure 2.17c for sample S-3. Whereas figure 2.17d represents the TEM image of γ-Al_2O_3 obtained by calcining at 600°C respectively, which have retained the same morphology as earlier, except that their sizes were considerably decrease due to the decomposition of acetic acid groups.

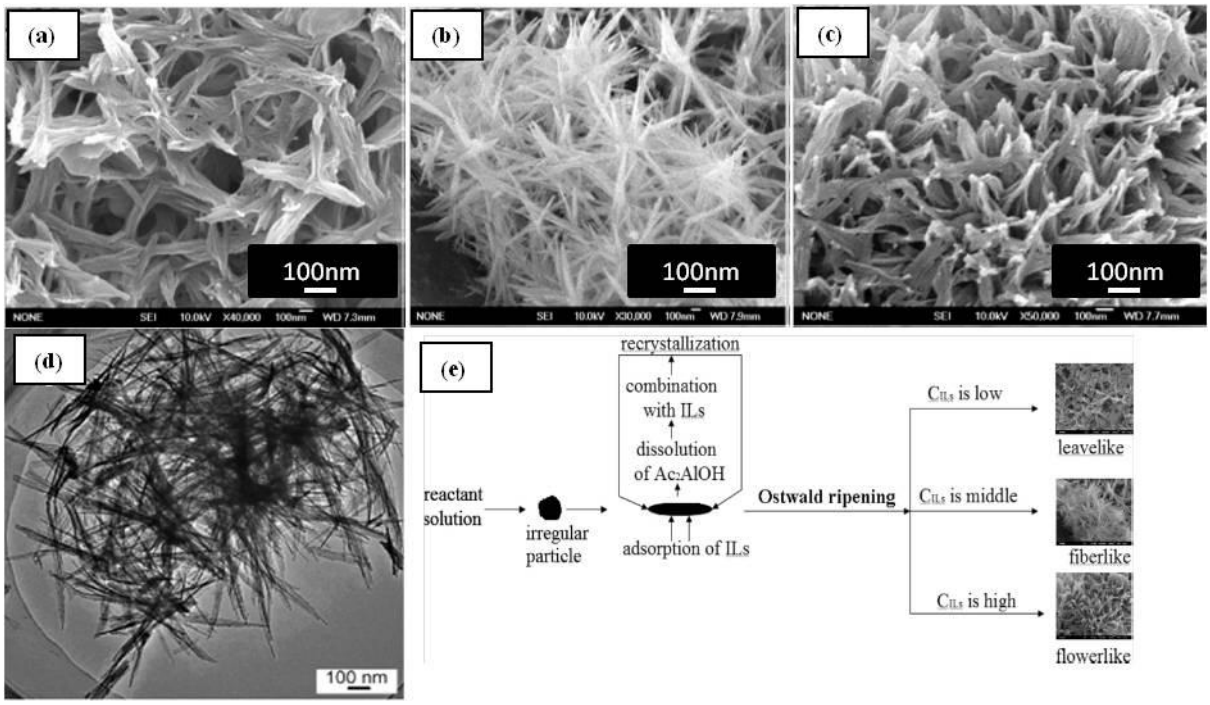

Figure 2.17: Typical SEM images of $(CH_3COO)_2Al(OH)$ obtained at 120°C for 12 h; (a) nanoleaf, (b) nanofibers (c) microflowers, (d) The TEM images of γ-Al_2O_3 at 600°C and (e) schematic illustration for the growth process of the precursor aluminum acetate hydroxide (Kim et al., 2010).

Yang et al. (2011) have investigated on synthesis of γ-Al_2O_3 nanowires through a boehmite precursor route. Crystalline γ-Al_2O_3 nanowires were synthesized by thermal decomposition of boehmite (γ-AlOOH) nanowires obtained via hydrothermal route at 200°C for 24h, using $AlCl_3$, NaOH and NH_3 as starting materials. The *γ* -AlOOH nanowires have a diameter of 20–40 nm and length above 600 nm. The pH value and the mixed precipitation play an important role in the formation of the γ-AlOOH nanowires. The size and morphology of γ-Al_2O_3 can be well preserved during the transformation from γ-AlOOH to γ-Al_2O_3.

Recently, synthesis of rod-like mesoporous γ-Al_2O_3 with enhanced affinity towards Congo red removal was observed by Cai et al. (2012). To synthesize γ-Al_2O_3, freshly precipitated amorphous alumina gel using aluminium sulfate, aluminium nitrate and aluminium chloride are used as aluminium sources and Pluronic P123 and F127 as structure-directing agents, respectively. For controlling the nucleation and growth of alumina nanorods, these structure directing agents were highly effective and also the anions (SO_4^{2-},Cl^- and NO_3^-) of aluminium sources have effect on their physico-chemical properties and adsorption performance. Among all, γ-Al_2O_3 prepared from alminium sulfate using P123 shows best adsorptive performance for Congo red, with adsorption capacity of nearly 99.2 mg g^{-1}.

2.2.3 Mixed metal oxide nancomposite by hydrothermal method

Mixed oxide systems have the ability to obtain structures in combination with the properties that individual oxide doesn't possess. The production of homogeneous nanosized binary ceramics or nanocomposite materials can improve certain properties because of quantum-confinement effects or greatly increased surface area. The main purpose of the preparation of the nanocomposite is to obtain the synergic effect of the imorganic compounds. Nanocomposites have a peculiar structure, i.e. a phase separated structure, with a nanoscale interface between the two matrixes.

Makovec et al. (2008) have started a new strategy for the synthesis of particles of cubic magnetite spinel with an anisotropic plate-like shape and of spinel-hexaferrite intergrowth nanocomposite particle. It was based on hydrothermal decomposition of presynthesized Ba-hexaferrite ($BaFe_{12}O_{19}$) particles in the presence of $NaHCO_3$ and a hydrazine reducing agent. The nanocomposite particles synthesized by the incomplete decomposition of hexaferrite contained a structural intergrowth of spinel and hexaferrite.

Microscopic studies of a SnO_2-α-Fe_2O_3 nanocomposite were investigated by Hayashi et al. (2008). The SnO_2-α-Fe_2O_3 nanocomposite hierarchical architectures were synthesized by hydrothermal method. The α-Fe_2O_3 nanotubes grown along the c-axis were first synthesized by a coordination-assisted dissolution process, and were then dispersed in a $Sn(OH)_6^{2-}$containing solution and converted to the SnO_2/α-Fe_2O_3 hierarchical architectures. The SnO_2-α-Fe_2O_3 nanocomposite was made by α-Fe_2O_3 nanotubes with SnO_2 nanorods grafted centripetally around them.

Jayalakshmi et al. (2009) have worked on hydrothermal synthesis of CuO-SnO_2 and CuO-SnO_2-Fe_2O_3 mixed oxide and their electrochemical characterization in neutral electrolyte. In the synthesis procedure Urea is used as the hydrolytic agent and their electrochemical behavior was studied by cyclic voltammeter. The morphology of CuO-SnO_2 mixed oxide reflects larger platelets of SnO_2 dispersed with much smaller CuO particles. Particle sizes range from 47 to 500nm. The morphology of CuO-SnO_2-Fe_2O_3 differed entirely from the binary oxide. The particles were almost spherical in shape and their sizes were in the range of 30 to 76 nm.

Fabrication of CuO-Fe_2O_3 hollow hybrid microspheres were studied by Liu et al. (2009). In the hydrothermal synthesis procedure $FeSO_4.7H_2O$ and $CuSO_4.5H_2O$ were used as iron and copper precursors and urea was used as homogeneous precipitant. Hollow CuO/Fe_2O_3 microsphere shell formed was composed of uniform metal oxide nanorods with

about 20-40 nm in diameter and 100-200 nm in length as shown in figure 2.18. These metal oxide hollow spheres can be used in applications such as chemical sensors or in catalysis.

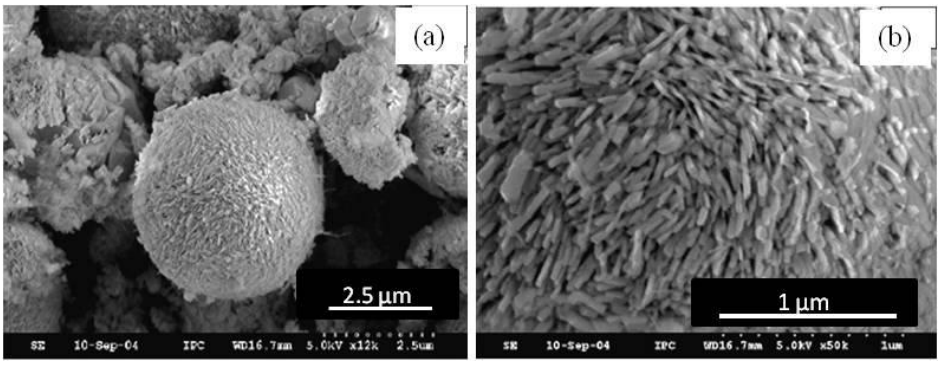

Figure 2.18: SEM images of CuO-Fe_2O_3 (a) hollow microspheres and (b) mixed oxides nanorods (Liu et al., 2009).

Epitaxial growth of branched α-Fe_2O_3-SnO_2 nano-heterostructures was studied by Zhou et al. (2011). A novel six-fold-symmetry branched α-Fe_2O_3 /SnO_2 nano-heterostructure was prepared by hydrothermal growth of α-Fe_2O_3 precursor branches on pre-obtained SnO_2 nanowire stems. The synergetic effects exerted by SnO_2 and α-Fe_2O_3 as well as the unique branched structure are probably responsible for the enhanced performance. These α-Fe_2O_3-SnO_2 composite materials were used as lithium-ion batteries.

Recently, Tomar et al. (2013) have synthesized TiO_2-ZrO_2 nanocomposite by hydrothermal method. A series of titania-zirconia mixed oxide with various TiO_2-ZrO_2 content of 10 to 90 mol % was prepared at 240°C for 24h in hydrothermal pot. From the XRD pattern it was observed that, in case of TiO_2, both anatase and rutile phase was formed and in case of ZrO_2, both monoclinic and tetragonal structures were formed. The SEM images confirmed the formation of highly porous material. The average crystallite size was found to be 9 to 26 nm.

2.3 Electrospinning method

Electrospinning represents a simple and convenient method for generating continuous polymer fibers with diameter ranging from tens of nanometer to several micrometers. The origin of electrospinning as a viable fiber spinning technique can be traced back 100 years ago. It was first conceived by Lord Rayleigh in the late 19th century. Electrospinning is nothing but an electrostatic fiber fabrication technique. Electrospinning method has the capability and feasibility in the generation of large quantities of nanofibers. Nanofibers often serve as the basic platform where other components are built on. Nanofiber exhibits certain distinct advantages since it has been used as the basic building block in living things (Teo et

al., 2009). Moreover, spun nanofibers offer several advantages such as, an extremely high surface-to-volume ratio, tunable porosity, malleability to conform to a wide variety of sizes and shapes and the ability to control the nanofiber size & morphology to achieve the desired properties.

The standard electrospinning set up consists of three major components: a high-voltage power supply, a syringe pump attached with syringe having metallic needle and an electrically conductive collector. The needle of the syringe typically serves as an electrode containing electrically charge the solution and the counter-electrode is connected to the conductive collector. A polymer, sol-gel or a composite solution is loaded into the syringe and this viscous liquid is pushed towards the needle tip by using a syringe pump, forming a droplet at the tip. Under the influence of strong electrostatic field, charges are induced in the solution and the charged polymer is accelerated towards the grounded metal collector. Because of the induced charges on the liquid, the liquid surfaces repel each other and create shear stress. These repulsive forces act in a direction opposite to the surface tension, which results in the extension of the pendant drop into a structure called as Taylor cone of conical shape and serves as an initiating surface (Baji et al., 2010). After formation of tailor cone, at the top of metallic needle the electrostatic forces will cause the ejection of a charged and thin jet. The jet undergoes a whipping process, which leads to formation of ultra-thin fiber mats as a result of solvent evaporation. In electrospinning process, the solution plays a significant part for the resultant fiber morphology. The electrical property of the solution, surface tension and viscosity will determine the amount of stretching of the solution (McCann et al., 2005). Instability occurs if the applied external electrostatic field is not above the critical value, which would cause the jet to break up into droplets. Such phenomenon is called Rayleigh instability. Therefore, the formation of nanofibers is a function of operating parameters such as, applied voltage, solution feeding rate and solution properties, mainly conductivity, viscosity and surface tension (Thavasi et al., 2008). Apart from solution and processing parameters, there are also ambient parameters that include humidity and temperature, which affect the electrospinning process. It is found out that there is an inverse relationship between viscosity and temperature (Bhardwaj et al., 2010).

Fabrication of one-dimensional ceramic nanofibers has gained increasing interest in the last decade. For synthesis of ceramic nanofibers, combination of two conventional techniques such as electrospinning and sol-gel process is widely used. Combination of both the techniques provides a way to fabricate ceramic nanofibers of different sizes, composition,

and morphologies such as tubular, ribbons and porous fibers in a single step (Chronakis, 2005). The procedure for synthesizing ceramic nanofiber consists of three major steps: (i) Preparation of an inorganic sol containing a matrix polymer together with an alkoxide, salt, or polymer precursor by sol-gel method (ii) Electrospinning of the solution to generate composite nanofibers consisting of the matrix polymer and precursor. (iii) Calcination, sintering, or chemical conversion of the precursor into the desired ceramic at an elevated temperature, with removal of all polymers from the precursor fibers (Li et al., 2006). Generally, ceramic nanofibers are made by electrospinning of inorganic precursors in the presence of polymer followed by calcinations at higher temperatures. In last few years, various groups reported the preparation of different iron oxide; alumina and mixed metal oxides were prepared by electrospinning method.

2.3.1 Iron oxide nanofiber by electrospinning method

In recent years, electrospinning method has been explored as an advantageous method to synthesize metal oxides and ceramics nanofibers with diameters around tens of nanometer.

Zhu et al. (2006) have studied on preparation of superhydrophilic α-Fe_2O_3 nanofiber with tunable magnetic properties. In the present study, the α-Fe_2O_3 nanofibers were prepared using ferrous acetate ($FeAc_2$) mixed with polyvinly alcohol (PVA) as precursors. A 10 wt % PVA aqueous solution was prepared and mixed with $FeAc_2$ at 50°C in water bath for 8 h. Then the solution was aged for 12 h at room temperature. A light brown colour sol was obtained was used for electrospinning procedure. The as-spun nanofibers obtained were calcined for 4 h in air at different temperatures to form α-Fe_2O_3 nanofibers. A series of α-Fe_2O_3 nanofiber with different $FeAc_2$ contents ranging from 20 to 50 wt. % have been fabricated. Figure 2.19 shows the SEM images of as-spun PVA/$FeAc_2$ composite nanofibers prepared with different contents of $FeAc_2$. It displays a fully interconnected pore structure, i.e. netlike microstructure, and the surface of the nanofibers was smooth and uniform, due to the amorphous nature of the PVA. The fiber diameter was in the range of 70 to 190 nm with increase in $FeAc_2$ content from 20 to 50 wt%. It was also observed that after calcinations at 800°C, the surface of the nanofibers is rough and the fibers are broken and its diameter was found to be near 130-180nm. The super hydrophilicity of α-Fe_2O_3 nanofibers film may be widely used as fast magnetic filter in the industrial applications.

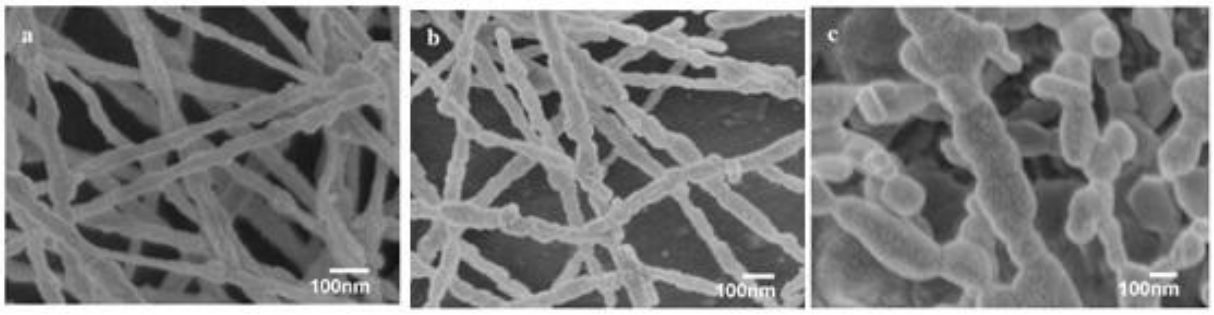

Figure 2.19: SEM images of as-calcined α-Fe_2O_3 nanofibers with 40 wt. % $FeAc_2$ at different calcination temperature for 4 h (a) 400; (c) 600; (d) 800°C (Zhu et al., 2006).

Zhan et al. (2007) have studied on the fabrication of long α-Fe_2O_3, and γ-Fe_2O_3 hollow fibers using both sol-gels combined two spinneret co-electrospinning method. In the present work, an inorganic ferric citrate sol was taken in outer spinneret and immiscible liquid machine oil was taken in inner tube and was electrospun at 25kV to form core shell structured fibers. Then the obtained core-shell fibers were soaked in cyclohexane to extract the machine oil and were dried at room temperature to form xerogel hollow fibers. The hollow xerogel fibers were calcined in air at 600°C to form α-Fe_2O_3 hollow fibres with diameter 0.5μm to 4 μm and uniform wall thickness of 200nm. Figure 2.20 represents the SEM micrographs of iron oxide hollow fibers. Furthermore, the authors have also reported the synthesis of hollow metallic Fe-nanofibers and γ-Fe_2O_3 hollow fibers by reducing and re-oxidizing the hollow hematite (α-Fe_2O_3) fibers under hydrogen flows at different temperature as shown in Figure 2.20 (c, d).

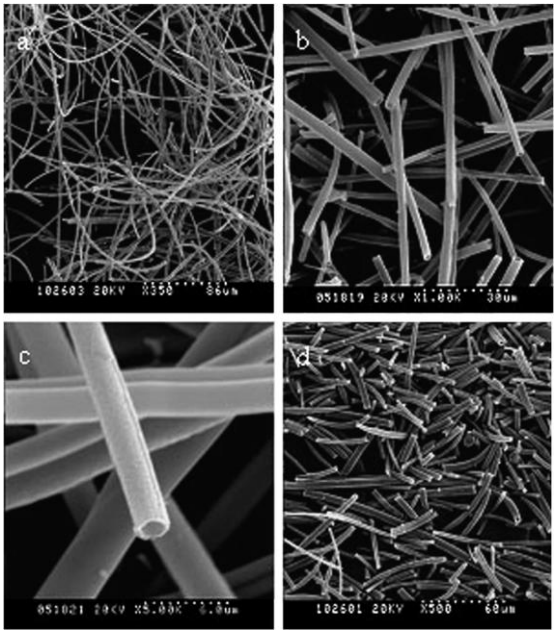

Figure 2.20: SEM images of the α-Fe hollow fibers (a, b), maghemite (γ-Fe_2O_3) hollow fibers (c), and short maghemite hollow fibers (d) (Zhan et al., 2007).

The synthesis of α-Fe_2O_3 nanofibers using electrospinning method was reported by Zheng et al. (2009). They have electrospun the PVA polymer aqueous solution containing ferric nitrate salt precursor at 15kV applied voltage. Upon sintering the as-spun composite fiber at 800°C, pure α-Fe_2O_3 nanofiber having average diameter of 150 nm were obtained. By using electrospun α-Fe_2O_3 nanofibres, the author's have studied the ethanol gas sensing properties. The electron microscopy of α-Fe_2O_3 nanofibers are shown in Figure 2.21.

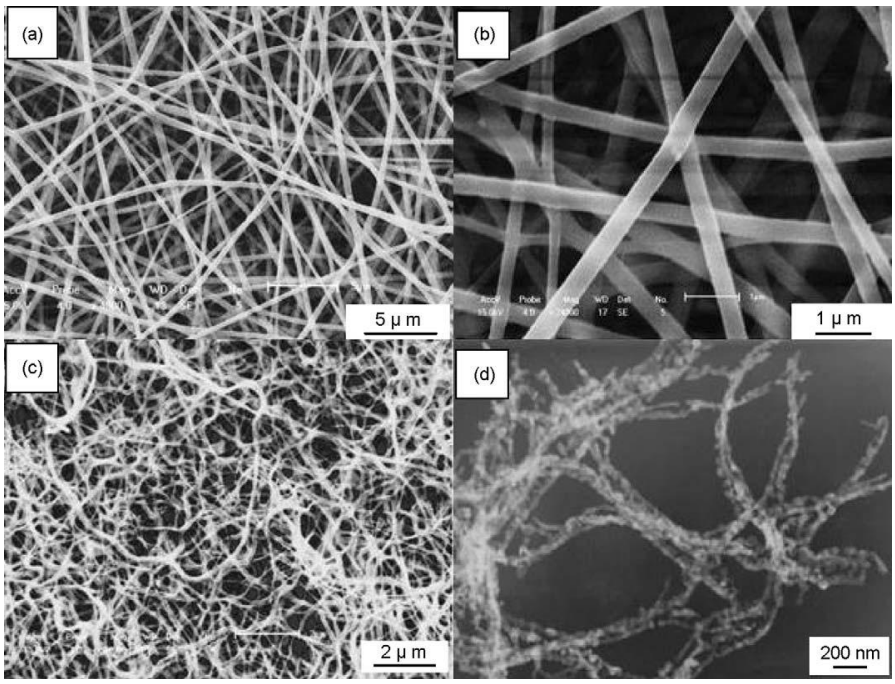

Figure 2.21: SEM images of electrospun nanofibers: (a) PVA/$Fe(NO_3)_3.9H_2O$ composite nanofibers, (b) magnified composite nanofibers, (c) calcined at 800°C and (d) TEM image of electrospun nanofibers calcined at 800°C (Zheng et al., 2009).

Similar way electrospun mediated synthesis of Fe_2O_3 nanofibers with diameter 180 nm were reported by Shao et al. (2011). They have also used PVA polymers and $Fe(NO_3)_3$ precursors for electrospinning and the obtained composite fibres were calcined in air at 550°C to from Fe_2O_3 nanofibers. The author reported here that it is also possible to fabricate metallic continuous nanofibers using electrospun metal oxide fibres. Furthermore, the obtained iron oxide nano fibres were calcined at 750°C in hydrogen atmosphere to form metallic Fe-nanofibres. The synthesized Fe-nanofibres were found to be in the diameter range 5-20 nm as shown in Figure 2.22.

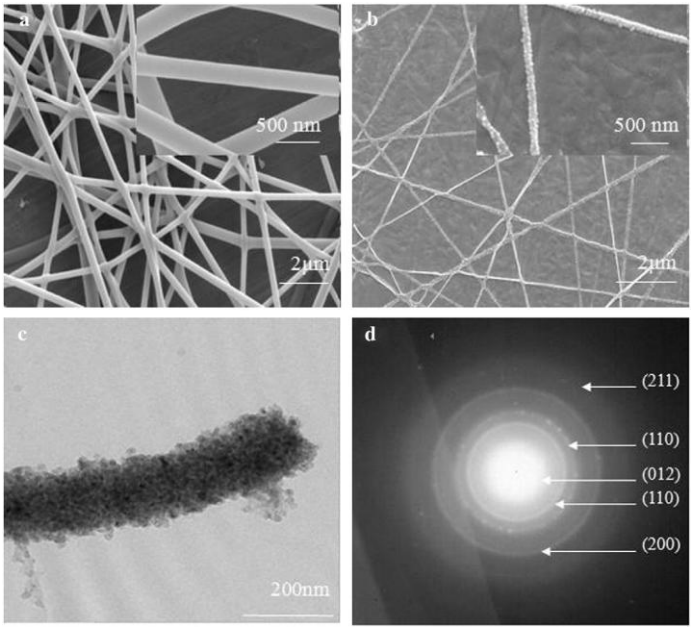

Figure 2.22: (a) SEM image of electrospun PVA/Fe $(NO_3)_3$ composite nanofibers; (b, c) SEM image of Fe nanofibers; and (d) SAED pattern of Fe nanofiber (Shao et al., 2011).

Eid et al. (2010) have reported on synthesis of iron-based one-dimensional nanostructures by electrospinning process and varying the pyrolysis atmospheres. 1D nanomaterials have strong shape anisotropy, which is not observed for bulk or particle counterparts. Fe based one-dimensional nanomaterials were obtained by electrospinning the PVP/ ethanol solution containing iron acetate in presence of acetic acid followed by heat treatment. The obtained as- spun composite fibers were heated at higher temperature in air to form Fe_2O_3 nanofibers, where Fe_2O_3 nanofibers were obtained after calcinations in presence of H_2/Ar atmosphere. Authors have also studied by varying the concentration of the polymer solution, which shows its direct effect on the diameter of the as-prepared nanotubes and nanowires. According to the authors, a single electrospinning method based on $FeAc_2$/PVP solution, two different kinds of Fe-based nanowires materials can be achieved.

Recently, Chaudhari et al. (2012) have studied on one-dimensional hollow α-Fe_2O_3 electrospun nanofibers as high performance anode material for lithium ion batteries. These hollow-structured α-Fe_2O_3 nanofibers were successfully synthesized by simple electrospinning technique using iron acetylacetonate ($Fe(acac_3)$)-polyvinylpyrrolidone PVP as the precursors. Further, composite fibers of ($Fe(acac_3)$)-PVP were calcined at 500°C to form pure α-Fe_2O_3 phase. Figure 2.23 shows the surface morphology of the as-spun Fe ($acac_3$)-PVP composite fibers. These fibers are randomly oriented, interconnected and have individual length ranging up to tens of micrometers. The α-Fe_2O_3 hollow structures of α-

Fe_2O_3 nanofiber can be considered as a potential high capacity anode for next generation lithium ion batteries.

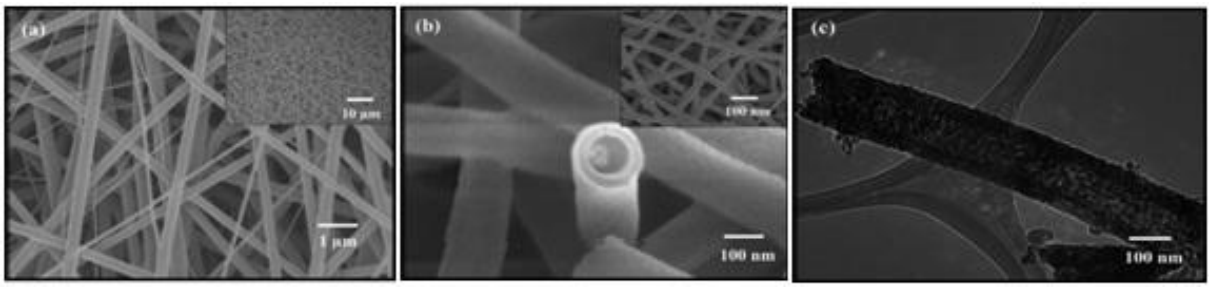

Figure 2.23: FESEM images of (a) $Fe(acac)_3$–PVP composite fibers, (b) α-Fe_2O_3 hollow fibers and (c) TEM of α-Fe_2O_3 hollow fibers (Chaudhari et al., 2012).

2.3.2 Alumina nanofiber by electrospinning method

Alumina is one of the most widely used ceramic materials, which finds applications as structural component for high temperature applications, heat engine, aerospace applications etc. it is also used for adsorption/chemisorptions of heavy metal ions, which depends on exposed surface area. Therefore, alumina and ceramics nanofibers with high surface area can be produced by electrospinning method. It has various applications including high-temperature insulation, catalyst support in high-temperature reactions, fire protection and as reinforcement for resins, metals and ceramic. Alumina fibers have various properties like high strength and elastic modulus, corrosion resistance, low thermal conductivity, chemical stableness, and good electrical insulation. Commercially available alumina nanofibers have limited properties. For that a large number of researchers have prepared by various methods, but electrospinning is one simple and versatile method in producing continuous ultrafine alumina and other fibers.

Dai et al. (2002) have studied on a novel method for preparing ultra-fine alumina-borate oxide fibers via an electrospinning technique. Alumina-borate/PVA composite fibers were prepared using both sol-gel and electrospinning method. PVA aqueous solution was prepared and aluminium acetate was mixed with it, and boric acid was added as stabilizer into the solution. The obtained sol was electrospun at a high voltage of 19kV. Further the electrospun fiber was calcined at 1000-1400°C for 2h to form alumina fibres. Figure 2.24 shows the SEM image of alumina-borate/PVA composite fibers and calcined fibers. Figure 2.24 (a) shows the as-spun fiber, which is smooth and amorphous in nature. After sintering at higher temperature (figure 2.24 (b-d)), the surface of fiber becomes rough due to development of grain boundaries. However the grains disappeared at 1400°C and surface

become smooth due to formation of a homogeneous α-Al_2O_3 crystalline phase. The average diameter of fibre was about 550 nm at 1400°C.

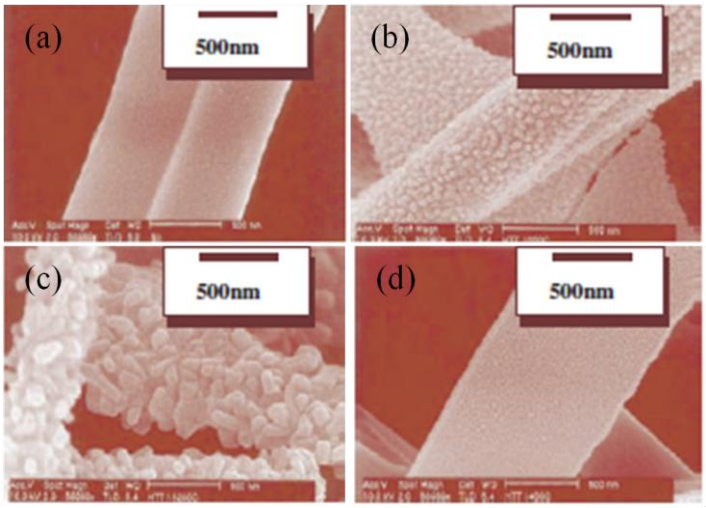

Figure 2.24: SEM images of alumina-borate/PVA composite fibers (a) as-spun composite fiber, and calcined at (b) 1000°C, (c) 1200°C and (d) 1400°C (Dai et al., 2002).

Transparent alumina noanofibers have been synthesized using aluminium 2, 4, pentadionate in acetone and PVP polymer via electrospinning by Azad A.M., in 2006. The as-spun composite fibers were calcined at 1000 to 1500°C to obtain pure, crystalline and transparent α-Al_2O_3 nanofibers. It was reported that the formation and crystallization of alumina nanofibres proceeds through a series of phase transformation starting from boehmite phase to α-Al_2O_3 phase followed by dehydration and polymer matrix decomposition process.

Panda and Ramakrishna, (2007) have again studied on synthesis of alumina nanofibers by electrospinning method using different aluminum precursors. They prepared alumina nanofiber by using different precursors such as PVA and PEO as polymer precursor, aluminum acetate and aluminum nitrate as alumina precursor. According to them, a solution containing upto 50% Al precursor can also be electrospun. A comparative study between PVA/aluminum nitrate, PVA/aluminum acetate and PEO/aluminum nitrate were reported. It was observed that smooth, continuous and uniform fibers were formed when aluminum acetate precursor was used. But upon using alumininum nitrate precursor's the fibers formed were not uniform and fused together due to hygroscopic nature of aluminium nitrate salt. Moreover, in this case large scale production is also not possible due to strong repulsion between similar charges. Upon sintering the composite fiber at 900 to 1300°C, alumina fibres with diameter range 20-500nm were formed.

Maneeratana et al. (2008) have worked on continuous hollow alumina gel fibers by direct electrospinning of an alkoxide-based precursor. In this study, continuous fibrous

bundles were produced with consistent tubular structures by electrospinning using aluminum tri sec butoxide, in presence of sec butyl alcohol and diethylene glycol monoethyl ether solvents. It was observed that the hydrolysis and condensation reaction plays an important role in the formation of hollow structure.

Kang and co workers, in 2011 have reported on the synthesis of alumina nanofibers by electrospinning method. In this work, high quality alumina nanofibers were prepared using sol-gel spinning solutions of $AlCl_3$-PVP as precursors. Further, it was sintered in muffle furnace at different temperature such as 450, 900 and 1100°C for 5 h in air to obtain amorphous Al_2O_3, γ-Al_2O_3 and α-Al_2O_3 respectively. The diameter of alumina nanofibers obtained were in the range of 100-800nm.

Recently, Yu et al. (2012) have synthesized continuous alumina nanofibers via electrospinning of method. The polymer-aluminium composite nanofibers were fabricated via electrospinning solution containing polyacrylonitrile (PAN), polymer in N,N-Dimethylformamide (DMF) solvent and aluminum 2,4-pentanedionate as aluminum precursors. The weight ratio between aluminum precursor and PAN polymer was maintained 1:1. Figure 2.25 (a) shows SEM images of the as-spun composite fibers, where diameter of the fibers was in the range of 500nm to 1µm. After calcination at 1200°C, as shown in figure 2.25 (b, c) a well-defined crystalline α-Alumina nanofibres were with a reduced size of 250 nm.

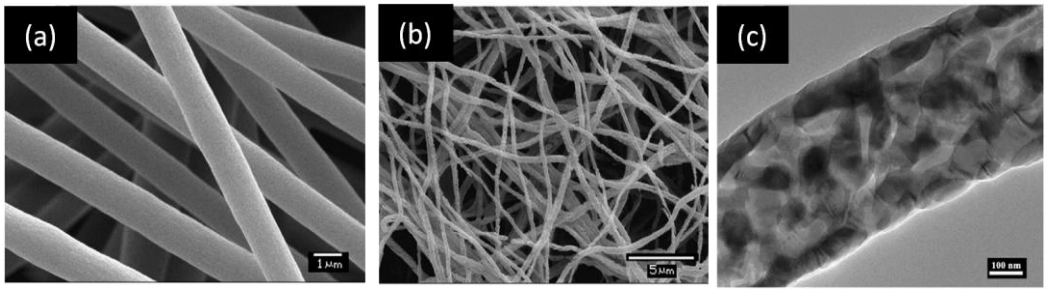

Figure 2.25: SEM images of alumina nanofibers (a) as-spun composite fibers, (b) after calcinations at 1200°C and (c) TEM images of after calcination (Yu et al., 2012).

More recently, Milanovic´ et al. (2013) have used electrospinning method to synthesize alumina nanofibers. The solutions used for electrospinning process were aqueous aluminium chloride hydroxide and poly vinyl alcohol solution. The as-spun composite fibers were heated at 1100°C, in air to form the crystalline alumina fibre. From XRD data, crystalline corundum structure of the fiber was confirmed. Figure 2.26 shows the FESEM micrograph. It is clear that the fibers are well formed without formation of any drops in the fiber morphology. The average diameter of the calcined fiber was found to be 470 nm.

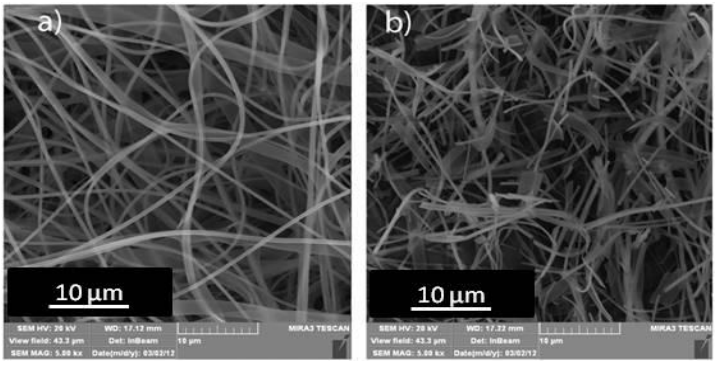

Figure 2.26: SEM image of ceramic fibers, (a) as-spun and (b) calcined at 1100°C (Milanovic´ et al., 2013).

2.3.3 Mixed oxide nanofiber by electrospinning method

Materials with nanometer size particles possess unique chemical and physical characteristics. To synthesize this mixed oxide nanocomposite, sol-gel method and electrospinning method are novel methods for making inorganic-inorganic, inorganic-organic composite nanomaterials. The small fiber diameters and porous structure of electrospun fibers will result in a high specific surface area that is beneficial in a variety of applications.

Yang et al. (2007) have fabricated Cr_2O_3/ Al_2O_3 composite nanofibers by combining both sol-gel and electrospinning method. By using sol-gel method chromium nitrate, aluminium nitrate and PVA in ethanolic solution was mixed in water bath at 60°C for 5h. A viscous solution of PVA/Cr $(NO_3)_3$/Al $(NO_3)_3$ composites for electrospinning was obtained. A voltage of 8 kV was applied to the solution for electrospinning. The as-spun fibers were calcined at 700°C to get oxide phase. From XRD study, it was observed that chromium oxide was crystalline in nature but aluminium oxide formed in the composite found to be in amorphous nature. From SEM analysis the calcined composite fibers obtained had smooth surface with diameters in the range of 50-150 nm. BET surface area of calcined sample were around 103 m^2/g, which indicates that the Cr_2O_3/ Al_2O_3 composite fibers might possess high catalytic activity due its high surface area.

Asokan et al. (2010) have reported on mixed oxide nanocomposite nanofiber of ZnO-SnO_2 synthesized by electrospinning method. One-dimensional nanostructure metal oxides such as TiO_2, ZnO_2 and SnO_2 have to be excellent property for ultrasensitive and highly chemical sensors. A better understanding of such coupled oxides is important in tailoring the properties of next-generation chemical sensors. A mixed solution of polyvinyl alcohol, zinc acetate and tin chloride dehydrate were used as precursor materials to synthesize the nominal stoichiometry of (1-x) ZnO-(x) SnO_2 nanofibers. SEM analysis shows that the as-spun nanofibers exhibited uniform, smooth fibrous morphology for the composition of $x \leq 0.45$,

however, above x > 0.45, there was a formation of nanoclusters. The diameter of nanocomposite depended on Sn content. The PL measurements showed that there was a change in the blue/violet luminescence confirming the presence of Sn in Zn-rich composition.

Fabrications of TiO_2/ZnO composite nanofibers, with diameter in the range of 85-200 nm were synthesized by electrospinning method (Liu et al., 2010). For synthesis zinc acetate and titanium tetra-isopropoxide were used as precursors and cellulose acetate as the fiber template. The composite solution was electrospun, followed by calcinations at 500 and 700°C for 5 h. The diameter of the TiO_2/ZnO composite nanofibers as shown in the TEM image (figure 2.27) is 175 nm. The TiO_2/ZnO composite nanofibers showed much higher photocatalytic efficiency than pure TiO_2 nanofiber in degrading Rhodamine B and phenol molecules in water.

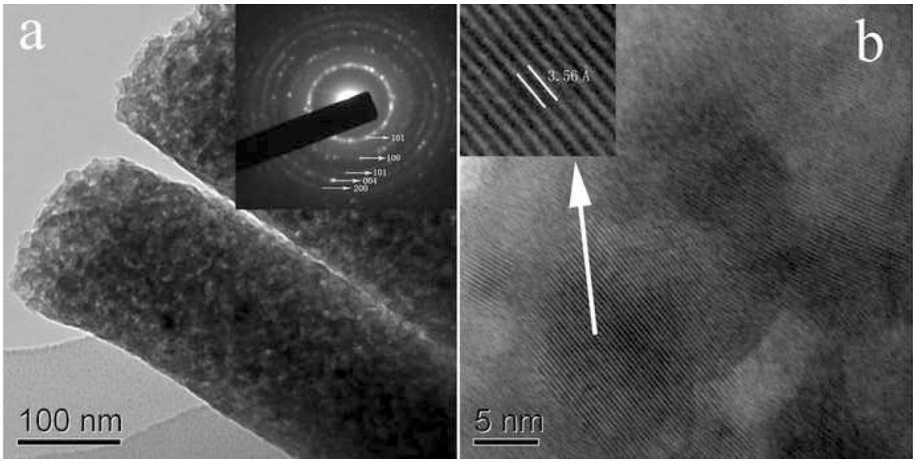

Figure 2.27 (a) TEM image of TiO_2/ZnO nanofibers, inset is SAED image of TiO_2/ZnO and (b) HR0TEM image of TiO_2/ZnO nanofibers (Liu et al., 2010).

Recently, Moon et al. (2012) have studied on electrospun poly (ethylene oxide)/ hydrated iron oxide (HIO)/ sodium alginate (SA) composite nanofibers with multifunctional properties. The hydrated iron oxide have honeycombed and duplex structure and high specific surface area, so it can be used by mankind as a bio-material with bacterial affinity, absorbing material and filler. In this work, the aqueous solution of PEO/HIO/SA was prepared and electrospun with an applied voltage of 9-14kV. As-spun fiber has an average diameter of 159-475 nm with smooth surface. The composite nanofibers, prepared by using 50% HIO shows 92.5% removal of V.vulnificus bacteria and with 10% SA shows good anti-bacterial property based on PEO polymer concentration. This PEO/HIO/SA composite nanofiber could also be used as a biomedical, absorptive and precipitative material for public benefit such as clinical, food and environmental applications.

Hassan et al. (2012) have studied on toxicity of Ce_2O_3-TiO_2 composite nanofibers against *S.aures* and *S. Typhimurium* synthesized by sol-gel mediated electrospinning method for disinfection of food pathogens. For synthesis cerium nitrate hexahydrate, titanium isopropoxide and poly(vinyl acetate) were used as the precursor. The diameter of the fiber was found to be 300 nm. The bactericidal effects of Ce_2O_3-TiO_2 composite nanofibers are found to be very promising. The antibacterial activity was attributed to the release of reactive oxygen species which caused cell membrane damage followed by damage to the interior molecules eventually causing the death of the bacteria.

Very recently, Lee et al. (2013) have synthesized ZnO-In_2O_3 composite nanofiber for selective and sensitive detection of trimethylamine (TMA). Three different compositions of ZnO-In_2O_3 composite nanofiber were prepared by electrospinning method and were compared with those of pure ZnO and In_2O_3 nanofibers as shown in figure 2.28. In the synthesis procedure, zinc acetate and indium nitrate was used as the precursors and PVP as the polymer for binding agent followed by heat treatment of 600°C for 2 h in air. Both the selectivity and response to TMA of three different compositions of ZnO–In_2O_3 nanofibers were significantly higher than those of pure ZnO and In_2O_3 nanofibers.

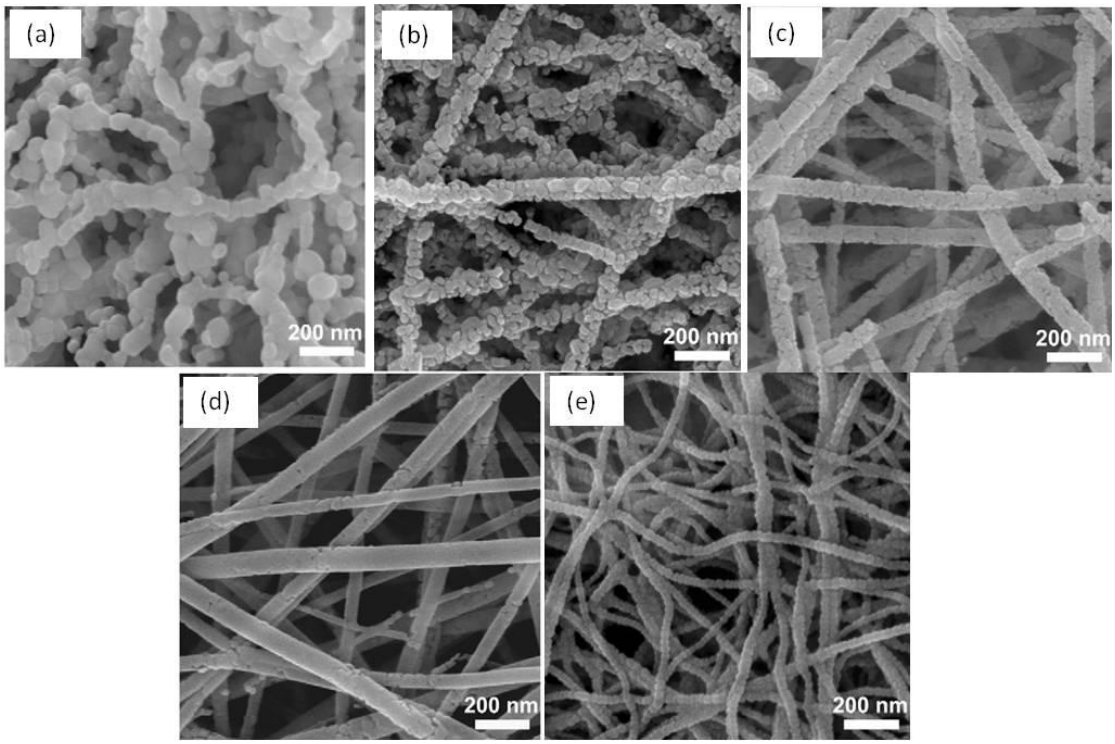

Figure 2.28 SEM images of (a) ZnO nanofiber, (b) 67Zn33In nanofibers, (c) 50Zn50In nanofiber, (d) 33Zn67In nanofibers and (e) In_2O_3 nanofibers after heat treatment at 600°C (Lee et al., 2013).

2.4 Characterization techniques

A large number of analytical techniques are there which are used for the characterization of nanomaterials and mixed oxide nanocomposites. In this section basic principle of these techniques, which have been used during the result analysis part of this thesis was discussed. They are absorption spectroscopy (UV-Vis), Infrared spectroscopy (FT-IR), X-ray Diffraction (XRD), Scanning electron microscopy (SEM), Transmission electron microscopy (TEM), Brunauer Emmet Teller (BET), Thermogravimetric analysis (TGA-DTA), and Atomic absorption Spectroscopy (AAS).

2.4.1 UV-Vis spectroscopy

Electronic absorption or UV-visible spectroscopy is one of the simplest and yet most useful optical techniques for studying optical and electronic properties of nanomaterials. Most of the organic molecules and functional groups are transparent in the portion of the electromagnetic spectrum which we call the ultraviolet and visible regions. That is the region, where wavelength ranges from 190 nm to 800nm. The basic principle of electronic absorption spectroscopy is based in the measurement of light absorption due to electronic transition in the sample. The energy adsorption due to absorption spectrum, atoms and molecules pass from a state of low energy i.e. ground state to a state of higher energy i.e. excited state. The electromagnetic radiation that is absorbed has energy exactly equal to the energy difference between the excited and ground state (Pavia et al., 2007). The operating principle is based on Beer's law, the absorbance or optical density as a function of wavelength, A, is related to the incident light intensity, I_0 and transmitted light intensity, I, concentration of a solution sample, c, path length of the sample, l, absorption coefficient, α, and molar absorptivity (formerly known as molar extinction coefficient), ε, by the following equation:

$$A = log\frac{I_0}{I} = \varepsilon lc = \alpha c \qquad (2.1)$$

Compounds which are colored have absorption in the visible region and are likely to contain a long chain conjugation system or a polycyclic aromatic chromophore. Few functional groups like nitro, azo, nitroso, polybromo, α-diketo etc containing compounds also exhibits color in visible region.

UV-Vis spectroscopy has been used by researchers. Few of them are Shu-hua et al. (2007) studied for sodium aluminate, α-Fe_2O_3 nanoparticle (Janardhanan et al., 2008), silver nanoparticles in composite nanofiber membrane (Saquing et al., 2009, Dong et al., 2010), Bovine serum albumin (Yang et al., 2009).

2.4.2 Fourier transforms infrared spectroscopy (FT-IR)

Infrared is a common vibrational spectroscopy technique useful for determination of compounds functional groups. Compounds having covalent bond, whether organic or inorganic absorbs various frequencies of electromagnetic radiation in the infrared region of the electromagnetic spectrum. In terms of wave numbers, the vibrational infrared extends from about 4000 to 400 cm^{-1}. In Infrared absorption process molecules are excited to a higher energy state when they absorb infrared radiation. Radiation in this energy range corresponds to the range encompassing the stretching and bending vibrational frequencies of the bonds in most covalent bonds. As for many harmonic oscillator, when a bond vibrates, its energy of vibration continuously and periodically changing from kinetic to potential energy and back again. The total amount of energy is proportional to the frequency of vibration, i.e.

$$E_{osc}\ \alpha\ h\nu_{ocs} \qquad (2.2)$$

The natural frequency of vibration of a bond is given by the equation,

$$\nu = \frac{1}{2\pi c}\sqrt{\frac{K}{\mu}} \qquad (2.3)$$

which is derived from Hooke's Law for vibrating springs. K represents the force constant of the spring and μ represents the reduced mass of the system. FTIR spectroscopy is a preliminary test to detect both organic and inorganic molecule in a compound. Many researchers have studied their compounds using FTIR spectroscopy. Many researchers have also reported IR analysis data viz. Alumina nanoparticles loaded with and without phenanthrene (Yang et al., 2005), iron oxide reinforced vinyl-ester resin nanocomposite; (Guo et al., 2008), iron oxide nanocrystals (Willis et al., 2005), Pt nanoparticle interaction with alumina (Dablemont et al., 2008), Poly (methyl methacrylate) interaction with aluminium oxide to form nanocomposite (Viratyaporn et al., 2010), Strong, broad band at around 610 cm^{-1} is for Al-O stretching vibration (Naskar et al., 2010), hybrid gold coating on iron oxide nanoparticle was monitored (Hoskins et al., 2012).

2.4.3 X-Ray diffraction

X-ray diffraction (XRD) is an important structural technique for characterization of nanocrystals. Apart from providing the structural phase of the nanocrystals, this technique also provides an estimate of the size of the nanocrystals (Cullity et al., 1956). X-ray

diffraction patterns of the nanocrystals are recorded with a X-ray diffractometer using Cu Kα radiation (λ = 1.5418 Å). X-Ray Diffraction follows the principle of bragg's law

$$n\lambda = 2d\sin\theta \qquad (2.4)$$

Where, d is perpendicular distance between lattice planes of miller indices, λ wavelength of the incident X-ray and θ is glancing angle. Bragg's law states that, when a chromatic intense beam of light falls on a parallel lattice plane of crystal, the incident beam reflected secularly from various planes of crystal. In this case, the phenomenon of reflection is known as crystal diffraction of scattering. Diffraction is essentially a scattering phenomenon in which large numbers of atoms co-operate. The finite size of the crystallites has a marked effect on the X-ray diffraction line widths. With reduction in the particle size, X-ray diffraction lines broaden significantly. This is due to the finite size of the nanocrystals. The particle size can be estimated from the width of the diffraction line corresponding to a particular (*hkl*) reflection using the Scherer's formula.

$$\tau = \frac{K\lambda}{\beta \cos\theta} \qquad (2.5)$$

where τ is the mean size of the ordered (crystalline) domains, which may be smaller or equal to the grain size,

K is a dimensionless shape factor, which is equal to unity,

λ is the X-ray wavelength,

β is the line broadening at half the maximum intensity and

θ is the Bragg angle.

XRD technique is used to study structural phase and also the crystallite size. With change in temperature from 600 to 1200°C, boehmite phase changes to predominant oxides i.e. γ-Al_2O_3, θ-Al_2O_3 and α-Al_2O_3, which clearly shows XRD spectra (Park et al., 2005). Similarly crystal structure analysis is studied by many researchers such as TiO_2 (Choi et al., 2006) having a crystallite size of 9 nm. Few more examples such as zero-valent iron nanoparticle were confirmed by XRD (Sun et al., 2006), α-Fe_2O_3 nanoparticle powder shows hexagonal structure with the crystal size ranged from 34.2 nm to 53.9 nm calculated from Scherrer equation (Zhao et al., 2007), Al_2O_3-Fe_2O_3 nanocomposite (Braga et al., 2010), alumina nanoparticles (Akbari et al., 2011), γ- Al_2O_3 and α-Al_2O_3 nanoparticles (Kulkarni et al., 2011, Firmansyah et al., 2012) and γ-Fe_2O_3 and Fe_3O_4 (Baykal et al., 2012). Recently, Pavani et al. (2013) has got a green approach to synthesis nano-sized iron oxide. The XRD results shows α-Fe_2O_3 which is comparable with JCPDS files 33-0664. The highest peak

shifts towards 35° which indicates formation of γ-Fe_2O_3 which is confirmed by JCPDS file 39-1346.

2.4.4 Scanning electron microscopy (SEM)

SEM is a type of electron microscope that creates various images by focusing a high energy beam of electrons onto the surface of a sample and detecting signals from the interaction of the incident electron with the sample's surface. SEM images have greater depth of field (curved surfaces are resolved properly) yielding a characteristic 3D appearance useful for understanding the surface structure of a sample. Magnification is of order 10,000X and resolution 10 nm. A stream of electrons is formed by electron surface and accelerated towards the specimen using positive electric potential. The stream is confined and focused using metal apertures and magnetic lenses into a thin focused monochromatic beam. The beam is focused onto the sample using a magnetic lens. Interactions occur inside the irradiated sample affecting the electron beam.

To study morphology of nanostructured materials the preliminary experiment is SEM. Examples include; one dimensional iron oxide/silica nanostructures (Zhang et al., 2008), aluminium hydroxide nanorods (Chang et al., 2009), hematite nanorod (Li et al., 2009), alumina nanotube (Wakihara et al., 2009), magnetic polyacrylonitrile-Fe@FeO nanocomposite fibers (Zhu et al., 2011, Horzum et al., 2012) and so on. Recently, Wang et al. (2012) have reported on multifunctional magnetic mesoporous silica nanocomposites. SEM images shows spherical in morphology, which are uniform in nature. Its mean diameter was around 200 nm with a rough surface. The surface roughness was attributed to the fact that the particles formed by packing many nanocrystals. On silica deposition on magnetite particle, the obtained mesoporous structure exhibit a more regular spherical shape with smooth surface on it. More recently, Milanovic´ et al. (2013) have studied on alumina nanofibers via electrospinning of aluminium chloride hydroxide with poly vinyl alcohol solution. The morphology of the fiber was examined using the FeSEM at 20 kV. The FESEM images shows that the fibers are well formed but after heat treatment the fiber size got shrink and its diameter decreases, which is found to be 1000 nm.

2.4.5 Transmission electron microscopy (TEM)

Transmission electron microscopy (TEM) is a high spatial resolution structural and chemical characterization tool. A modern TEM has capability to directly image atoms in crystalline specimens at resolution close to 0.1 nm, smaller than inter-atomic distance (Zhang et al.,

2005). TEM can be used to characterize nanomaterials to gain information about particle size, shape, crystallinity, and interparticle interaction. TEM carry out same working principle as of TEM the only difference is that TEM detects "transmitted electrons" and SEM detects "backscattered" and secondary electrons. TEM can also provide crystallographic information as well. The diffraction patterns can be detected which contains useful crystallographic information about the sample. TEM can also be used as an elemental analysis tool, capable of identifying the elements in areas less than 0.5μm in diameter.

This technique has been used to characterize the different type of nanostructure materials. Few examples are shown here such as, iron oxide tube-in tube nanostructure (Jia et al., 2007), α-Fe_2O_3 nanorod (Wang et al., 2008), Titanate nanofiber (Yang et al., 2008), ZnO nanoparticle (Prasad et al., 2009), Alumina nanotubes (Wakihara et al., 2009), carbon nanotube-reinforced electrospun polymer nanofiber containing zero-valent iron nanoparticles (Xiao et al., 2010), alumina nanoparticle (Dorigato et al., 2011), α-Al_2O_3 nanoparticles (Dringen et al., 2011), flower-like α-Fe_2O_3 nanostructure (Cao et al., 2012), 1D hollow α-Fe_2O_3 electrospun nanofiber (Chaudhari et al., 2012), Au/Fe_3O_4 nanocrystals (Goergen et al., 2013) and so on. More recently, both low resolution and high resolution TEM has been used to characterize α-Fe_2O_3 nanofiber, which is very thin with an average diameter of 40 nm. At the same time clear and regular lattice fringes are observed throughout the nanofiber, which indicates single crystal nature of the nanofiber and the lattice spacing is determined to be 0.27 nm, corresponding to the interspacing of the plane of hematite with a rhomohedral structure, which is in good agreement with the produced XRD analysis. We have used this technique to characterize the size and morphology of Al_2O_3, Fe_2O_3 and Al_2O_3-Fe_2O_3 nanocomposite prepared by sol-gel, hydrothermal and electrospinning technique.

2.4.5 Brunauer, Emmett Teller (BET)

The BET theory was developed by Stephen Brunauer, Paul Emmett and Edward Teller in 1938. It was an extension of Langmuir theory. BET theory is a rule for the physical adsorption of gas molecules on solid surfaces and for an important analysis technique for the measurement of the specific surface area of nanomaterial. Surface area is the means through which a solid interacts with its surroundings, especially liquids and gases. However, this surface area is created by reduction of particle size using T_g, melting or Ostwald ripening and porosity is generated within the particle. The concept of the theory is an extension of the

Langmuir theory, which is a theory for monolayer molecular adsorption, to multilayer adsorption with the following hypotheses:

(a) Gas molecules physically adsorb on a solid in layers infinitely;
(b) There is no interaction between each adsorption layer; and
(c) Langmuir theory can be applied to each layer.

Using BET method, determination of surface area, pore volume, pore size distribution and pore density measurements is carried out. For example BET surface area of zero-valent iron nanoparticle is around 14,500 m^2/kg, with a particle size around 53 nm (Sun et al., 2006), mesoporous Fe_2O_3 have a high surface area of 111 m^2/g (Yu et al., 2008), γ-Al_2O_3 nanofiber with a surface area of 160 m^2/g (Yang et al., 2010), calcined SnO_2 nanotube shows a high BET surface area of 1200 m^2/g (Ye et al., 2010), BET surface area of flower-like Fe_3O_4 microspheres is 70.28 m^2/g and Fe_3O_4 nanoparticle is 62.55 m^2/g (Li et al., 2011), mesoporous alumina (γ-Al_2O_3 nanorod) using aluminium sulfate by hydrothermal method has a BET surface area of 145 m^2/g (Cai et al., 2012), γ-alumina nanotube synthesised by hydrothermal method using CTAB has a surface area of 203.73 m^2/g, pore volume of 0.14 ml/g and average pore diameter of 2.78 nm (Dahlan et al, 2012), specific surface area of the sample were found to as 75 and 134 m^2/g for bare TiO_2 and Fe doped TiO_2 nanoparticle respectively (Pongwan et al., 2012) and so on. Recently Asuha et al. (2012) have synthesized γ-Fe_2O_3 nanopowder using CTAB surfactant and it is found that the maximum BET surface area was 149.8 m^2/g.

2.4.6 Thermogravimetric analysis (TGA-DTA)

Thermogravimetric analysis (TGA) is a technique in which the mass of the sample is measured against time or temperature while the temperature is changed under a certain atmosphere. This method is used for the determination of sample purity, water content, carbonate or organic content present in it and also for studying decomposition reactions. The graph of the resultant change in mass with respect to temperature is called a thermogravimetric curve (McMahon G., 2007). In fact the kinetics i.e. the rate at which the property changes with temperature can also be measured. The instrument or the detector for TGA is a balance, called a thermobalance or thermogravimetric analyser. The TGA apparatus detects small mass changes of a specimen, kept in thermobalance, which caused with change in temperature of the furnace. The flow of temperature in furnace is under a controlled temperature program. Any change in sample weight can be detected by

thermobalance. Sensitivities of the order of 0.1 μg or less are determined. It can be carried out in both inert or air atmosphere. Continuously, mass change with time and temperature is recorded. Some of the major factors affecting TGA measurements include sample size, heating rate, buoyancy, electrostatic effects, gas flow and sample holder. By analyzing the TGA curve, relative mass change with respect to the initial quantity (%) is obtained.

Differential thermal analysis (DTA) is a method for detecting the thermal behavior of a sample in terms of the temperature change. DTA helps in detecting physical properties, phase transitions, crystal polymorphism or thermal behavior such as heat evolution or absorption accompanying thermal degradation or chemical reaction. In case of DTA, difference in temperature i.e. ΔT between a sample and a reference material can be measured and both are heated at the same controlled temperature. Any physical or chemical change occurs in the sample, is because of change in phase or change in enthalpy that is nothing but the heat content of the material. Each and every change in temperature between the sample and reference is also recorded in the DTA analysis. However, the heat flow in sample and reference will be same rather than the temperature. DTA results helps to construct phase diagram and study phase transition and also finds the change in enthalpy. Both TGA-DTA can be measured at the same time, with different properties. It is very important that the time at any temperature should be sufficient in order to permit completeness of reaction.

These days, materials thermal behavior by combining both TGA-DTA is very common. Few examples are: Alumina synthesis by sol gel method represents both TGA and DTA graphs, which displays the same behavior. Few endothermic peaks are shown at 100, 130 and 150°C, which is for water loss. At the same large endothermic peak is visible at about 300°C, which might be due to destruction of Al-O-Al and Al-OH bond of the amorphous gel and also sublimation of ammonium chloride. An exothermic peak is also visible for small mass loss, due to combustion of remaining components. During 300-500°C, a metastable phase of γ-alumina is originating. A transformation around 1000°C indicates a phase transformation of γ-alumina into δ-alumina; it is seen in DTA curve with an exothermic peak around 850°C (Alves et al., 2005). Machala et al. (2007) have reviewed on amorphous iron (III) oxide, where they have studied on DTA curve of amorphous ferric oxide nanopowder. An exothermic peak observed at 292°C can be attributed to the process of crystallization of amorphous Fe_2O_3 to γ-Fe_2O_3, while an intensive peak at 396°C corresponds to the polymorphous isochemical transformation of γ-Fe_2O_3 to α-Fe_2O_3. Asmatulu et al. (2010) have studied on TGA analysis, for graphene containing PVC

nanocomposite fibers. Peaks around 200 and 400°C indicates coming off of dimethylacetamide and PVC from electrospun fibers. At around 500°C graphene component was removed from the fiber. Recently, Rizov B., (2012) have studied in details on phase transformation from goethite to hematite and thermal decomposition in various nickeliferous laterite ores.

2.4.7 Atomic absorption spectroscopy (AAS)

AAS is a technique for measuring quantities of chemical elements present in environmental samples by measuring the absorbed radiation by the chemical element. When energy is absorbed, electronic transitions take place and are seen as sharp lines as opposed to broad bands in molecular spectra. These line spectra are specific for the element being studied and contain information on its atomic structure. If energy is provided to an atom, there are three possible transitions: absorption, emission and fluorescence. Atomic absorption spectroscopy (AAS) is based on ground state free atoms absorbing visible or UV radiation at specific wavelength. However, in AAS selectivity is also very important, since each element has a different set of energy levels and gives rise to very narrow absorption lines. Thus, to get a linear calibration curve, the selection of the monochromator is vital to obtain. This linear calibration curve obeys Beers' law. In fact, the bandwidth of the absorbing species must be broader than that of the light source, which depends on monochromators. The monochromator is a very important part of an AAS because it is used to separate the thousands of lines generated by all of the elements in a sample (Garcia et al., 2012). The light from monochromator is directed to detectors, who convert the light signal into an electrical signal proportional to the light intensity. The prepared sample used to supply instrument in a form it depends on the atomization technique used. The function of atomizer is to produce as many free atoms a possible for the purpose of sensitivity. There are three considerations when choosing the atomizer: the type of the sample (solid, liquid or gas), the concentration of the sample and the size of the sample. There are three types of atomization techniques: (1) flame atomic absorption spectrometry, elements like copper, chromium, nickel, lead and many more can be detected here. (2) graphite furnace atomic absorption spectrometry and (3) hydride generation atomic absorption spectrometry used for arsenic and mercury.

Recently, adsorption by nanoparticles has been an innovative treatment for the purification of water from heavy metals with low cost and no residual metal sludge. Many works are going on by using Atomic absorption spectroscopy for metal ion removal. Few

examples are: Liu et al. (2009) have used magnetic chitosan nanocomposite for the removal of heavy metal ions like Pb^{+2}, Cu^{+2} and Cd^{+2} from water using AAS. Similarly, Huang et al. (2009) have studied on removal of heavy metal (Cu (II) and Cr (VI)) cations and anions using amino-functionalized magnetic nanoadsorbent. An investigation on the removal of Cr (III), Cd (II) and Pb (II) by using newly synthesised Al_2O_3/PES and ZrO_2/PES (polyethersulfone) membrane was studied by Maximous et al. (2010). Recently, Saberi A., (2012) has studied on preparation of zero-valent iron nanoparticles and Ni/Fe bimetallic nanoparticles and their application to remove Pb^{2+} in aqueous solution. Similarly, Predescu et al. (2012) have worked on nano-sized crystals of maghemite iron oxide (γ-Fe_2O_3) on resin surface, which showed remarkable adsorption efficiency in removal of some toxic metal ions as Zn, Cu and Cr. Wang et al. (2012) have used Fe_3O_4 nanoparticles for removal of heavy-metal ions i.e. Pb^{+2} and Cr^{6+} from waste water. Very recently, Nadeem U., (2013) have studied on magnetic ferrofluid loaded with maghemite nanoparticles, used for adsorptive removal of zinc ions in presence of applied magnetic field. Results show that maximum sorption efficiency of 97% was attained at pH 3 at time 60 min.

2.5 Concluding remarks

In this chapter we reviewed on the preparation and applications of different 1D nanomaterials. Although a large numbers of work have been reported on different 1D metal oxides, less work has been reported on one dimensional alumina and iron oxide system. However, a very less literature is available on mixed iron oxide- alumina composite nanomaterials. Our work is based on three convenient techniques of preparation i.e. sol-gel, hydrothermal and electrospinning method. As we have basically focused on one-dimensional nanomaterials, so we have adopted these three techniques. For synthesizing continuous nanofibers electrospinning is the simplest and best method. These one-dimensional nanomaterials can be used in a large number of applications such as adsorption, organic dye removal, anti-bacterial activity and many more. As very few literatures are available on the application of nanomaterials for environmental clean-up hence more focused studies are needed to develop composite nanomaterials for solving environmental issues.

CHAPTER 3

SOL-GEL MEDIATED SYNTHESIS OF BOEHMITE (ALOOH) NANOMATERIALS FOR REMOVAL OF CONGO RED (CR) DYE FROM AQUEOUS SOLUTIONS

3.1 Introduction

Nanometer sized materials have evoked a lot of interest due to their unusual physical characteristics which differ strongly from their conventional coarser counterparts in several aspects (Mandal et al., 2008, Deb et al., 2001). Nanoparticles are essentially larger than individual atoms and molecules but are smaller than bulk solid. Hence, they obey neither absolute quantum chemistry nor laws of classical physics and have properties that differ markedly from those expected from the bulk materials. Arising out of their ultra-fine sizes, high surface areas, useful interfacial defects and interface dominated character, nano-phase and nanostructure materials are used as key components in many areas such as electronics and optical devices (Yang et al., 2007), pharmaceuticals (Sadiq et al., 2009), paints, coatings, superconductors, semiconductors (Cao et al., 2001) and catalysis (Yang et al., 2007, Hwang et al., 2001) and in general in nanotechnology. In recent years, the applications of dye and pigments have increased considerably (Dong et al., 2011, Zhou et al., 2010). Dyes are known pollutants that are considered toxic and even carcinogenic for human health (Wang et al., 2005, Zhu et al., 2012). The presence of these dyes in water even at very low concentration is highly visible and undesirable (Hu et al., 2010). Two key components are responsible for dye molecules, one is the chromophores, which is responsible for producing colors and the auxochromes, which can not only supplement the chromophore but also render the molecule soluble in water and give enhanced affinity (Gupta et al., 2009).

Congo red [1-naphthalene sulfonic acid, 3, 30-(4, 40-biphenylenebis (azo)) bis(4-amino-) disodium salt, CR] is toxic to many organisms and is a suspected carcinogen and mutagen. It is the first synthetic dye, which is capable of dying cotton directly. Benzidine, a

human carcinogen and Congo red are however, banned in many countries because of health concerns. Congo red are difficult to biodegrade due to its structural stability, that is their complex aromatic structures, which provide them physico-chemical, thermal and optical stability (Chatterjee et al., 2009). Generally, biological aerobic wastewater systems are not successful for decolorization of majority of dyes. Therefore, in order to achieve the desired degree of treatment, it is necessary to integrate biological, chemical and physical processes as coagulation, ultra-filtration, electro-chemical adsorption, and photo-oxidation (Kargi et al., 2004, Pradhan et al., 2011).

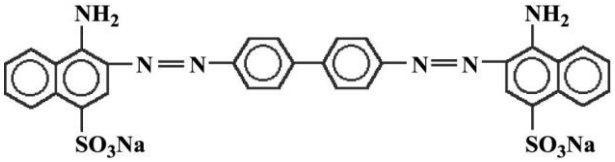

Scheme 1. Molecular structure of Congo Red.

Jain et al., has studied the removal of hazardous dye Congo red from waste water (2008). They have investigated and developed cheap adsorbent methods for color removal using sawdust as adsorbent. Effect of pH, temperature, amount of adsorbent, contact time, and concentration of adsorbate was studied. After adsorption, to observe the quality of waste water, a COD measurement was also carried out. Recently, Iqbal et al. (2010) has studies both the thermodynamics and kinetics of adsorption of dyes from aqueous media onto alumina. The removal of many dyes by change in different parameters has been investigated which obeys all the isotherms and also obeys pseudo-second order kinetics. The dyes were found to be chemisorbed onto alumina. It is also found that adsorptive removal of Congo red, from aqueous solutions by maghemite nanoparticle is also 100% at pH 6. The Langmuir adsorption capacity was also found to be 208.33 mg g^{-1} of the adsorbent (Afkhami et al., 2010). Similarly more recently Cheng et al. (2011) have described the adsorption kinetics and isotherms for the study of Congo red in water by using synthesized hierarchical $Ni(OH)_2$ and NiO nanosheets. Comparison between Ni $(OH)_2$ nanosheets , NiO nanosheets and NiO nanoparticles has been observed. Among them Ni $(OH)_2$ and NiO nanosheets were found to be effective adsorbents for the removal of Congo red from waste water.

3.2. Experimental section

3.2.1. Materials and methods

Aluminium iso-propoxide (AIP) of analytical grade with purity 99.0 % was obtained from S D fine, India. Iso-propanol (IPA) and acetic acid (AA) were purchased from SRL, India.

Congo red, sodium hydroxide and nitric acid were bought from Merck, India ltd. All chemicals are used without further purifications. Double distilled water was used throughout the experiments for preparation and dilution of the solutions. Boehmite (AlOOH) nanomaterials were prepared by sol-gel method. The experimental method was based on hydrolysis and condensation reactions of aluminum isopropoxide (AIP), which occurred to precipitate aluminum in the form of fine hydroxide gel. Initially AIP was dissolved in 2-propanol with continuous stirring in which controlled amount of acetic acid and water was added slowly. The molar ratios of AA/AIP ~0.02, Molar ratio of H_2O/AIP ~ 0.4 and molar ratio of IPA/AIP ~ 19 were maintained during the process. The precipitate obtained was heated at 80°C using water bath for 20 hours and then filtered and washed with 2- propanol for several times and then dried at 60°C for 8 hours.

3.2.2 Characterization techniques

Surface morphology of Boehmite nanomaterials were characterized by using a (JEOL JSM-6084LV) SEM equipped with Oxford INCA energy dispersive X-ray analyzer (EDAX) system and was operated at 15 kV. In order to increase the conductivity of the samples, they were gold coated using a JEOL FRC 1200 fine coater before taking SEM. The powder X-ray diffraction patterns were obtained on a Pan analytical X-ray diffractometer (PW1830) using Cu Kα (λ = 1.541 Å) radiation. The BET adsorption-desorption data was recorded using AUTOSORB-1 with nitrogen atmosphere by keeping it for degassing for 2 hrs at 100°C. A JEOL 200 HR-TEM was used to characterize the AlOOH nanomaterial which was operated at 200 kV. The boehmite nano-powders were dispersed in ethanol and then a drop of the above dispersion was taken on a carbon coated copper grid (300 meshes) for TEM imaging. A digital pH meter (Satorius Model PB-11) combined with glass electrode was used for all experiments. A Shimadzu UV-Visible spectrophotometer (Shimadzu-2450) has been used for adsorption study of Congo red dye. The measurement of nanomaterials has been carried out using soft imaging system software (analySIS FIVE, GmbH) attached with an Olympus (BX-5175E21P) optical microscope.

3.2.3 Adsorption experiments

An adsorption study for Congo red was performed by batch experiments. The Congo red dye adsorption on Boehmite nanopowder was carried out as follows known weight of boehmite (0.1 gm) was added to different glass bottles containing 20 ml of Congo red dye solution. Initial dye concentrations were 100 and 1000 mg/L. The pH of the Congo red solution was

adjusted at 8 using 0.1M HNO_3 or 0.1M NH_4OH solution (Lian et al., 2009). After the adsorption study, the concentration of Congo red solution was measured by using UV-Vis spectrophotometer at 498nm. The adsorption experiments have been conducted three times and the data are presented in the figures with an appropriate error bars. The error bars are found to be within ±3%.

3.3 Result and discussion

3.3.1 Structural properties

We have used sol-gel method for preparation of Boehmite (AlOOH) nano-sized powder by hydrolysis and condensation reaction of aluminum iso-propoxide. The formation of boehmite phase has been confirmed from XRD study. Figure 3.1 shows the XRD pattern of the as-synthesized boehmite materials. This result revealed that the formed materials are crystalline in nature. All of the diffraction peaks can be indexed to the boehmite, orthorhombic γ-AlOOH phase of alumina (JCPDS card No 76-1871). No peaks from any other phase of alumina or impurities are found, indicating the formation of pure boehmite nanopowder. Upon calcinations in air at around 1000^0C, the γ-AlOOH phase has been transformed into α-Al_2O_3 (JCPDS-42- 1468) as shown in figure 3.1(b).

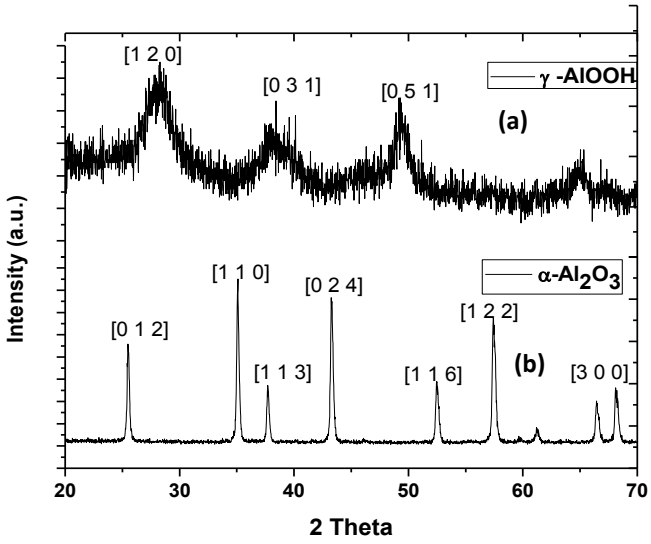

Figure 3.1: XRD pattern of (a) γ-AlOOH and (b) α-Al_2O_3 (Calcined at 1000^0 C).

Figure 3.2 displays the N_2 adsorption-desorption isotherm for the boehmite nanoparticle. According to IUPAC classification, the nitrogen adsorption-desorption isotherm can be classified as a type III isotherm, which is characteristic of non-porous materials. It represents extremely weak adsorbate-adsorbent interaction. The specific surface area is found to be 40 m^2g^{-1} for boehmite nanopowder.

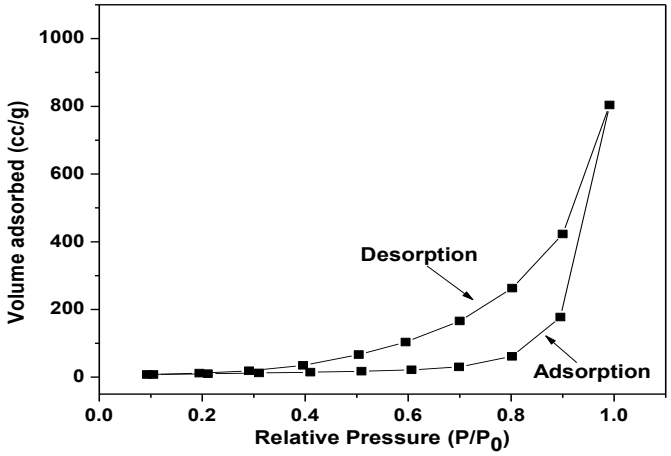

Figure 3.2: Nitrogen adsorption–desorption isotherm graph of AlOOH.

3.3.2 Morphology

The surface morphology and elemental detection X-ray analysis of the prepared boehmite nanopowder were carried out using scanning electron microscope. Figure 3.3 shows the SEM and EDAX studies of AlOOH nanomaterials. The EDAX image of AlOOH shows the presence of aluminium and oxygen, which indicates the formation of AlOOH. The SEM image of the boehmite suggests the presence of ultra-fine as well as agglomerates particle in the powder with irregular morphology.

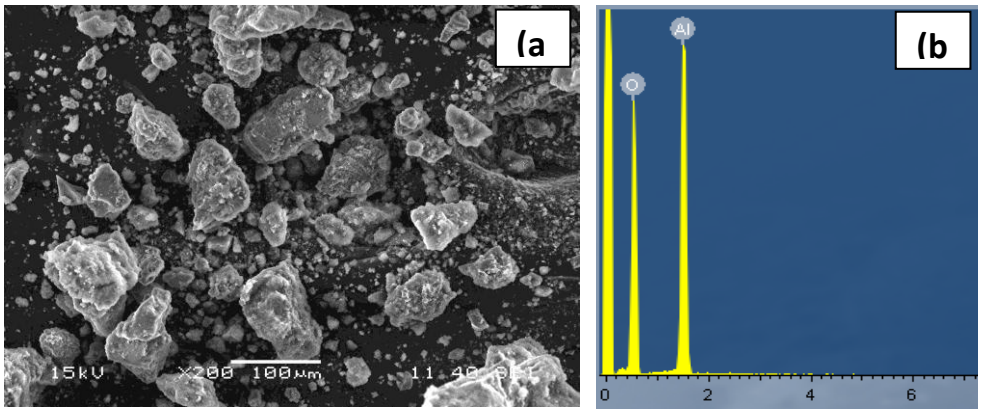

Figure 3.3 (a): SEM image of AlOOH powder and (b) EDAX analysis

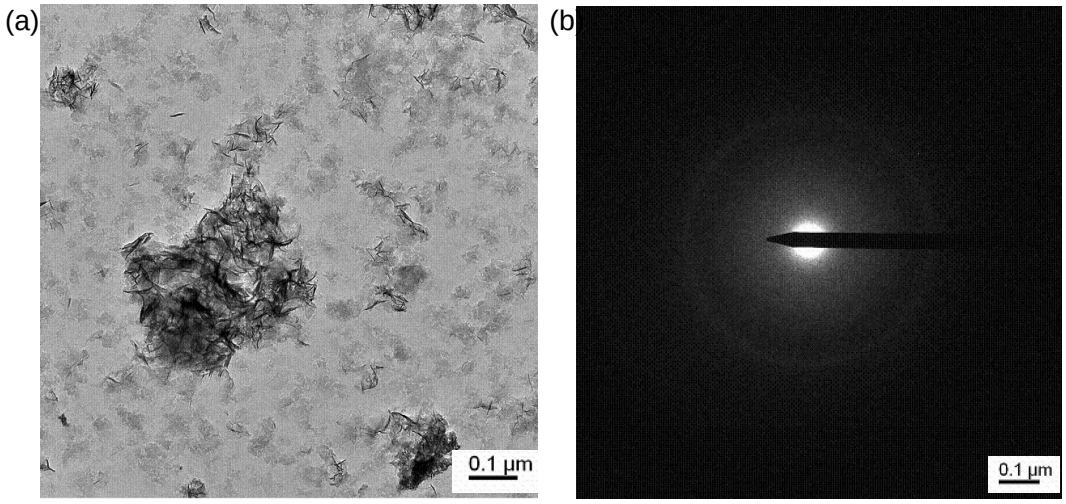

Figure 3.4: TEM image of (a) AlOOH and (b) Electron diffraction pattern of AlOOH

We have carried out the TEM analysis in order to obtain the particle size and morphology of boehmite nanopowder. Figure 3.4 shows the TEM image of the synthesized boehmite nanomaterials. From figure 3.4a, it is observed that the needle shaped boehmite nanomaterials formed. The diameter of these materials are found to be 10-20 nm and 80-100 nm length as measured from the TEM image. Figure 3.4b shows the electron diffraction pattern of boehmite nanomaterials. The formation of ring pattern in the electron diffraction suggests the boehmite materials are polycrystalline in nature.

3.4 Adsorption Studies

3.4.1 Effect of pH on adsorption of Congo red dye

pH of the solution plays an important role in controlling the adsorption of dye on to adsorbent surface. The pH would affect both aqueous chemistry and surface binding- sites of the adsorbent. To determine the optimum pH conditions for the adsorption of Congo red, the effect of pH was studied over the pH range of 4.0 – 8.0, with a stirring time of 30 min. Here the initial concentration of dye and adsorbent dosage were set at 100 mg/L and 0.1g respectively, for all batch tests in this experiment. The pH value of Congo red solution was adjusted using 0.1M HNO_3 and 0.1M NH_4OH. The results obtained are presented in figure 3.5, which describes maximum adsorption, around 100 % approx for γ-AlOOH, at pH 7. It is observed from the figure 3.5(a), that dye adsorption increases with increasing the pH from 4 to 8. It may be due to the variation of surface charge of boehmite nanoparticle as a function of pH of the solution. Figure 3.5(c) shows the effect of pH on the zeta potential of boehmite nanoparticle. The isoelectric point (Iep) of boehmite nanoparticle is 7.3, so the charge on the

particles nears this pH is zero (Singh et al., 2005). The surface charge is positive at pH values lower than Iep, neutral at Iep, and negative at pH values higher than it. At lower pH, the dye molecules exist in protonated form. These positively charge dye molecules experience electrostatic repulsion from positively charge boehmite surface, which is responsible for decrease in adsorption (Iram et al., 2010). Hence, all the succeeding investigations were performed at pH 7. Figure 3.5 (b) shows the UV-Vis absorption spectra of Congo red dye solution (100 ppm). It shows the characteristic absorption peak at 498 nm. This characteristic absorption peak of the dye molecules disappeared completely after 30 min of contact time with boehmite nanomaterials, at pH 7 and the dye solution become colorless. This suggests the complete adsorption of dye molecule onto boehmite surface.

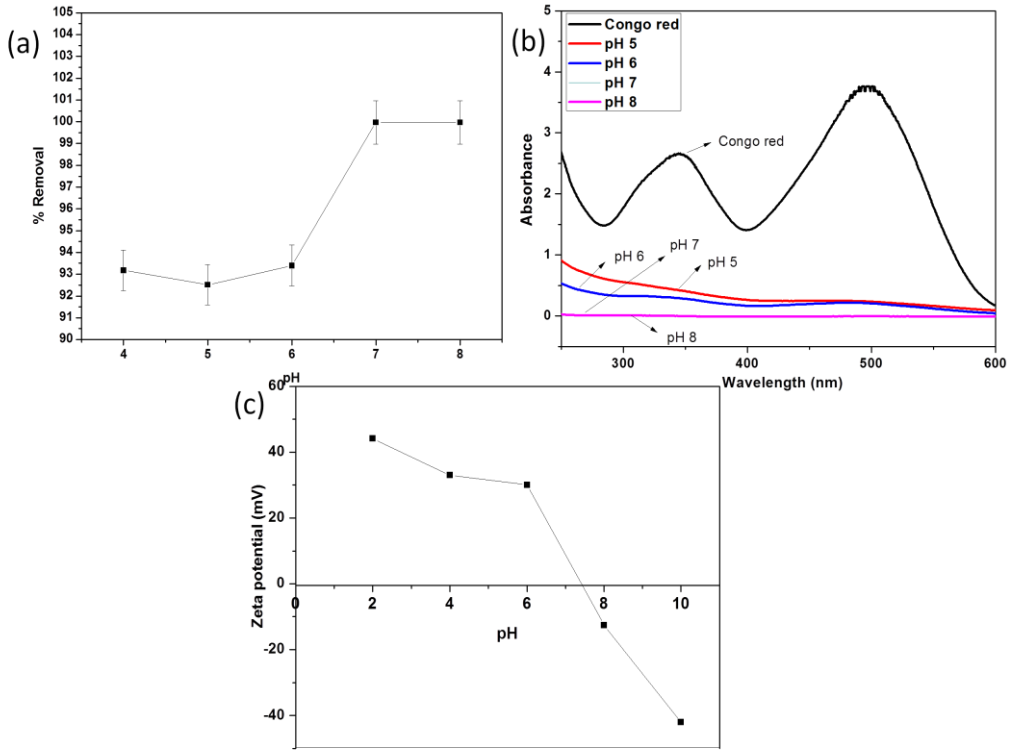

Figure 3.5: (a) Percentage removal as function of pH, (b) absorption spectra of Congo red dye (100mgL^{-1}, 30 min) and (c) Zeta potential of boehmite nanoparticle as a function of solution pH.

3.4.2 Effect of contact time on adsorption of Congo red

The effect of contact time on the sorption capacity of the boehmite nanoparticle for Congo red dye removal is shown in figure 3.6. Studies of contact time are helpful in understanding the amount of dye adsorbed by a fixed amount of the adsorbent (0.1 g of boehmite) at room temperature. Within a short contact time (10 min) 99% of Congo red dye are adsorbed on the surface of boehmite. The graph reveals the rate of initial removal of Congo red was fast

adsorption was fast. However, with increase in contact time the system attains a steady state. The rapid rate of adsorption at the initial contact time was due to the fact that a large number of vacant surface site were available for adsorption. Afterwards the gradual occupancy of remaining vacant sites become difficult due to the repulsive force between the Congo red molecules adsorbed on the surface and the adsorbate. Therefore, it is observed that removal of Congo red dyes by boehmite nanoparticle was rapid and after 10 mins of contact time 99.8 % removal of Congo red was obtained.

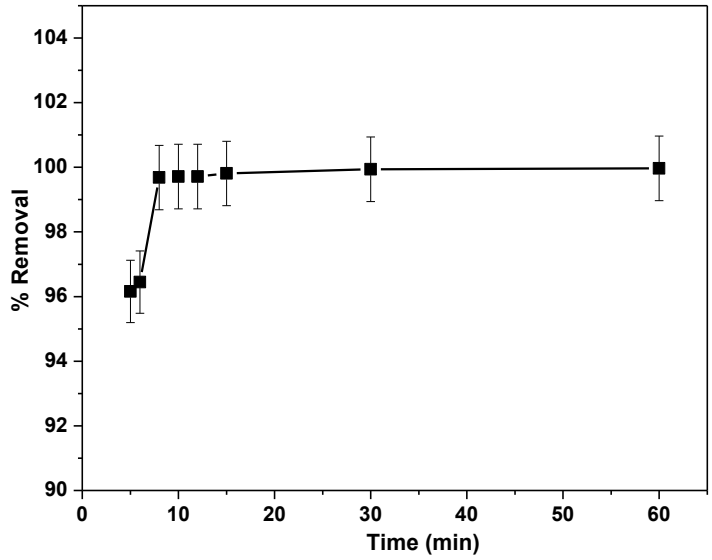

Figure 3.6: Percentage removal of Congo red using boehmite as a function of time (min).

We have also studied the dye removal capacity of α-Al_2O_3 having initial Congo red dye concentration of 100 mg/L and 1000 mg/L as a function of contact time. α-Al_2O_3 nanomaterials were obtained by sintering boehmite nanomaterials at 1000^0C for 2 h in air. The adsorption data obtained was shown in figure 3.7. Adsorption data of both 100 mg/L and 1000 mg/L solution by AlOOH, reveals complete (100%) removal of congo red with change in contact time (Figure 3.7b). However, the removal capacity of congo red by α-Al_2O_3 was found to be 90% for 100 mg/L solution (Figure 3.7a), which further reduced to 80% by increasing the concentration of dye solution to 1000 mg/L. Thus we can confirm that presence of oxy hydroxide in boehmite nanomaterials is responsible for dye removal which is markedly absent in Al_2O_3 adsorption plot.

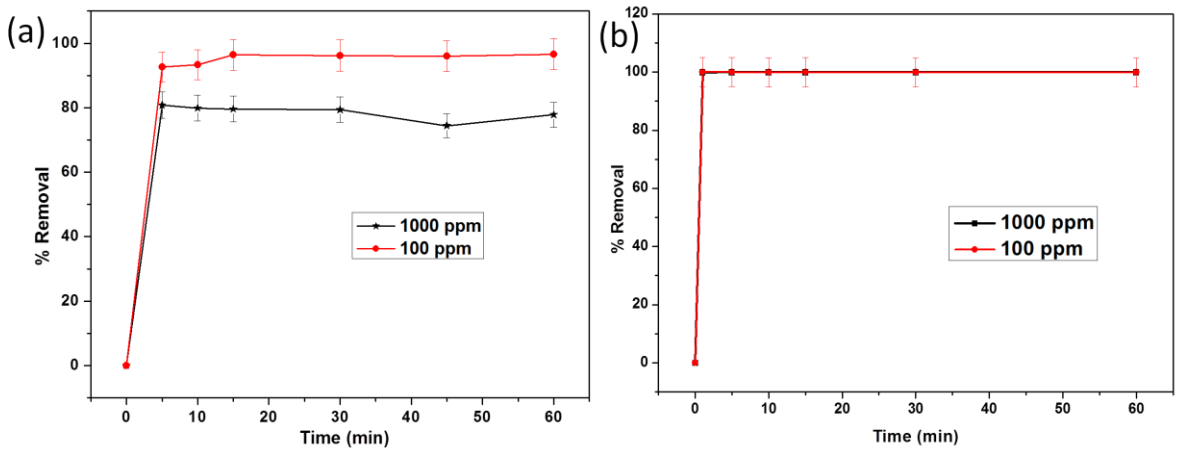

Figure 3.7: Percentage removal graph of (a) Al_2O_3 nanoparticle and (b) γ-AlOOH nanoparticle as a function of time (min) at two different concentration of 100 mg/L and 1000 mg/L

3.4.3 Effect of adsorbent dosage on adsorption of Congo red

The study of adsorbent dosage gives an idea of the effectiveness of an adsorbent and also shows the ability of dye to be adsorbed with a minimum dosage (Dawood et al., 2012). The effect of adsorbent dose was investigated by adding various amounts of adsorbent in the range of 0.01-0.1 g into the bottle containing 20 mL of 100 mg/L dye solution at pH 7, for all batch experiments. The removal of Congo red at different doses is shown in figure 3.8. It was found from the figure 3.8 that with the increase in adsorbent dosage a very minimal change is found in the removal percentage. At equilibrium the percentage of dye removal was increased from 99.5% to 99.8% with the increase of adsorbent mass from 0.08 g to 0.1 g, respectively. The increase in percentage of dye removal with increasing adsorbent dosage is due to increase of sorption active sites at the adsorbent surface (Royer et al., 2009). It was also observed from the experiment that, when the adsorbent dose is high, even at 10 min contact time, 99.9% removal was achieved. This is due to the extent of adsorption is directly proportional to the adsorption sites which is nothing but the amount of dosage. The adsorption capacity was found to be 200 mg/g using 0.1 g adsorbent dose onto 20 ml of 1000 ppm dye solution. Consequently, the adsorbent dose was maintained at 0.1 g for 20 ml of Congo red of 100 mg/L in all the experiments, which was considered to be sufficient for the removal of Congo red.

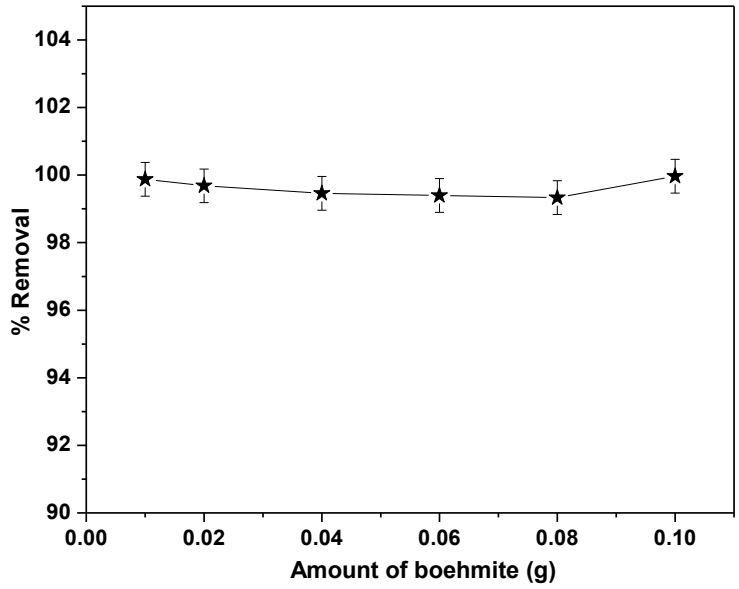

Figure 3.8 : Percentage removal graph of Congo red as a function of dosage (g/L) by boehmite nanoparticles.

3.4.4 Effect of change in initial concentration on adsorption of Congo red dye

The adsorption is greatly influenced by the concentration of the solution, as the adsorptive reactions are directly proportional to the concentration of the solute. To determine the adsorption of Congo red, as a function of initial concentration, we have carried out batch experiments, taking 0.1 g of adsorbent in 20 ml dye solution, for 1 h contact time, at pH 7. The concentration of Congo red solution was varied from 100 mg/L to 1000 mg/L, maintaining same experimental condition. It is clear from figure 3.9 those removal percentages of the Congo red dye is high at lower concentration and comparatively decreases with increase in adsorbate concentration. The percentage of dye removal was 99.9% at 100 mg/L dye solution, which decreases slightly to 97.2% at 1000 mg/L. Overall, it is found that the prepared γ-AlOOH nanoparticle has high affinities for Congo red removal and the electrostatic attraction between the dye molecules (negatively charged) and γ-AlOOH surface (positively charged) might be the predominant adsorption mechanism.

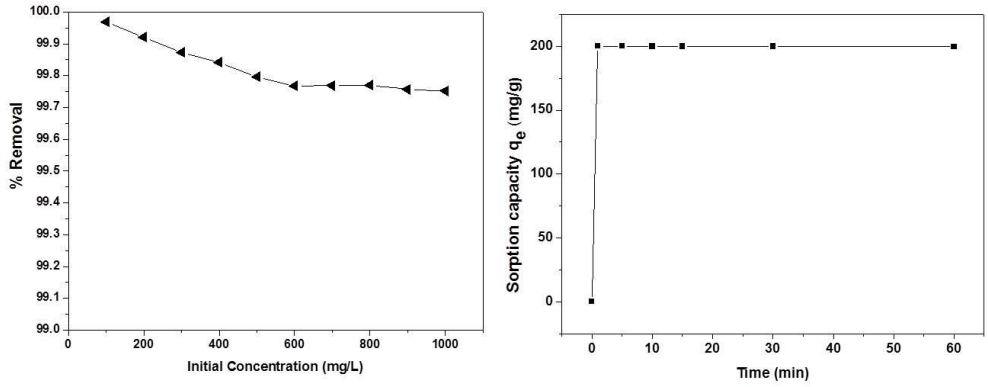

Figure 3.9: (a) Percentage removal of Congo red by boehmite nanomaterials as a function of initial concentration (mgL^{-1}) and (b) The sorption capacity of boehmite nanomaterials as a function of time.

3.4.5 Adsorption Isotherms

The interactive behaviour between the adsorbate and adsorbents are fundamentally described by adsorption isotherm and are important for investigating the mechanisms of adsorption. The isotherm assumes that adsorbent surface sites have a spectrum of different binding energies. Hence it is the relationship between the removal ability of the material and the concentration of the contaminant solution. Several isotherms equations are available, and the two important isotherms were selected for this study i.e. the Langmuir and Freundlich isotherms.

These isotherms are useful for estimating the total amount of adsorbent needed to adsorb a required amount of adsorbate from solution. In order to describe the Congo red adsorption onto the boehmite nanoparticle surface isotherm data obtained were fitted to the Langmuir and Freundlich adsorption models. Isotherm studies were conducted by varying the initial Congo red concentration from 100 to 1000 mg/L and maintaining the adsorbent dosage of 0.1 g at a time variation of 1 hour.

The Langmuir isotherm describes the interactive behaviour between the solutes and adsorbents. It is based on the assumptions of monolayer adsorption on a structurally homogeneous adsorbent, where all the sorption sites are identical and energetically equivalent (Zhua et al., 2011, Bulut et al., 2008).

Linearized Langmuir equation is represented as follows:

$$\frac{C_e}{Q_e} = \frac{1}{q_m b} + \frac{1}{q_m} C_e \qquad (1)$$

where C_e (mgL^{-1}) is equilibrium concentration of Congo red in solution, q_e (mg g^{-1}) is the adsorption capacity at equilibrium, q_m (mg g^{-1}) is maximum amount adsorbed per unit mass of adsorbent required for monolayer coverage of the surface, b (L mg^{-1}) is a constant related to the heat of adsorption. The slope and intercept of linear plots of C_e/q_e against C_e yield the values of $1/q_m$ and $1/q_m b$ for Eq (1).

Table 3.1 Adsorption isotherm parameters of boehmite nanoparticle

Langmuir Isotherm model			**Freundlich Isotherm model**		
q_m(mg/g)	b(L/mg)	R^2	K_F(mg/g)$(L/mg)^{1/n}$	n	R^2
243.9	12.82	0.836	109.06	1.907	0.9851

The Freundlich isotherm is the known relationship describing the adsorption equation. This fairly satisfactory empirical isotherm can be used for non-ideal adsorption that involves heterogeneous surface energy systems. Here the adsorbent surface phase is also considered as multilayer. The favorable adsorption of the adsorption model can be determined from Freundlich constants from equation (2). The Freundlich isotherm is commonly given by

$$\ln q_e = \ln K_F + (1/n) \ln C_e \qquad (2)$$

Where K_F (mg/g)$(L/mg)^{1/n}$ is related to the adsorption capacity of the adsorbent and 1/n is another constant related to the surface heterogeneity (Karaoglu et al., 2009). Freundlich adsorption isotherm of Congo red is shown in figure 3.10. The slope and intercept of linear plots of ln q_e against ln C_e yield the values of 1/n and ln K_F for Eq (2). The values of regression coefficients say that the experimental data obtained are fit well to the Freundlich isotherm model as compared to Langmuir isotherm as shown in table 3.1.

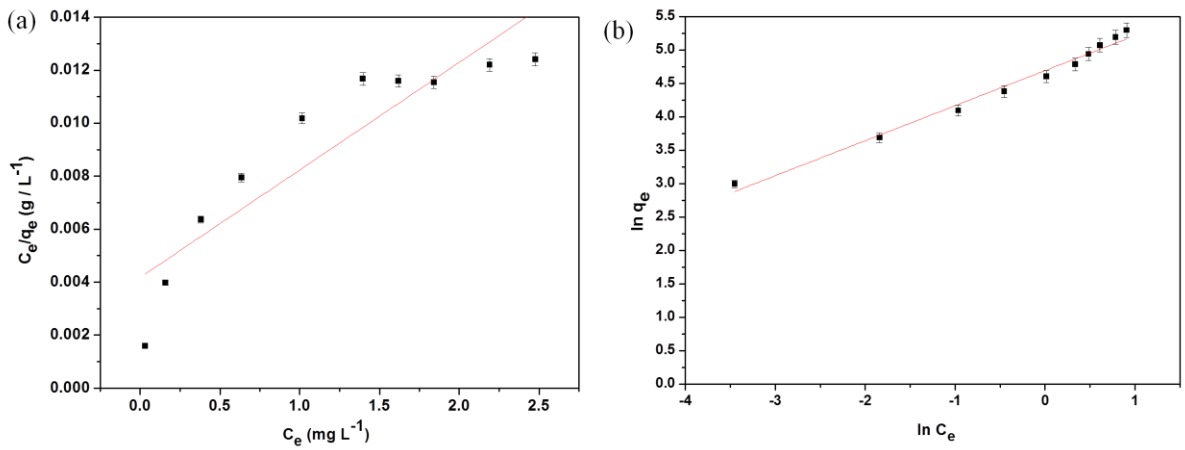

Figure 3.10: Langmuir and Freundlich isotherm for the adsorption of Congo red onto boehmite nanoparticle at room temperature.

3.4.6 Adsorption Kinetics

The adsorption kinetics is important for adsorption studies in order to identify the mechanism and the potential rate controlling steps involved in the process of adsorption (Wu et al., 2005). Two kinetic models, pseudo-first-order and pseudo-second-order are studied and adopted to investigate the adsorption process. Figure 3.11 shows the sorption kinetics of Congo red onto boehmite surface obtained by batch experiments for an initial Congo red concentration of 100 mg/L at pH 7.0. From the regression coefficient value i.e. R^2 = 1, confirms that the adsorption obeys pseudo-second order kinetics. The pseudo-second order model can be expressed as follows:

$$\frac{dQ}{dt} = k_2\,(q_e - q_t)2 \qquad (3)$$

Where k_2 (g.(mg.min)$^{-1}$) is the rate constant of the pseudo-second order equation. The integrated form of the above equation can be expressed as follows:

$$\frac{t}{q_t} = \frac{1}{k_2 q_e 2} + \frac{1}{q_e}t \qquad (4)$$

The value of q_e and k_2 can be determined by the slope and intercept of the straight line of the plot t/q_t versus t respectively (Liu et al., 2011).

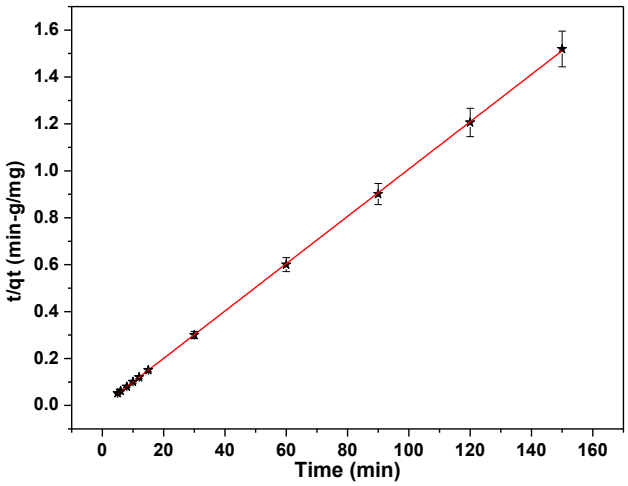

Figure 3.11: Pseudo-second-order kinetic plots for Congo red adsorption onto boehmite nanoparticle.

3.5 Conclusion

Boehmite nanoparticles with diameter 10-20 nm have been synthesized using sol-gel method. Batch experiments were performed for the removal of Congo red dye from aqueous solution, by using boehmite nanoparticle as adsorbent materials. The adsorption characterization have been examined at different pH, initial metal ion concentration, contact time and different adsorbent dosage. Highest removal was achieved in neutral range, that is, pH 7-8. Adsorption equilibrium is attained within a short contact time of 30 min. With increase in amount of adsorbent dose, the percentage of adsorption increases, due to increase in number of adsorption sites. The adsorption capacity of boehmite nanomaterials was found to be 200 mg/g. Order of adsorption was governed by pseudo-second order kinetics. Experimental data of Congo red adsorption obtained was successfully fits to Freundlich isotherm model over all concentration range studied, which suggest the multilayer adsorption mechanism.

CHAPTER 4

STUDIES ON ELECTROSPUN ALUMINA NANOFIBERS FOR REMOVAL OF Cr (VI) & F^- TOXIC IONS FROM AQUEOUS SYSTEM

4.1 Introduction

One dimensional nanostructure such as nanorods, nanotubes, nanowires, nanofibers etc., have attracted much interest over the past decade as they can address the needs of a wide range of advanced applications (Shen et al., 2009). The nano-sized fibrous structures are unique as compared to bulk fibers due to their high surface to volume ratio, fiber interconnectivity, micro scale interstitial space and also high porosity. These properties attract a lot of attention of present research on ceramic nanostructure, which also improves the performance for many modern applications (Ramakrishna et al., 2005). Alumina (Al_2O_3) is one of the most excellent ceramic oxides (El-Shaarawy et al., 2009) and has been studies extensively over a long period of time because of their potential for broad applications in adsorbents, catalysts and catalyst support (Raybaud et al.,2001, Zhang et al., 2008, Hou et al., 2005), and reinforcements for composite materials. Alumina is also used for adsorption /chemisorption of heavy toxic metal ions such as arsenic or arsenate (Li et al., 2011). The adsorption depends on exposed surface area; therefore, nanofibers with high surface area produced by different synthetic methods might be ideal for this application. Various methods have been adopted for the synthesis of nanosized alumina materials (Chandradass et al., 2009) which includes mechanical milling, sol-gel method (Kim et al., 2007), hydrolysis & precipitation, hydrothermal method (Chen et al., 2007), combustion synthesis (Ianos et al., 2009), electrospinning method (Teo et al., 2007, Sun et al., 2009) etc. Among them, electrospinning, a non-equilibrium electro-hydrodynamic process, is a platform technology for the production of nanofibrous materials. Recently, electrospinning is used as a novel method for preparing various inorganic & ceramic fibers with a diameter ranging from several micrometers to tens of nanometers (Guan et al., 2003, Zhang et al., 2009, Ding et al.,

2008). The morphology of the fibers depends on the process parameters; including solution concentration, applied electric field strength, distance between two electrode, feed rate and viscosity of polymer (Fong et al., 1999, Shin et al., 2001). Arising out of their specific surface area and highly porous structure electrospun fibers can be used in a number of applications including membranes, tissue engineering and other biomedical applications (Deitzel et al., 2002). Electrospun nanofibers have diameters 5 to 10 times smaller than that of melt blown fibers. Most of the recent work on electrospinning has focused to understand deeper the fundamental aspects of the process in order to gain control of nanofiber morphology, structure, surface functionality, and strategies for assembling them or on determining appropriate conditions for electrospinning of various polymers and biopolymers (Frenot et al., 2003, Huang et al., 2003).

Li et al. (2006) have reported a brief overview of recent progress in preparation of ceramic nanofibers using electrospinning method. They have highlighted several unique features associated with electrospinning technique and illustrate the potential of electrospinning in ceramic nanofibers processing and applications. Similarly, the recent advances in nanostructured ceramics by electrospinning methods have been reviewed by Ramaseshan et al. (2007). In this review they have reported the electrospun mediated synthesis of various ceramics nanofibers in details along with their many useful applications. The fabrication of transparent alumina nanofiber by electrospinning method has also been reported (Azad et al., 2006). This author has used aluminum 2, 4-pentanedionate and PVP polymer solution to prepare inorganic-organic composite fibers which upon sintering at high temperature yield high-purity and crystalline α-alumina nanofibers. Dia et al. (2002) have prepared ultra-fine alumina-borate oxide fiber via sol-gel mediated electrospinning method. The average diameter of the alumina-borate fiber was found to be about 550 nm and upon crystallization; the surface of the fibers became rough due to development of the grain boundaries. The authors have also reported that the alumina-borate phase was unstable & was formed at calcination temperature 1000-1200 $^{\circ}$C. However, a new stable crystalline phase of α-alumina was formed at 1400 $^{\circ}$C. More recently, Yang et al. (2007) synthesized composite Cr_2O_3/Al_2O_3 nanofibers with the fiber diameter in the range of 50-100 nm, after calcination of PVA/chromium nitrate/ aluminium nitrate composite fibers at certain temperature. They have adopted a modified sol-gel method followed by electrospinning method for fabrication of nanosized Cr_2O_3/Al_2O_3 composite fibers. Panda et al. (2007) has successfully prepared alumina nanofibers by electrospinning method using different precursors from a combination

of PVA and PEO polymer precursor, alumina nitrate as alumina precursor. Maneeratana et al. (2008) have reported direct synthesis of continuous hollow alumina fibers via sol-gel mediated electrospinning method using aluminium alkoxide precursors. Kang et al. (2011) have synthesized alumina nanofibers with average diameter 100-800 nm by electrospinning $AlCl_3$/PVP solution followed by calcinations at high temperature. However, preparation of continuous alumina nanofibers via electrospinning of PAN/DMF solution was reported by Yu et al. (2012). Aluminum 2, 4-pentanedionate was used as alumina precursor, which on calcinations at 1200 °C, forms alumina nanofibers with diameters ranging from 150 to 500 nm. XRD data confirms the formation of α-alumina with a crystallite size of 10 nm approximately. More recently, Milanovic et al. (2013) have studied on preparation of low cost alumina nanofibers by electrospinning. Aluminum chloride hydroxide and PVA composite mixture was used as precursor. On further calcinations of electrospun nanofiber at 1100 °C shows average diameter of 470 nm and well defined corundum structure.

Removal of toxic heavy metal ions from wastewater has received significant attention due to their high impact on environment and public health (Lia et al., 2003). It is a major concern because of their nondegradability and threat to human life and environment. This heavy metal removal from aqueous solutions has been traditionally carried out by chemical precipitation (Demirbas et al., 2008). Many more pre concentration methods are well known (Amin et al., 2001). Most of them are complicated and time-consuming. Among these methods, however, the adsorption method is simple and convenient (Boddu et al., 2003, Fang et al., 2007, Fathima et al., 2005, Hu et al., 2005, Noroozifar et al., 2008). Adsorption is the accumulation of gas, vapor or liquid molecules on an interface (Uysal et al., 2007). The adsorption processes appear to be multi determined and depend on both the characteristic of the adsorbent and the operating conditions. The primary need for a better adsorption process is an adsorbent with sufficient selectivity, high sorption capacity and resistance to high temperatures and high radiation levels (Bishnoi et al., 2004). A literature survey shows that some scientists have already studied different ways for the removal of heavy metals and hazardous waste management (Baily et al., 1999). Chromium is one of the regulated toxic metals in environment and is found in various oxidation stages ranging from –II to +VI but mainly in two states, as Cr (III) and Cr (VI). Between the two forms, Cr (VI) is the most toxic and it is carcinogenic and mutagenic to living organisms (Pagana et al., 2011, Wang et al., 2009). It is highly toxic because of its oxidizing properties and tends to accumulate in living organisms causing serious damages for bacteria, plants and animals. Cr (VI) has high water

solubility and mobility (Mohan et al., 2006, Silva et al., 2009) and because of its negative impact on the aquatic ecosystem, the hexavalent state is more concerned by the research (Rajesh et al., 2007). The maximum permissible level of Cr (VI) in drinking water according to World Health Organization (WHO) is 50 µg/L (Ajouyeda et al., 2009). Similarly, fluoride is also considered as both an essential element and potent environmental pollutant at high concentrations, causing a number of disorders (fluorosis) among the consumers (Castillo et al., 2007). According to W.H.O reports, a value more than 1 mg/L in drinking water can cause dental and sketal fluorosis (Kamble et al., 2010, Valdivieso et al., 2006). However, by crossing a certain level of fluoride intake, it causes many bone diseases, including mottling of teeth and lesions of the endocrine glands, thyroid, liver and other organs (Cengelolu et al., 2002). Hence it is an important task to supply water with safe fluoride levels. Fluorine is the most electronegative and reactive among all the elements in the periodic table. Because of its great reactivity, fluorine cannot be found in nature in its elemental state. It exists either as inorganic fluorides (including the free anion F^-) or as organic fluoride compounds (Jagtap et al., 2012).

These electrospun nanofibers have large specific surface areas and high adsorption rates, which have attracted a great attention in heavy-metal removal from wastewater in recent years (Sanga et al., 2008, Haider et al., 2009). Similar type of work has been done by Hota et al. (2008) for the removal of heavy-metal ion like Cd (II). Here the sorption of Cd (II) by using a boehmite impregnated electrospun membrane. The adsorption capacity was found to be 0.20 mg/g. Zhu et al. (2010) have reported the preparation of PVC ultrafine fibrous membrane using electrospinning method, and used for adsorption of cationic dye. The adsorption of metal ions from aqueous solutions to adsorbents is usually controlled by the properties of the surface functional groups of the adsorbents (Deng et al., 2003).

The defluoridation performance of five different types of aluminas such as aluminium oxides, hydroxide and oxy-hydroxide were investigated by Gong et al. (2012). Five different types of aluminas were synthesized at different pH values and calcination temperatures, and their fluoride removal behavior was studied. Similarly, Kamble et al. (2010) have also reported the adsorption potential of commercially available alkoxide origin alumina materials for defluoridation of drinking water using batch and continuous mode of operations.

Recently, Vu and co-workers (2013) have studied on different phases of TiO_2 nanofiber synthesized by electrospinning technique with subsequent heat treatment and acidic-dissolution. Subsequently, an adsorption study of arsenic (As (III)) was investigated. Among all of the phases, amorphous TiO_2 nanofibers have highest adsorption capacity and

rate than the crystalline TiO_2 nanofibers due to its higher surface area and pore volume. Again the same group has also studied on adsorption of Cu (II) by anatase mesoporous TiO_2 nanofibers of diameter 90 nm. A comparison of adsorption studies between both anatase TiO_2 nanofiber and mesoporous TiO_2 nanofiber was carried out. It was observed that mesoporous TiO_2 nanofiber shows better adsorption capacity than anatase TiO_2 nanofiber.

In this study, we have reported the synthesis of α-Al_2O_3 ultra-fine fibers by electrospinning aluminium acetate (AlAc) sol precursor and PVP/ethanol polymer solution followed by calcination at higher temperature. The commercially available aluminium acetate is found to be either boric acid stabilized form or basic acetate form, which is sparingly soluble in water & alcohol. Therefore, direct synthesis of alumina fiber by electrospinning method using commercially available acetate precursors is a tedious task. Hence, we have prepared aluminum acetate aqueous sol, by co-precipitation method and have used the prepared sol as a precursor for alumina fiber synthesis. The effect of organometallic precursor and calcination temperature on the formation, morphology and crystallization of nanofibers has been discussed here. In the present work, we have also investigated on the adsorption of Cr (VI) and F^- ion from aqueous solution by using alumina nanofiber as adsorbent materials. Batch studies were conducted at room temperature and the effect of contact time, pH, adsorbent dose, initial metal ion concentration were investigated to optimize the conditions for maximum chromium (VI) and fluoride removal. The experimental data obtained were calculated and fitted using adsorption isotherms, kinetic model in order to understand the nature of adsorption.

4.2 Experimental procedure

4.2.1. Materials

The polymer poly vinyl pyrrolidone (PVP; Mn =1300 000) was obtained from Sigma-Aldrich (USA). Ethanol was obtained from Merck, Germany, Aluminium sulphate 16 hydrate (GR) was purchased from Merck India. Barium acetate ($Ba(Ac)_2$, AR grade) was supplied by S.D Fine Chem Ltd, India. Acetic acid (AA) was purchased from Rankem, India. The rest of the chemicals, as potassium dichromate, sodium fluoride, HNO_3, NH_4OH were purchased from Merck, India. Merck Chromium standard is being used for standardization of atomic absorption spectroscopy (AAS). All the chemicals were used without further purifications. Double distilled water and 25 ml neat & cleaned glass bottles were used throughout the experiments.

4.2.2. Fabrication of alumina nanofibers

The PVP solution (10 wt %) was prepared by dissolving PVP polymer powder in absolute ethanol under constant and vigorous stirring. Aluminium acetate was used as aluminium precursors and was prepared by mixing saturated solution of barium acetate and aluminium sulphate. The aluminum precursor sol was mixed with the previously prepared PVP/ethanol solution followed by addition of 1-2 drops of acetic acid. The polymer to aluminium precursor's weight ratio was maintained at 3:1. The resulting PVP-aluminium acetate solution was loaded into a 3 ml plastic syringe fitted with a metallic needle. The polymer solution was pushed to the needle tip using the syringe pump and the feed rate was kept at 1.0 ml/hr. The positive terminal of a variable high voltage (Glassman Japan) power supply (14 kV) was applied to the metallic needle, whereas the negative terminal was connected to the grounded collector which was covered with the aluminium foil served as counter electrode. The distance between the needle tip and collector was maintained 10 cm. All the experiments were conducted at room temperature with a relatively low humidity (45-50 %) condition. After electrospinning, the as-spun PVP/aluminium acetate composite fibers were calcined in air for 2 hours at higher temperatures (1000 °C) at a heating rate of 20 °C/min in order to obtain pure Al_2O_3 nanofibers.

Further the alumina nanofiber obtained from PVP/aluminum acetate as precursors were used for adsorption studies of Cr (VI) and F^- ions from aqueous system.

4.2.3 Adsorbent characterization techniques

The powder X-ray diffraction (XRD) patterns were recorded on a PAN analytical diffractometer (PAN) using nickel-filtered Cu Kα (λ = 1.541 Å) radiation. The surface morphology of Al_2O_3 nanofibers were characterized using JEOL JSM-5300 scanning electron microscopy, operating at 20kV. The SEM was equipped with Oxford INCA energy dispersive X-ray analyzer (EDAX) system. The nanofibers were deposited on a carbon tape before mounting on a sample holder for scanning electron microscopy (SEM) analysis. Philips 200 TEM equipment was used to characterize the Al_2O_3 nanofibers and was operated at 200 kV. The Al_2O_3 nanofibers were dispersed in ethanol and then a drop of the above dispersion was taken on a carbon-coated copper grid (300 meshes) for transmission electron microscopy (TEM) imaging. The IR spectra of the samples were recorded using a Perkin-Elmer infrared spectrophotometer (Spectrum RX-1) with resolution of 4 cm^{-1}, in the range of 400–4000 cm^{-1}. The BET surface area of the fibers was measured using AUTOSORB-1 equipment. The

samples were degassed at 120°C for 2 hrs prior to the surface area measurement. Thermal decomposition of alumina precursor membrane was studied with thermogravimetric and differential thermal analysis (TG-DTA) using SHIMADZU (TA-60 WS) model. The data were obtained by heating the sample at 20°C/ min in air atmosphere. Adsorption studies were carried out by Perkin-Elmer (Analyst 200), atomic absorption spectroscopy (AAS). The residual concentration of Cr (VI) following sorption experiments were determined by using AAS fitted with a chromium lamp. A digital pH meter (Sartorius Mechatronics India Pvt. Ltd), fitted with a glass electrode was used for pH adjustment. The concentration of fluoride in the test solution was measured using an Orion ion selective electrode and Orion 720 A+ ion analyzer. A total ionic strength adjusting buffer (TISAB III) solution was added to both samples and standards in the ratio 1:10 (Instruction Manual, 1983). TISAB-III contains 300 g sodium citrate·$2H_2O$ (fw = 294.10), 22 g of 1, 2-cyclohexanediamine-N,N,N',N'-tetraaceticacid (CDTA) and 60 g of NaCl in a volume of 1000mL (pH 5–5.5). CDTA forms stable complexes with polyvalent metal cations (e.g. Al (III) and Fe (III)) in water and/or aqueous solution (eg. Al^{3+} and Fe^{3+}) which are more stable than metal–fluoride complexes in solution (Islam et al., 2007).

4.2.4. Adsorption experiments

The electrospun alumina nanofibers were used as adsorbent materials for removal of chromium (VI) and fluoride from aqueous system. We have conducted the batch adsorption studies in order to determine the optimum conditions for removal of chromium (VI) and fluoride from aqueous system, which were performed using small (50 ml) neat and clean screw-capped glass and polypropylene lined bottle respectively. A stock solution (1000 mg/L) of chromium (VI) and fluoride ions was prepared by dissolving exact amount of $K_2Cr_2O_7$ (merck) and sodium fluoride (merck) in deionized water. Solutions with the desired concentrations (10-100 mg/L) of chromium (VI) and fluoride were prepared by successive dilutions of the stock solution. Batch adsorption experiments were performed by addition of different quantities of alumina nanofibers (10-100 mg) into a 20 ml stock solution of chromium (VI) and fluoride of varying concentrations (10-100 mg/L). All the adsorption experiments were carried out at room temperature (27°C) with constant stirring by using orbital shaker. The effect of pH on adsorption of chromium (VI) and fluoride ions by alumina nanofibers were studied by varying pH of the solution over the range of 3-9 by adding 0.1 M NH_4OH and 0.1 M HNO_3 aqueous solution. A separate set of experiments were conducted to test the time required to reach the equilibrium condition, by keeping the initial concentration

of the test solution 10 mg/L and adsorbent dose at 0.01 g for a chromium (VI) solution and 0.1 g for a fluoride solution at optimum pH values of 5 and , respectively. Similarly, the effect of the adsorbent dosage on adsorption of chromium (VI) and fluoride ions was performed by shaking 20 ml of 10 mg/L stock solution for 1 hr with different adsorbent doses (0.01 - 0.1 g) at room temperature. After equilibrium was reached, the adsorbent was separated from the aqueous solution by filtration using whatman-42 filter paper again was centrifuged for removal of fine dispersion of nanoparticle. The residual concentration of the metal ions in the aliquot was determined by AAS and an Orion ion selective electrode. Adsorption data obtained in this experimental study were evaluated with Freundlich, & Langmuir isotherms models. The adsorption experiments have been conducted three times and the data are presented in the figures with an appropriate error bars. The error bars are found to be within ±3%.

The percentage of chromium (VI) and fluoride ions adsorbed were determined from the difference between initial C_i and final C_f concentrations of both ions in aqueous solution, before and after contact.

$$\% \text{ Removal} = \frac{C_i - C_f}{C_i} 100 \qquad (1)$$

4.3 Results and discussion

The preparation of α-Al_2O_3 using electrospinning method has been reported earlier. In these reports, α-Al_2O_3 was prepared using organometallic precursors such as aluminium acetate stabilized boric acid, aluminium acetyl acetonate & inorganic precursors such as aluminium nitrate and aluminium chloride (Shin et al., 2001, Azad et al., 2006, Dia et al., 2002, Panda et al., 2007, Kang et al., 2011). However, use of above precursors for the preparation of alumina in electrospinning method has many disadvantages. For example formation of aluminium borate ($Al_4B_2O_9$) fibers was observed when aluminium acetate stabilized boric acid was used as precursor. In some cases aluminum acetyl acetonate is carcinogenic in nature. Similarly, in case of inorganic salt precursors, due to their hygroscopic nature & highly charge species; formation of homogeneous and large scale production of fibers is extremely difficult. Hence, in order to overcome the above difficulties and for large scale production of alumina nanofibers we have reported here the use of aluminium acetate aqueous sol as aluminium precursors and PVP as polymer.

In this work, PVP/aluminium precursor composite fibers were prepared by electrospinning of aluminium acetate sol mixed PVP-ethanol solution. Upon calcinations of above composite fibers in air, pure Al_2O_3 ultra-fine fibers were obtained. The schematic representation of the preparation of electrospun nanocomposites membrane is shown in figure 4.1. The saturated solution of aluminium acetate was freshly prepared using aluminium sulfate and barium acetate salts. The chemical reactions occur in this process are presented below. (Note: Ac → Acetate, CH_3COO^-)

$$Al_2(SO_4)_3 + 3Ba(Ac)_2 \longrightarrow 2Al(Ac)_3 + 3BaSO_4$$

$$Al(Ac)_3 \xrightarrow{\Delta} Al_2O_3$$

The barium sulphate precipitate obtained was filtered out and the filtrate containing the aluminium acetate solution was mixed with PVP-ethanol solution to prepare PVP-aluminium acetate composite fibers. We have maintained the PVP to alumina precursor weight ratio 3:1 in this case. In order to obtain the pure alumina nanofibers, the PVP/alumina precursor's composite fibers were calcined in air at two different temperatures i.e., 500 °C & 1000 °C for 2 h.

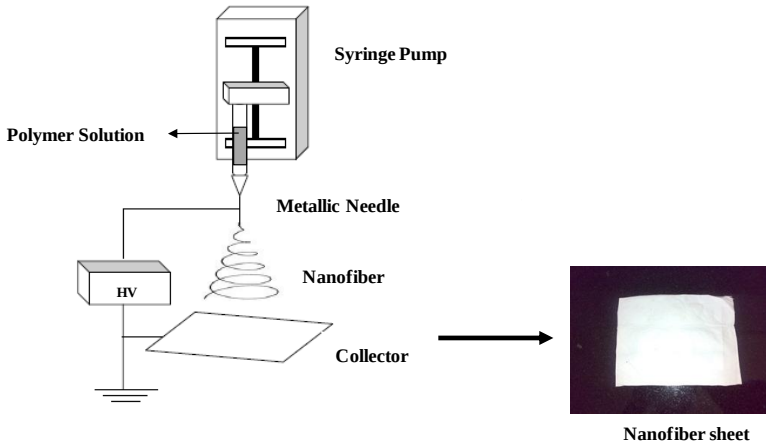

Figure 4.1 Schematic diagram of electrospinning setup.

XRD analysis has been used to determine the structure and purity of the electrospun alumina nanofibers. Figure 4.2 shows the XRD curve for the calcined alumina fibers that are prepared by electrospinning of a PVP/aluminum acetate solution. Diffraction peaks corresponding to single phase α-Al_2O_3 have been found for the sample sintered at 1000 °C for 2 hours. The XRD patterns indicate that pure and highly crystalline α-Al_2O_3 is formed. No other peaks associated with the presence of impurities are observed. All the observed diffraction peaks be indexed to α- Al_2O_3 structure and are matching well with the literature value (JCPDS Card No: 42-1468).

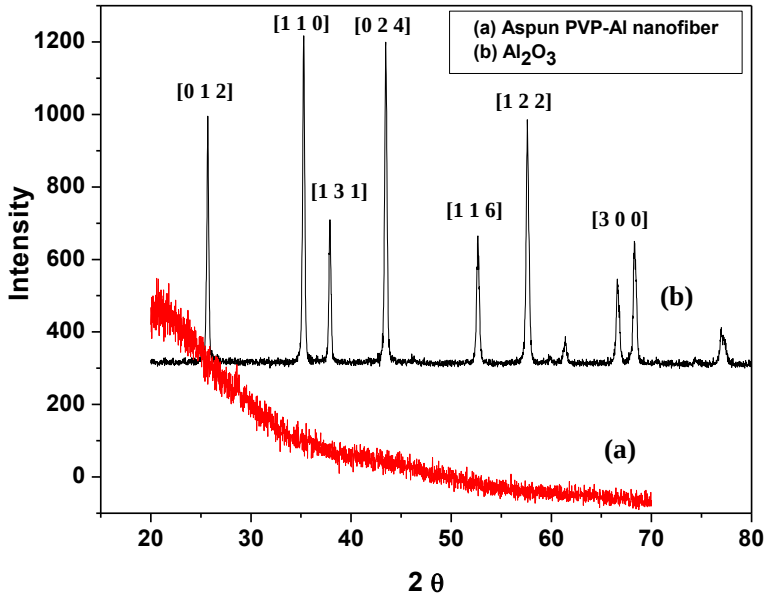

Figure 4.2 XRD pattern of alumina nanofiber (a) PVP-alac-aspun nanofiber (b) Al_2O_3 nanofiber obtained after sintering at 1000° C.

Figure 4.3 shows the FT-IR spectra of PVP-aluminium acetate as-spun composite fibers and alumina fibers obtained after calcination of composite fibers at 1000 °C. The spectrum of the as-spun ultra-fine fiber (figure 4.3a) shows the characteristic peaks at 1283, 1433 and 1647 cm^{-1}, corresponding to the stretching and bending vibrations of PVP (Frenot et al., 2003). The broad band observed around 3400 cm^{-1} indicates the O-H stretching frequency of acetate precursors. When the fibers were calcined at 1000 °C, the characteristic peaks of PVP and O-H stretching band disappeared as shown in figure 4.3b. This is because of removal of polymer and decomposition of acetate precursors at higher calcination temperature. However, appearance of new peaks in the range of 565-880 cm^{-1} may be attributed to the presence of alumina, which is also supported by XRD results.

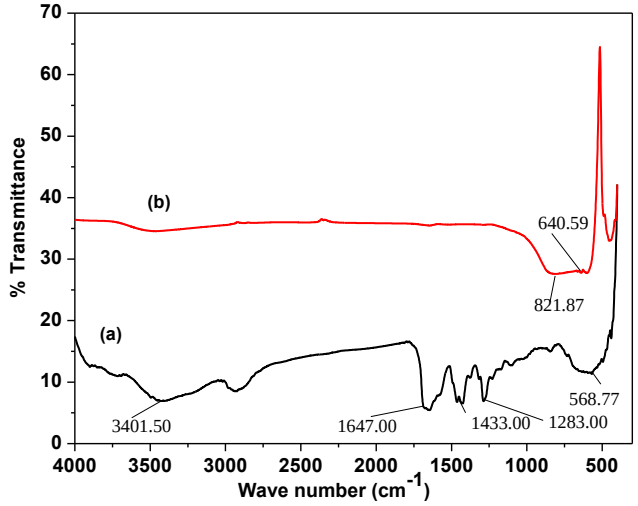

Figure 4.3 FTIR of (a) as-spun composite fiber and (b) fiber sintered at 1000 °C**.**

Thermal behavior of the PVP-aluminium acetate as-spun ultra-fine fiber membrane was studied by TGA-DTA analysis in air up to 1000 °C at a heating rate of 10 °C/min. Figure 4.4 represents the TGA-DTA curve of PVP-aluminum acetate as-spun ultra-fine fiber. It could be observed from the figure that the fibers have four major weight losses, represented by four peaks in DTA curve. An endothermic peak is observed in DTA curve with maxima at 98 °C, and three exothermic peaks are observed between 260 °C to 500 °C. It is believed that the first weight loss of 9 wt % was because of evaporation of residual moisture and ethanol molecules in the fibers. The second weight loss starting at 260 °C, with a weight loss of 11% resulted from decomposition and burning of PVP polymer fibers. The third & fourth weight loss, observed between 350-650 °C, with a loss of 73 wt%, corresponds to complete combustion of PVP polymers and organometallic aluminium acetate. When the temperature exceeds 650 °C, the TGA graph is nearly horizontal, which indicates the complete burning of polymer, and organic matters resulting the formation of pure aluminium oxide fibers.

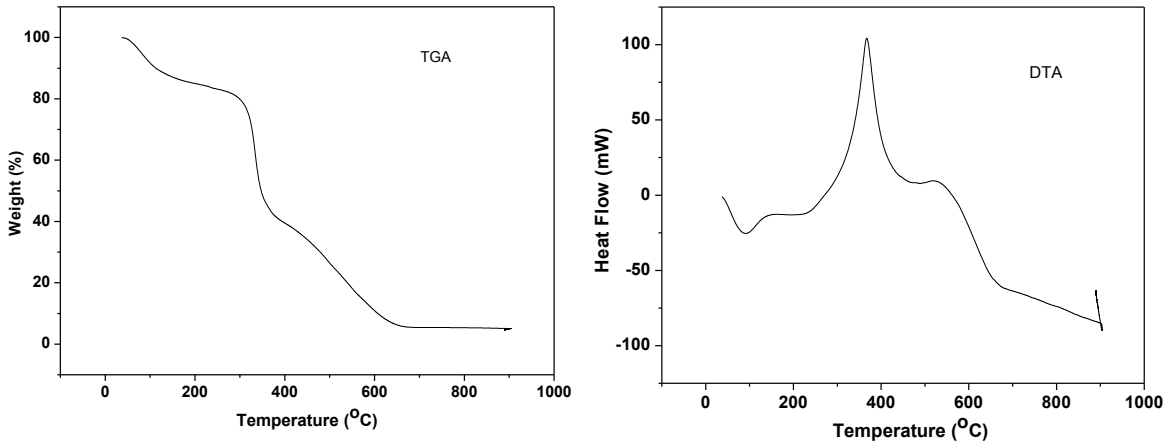

Figure 4.4 TGA/DTA curve of the PVP-Aluminium acetate as-spun nanofiber membrane.

The SEM images of as-spun PVP-aluminium acetate composite fibers and fibers sintered at 1000 °C have been shown in figure 4.5. It is observed from the figures that ultra-fine cylindrical composite fibers having diameter in the range of 200-600 nm can be successfully prepared using aluminium acetate as precursors (figure 4.5a, b). Pure Al_2O_3 ultra-fine fibers with smooth surface morphology have been obtained by sintering the above composite fibers as shown in figure 4.5 (c, d). It is observed from the figure that the fiber like structure in the as-spun composite membrane is fully retained in the sintered sample, with considerable decrease in fiber diameter.

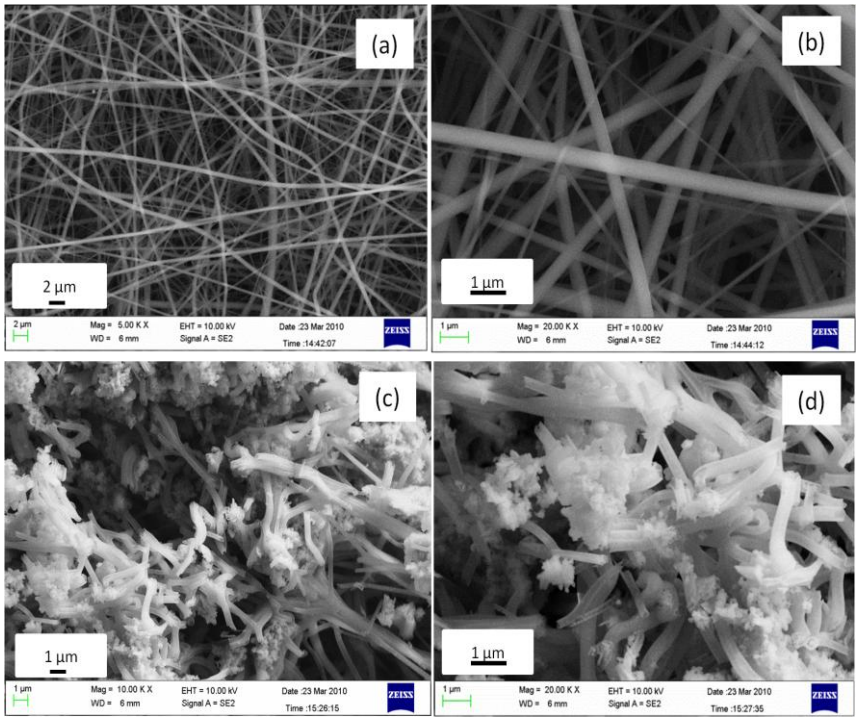

Figure 4.5 SEM images of (a, b) as-spun nanofibers of PVP-aluminum acetate precursor and (c, d) sintered at 1000 °C.

Figure 4.6 indicates the SEM images of alumina nanofibers obtained after sintering PVP-aluminium acetate composite fibers at 1000 °C. These figures indicate the formation of pure ultra-fine cylindrical Al_2O_3 fibers with smooth surface morphology. The diameter of alumina fibers (figure 4.6a) are found to be in the range of 200-600 nm. The SEM elemental detection X-ray analysis (SEM-EDAX) clearly suggest that the presence of aluminum and oxygen elements (figure 4.6 b). This result indicates the formation of pure alumina fibers. Figure 4.6c shows the SEM image of the alumina nanofibers after adsorption experiments. It is observed from the figure that the fiber like structure of alumina fibers was fully retained after adsorption studies without affecting the fiber morphology. The SEM-EDX of the alumina fibers after adsorption (figure 4.6d), suggests the presence of Al, Cr, and O. This result might be due to sorption of Cr ion the surface of alumina fibers.

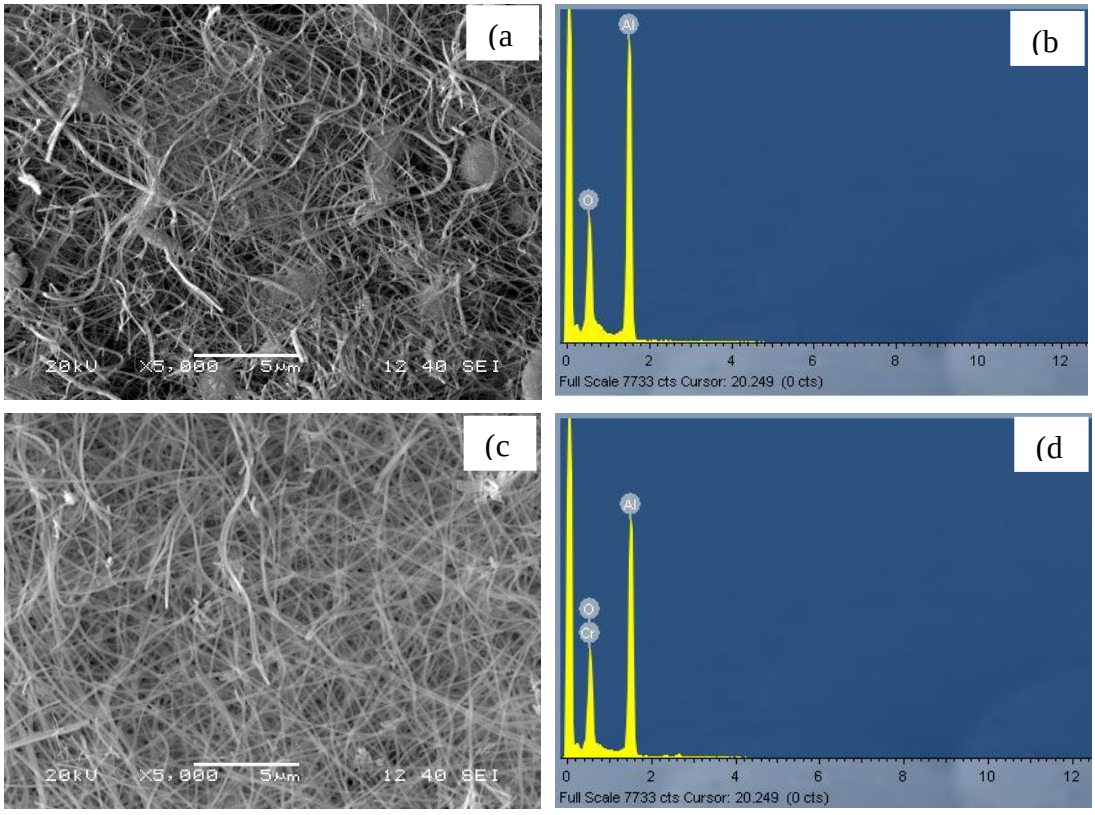

Figure 4.6 SEM images of alumina nanofibers (a) before adsorption, (b) EDX spectrum before adsorption, (c) alumina nanofiber after adsorption and (d) EDX spectrum after adsorption.

In order to obtain more information about the formation of individual Al_2O_3 ultra-fine fibers, we have carried out the TEM analysis. Fig. 4.7a shows the TEM microscopy of Al_2O_3 nanofibers after calcination at 1000^0C for 2 h at a heating rate of 20^0C/min. TEM microscopy (Fig. 4.7a) clearly indicates the formation of nano-sized fibers. Furthermore, it is observed

from the TEM studies that the diameters of nanofibers were not uniform, instead a broad range of fibers were formed (100-500 nm), which is also consistent with the fibers diameter observation by the magnified SEM microscopy. Figure 4.7b shows the selected area electron diffraction pattern of alumina nanofibers. The corresponding diffraction rings and bright spot on the electron diffraction pattern suggest that the alumina fibers obtained are highly crystalline in nature, which is also consistent with XRD results.

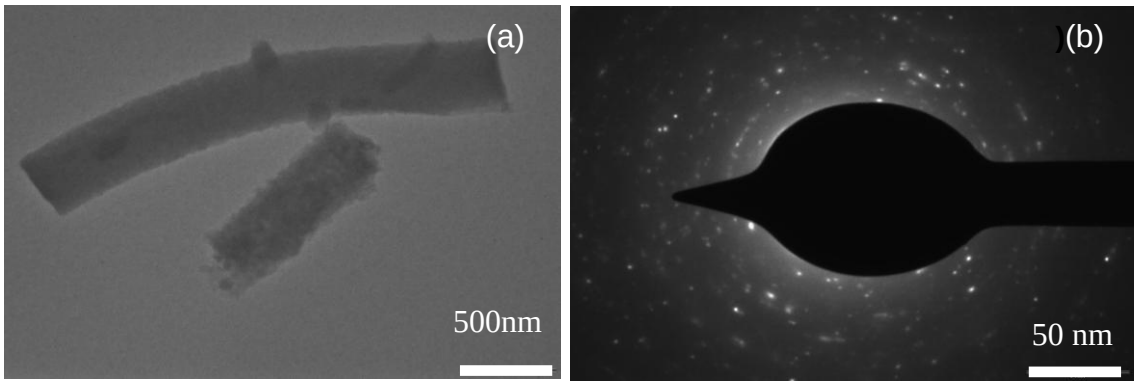

Figure 4.7 (a) TEM image and (b) Electron diffraction pattern of alumina nanofibers.

The surface area of the alumina fibers are found to be 40 m^2/g and are nonporous in nature as observed by BET studies.

4.4 Adsorption studies

4.4.1 Effect of pH on adsorption of Cr (VI) and Fluoride ions

The removal of Cr (VI) and fluoride ion from aqueous solution by alumina nanofiber adsorbents were studied by varying the pH of the solution over the range of 3-9 and the results obtained were shown in the figure 4.8. It is observed from the figure that the maximum adsorption of Cr (VI) on alumina nanofibers surface occurs at pH 5 whereas, in case of fluoride pH 7 shows maximum removal. Percentage removal efficiency increased from 38 % (pH 3) and reached 72% (pH 5). This result can be interpreted as follows. Depending on the solution pH values and concentration of Cr (VI) ions in solution, Cr (VI) species may be present in solution, as dichromate ($Cr_2O_7^{2-}$) hydrochromate ($HCrO_4^-$), or chromate (CrO_4^{2-}). In acidic environment (lower pH) the Cr (VI) is either exists as $HCrO_4^-$ or as $Cr_2O_7^{2-}$ and in alkaline environment predominately exists as CrO_4^{2-} ions (Selvi et al., 2001). Highly acidic conditions (pH 3) are not favorable due to competition between protons and anionic metallic species ($HCrO_4^-$) that explain weak adsorption. With increase in pH, the degree of protonation of anionic metallic species reduces gradually and the surface of the

alumina sorbent becomes positive as a result uptake of Cr (VI) ions increases. Hence, adsorption of Cr (VI) onto alumina surface increases at pH 5. Furthermore, increase in pH, there is competition between OH^- and chromate ions (CrO_4^{2-}), the former being the dominant species at higher pH values. The net positive surface potential of sorbent decreases, resulting in the weakening of electrostatic forces between sorbent and sorbate, which ultimately leads to reduced sorption capacity (Aklil et al., 2004, Naiya et al., 2009, Kwon et al., 2010). As maximum removal of Cr (VI) by alumina nanofibers was observed at pH 5 and no further significant change on adsorption capacity was noticed between pH 5 to 8; we have chosen pH 5 for all adsorption experiment of Cr (VI) ions. In case of fluoride ion the maximum removal percentage (50%) was observed at pH 7 as shown in figure 4.8. Fluoride adsorption may be due to the combined effect of both chemical and electrostatic interaction between the aluminium oxide surface and fluoride ion and also availability of active sites on the adsorbent surfaces (Mohapatra et al., 2011, Ruixia et al., 2002). At acidic pH, protonation creates positively charged alumina surface which attributed to a greater increase in the attractive force between positively charged surface and negatively charged fluoride ions. While at higher pH 9, adsorption percentage decreases. Here the efficiency decreases because the basic solution acquires negative charge in alkaline pH and there is repulsion between negatively charged alumina surface and fluoride ion. Here the negative hydroxyl ions also compete with fluoride ions leading to a decrease in its percentage removal. Whereas at highly acidic pH 3, the negatively charge fluoride ions are converted into hydrofluoric acid form and hence adsorption of fluoride onto the positively charge adsorbent surface decreases (Kamble et al., 2010, Maliyekkal et al., 2006).

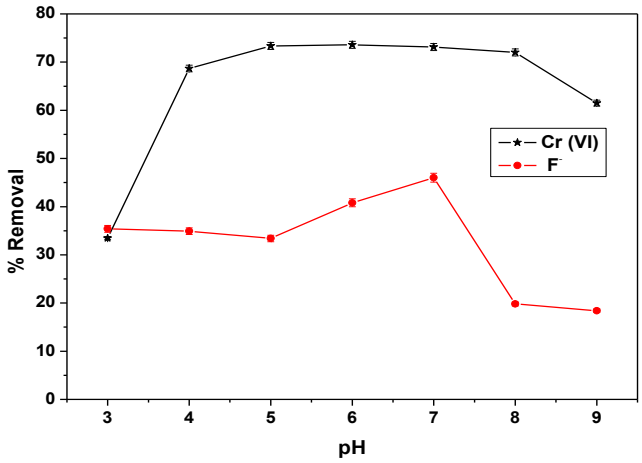

Figure 4.8 Percentage removal of Cr (VI) and fluoride by alumina nanofibers with variation in pH.

4.4.2 Effect of contact time on adsorption of Cr (VI) and Fluoride ions

The time of contact of adsorbate and adsorbent plays a significant role for the removal of pollutant species from aqueous solution during batch experimental studies. For determining the optimum time for complete removal of Cr (VI) and fluoride ions from the aqueous solution, we have carried out a number of adsorption experiments at different contact time from 0 min to 3 hours, keeping the initial Cr (VI) and fluoride ions concentration of 10 mg/L at pH 5 and pH 7 and adsorbent dose of 0.01 g and 0.1 g respectively. Figure 4.9 shows the effect of contact time on the adsorption of Cr (VI) and fluoride by alumina nanofibers. The result indicates that the adsorption rate reaches to the equilibrium after one-hour in case of both the ions. The percentage removal of Cr (VI) ions was found to be 70 %, whereas for fluoride ion it is 50% in 60 min of contact time. There was no significant change in equilibrium concentration from 1 h to 3 h contact time. Therefore, it is cleared that the adsorption of Cr (VI) and fluoride ions by electrospun alumina nanofibers is rapid and after 1 h complete adsorption equilibrium is obtained. In the figure 4.9 (b), the loading capacity is being plotted with change in time. This result indicates the sorption capacity of electrospun alumina nanofibers for Cr (VI) ion is 6.8 mg/g and for fluoride ion is 1.2 mg/g at equilibrium.

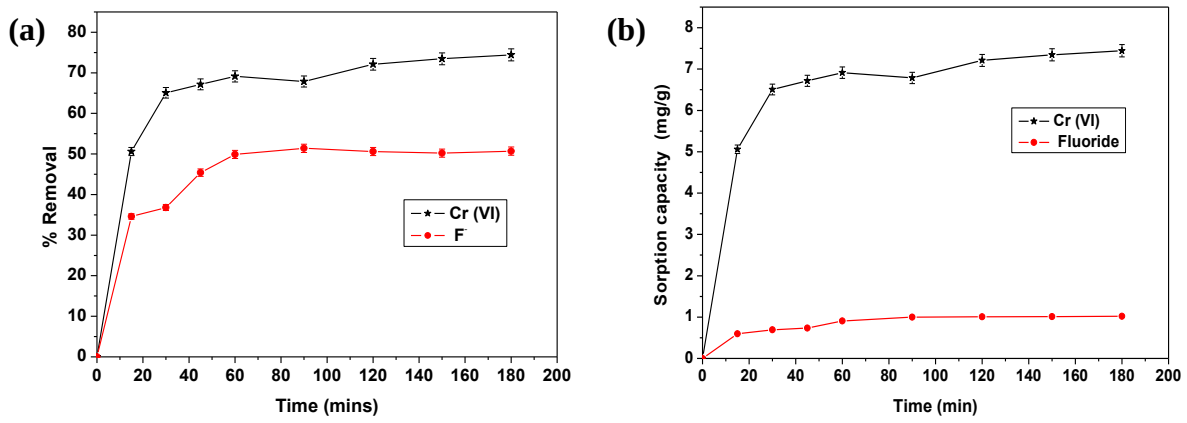

Figure 4.9(a) Percentage removal of Cr (VI) and fluoride ions as a function of time (min) by alumina nanofibers and (b) sorption capacity of alumina with time.

4.4.3 Adsorption kinetics

The study of adsorption kinetics is important as it provides valuable insight into the reaction pathways and the mechanism of adsorption. Adsorption mechanism depends on the physical and chemical characteristics of the adsorbent and also on the mass transfer process (Hameed et al., 2005). In this present work, we have studied the kinetics of the removal of Cr (VI) and fluoride ion for understanding the adsorption behavior of the alumina nanofiber. The

experimental data obtained are applied to pseudo-first order (Tseng et al., 2010) and pseudo-second order model (Ho Y.S., 2006) to clarify the sorption kinetics of Cr (VI) and fluoride ion onto alumina nanofiber surface. The pseudo-second order model can be expressed as follows:

$$\frac{dQ}{dt} = k_2 (q_e - q_t)^2 \qquad (2)$$

Where k_2 (g. (mg.min)$^{-1}$) is the rate constant of the pseudo-second order equation, q_e and q_t are the amount of solute adsorbed on the adsorbent at equilibrium and at time t, respectively. The integrated form of the above equation can be expressed as follows:

$$\frac{t}{q_t} = \frac{1}{k_2 q_e^2} + \frac{1}{q_e} t \qquad (3)$$

The value of q_e and k_2 can be determined by the slope and intercept of the straight line of the plot t/q_t versus t respectively (figure 4.10)

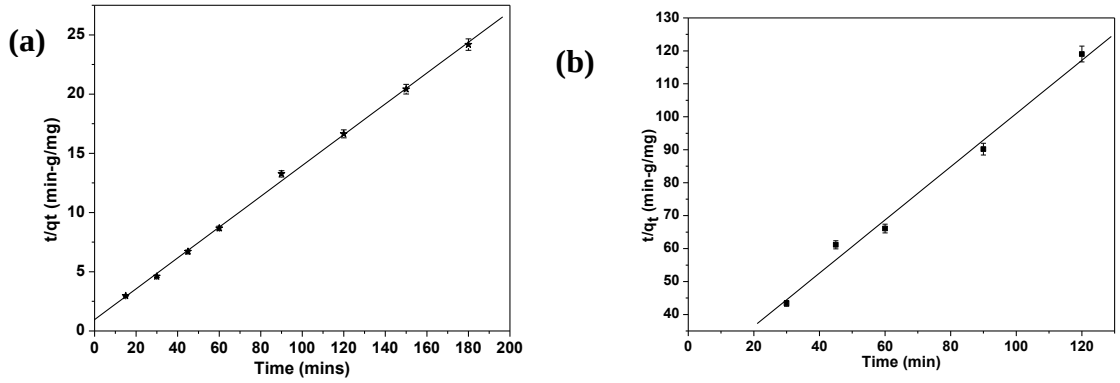

Figure 4.10 Pseudosecond-order plot for Cr (VI) and fluoride ion removal by alumina nanofiber.

Table 4.1 Values of Pseudo-second order kinetics parameters for removal of Cr (VI) and fluoride ions by alumina nanofiber

	Pseudo-second order reaction		
	K_2 min^{-1}	R^2	$Q_{e\,calc}$. mg/g
Cr(VI)	7.246	0.995	1
fluoride	0.032	0.988	1.239

The results obtained demonstrate a highly significant linear relationship for removal of Cr (VI) and fluoride ion on alumina nanofiber surface in table 4.1. The value of correlation coefficient (R^2 = 0.995, R^2= 0.9884) clearly indicates that the experimental data are in good agreement with pseudo-second order rate law based on adsorption capacity.

4.4.4 Effect of initial concentration on adsorption of Cr (VI) and fluoride ions

The effect of initial concentration on the adsorption of Cr (VI) and fluoride ion by alumina nanofiber were studied by varying the Cr(VI) and fluoride concentration from 10 mg/L to 100 mg/L for 1 hr contact time. Figure 4.11 shows the effect of initial concentration on the adsorption of Cr (VI) and fluoride ions by alumina nanofibers. We observed from this figure that the percentage removal of Cr (VI) increases with increase in initial concentration, the reason may be due to the availabilty of more number of Cr(VI) ions in the solution for sorption onto the available binding sites on the surface of alumina nanofiber adsorbent. The percentage removal of Cr (VI) increases from 70 % to 93% by increasing the initial concentration of the solution from 10 mg/L to 50 mg/L. Further increased in concentration of the initial solution (up to 100 mg/L), there is no further appreciable change in percentage removal is noticed. This is due to achievement of equilibrium and saturation of binding sites of the adsorbent surface (Dong et al., 2010, Jinhua et al., 2010). It is also observed from figure 4.11 that the percentage removal of fluoride ion decreases with increase in initial fluoride ion concentration. In this case, the percentage removal of fluoride ion was found to be 55 % at 10 mg/L and 42 % at 100 mg/L. This is probably due to the fact that for a fixed adsorbent dosage, the total available adsorption sites are limited, thereby adsorbing almost the same amount of fluoride (Tembhurkar et al., 2006).

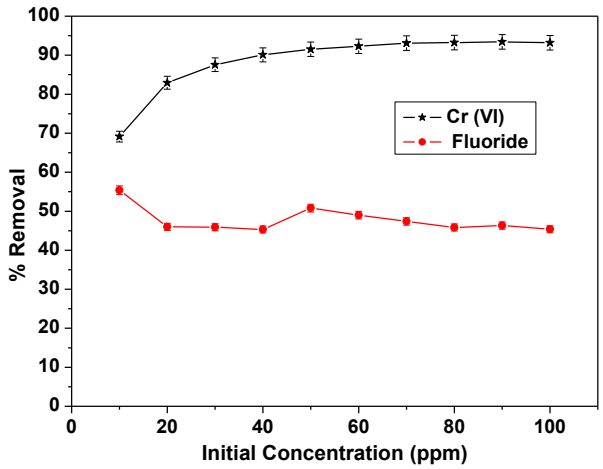

Figure 4.11 Percentage adsorption graph of Cr (VI) and fluoride ions with variation in concentration of metal ion by alumina nanofibers.

4.4.5 Adsorption isotherm

In order to describe the adsorption behavior of Cr (VI) and fluoride onto the alumina nanofiber surface, we have studied adsorption isotherms. The isotherm studies are conducted by varying the initial concentration of Cr (VI) and fluoride from 10 to 100 mg/L and maintaining the adsorbent dosage of 0.5 g/L and 5 g/L respectively. The equilibrium adsorption data obtained were analyzed using Langmuir and Freundlich isotherm models (Maliyekkal et al., 2006, Tor A., 2006, Sarkar et al., 2006). Langmuir adsorption isotherm model is based on the assumption of monolayer coverage of adsorbent surface, having a finite number of identical sites with equivalent energy. Therefore, the maximum adsorption corresponds to formation of a saturated monolayer of adsorbate molecule (Cr (VI) and fluoride ions) on the adsorbent surface. The Langmuir equation is represented as follow:

$$\frac{\boldsymbol{c_e}}{\boldsymbol{q_e}} = \frac{\mathbf{1}}{\boldsymbol{q_m b}} + \frac{\mathbf{1}}{\boldsymbol{q_m}}\boldsymbol{C_e} \qquad (4)$$

Where C_e and q_e are the concentration of adsorbate (mg/L) and amount adsorbed (mg/g) at equilibrium. q_m (mg/g) and b (L/mg) are the Langmuir constants and are related to adsorption capacity and energy of adsorption respectively. The equilibrium data obtained were also examined by Freundlich adsorption isotherm. This model is based on the assumption that adsorption of adsorbate molecules occurs on a heterogeneous adsorbent surface. This equation is employed to describe heterogeneous system and is characterized by the heterogeneity factor n. The equation is represented as follows:

$$\ln\ q_e = \ln K_F + (1/n) \ln C_e \qquad (5)$$

Where q_e is the amount of adsorbate adsorbed per specific amount of adsorbent (mg g^{-1}), C_e is equilibrium concentration (mg L^{-1}), K_f and n are Freundlich equilibrium constants. These constants K_f and n are incorporating factors affecting the adsorption process like adsorption capacity and intensity of adsorption. Figure 4.12 represents the liner plot of log q_e against log C_e. The values for the Freundlich constant and correlation coefficients (R^2) are calculated using Freundlich plot (figure 4.12) and are shown in table 4.2. The value of Freundlich coefficient 'n' fulfilled the condition $0 < n < 10$, this suggests that adsorption of Cr(VI) and fluoride on the surface of alumina fibers are favorable. Again from the correlation coefficient (R^2 = 0.998 and R^2= 0.997) it is observed that Cr (VI) and fluoride ion adsorption is better fitted for Freundlich adsorption isotherm. However, the equilibrium data are not fitted to

Langmuir isotherm model as shown in table 4.2, indicate the adsorption does not follows monolayer adsorption. Therefore uptake of Cr (VI) and fluoride ions preferably follows multilayer and heterogeneous adsorption process.

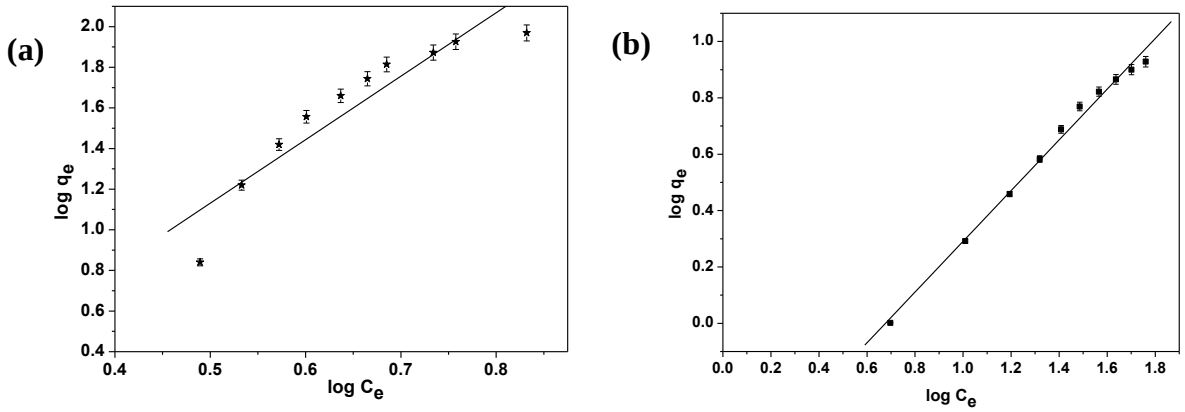

Figure 4.12 Freundlich isotherms for the adsorption of Cr (VI) and fluoride ion on alumina nanofiber.

Table 4.2 Values of Langmuir and Freundlich Constants for Adsorption of Cr (VI) and fluoride by alumina nanofiber

	Langmuir Isotherm model			**Freundlich Isotherm model**		
	q_m(mg/g)	b(L/mg)	R^2	K_F(mg/g)(L/mg)$^{1/n}$	n	R^2
Cr(VI)	14.36	6.563	0.462	0.649	0.319	0.866
fluoride	34.01	161.17	0.803	0.544	1.111	0.9925

4.4.6 Effect of adsorbent dosage on adsorption of Cr (VI) and fluoride ions

In order to study the effect of adsorbent dosage for removal of Cr (VI) and fluoride ions, we have carried out adsorption experiments by varying the amount of alumina nanofibers using 10 mg/L Cr (VI) and fluoride stock solution maintaining the contact time of 1 hr and pH of the solutions at 5 and 7 respectively. The results obtained are shown in figure 4.13.

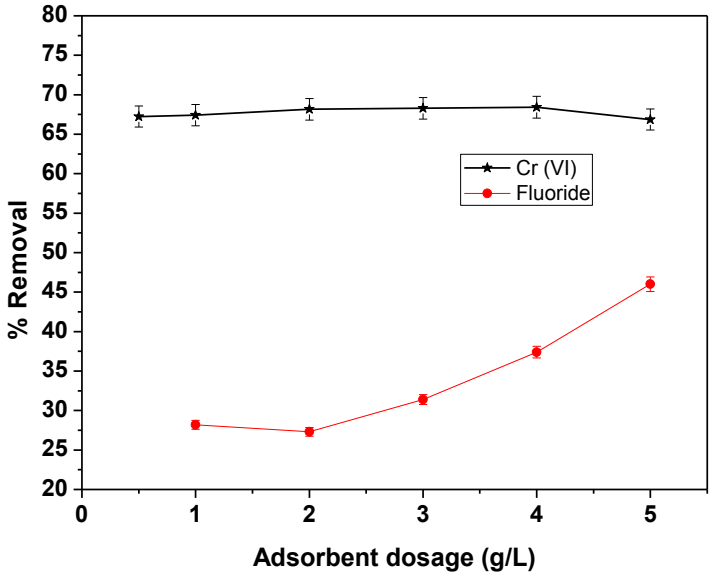

Figure 4.13 Percentage removal graphs of Cr (VI) and fluoride ions with variation in dosage (g/L) by electrospun alumina nanofibers.

It is observed from the figure 4.13 that with increase in adsorbent dosage from 0.5-5 g/L, there was no appreciable change in sorption of Cr (VI) ions. The percentage removal was found to be unchanged or maintained constant value even if more alumina nanofiber was added. From this result we concluded that 0.5 g/L of alumina nanofibers dosage is good enough for maximum removal of Cr (VI) ion present in 10 mg/L stock solution, and the maximum percentage removal was found to be about 70 % for Cr (VI) ions. In case of fluoride ion with increase in adsorbent dosage the percentage removal increases till 50 % maximum. The enhancement of adsorption in increase of dosage is due to availability of active binding sites and to the presence of a greater surface area for adsorption of fluoride. The results showed that alumina nanofiber was efficient for 50% removal fluoride ion at adsorbent dosage of 5 g/L of 10 mg/L stock solution and hence this dosage was selected for further studies (Chen et al., 2011).

4.5 Conclusions

Alumina nanofiber was synthesized by electrospinning of PVP and aluminium acetate salt precursors followed by calcination. The XRD, SEM, EDX and TEM characterization techniques confirmed the formation of pure nanosized alumina fibers. The diameters of the fibers are found to be in the range of 100-500 nm by TEM study. XRD analysis of the calcined fiber at 1000 °C confirms the formation of pure α-alumina phase. Batch experiments were performed for the removal of chromium (VI) and fluoride ions from aqueous solution,

by using alumina nanofiber as adsorbent materials. Adsorption characterization has been examined at different pH values, initial adsorbate concentrations, contact times, and adsorbent dosage. It was observed that the efficient removal of chromium (VI) and fluoride ions was achieved at pH 5 and 7, respectively. The maximum removal was found to be 70 % for Cr (VI) and 50 % for fluoride ions. Furthermore, in the case of chromium (VI), with an increase in the initial concentrations, the percentage of adsorption increases because of an increase in the number of adsorption sites. The maximum uptake of chromium (VI) and fluoride ion onto alumina nanofiber surface were found to be 6.8 and 1.2 mg/g, respectively. Adsorption equilibrium was attained within a short contact time of 1 hr, and the adsorption kinetics was governed by pseudo-second-order rate law. The isotherms studies indicate that the adsorption of chromium (VI) and fluoride ion onto alumina nanofiber surface was successfully fits to Freundlich isotherm model over all concentration range studied, which shows heterogeneous adsorption process.

CHAPTER 5

SYNTHESIS OF MIXED Fe_2O_3-Al_2O_3 NANOCOMPOSITES FOR ADSORPTIVE REMOVAL OF CONGO RED DYE

5.1 Introduction

Nanocomposite is a special nanostructure, consisting of two or more different materials present in some form and its dimension fall in nanometer range in atleast one direction. Nanocomposites materials can be broadly classified into three main categories that have implications in preparation techniques. They are inorganic-inorganic, inorganic-organic and organic-organic nanocomposites (Chronakis et al., 2005, Hussain et al., 2006). The synthesis of nanosized composite particles with controlled morphology and improve properties are important in many critical areas of modern research (Davis et al., 2003). Now-a-days, researchers are much more interested in mixed metal oxide (inorganic-inorganic) nanoparticle because of its broad class of catalytic, electronic, magnetic properties and also for its heterogeneous catalysis (Wang et al., 2007).

Recently, Dong et al. (2011) have synthesized iron oxide and alumina nanocomposite (Fe_2O_3-Al_2O_3) with a unique structure, which shows a remarkable catalytic performance in Fischer-Tropsch synthesis. These nanoparticles often exhibit superior properties and performance; it is because of its large specific surface area. Among various metal oxides the oxides of aluminium (Al) and iron (Fe) have large advantages because of their low cost, extensive availability, thermal stability and remarkable adsorption capacity (Wu et al., 2012, Masue et al., 2007). Violante et al. (2003) have studied on the adsorption of heavy metal ions on mixed Fe-Al oxides in absence or presence of increasing concentrations of oxalate or tartrate. Ground water and surface water pollution is a serious problem due to its high toxicity for the presence of dyes and organic waste. Among them Congo red dye is an important source of water pollution and a known human carcinogen (Chiou et al., 2004). Different process have been used to remove Congo red from colored effluents but among all, adsorption has been recognized as the most popular treatment process due to its simplicity, high efficiency, easy

recovery and the reusability of the adsorbent (Chatterjee et al., 2010, Kim et al., 2004, Darzi et al., 2009). Similarly, Gong et al. (2009) studied the removal of cationic dyes from aqueous solution using magnetic multi-wall composite carbon nanotube as adsorbent. Adsorption characteristics of the nanocomposite adsorbent were examined using methylene blue, neutral red and brilliant cresyl blue as adsorbates. Template-free hydrothermal synthesis of hierarchical spindle-like γ-Al_2O_3 materials was prepared and its removal affinity towards organic and inorganic pollutants was studied (Cai et al., 2010). During synthesis three different aluminium precursors were taken i.e. aluminium chloride, aluminium nitrate and commercially available boehmite. By maintaining a molar ratio between urea and aluminium precursor, 3.5:1, the hydrothermal reaction was carried out at 180°C. Adsorption studies of Congo red, phenol; Cd (II) and Cr (VI) were carried out by batch experiments using γ-Al_2O_3 adsorbents. On further comparison of adsorption capacity between three adsorbents, it was found that the sample prepared by commercially available boehmite shows very less adsorption capacity as compared to the other two samples. Adsorption capability of cadmium oxide nanostructure has also been investigated by Tadjarodi et al. (2012). Cadmium chloride monohydrate and ammonium oxalate monohydrate were used as the precursor with a molar ratio of 1:1. With addition of sodium hydroxide in the above solution alkaline pH was maintained and hydrothermal reaction was carried out at 160°C for 24 h. The resulting product was calcined at 450 °C for 2 h in air. The CdO formed were of rhombus-shaped with an average size of 29 nm. Moreover, these CdO nanostructures were used for Congo red removal study, which shows 99% removal in high concentration (5-50 ppm), with an adsorption capacity of 41.2 mg g^{-1}. Wu et al. (2005) have studied on magnetic powder MnO-Fe_2O_3 composite as a novel material for the removal of azo-dye i.e., acid red B from water. MnO-Fe_2O_3 composite were prepared by co-precipitation method, with different molar ratios of Mn: Fe. Maximum adsorption was shown in acidic range and adsorption capacity increases with increase in iron content in the mixed composite. The maximum adsorption capacity was found to be 105.3 mg g^{-1} at pH 3.5. These magnetic composite can be conveniently recovered by magnetic separation technology. Salehi and co-workers, (2010) have synthesized a novel biocompatible composite of chitosan–zinc oxide nanoparticle. Further, adsorption studies was also carried out for removal of two textile dyes i.e., direct blue 78 and acid black 26 using chitosan-zinc oxide nanocomposite as adsorbent. Maximum removal was observed at pH 2 and also the adsorption capacity was found to be 92 and 95.2 mg g^{-1} in case of acid black 26 and direct blue 78 respectively. Recently, Wang et al. (2011) prepared a graphene based magnetic Fe_3O_4 nanocomposite for effective removal of organic dye fuchsine from aqueous

solution. The adsorption equilibrium was attained with a short time of 30 min for 100% removal. Maximum adsorption capacity was found to be 89.4 mg/g.

In the present study, iron oxide-alumina mixed nanocomposite was prepared by hydrothermal method and their adsorption characteristic for the removal of Congo red dye from aqueous solution was studied. Synthesized mixed oxy-hydroxide sample was sintered at different temperatures to obtain mixed oxides nanocomposites. The adsorption experiments such as effect of contact time, pH, adsorbent dose and initial concentration variation were explored in batch experiments. The adsorption isotherm and kinetic studies were also carried out to elucidate the adsorption mechanism. A comparative study for maximum removal capacity of using different mixed oxide nanocomposite adsorbents was also reported here.

5.2 Experimental section

5.2.1 Materials

Ferrous sulphate ($FeSO_4.7H_2O$) and aluminium nitrate ($Al(NO_3)_3 \cdot 9H_2O$) of analytical grade with purity 99.0% was obtained from Merck, India. Both NaOH pellets and NH_3 solution were also obtained from Merck, India. All chemicals were used without further purifications. Double distilled water was used throughout the experiments for preparation and dilution of the solutions.

5.2.2 Synthesis of Fe_2O_3 –Al_2O_3 nanocomposites

In this work, Fe_2O_3-Al_2O_3 nanocomposites were prepared by hydrothermal method. The $Al(NO_3)_3 \cdot 9H_2O$ and $FeSO_4.7H_2O$ salts were taken in a molar ratio of 1:1 and were mixed in a 50 ml distilled water. Then the mixed solution was stirred vigorously. At the same time, a mixed precipitant was prepared by adding 25 ml of 2M NH_3 solution into 25 ml of NaOH solution so as to maintain a ratio of 1:1. The mixed precipitant was added drop wise to above mixture solution with vigorous stirring. Simultaneously, the pH of the solution was measured using pH meter. At pH 5.6 green precipitate was formed. The formation of precipitate in the whole mixture solution was transferred into a 100 ml teflon cupped pressure pot. The pressure pot was sealed and kept in an electric oven at 180°C for 6 h. After that the pressure pot was cooled at room temperature and the resultant product was centrifuged, washed with deionized water several times and dried at 50°C for 5-6 h followed by grinding. The obtained deep yellow powder was further calcined at 500°C and 1000°C, to form mixed Fe_2O_3-Al_2O_3 nanocomposite.

5.2.3 Characterization techniques

Scanning electron microscope (JEOL JSM-5300) was used for surface morphology characterization of iron oxide-alumina mixed nanocomposite which was operated at 15 kV. SEM was equipped with Oxford INCA energy dispersive X-ray analyser system (EDAX). In order to increase the conductivity of the samples, they were gold coated using a JEOL FRC 1200 fine coater before taking SEM. The powder X-ray diffraction patterns were obtained on a Pan analytical X-ray diffractometer (PW1830) using Cu Kα (λ = 1.541 Å) radiation. A JEOL 200 HR-TEM was used to characterize the iron oxide-alumina mixed nanocomposite materials, operated at 200 kV. The mixed nanocomposites were dispersed in ethanol and then a drop of the above dispersion was taken on a carbon coated copper grid (300 meshes) for HR-TEM imaging. A digital pH meter (Satorius Model PB-11) combined with glass electrode was used for all experiments. A Shimadzu UV-Visible spectrophotometer (Shimadzu-2450) was used for adsorption study of Congo red dye.

5.2.4. Adsorption experiments for Congo red dye by batch process

The unsintered and sintered mixed iron oxide-alumina nanocomposites samples were used as adsorbent for removal of organic dye pollutants. The adsorption study was carried out by taking 100mg of powder samples into 10ml of Congo red ($C_{32}H_{22}N_6O_6S_2Na_2$) solution (100 mgL^{-1}) under stirring condition. The adsorption study was carried out with change in different parameters viz. variation in time, pH, and initial concentration of Congo red. After appropriate time of stirring, the solution was filtered using whatman-40 filter paper and further it was centrifuged for fine removal of dispersed nanoparticle, and finally analyzed by UV-Visible spectrophotometer. The adsorption experiments have been conducted three times and the data are presented in the figures with an appropriate error bars. The error bars are found to be within ±3%.

5.3 Result and discussion

5.3.1 Structural properties

We have used hydrothermal method for preparation of iron-aluminium mixed oxide nanocomposite powder. The obtained powder was sintered at different temperatures and the formation of different phases was confirmed by XRD study. Figure 5.1 shows the XRD pattern of iron oxide-alumina mixed nanocomposite. This result revealed that the formed materials are crystalline in nature. Figure 5.1(a) shows XRD pattern of the as prepared mixed nanocomposite. It is observed from the XRD data that the hydrothermal mediated synthesis

of as prepared samples consists of mixture of boehmite (γ-AlOOH) and goethite (γ-FeOOH) phases, which is confirmed from the JCPDS Files (File no.84-0175) and (File no. 77-0247) respectively. The obtained mixed oxy hydroxide phases of iron-aluminium nanocomposite were sintered at 500°C and 1000°C in air for 2 h. Figure 5.1(b) and 5.1(c) represent the XRD pattern of Iron oxide-alumina nanocomposites obtained on sintering the as prepared mixed oxy-hydroxide at 500°C and 1000°C, respectively. It is also observed from the XRD data that the sintered sample contains the mixture of iron and aluminum oxides. The 2θ values of mixed oxides formed after sintering the sample at 500°C found to match with (JCPDS File no 89-8104) and (JCPDS File no 29-0062), this result confirmed the formation of mixed γ-Fe_2O_3-Al_2O_3 nanocomposite. Similarly, the formation of mixed α-Fe_2O_3-Al_2O_3 phase was obtained after sintering the as-prepared sample at 1000°C, which was confirmed from XRD pattern (Figure 5.1(c)).

The surface morphology of iron-alumina oxide mixed nanocomposites has been studied by scanning electron microscopy method. Figure 5.2 represents the SEM and EDAX analysis of mixed nanocomposites obtained by hydrothermal synthesis of as-prepared and sintered samples. It is observed from the SEM images that the as-prepared samples (figure 5.2 a) are rod shaped and are in the size range of 100-300 nm. It is also observed that the rod like morphology of mixed nanocomposites is retained after sintering the as prepared samples at higher temperature. The presence of Fe, Al and O elements in the mixed composite were confirmed by the EDAX spectrum (figure 5.2d).

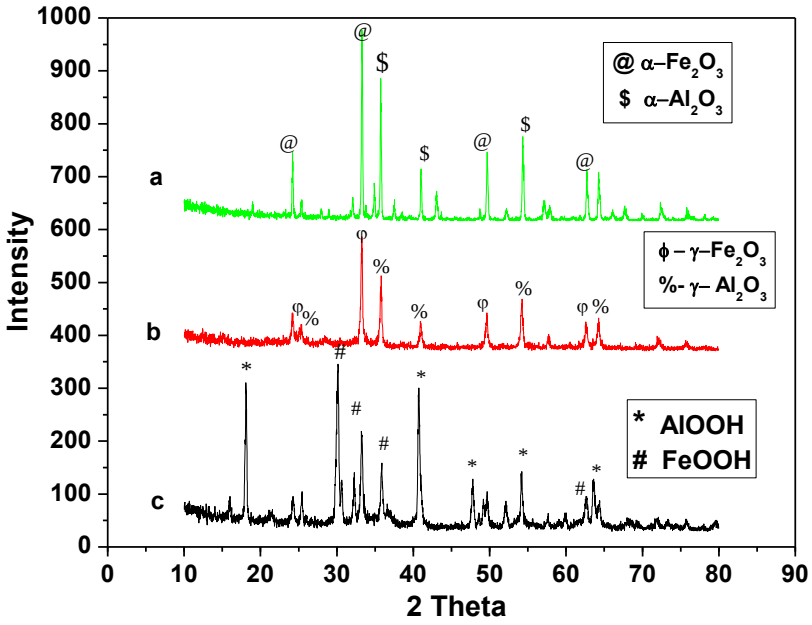

Figure 5.1: XRD data of (a) unsintered mixed oxy-hydroxide nanocomposite, (b) mixed oxide sintered at 500 °C, (c) mixed oxide sintered at 1000 °C.

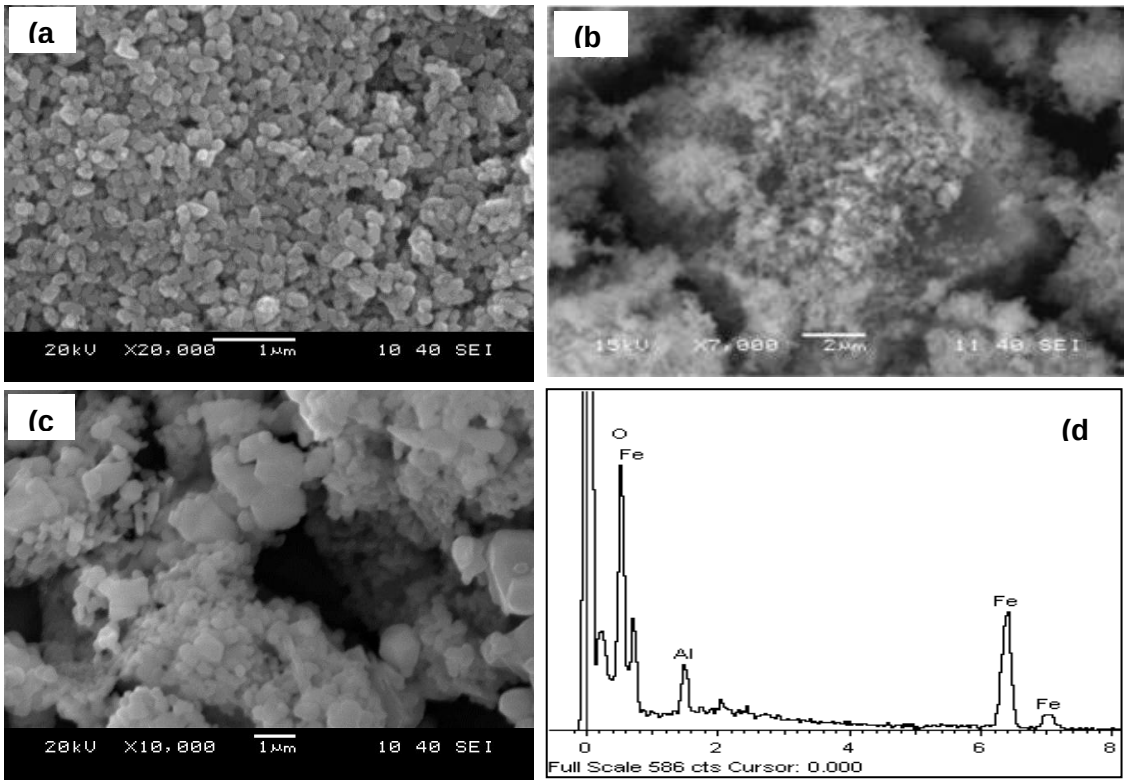

Figure 5.2: SEM image of (a) mixed FeOOH and AlOOH nanocomposite, (b) mixed γ-Fe_2O_3 and γ-Al_2O_3 nanocomposite sintered at 500 °C, (c) mixed α-Fe_2O_3 and α-Al_2O_3 sintered at 1000 °C, (d) EDAX image of mixed iron oxide and alumina nanocomposites.

In order to obtain more information about the formation, morphology and dimensions of mixed oxide nanocomposite, we have carried out the HRTEM imaging. Figure 5.3a shows the HRTEM image of Fe_2O_3-Al_2O_3 mixed oxide nanocomposite sintered at 500 °C. It was observed from the HRTEM imaging that the nanoparticle formed were not having uniform size; instead a size range from 100-300 nm was found. Figure 5.3 b shows the selected area diffraction pattern of mixed oxide nanocomposites. The corresponding diffraction rings and bright spot on the electron diffraction pattern indicate the formation of highly crystalline Fe_2O_3-Al_2O_3 mixed oxide nanocomposite, which is also consistent with XRD results.

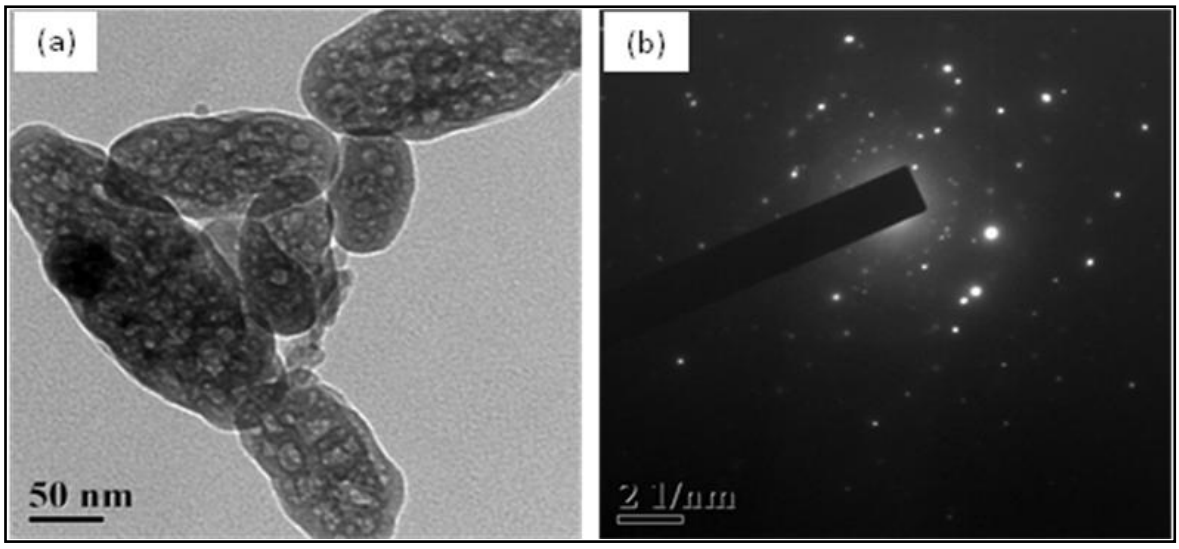

Figure 5.3: HRTEM image of (a) mixed γ-Fe_2O_3 and γ-Al_2O_3 nanocomposite sintered at 500 °C, and (b) SAED image of mixed oxide nanocomposite.

5.3.2 UV-Vis adsorption spectroscopy analysis

Figure 5.4(a) shows the UV-Vis absorption spectrum of iron-alumina mixed oxide nanocomposite prepared by hydrothermal method and sintered at different temperatures. Optical band gap is also measured using UV-Vis spectra analysis. The spectral absorption coefficient, α, is defined as

$$\boldsymbol{\alpha(\lambda) = 4\pi k(\lambda)/\lambda} \qquad (1)$$

Where *k(λ)* is the spectral extinction coefficient obtained from the absorption curve and λ is the wavelength. The band gap, E_g, is obtained by fitting the experiment absorption data with the following equation

$$\boldsymbol{(\alpha h\nu)^2 = A(h\nu - E_g)} \qquad (2)$$

Where hν is the photon energy, α is the adsorption coefficient, E_g is the band gap, and A is a characteristic parameter independent of photon energy. The value of band gap E_g has been obtained from the intercept of the extrapolated linear part of the $(\alpha h\nu)^2$ versus hν curve with the energy (hν) axis (Kharlamova et al., 2008, Gangwar et al., 2011). The band gap for mixed oxy hydroxide nanocomposte is 1.9 eV, for gamma phase the band gap is 1.7eV and the alpha phase mixed oxide nanocomposite has band gap value 1.95 eV as shown in Figure 5.4 (b). The value of band gap shows that all of the mixed oxide nanocomposites are semiconductor in nature with narrow band gap even after sintering at different temperature.

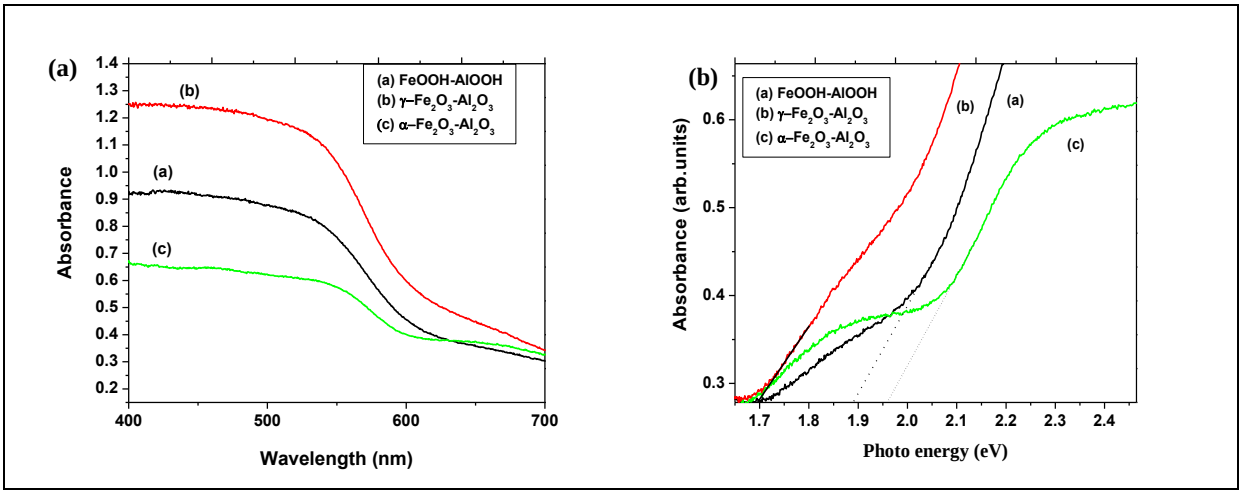

Figure 5.4: UV-Vis analysis of (a) mixed FeOOH and AlOOH nanocomposite, mixed γ-Fe_2O_3 and γ-Al_2O_3 nanocomposite sintered at 500 °C, mixed α-Fe_2O_3 and α-Al_2O_3 sintered at 1000 °C, (b) optical property of all the samples.

5.4 Adsorption study of Congo red by mixed nanocomposites

The FeOOH-AlOOH and Fe_2O_3-Al_2O_3 mixed nanocomposites prepared by hydrothermal synthesis method has been used for removal of Congo red dye from aqueous solutions. We had carried out the adsorption process by batch experiments using 25 ml of neat and cleaned capped glass bottles. The colour photograph of Congo red dye molecules before and after adsorption studies using both un-sintered (FeOOH-AlOOH) and sintered (Fe_2O_3-Al_2O_3) mixed nanocomposite materials are shown in figure 5.5. The adsorption experiments have been conducted three times and the data are presented in the figures with an appropriate error bars. The error bars are found to be within ±3%.

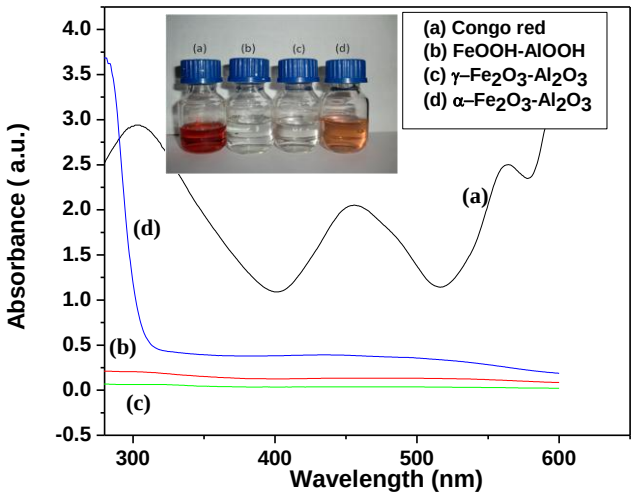

Figure 5.5 UV-Vis absorption spectra of Congo red solution and after being treated by three different samples, the initial concentration of Congo red are 100 mg/L. (a) before adsorption, after adsorption by 0.1 g (b) un-sintered, (c) sintered at 500 °C and (d) sintered at 1000 °C mixed iron oxide and alumina nanocomposite, in 15 min at pH 7.

5.4.1 Effect of pH on adsorption of Congo red dye

The pH values of dye solutions affect the chemistry of both the dye molecules and the adsorbent materials. Simultaneously, the pH of dye solution plays an important role in the whole adsorption process and also on the adsorption capacity. Original pH of Congo red solution (100 mg L^{-1}) is about 7.5. It was seen that the dye solution changes its colour from red to dark blue when pH was adjusted in highly acidic range and becomes dark blue in highly basic range i.e. pH 9 and above (Acemioglu et al., 2004, Wang et al., 2012). Therefore, the range of pH for Congo red adsorption was kept in the range of 3 to 8. The pH of the solution was adjusted by using 0.01 mol L^{-1} HCl or NaOH solutions. The graph of Congo red adsorbed with change in pH of the solution is shown in figure 5.6. From the figure it was observed that the percent removal of Congo red, has no effect on the pH of the solution and therefore we have carried out all the adsorption experiment at neutral pH 7. It was also observed that percentage removal of Congo red by both sintered and un-sintered samples with different pH have almost same values. But the sample sintered at 1000°C showed less removal percent as compared to the oxy-hydroxy sample and the sample sintered at 500 °C. FeOOH-AlOOH nanocomposite shows better adsorption as compared to α-Fe_2O_3-Al_2O_3, it can be explained that there is a large proton on the surface of the nanocomposite, which brings out larger adsorption capacity of Congo red, compared with that of the α-Fe_2O_3-Al_2O_3 mixed oxide nanocomposite (Fei et al., 2011). Zhua et al. (2011) studied that Congo red

anions in acidic and neutral solutions were easily adsorbed to Fe_3O_4 with positive surface charge but at higher pH values, Congo red anions were generally excluded away from the negatively charged surface of adsorbent, thus decreasing in percent removal of Congo red.

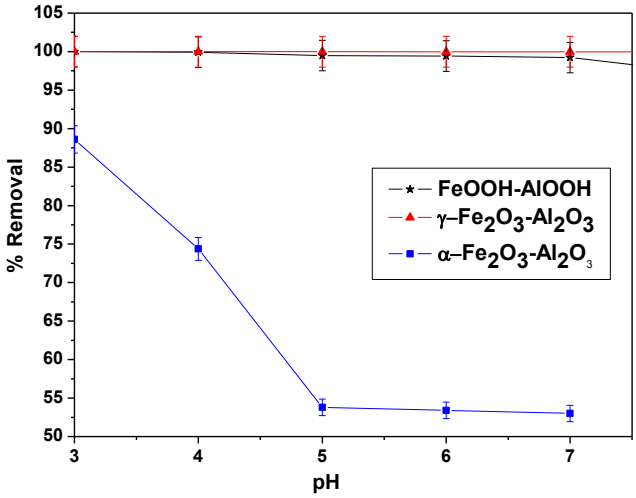

Figure 5.6: Effect of pH on percentage removal of the Congo red dye.

5.4.2. Effect of Contact time on adsorption study on Congo red dye

The effect of contact time on the adsorption of Congo red was studied to determine the time taken by samples to remove 100 mgL^{-1} Congo red solutions. 0.1 g of the sample was added into a 10 mL of 100 mg/L Congo red solution. The variation of Congo red adsorbed with time is shown in the figure 5.7. It was observed from the figure that the adsorption of Congo red by fixed amount of γ-Fe_2O_3-Al_2O_3 (sintered at 500°C) nanocomposite increases with increase in time and complete removal of Congo red dye was achieved after 15 min contact time. This is because, a large number of vacant surface sites were available for adsorption during initial stage. However, with a lapse of adsorption time, the remaining vacant surface sites were difficult to be occupied due to repulsive forces between Congo red adsorbed on the surface of sample (Zhua et al., 2011, Cai et al., 2012). The concentration of Congo red in the solution was measured spectrophotometrically at 498 nm. The decrease in concentration of Congo red with time determines its adsorption onto the adsorbent surface. It was observed that within 15 min contact time, there was 100% removal of Congo red shown by both the oxy-hydroxide nanocomposite and the gamma mixed oxide nanocomposites. But in case of mixed α-Fe_2O_3-Al_2O_3 the adsorption capacity decreases as this is associated with loss of water of hydration and oxy-hydroxyl group in the crystalline structure. Thus mixed γ-Fe_2O_3-Al_2O_3 and oxy hydroxide of iron and aluminum nanocomposite showed better adsorption as compared to α-Fe_2O_3-Al_2O_3 mixed nanocomposite.

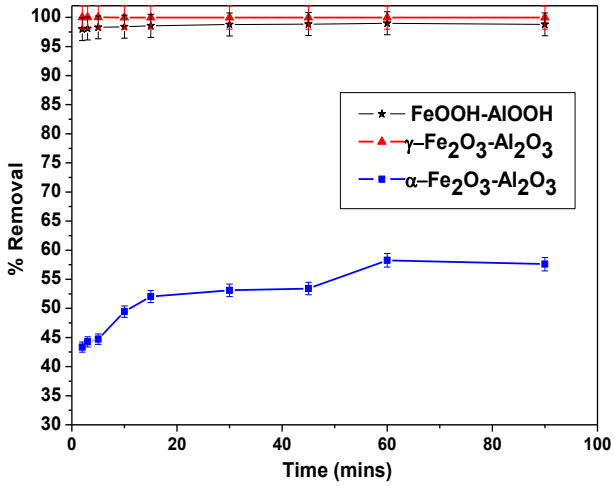

Figure 5.7 Effect of contact time on removal of the Congo red dye.

5.4.3. Effect of initial concentration on adsorption study of Congo red dye

The variation of Congo red adsorbed with concentration of the solution is shown in figure 5.8. It was observed from this figure that, the percent removal of Congo red onto the as prepared FeOOH-AlOOH and γ-Fe_2O_3 -Al_2O_3 nanocomposites is maximum and the value remain unaltered with increase in concentration of Congo red. It is also observed that within very short span of contact time both cases the adsorption attain the equilibrium value. It may be due to Congo red can absorb onto the metal oxide surface by coordination effect between metal ions and amine groups at the ends of Congo red molecules (Abd El-Latif et al., 2010, Yu et al., 2008). In case of mixed γ-Fe_2O_3-Al_2O_3 nanocomposites possesses water of hydration which form complexation via hydrogen bonding between the hydroxyl group and amine group of Congo red molecule for better adsorption of dye molecules on the surface. After sintering at higher temperatures the metastable γ-Fe_2O_3-Al_2O_3 phase gets converted into α-Fe_2O_3-Al_2O_3 and the removal capacity decreases as the availability of binding sites decreases as compared to that of oxy-hydroxy form and gamma mixed oxide. Thus among the three adsorbent materials γ-Fe_2O_3-Al_2O_3 can be considered as the most efficient adsorbent.

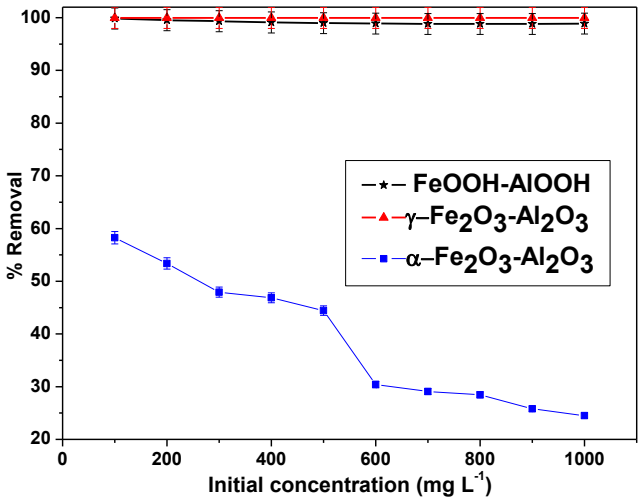

Figure 5.8 Effect of initial concentration on percentage removal of the Congo red dye.

We have also studied the dye removal capacity and rate of adsorption by varying the adsorbent doses. In case of Congo red removal onto metal oxide surfaces, electrostatic attraction is the cause behind adsorption (Lu et al., 2010, Huang et al., 2005), but when the amount of dye is more and the dose increases, the unsaturated bonds gets agglomerated within itself, and removal takes place. So to get the exact value of highest removal capacity, minimum amount of dose is taken while other experimental conditions remain the same. Figure 5.9 shows the adsorption rate by gamma mixed oxide nanocomposite in a solution of 10 ml and 100 mg L^{-1} of Congo red where mass of the sample is 0.002 g. Similarly the Congo red removal percentage becomes 100%, when the mass of adsorbent is 0.002 g where as it is less in case of adsorbent having 0.001 g. The results are presented in figure 5.9. The rate of adsorption of Congo red markedly slowed down due to small amount of porous structure. But the adsorption capacity reached 498 mg g^{-1} for 0.002 g of adsorbent in 60 min, with a removal percentage of 90 % of Congo red. For further confirmation we have kept the solution for overnight after 2 h of stirring. It was observed that the solution become clear and the deep red colour adsorbent was settled down at the bottom of the beaker. Thus, based on the above experimental result, it is concluded that the physical adsorption is responsible for decolorization of the dye and the oxidative degradation may also plays a secondary role in the whole process (Lu et al., 2010).

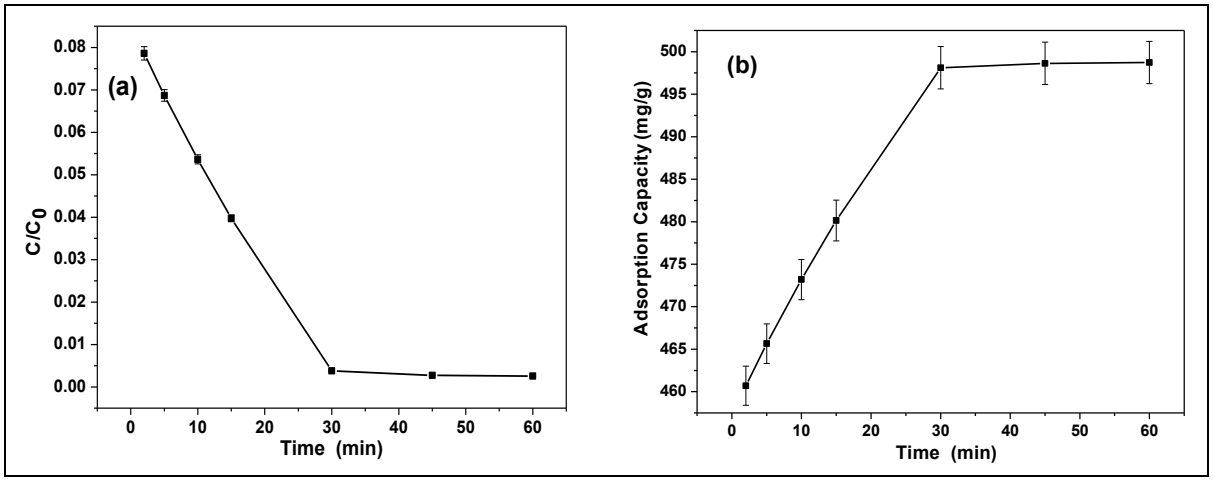

Figure 5.9: (a) Adsorption rate and (b) adsorption capacities of mixed nanocomposite for Congo red (100 mg L^{-1}, 10 ml) where mass of the sample were 0.002 g.

5.4.4. Adsorption isotherm study of Congo red dye

To describe the adsorption behaviour of Congo red onto the three different phases of iron-alumina mixed oxide nanocomposite, we have studied adsorption isotherms. The isotherm studies were carried out by varying the initial concentration of Congo red from 100 to 1000 mg/L and maintaining the adsorbent dosage of 0.1 g/L. An adsorption isotherm is an invaluable curve which describes the process governing the release or mobility of a substance from the aqueous porous media to a solid-phase at a constant temperature and pH (Limousin et al., 2007). The amount of dye adsorbed at equilibrium q_e (mg/g) was calculated from the following equation:

$$\boldsymbol{q_e = \frac{(C_o - C_e)v}{m}} \qquad \textbf{(3)}$$

where C_0 (mg/L) is the initial dye concentration, *Ce* (mg/L) the equilibrium concentration of dye solution, *v* (L) the volume of dye solution, *m* (g) is the mass of adsorbent.

The equilibrium adsorption data obtained were analyzed using Langmuir and Freundlich isotherm models, which are represented by the following equations, respectively:

$$\boldsymbol{\frac{C_e}{q_e} = \frac{1}{bq_m} + \frac{C_e}{q_m}} \qquad \textbf{(4)}$$

$$q_e = K_f C_e^{1/n} \qquad \textbf{(5)}$$

A linear form of the Freundlich isotherm can be obtained by taking logarithms of Eq (3):

$$\log q_e = \log K_f + \log C_e \qquad \textbf{(6)}$$

where q_m (mg/g) and b (L/mg) are Langmuir isotherm coefficients. The value of q_m represents the maximum adsorption capacity. K_f (mg/g) and n are Freundlich constants.

The Langmuir isotherm theory assumes monolayer coverage of adsorbate over a homogenous adsorbent surface and so the Freundlich isotherm is used to describe the surface heterogeneity of the sorbent (Bulut et al., 2008, Allen et al., 2004). It considers multilayer adsorption with a heterogeneous energetic distribution of active sites, accompanied by interactions between adsorbed molecules. Figure 5.10 shows the Langmuir and Freundlich isotherm. Experiments on removal of Congo red dye by mixed oxide nanocomposites. The parameters of both the isotherms data are listed in table 5.1. Here we observed that, oxy-hydroxide phase obeys Freundlich isotherm more than Langmuir isotherm. Similarly, in the case of gamma mixed oxide nanocomposite it slightly obeys Langmuir and perfectly fits for Freundlich isotherm. But in case of α-Fe_2O_3-Al_2O_3 mixed oxide nanocomposite it obeys Langmuir isotherm.

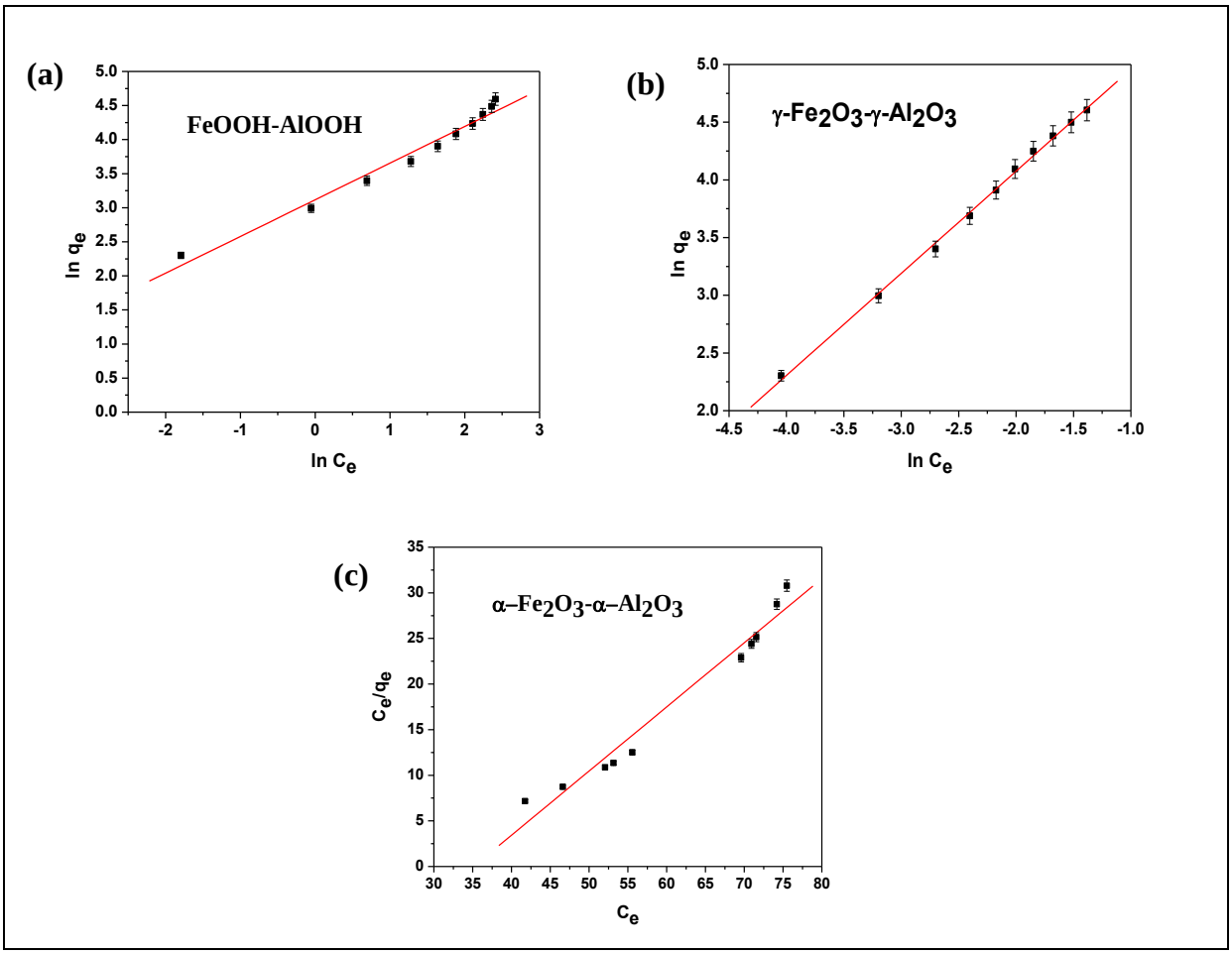

Figure 5.10 Langmuir and Freundlich isotherm as obeyed of all the three different phases (a) FeOOH-AlOOH, (b) γ-Fe_2O_3-Al_2O_3 and (c) α-Fe_2O_3-Al_2O_3 of mixed oxide nanocomposite.

Table 5.1 Adsorption isotherm parameter of mixed oxide nanocomposite.

	Langmuir Isotherm model			**Freundlich Isotherm model**		
	q_m(mg/g)	b(L/mg)	R^2	K_F(mg/g)(L/mg)$^{1/n}$	n	R^2
FeOOH-AlOOH	126.58	5.696	0.793	22.42	1.85	0.976
γ-Fe_2O_3-γ-Al_2O_3	416.66	0.791	0.76	345.15	1.13	0.998
α-Fe_2O_3-α-Al_2O_3	1.422	0.061	0.968	100.34	-0.665	0.974

5.4.5. Adsorption kinetics study

The applicability of the pseudo-first-order and pseudo-second-order model was tested for the adsorption of Congo red onto the three different phases of mixed oxide nanocomposite. The best fit model was selected according to the linear regression correlation coefficient, R^2 value. Here from the graph figure 5.11, it is clear that only pseudo-second–order kinetics is possible for all the three phases mixed oxide nanocomposite. The linearized form of pseudo-second-order rate equation is given as:

$$\frac{t}{q_t} = \frac{1}{k_2 q_e^2} + \frac{1}{q_e} t \qquad (7)$$

where k_2 (g.(mg.min)$^{-1}$) is the rate constant of the pseudo-second order equation. The value of q_e and k_2 can be determined by the slope and intercept of the straight line of the plot t/q_t (min-g/mg) versus t respectively. Figure 5.11 shows the sorption kinetics of Congo red onto mixed oxide nanocomposite surface obtained by batch experiments for an initial Congo red concentration of 100 mg/L at pH 7.0. The regression coefficient value (i.e. R^2= 1 approximately), in every case confirmed the adsorption obeys pseudo-second order kinetics.

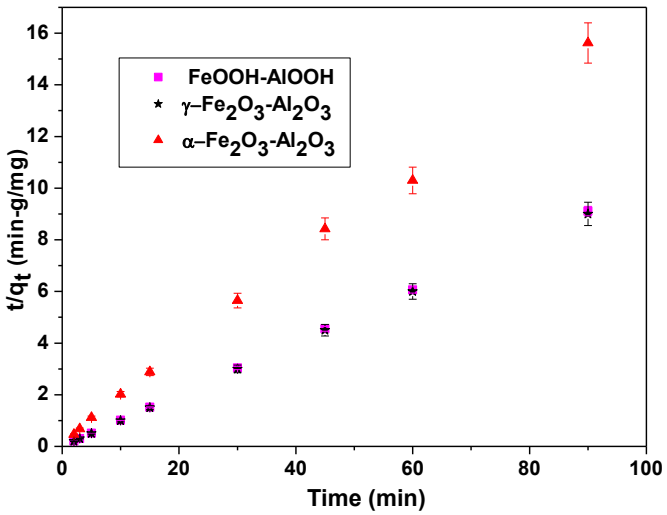

Figure 5.11 Kinetic study of mixed oxide nanocomposite of three different phases.

5.5 Conclusion

The mixed iron oxide-alumina nanocomposites have been synthesized using hydrothermal method. Batch experiments were performed for the removal of Congo red dye from aqueous solution, using three different phases of mixed oxide nanocomposite as adsorbent materials. Adsorption study was carried out by changing different parameters such as effect of time, pH and solution concentrations. A quantitative removal of Congo red dye by mixed oxide nanocomposite was achieved within a short contact time of 15 min. The adsorption capacity was found to be 498 mg/g approximately in case of gamma mixed oxides. The order of Congo red adsorption was governed by pseudo-second-order kinetics. The mixed nanocomposites obeyed Freundlich isotherm model as compared to Langmuir isotherm. Among the obtained nanocomposites gamma phase can act as a very good adsorbent for the 100% removal of Congo red.

CHAPTER 6

ELECTROSPUN Fe_2O_3-Al_2O_3 NANOCOMPOSITE FIBERS AS EFFICIENT ADSORBENT FOR REMOVAL OF HEAVY METAL IONS FROM AQUEOUS SOLUTION

6.1 Introduction

One dimensional nanostructure in the form of fibers, wires, rods, belts, and tubes has attracted plenty of attention due to their novel properties and diverse applications in last decade (Baji et al., 2010, Wang et al., 2000, Xia et al., 2003). A large number of advanced techniques have been developed to fabricate one dimensional (1D) nanostructure with well-controlled morphology and chemical composition. Among all 1D nanostructures, nanofibers exhibit high specific surface area due to their small diameter and porosity. The requirement for ultra-light weight yet strong structures for devices and miniaturized application has motivated novel designs using polymer nanofiber. Electrospinning is currently one of the most promising techniques to produce continuous and ultrathin nanofibers (Bhardwaj et al., 2010, Greiner et al., 2007). The electrospinning method provides operational flexibility for nanocomposite formation using different species into fibers. A number of metal and inorganic nanoparticles have been incorporated into electrospun nanofibers, which helps the nanocomposite fibers to achieve desired functional properties (Wang et al., 2010, Zhang et al., 2009, Zheng et al., 2009, Kim et al., 2007, Asokan et al., 2010, Machala et al., 2007). Recently, Kaewsanee et al. (2010) have reported the fabrication of aluminum-doped titanium oxide fiber by combined sol-gel and electrospinning method. In the composite fiber, the aluminum dopant helps in the reduction of the crystallite size of titania. Song et al. (2012) have also studied on preparation and characterization of tetra component $ZnO/SiO_2/SnO_2/TiO_2$ composite nanofiber by electrospinning method. This composite nanofibers were fabricated by calcination of the electrospun [$Zn(CH_3COO)_2$ +

PVP]/[$(C_2H_5O)_4Si$ + PVP]/[$SnCl_4$ + PVP]/[$Ti(OC_4H_9)_4$ + CH_3COOH + PVP] precursor composite fibers at 900°C for 8h. This precursor sol were placed in four different syringes, with plastic capillaries and delivered at a constant flow rate and collected in a copper wire collector.

One dimensional nanofibers are used in many fields viz. catalysis (Dong et al., 2010), photoluminescence (Hao et al., 2010), adsorption (Xu et al., 2012) etc. Presently heavy metals are among the most important pollutants in waters. They are non-degradable and therefore continue to accumulate in water bodies (Ozverdi et al., 2006). According to the World Health Organization (WHO, 1984), the metals of most immediate concern are lead, cadmium, arsenic, chromium, manganese, nickel and mercury (Mohapatra et al., 2010). Their presence in the environment can be detrimental to people, plants and animals. These heavy metals may cause serious disorders like, anemia, kidney disease, nervous disorder and even death. A large number of different methods are there for the removal of these heavy metal ions. But among all, recently, adsorption techniques for waste water treatment have become more popular with regard to their efficiency and economic method in removal of pollutants (Dai et al., 2013).

Recently, Parham et al. (2012) have shown effective removal of mercury(II) ions from contaminated water by modified magnetic iron oxide nanoparticles with 2-mercaptobenzothiazole as adsorbent. After modification of magnetic iron oxide nanoparticle the efficiency improved from 43.47 % to 98.6% for the same condition. As reported earlier by Srivastava et al. (2011) the adsorption of nickel ions from aqueous solutions by nano alumina, synthesized by sol-gel method, was found to show 90% removal at lower adsorbate concentration, which was very efficient for large scale removal. Cao et al. (2012) have also synthesized flower like α-Fe_2O_3 nanostructures, which was used for adsorption of As (V) and Cr (VI). These flowers like α-Fe_2O_3 nanostructures were synthesized by template-free microwave-assisted solvothermal method by using low-cost salt precursor's i.e., $FeCl_3.6H_2O$ and urea in ethanolic medium. The surface area was found to be 130m^2/g. The maximum adsorption capacities for As (V) and Cr (VI) were 51 and 30mg/g, respectively. Teng et al. (2011) have focused on thioether functionalized mesoporous fiber membrane, which is a combination of sol-gel and electrospinning fabrication and their applications for Hg^{2+} removals. The composite were used as a good adsorbent for Hg^{2+} removals due to modification with thioether groups. Similarly, Xiao et al. (2011) have synthesized zero-valent iron nanoparticle-immobilized hybrid electrospun polymer nanofibrous mats, which show excellent copper (II) removal. To synthesize hybrid nanofibrous mat by electrospinning

method, a polymer mixture solution of polyacrylic acid (PAA) and polyvinyl alcohol (PVA) was used, with incorporation of multiwalled carbon nanotubes (MWCNT). The MWCNT-reinforced PAA/PVA nanofiber mats were immersed in Fe (III) solution. Here zero-valent iron nanoparticle act as active agent. The maximum adsorption capacity of these nanofiber mats was found to be 75.3 mg/g. Very recently, Choi et al. (2013) have studied on high surface area ($248 m^2/g$) mesoporous titanium-zirconium oxide nanofibrous web for removal of heavy metal ion. A typical electrospinning technique combined with sol-gel reaction was adopted to synthesize this TiO_2/ZrO_2 nanofibrous web by further calcinations at 450°C. Titanium isopropoxide, zirconium propoxide, PVP, 2-amino-ethylphosphosphonic acid, amino tris (methylene phosphonic acid), were used as precursor for electrospinning methods. The fibre diameter, after calcinations was found to be 226nm. The TiO_2/ZrO_2 nanofibre surface was modified via phosphonate coupling to attach amine and phosphonate functionalities. The phosphonate-modified TiO_2/ZrO_2 nanofibrous web exhibited enhanced cadmium uptake, up to 10 times higher than the non-modified TiO_2/ZrO_2 nanofibrous web. However, the amine-modified TiO_2/ZrO_2 nanofibrous web performed slightly lower than the non-modified TiO_2/ZrO_2 nanofibrous web. In addition, the three types of nanofibrous webs exhibited slightly different affinity strengths to different metals (i.e., Cd, Pb, Cu, Ni and Zn) but the affinity of all three nanofibrous webs to lead and copper was higher than the affinity of the webs to cadmium.

The present study deals with the synthesis and characterization of Iron oxide-alumina mixed nanocomposite fibers by electrospinning method. The obtained electrospun Iron oxide-alumina nanocomposite fibers were further explored as adsorbents for removal of Copper (II), Nickel (II), Lead (II) and Mercury (II) metal ions from waste water by batch adsorption procedure.

6.2 Experimental section

6.2.1 Materials and methods

Iron acetylacetonate and Polyvinyl pyrrolidone polymer (PVP; Mn= 1,300,000) of analytical grade with purity of 99.0% was obtained from Sigma-Aldrich. Ethanol, acetone and acetic acid (AA) were purchased from Merck, India Ltd. All the chemicals were used without further purification.

6.2.2 Fabrication of iron oxide and mixed nanocomposite fibers

Prior to synthesis of mixed oxide Fe_2O_3-Al_2O_3 composite nanofibers, we have also synthesized Fe_2O_3 nanofibers by electrospinning method. The PVP solution (10wt %) was prepared by dissolving PVP polymer power in absolute ethanol under constant and vigorous stirring. Iron acetylacetonate was used as iron precursors. The iron precursor sol using acetone was mixed with the prepared PVP/ ethanol solution followed by addition of 1-2 drops of acetic acid. The polymer to iron precursor's weight ratio was maintained at 2:1. The resulting PVP-iron acetylacetonate solution was loaded in a 3ml plastic syringe fitted with a metallic needle. The polymer solution was pushed to the needle tip using the syringe pump and the feed rate was kept at 1.5 ml/h. The positive terminal of a variable high voltage (Glassman, Japan) power supply (12.5 kV) was applied to the metallic needle, whereas the negative terminal was connected to the grounded collector which was covered with the aluminium foil served as counter electrode. The distance between the needle tip and collector was maintained 10 cm. All the experiments were conducted at room temperature with a relatively low humidity (45–50%) condition. The obtained as-spun composite fibers were calcined at high temperature to form Fe_2O_3 nanofibers.

To synthesize the iron oxide-alumina mixed nanocomposite fibers, the combination of electrospinning and sol-gel process was carried out. For electrospinning, initially a solution was prepared by dissolving 12 wt % of polyvinyl pyrrolidone (PVP) in absolute ethanol under constant and vigorous stirring. Iron acetylacetonate was mixed with acetone and acetic acid. Later solution was mixed with previous solutions and was constantly stirred for overnight. The obtained solution was here after referred to as the neat spinning solution. An aqueous suspension of AlOOH nanopowder synthesized by sol-gel method was added to the spinning solution and again the mixture was constantly stirred for 5-6 hours (Kim et al., 2007). The weight ratio between the polymers to iron-aluminum precursor was maintained at 2:1:1. The resulting solution mixture of PVP–iron-aluminum was loaded into a 3 ml syringe fit with a metallic needle. The polymer solution was pushed to the needle tip using the syringe pump and the feed rate was kept at 1.0 ml/h. The positive terminal of a variable high voltage (Glassman, Japan) power supply (14 kV) was applied to the metallic needle, whereas the negative terminal was connected to the grounded collector which was covered with the aluminium foil served as counter electrode. After electrospinning, the as-spun nanocomposite fibers were calcined in air at 1000°C for 2 h, in order to obtain the crystalline mixed nanocomposite fibers.

6.2.3 Adsorbent characterization techniques

Surface morphology of mixed nanocomposite fiber was characterized by using a JEOL-JSM-6390LV scanning electron microscope operating at an acceleration voltage of 10 and 20 kV equipped with Oxford INCA energy dispersive X-ray analysis (EDAX). The X-ray diffraction patterns of the composite fibers were recorded using a PAN analytical diffractometer (PAN-PW 1830) using Ni filtered Cu Kα (λ = 1.541A°) radiation. The transmission electron micrographs were taken using a Philips 200 transmission electron microscope at an acceleration voltage of 200 kV. The composite fibers were dispersed in ethanol and a drop of this dispersion was added to a carbon coated Cu grid (300 meshes) for TEM imaging. The thermogravimetric analysis of the composite fibers was performed using a TGA/DTA, SHIMADZU (TA-60 WS) model equipment. The samples were heated in air atmosphere from ambient temperature to 1000^{o}C at a linear heating rate of 10°C/min. BET surface area was measured with Beckman Coulter SA3100. UV-Vis-DRS spectra were investigated using SHIMADZU 2045 spectrophotometer.

6.2.4 Adsorption experiments of mixed oxide nanocomposite fiber

The electrospun Iron oxide-alumina mixed nanocomposite fibers were used as adsorbent for the removal of heavy metal ions i.e. Cu^{2+}, Ni^{2+}, Pb^{2+} and Hg^{2+} from aqueous system. A stock solution (1000 ppm) of all the four ions were prepared by dissolving exact amount of copper chloride (Merck), nickel chloride (Merck), lead nitrate (Merck) and mercury chloride (Merck) in deionized water. Solutions with the desired concentration were prepared by successive dilutions of the stock solution. We have studied the effect of pH (2.0-8.0), sorption kinetics time (0-180 mins) and adsorption isotherms (initial concentration 5-50 mg L^{-1}) of metal ions (Cu^{2+}, Ni^{2+}, Pb^{2+} and Hg^{2+}). While analyzing adsorption behavior of the iron oxide-alumina mixed nanocomposite fiber, 0.05 gm in 20 ml of solution of metal ions at different concentration was taken. The pH was maintained at pH 6 in every solution. The contact time was maintained 60 min, for all the adsorption experiments. After reaching the equilibrium the residual concentration of the metal ions in the aliquot were determined by atomic absorption spectroscopy (AAS). Adsorption data obtained in this experimental study were evaluated with Freundlich, & Langmuir isotherms models. The adsorption experiments have been conducted three times and the data are presented in the figures with an appropriate error bars. The error bars are found to be within ±3%.

6.3 Result and discussion

6.3.1 Structural properties of iron oxide-alumina mixed oxide nanocomposite fiber

To determine the structure and purity of the electrospun nanocomposite fibers, the XRD analysis has been performed. The XRD pattern of the nanocomposite fiber recorded after calcinations at 1000^{o}C is presented in Figure 6.1(c). The XRD study revealed the crystalline nature of the sintered fibers. Figure 6.1(a) shows XRD pattern of alumina nanoparticle, which we got after sintering boehmite nanoparticle at 1000°C. XRD data consists of α-alumina phase, which is confirmed from JCPDS File no. 83-2081, whose crystal structure is corundum. Figure 6.1(b) represents the Iron oxide nanofiber obtained on sintering the as prepared PVP-Iron acetyl acetonate nanofiber at 1000°C, which is confirmed from JCPDS File no. 84-0311 having rhombohedral crystal structure. Similar type of characteristic diffraction peaks corresponding to the α-Fe_2O_3 and α-Al_2O_3 were also observed for boehmite doped PVP-Iron acetylacetonate mixed nanocomposite fibers sintered at 1000°C for 2 hrs (JCPDS Card No: 84-0311 and No: 83-2081 respectively).

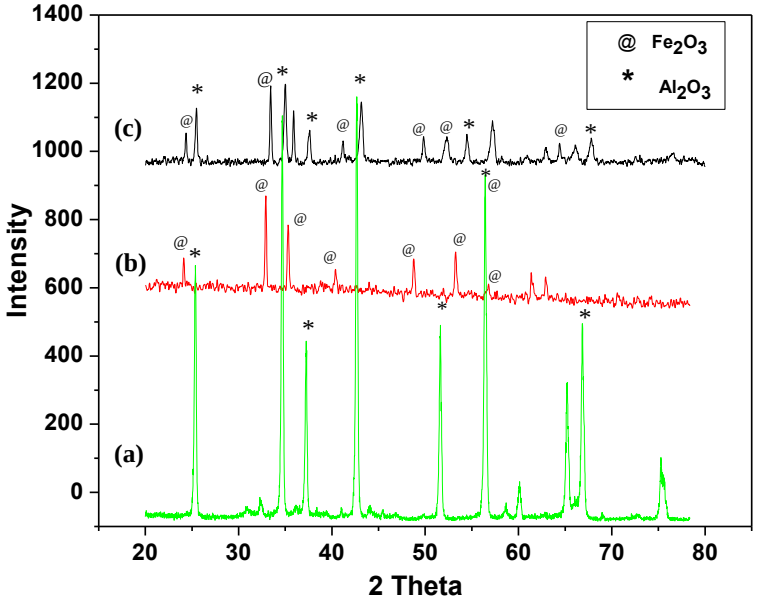

Figure 6.1 XRD pattern of Fe_2O_3-Al_2O_3 mixed nanocomposite sintered at 1000°C where (a) Al_2O_3, (b) Fe_2O_3 and (c) Fe_2O_3-Al_2O_3 nanomaterials.

6.3.2 Thermal behavior by TGA-DTA studies

Thermal behavior of the AlOOH mixed PVP-iron acetylacetonate as-spun ultra-fine fiber membrane was studied by TGA-DTA analysis in air up to 700°C at a heating rate of 10°C/min. Figure 6.2 represents the TGA-DTA curve of mixed as-spun nanocomposite ultra-fine fibers. TGA graph shows three major weight loss regions, at three different temperature ranges. The initial weight loss region between 50-150^{o}C, can be ascribed to desorption of the physically absorbed water from the sample. The second weight loss between 260°C and 290°C can be regarded as the thermal decomposition of iron acetylacetonate $Fe(acac)_3$. The

$Fe(acac)_3$ precursor decomposes into Fe_2O_3 and give off heat to the crystal and a corresponding strong exothermic peak occurs at 275°C in DTA curve. The third weight loss region between 290°C above 350°C corresponds to the complete decomposition of the PVP polymer. Correspondingly, a strong exothermic peak was observed in the temperature range of 290°C to 335°C in the DTA curve. This peak corresponds to a combined contribution from the decomposition of the polymer as well as the phase transformation of γ-Fe_2O_3 to α-Fe_2O_3. At about 320°C to 500°C the weight loss is more gradual which corresponds to the decomposition of AlOOH to Al_2O_3 (Teoh et al., 2007).

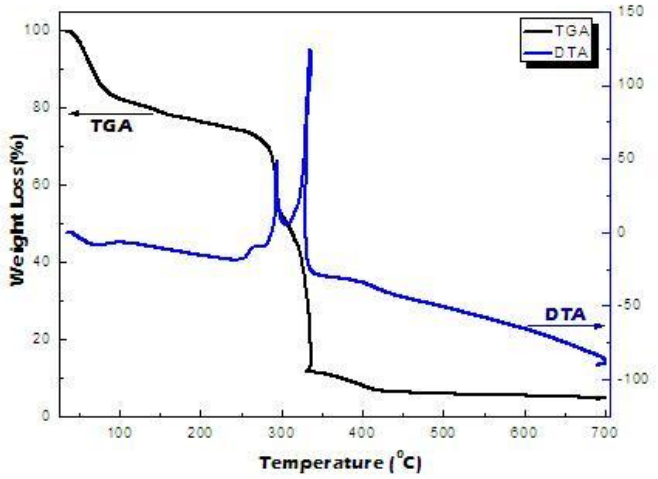

Figure 6.2: TGA/DTA profile of as-spun AlOOH–PVP–$Fe(acac)_3$ mixed nanocomposite fiber.

6.3.3 N_2 adsorption-desorption isotherm graph

N_2 adsorption-desorption isotherm is used to investigate the surface area of iron oxide-alumina mixed nanocomposite fibers as shown in Figure 6.3. The BET surface area of mixed nanocomposite is 9.6m^2/g. The BET analysis reveals that the mixed oxide nanocomposite fibers own lower surface area after calcinations at 1000°C. Figure 6.3 also presents Barret-Joyner-Halenda (BJH) pore size distribution curve (in the inset) of the figure. The composite oxide shows adsorption isotherm corresponding to nonporous materials. The presence of intra-particle pores can be observed from the pores size distribution curve obtained using BJH analysis. The corresponding pore size distribution curve obtained by BJH method shows a narrow pore size at 5.21 nm.

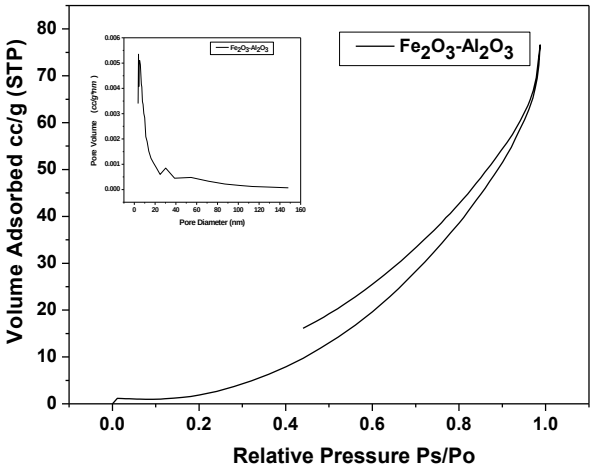

Figure 6.3: Nitrogen adsorption–desorption isotherm and pore size distribution curve (inset) of Fe_2O_3–Al_2O_3 nanofibers.

6.3.4 Morphology studies by SEM and TEM analysis

The SEM images of α-Fe_2O_3 is presented below (Figure 6.4). Figure 6.4 represents the SEM images of as-spun PVP-$Fe(acac)_3$ fibers. It is observed from this figure that the as-spun fibers are in the diameter of 700-900nm. Upon sintering at 1000°C α-Fe_2O_3 fibers were formed with a reduced diameter of around 200-400nm (figure 6.4b). The SEM-EDX confirms the formation of iron oxide nanofiber.

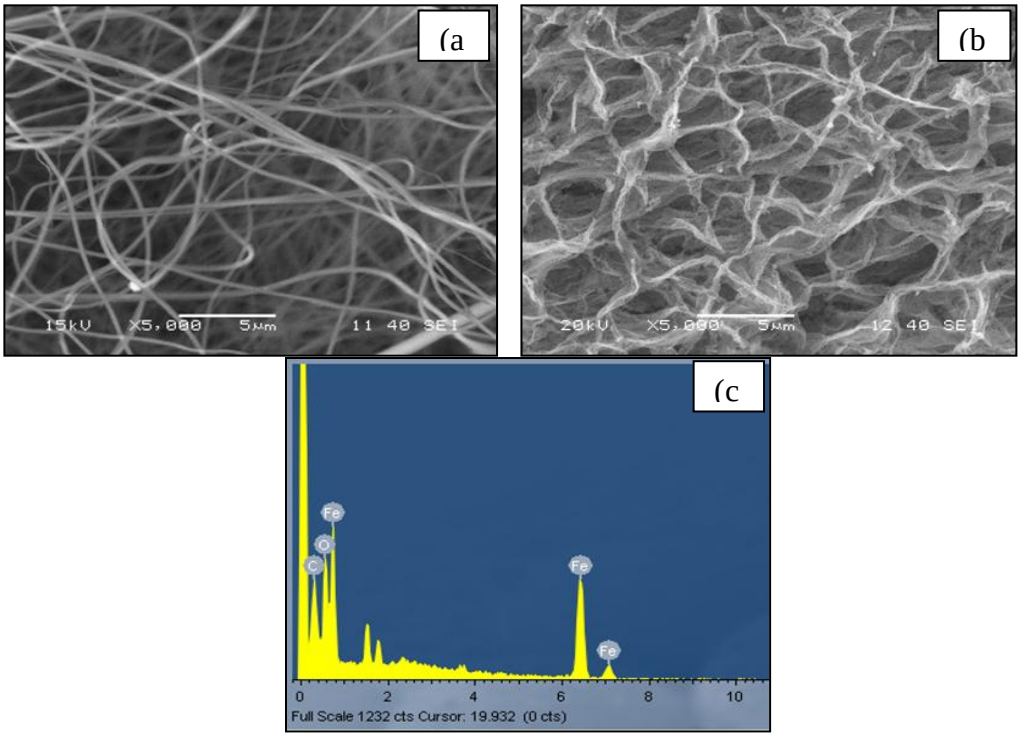

Figure 6.4: SEM image of Fe_2O_3 nanofiber (a) as-spun fiber, (b) sintered at 1000°C and (c) EDX pattern of sintered fiber.

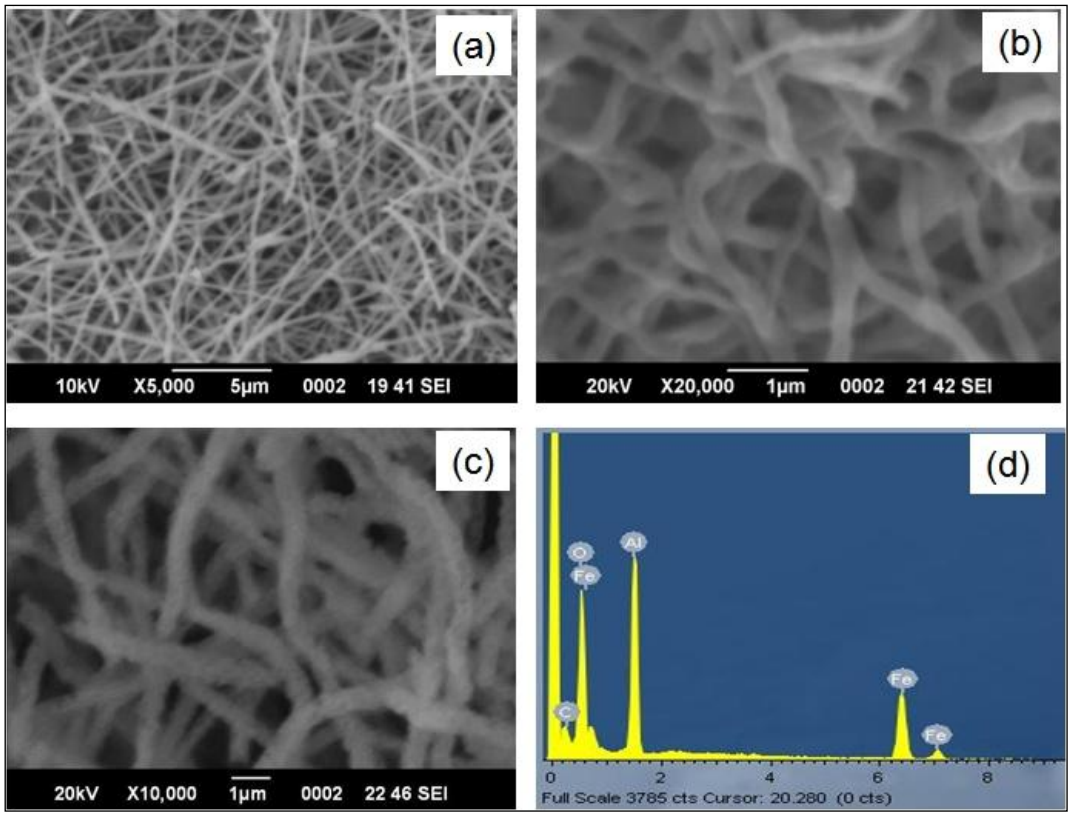

Figure 6.5 SEM image of Fe_2O_3-Al_2O_3mixed nanocomposite sintered at (a) 500°C (b) 700°C, (c) 1000°C, and (d) EDAX analysis of 1000°C sintered fiber.

The SEM images of sintered nanocomposite fibers are shown in Figure 6.5. The SEM images represent the formation of ultra-fine cylindrical nanocomposite fibers having diameter in the range of 200-700 nm. The fibers have smooth surfaces in Figure 6.5(a) which was sintered at 500°C, and have diameters in the range of 200-500 nm. It was also found that the size and smoothness of the fiber slightly changes with change in sintering temperature. Figure 6.5(b) and 6.5(c) represent the SEM picture of nanocomposite fibers sintered at 700°C and 1000°C. The average diameter of the sintered fiber in both cases was found to be 200-500 nm range. The smoothness of the surface decreases with increase in sintering temperature. This might be due to grain formation on the surface of fibers. The SEM elemental detection X-ray analysis (SEM-EDAX) clearly suggest that the presence of aluminium, iron and oxygen as elements (Figure 6.5d).

In order to obtain more information about the formation of nano-sized Fe_2O_3-Al_2O_3 nanocomposite fibers, we have carried out the TEM analysis. Figure 6.6a shows the TEM image of Fe_2O_3-Al_2O_3 nanocomposite fibers obtained by sintering the as-spun composite fibers at 1000°C for 2h. It is observed from the TEM studies that the diameters of nanocomposite fibers were not uniform, instead a broad range of fibers were formed (200-500 nm). This result is also consistent with the fibers diameter observed by the magnified

SEM images. Furthermore, it is also observed TEM images that there is uniform distribution of the nano-sized particles in all over the fiber surface. The corresponding diffraction rings and bright spot on the electron diffraction pattern (Figure 6.6b) suggest that the nanocomposite fibers obtained are highly crystalline in nature, which is also consistent with XRD results.

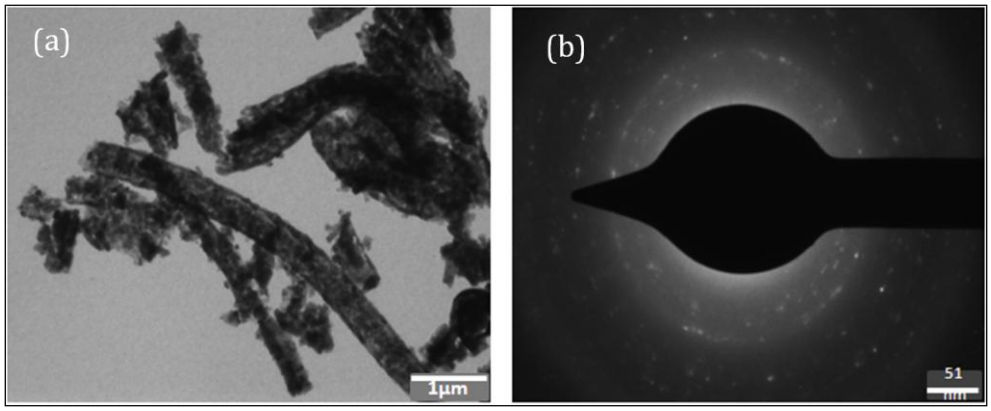

Figure 6.6: Electron microscopic study of Fe_2O_3-Al_2O_3 mixed nanocomposite fiber (a) TEM image (b) electron diffraction pattern.

6.4 Adsorption studies of mixed oxide nanocomposite fibers

6.4.1 Effect of pH on adsorption study of metal ions

pH is an important parameter for adsorption of metal ions from aqueous solution as it affects the solubility of the metal ions, concentration of the counter ions on the adsorbent and the degree of ionization of the adsorbate during reaction. On the other hand, hydrolysis, complexation by organic or inorganic ligands, redox reactions and precipitation are strongly influenced by pH. pH also strongly influences the adsorption availability of heavy metals (Esposite et al., 2002). To study the effect of this parameter on the metals sorption by mixed oxide nanocomposite, the solution initial pH was varied within the range of 2 to 7. This pH range was chosen to avoid metal solid hydroxide precipitation. The experiments were performed for an initial concentration of 50 mg/L and 0.05g adsorbent dose in 20ml of solution at room temperature (Figure 6.7). At lower pH, the concentration of H^+ ion is high causing a competition for vacant adsorbent site between the H^+ ion and metal ions. Therefore, at low pH, the removal efficiency is low. This result is consistent with the results obtained by Boudrahem et al. (2011). They have also studied adsorption of lead using date tree leaves at an optimized pH 5.8. After pH 6, the adsorption capacity remains constant and uptake of metal ions is observed which could be attributed due to metal hydrolysis and the precipitation at higher pH. Hence the overall graph indicates that the maximum uptake of these ions is

obtained at pH 5.5. Subsequently studies were conducted at pH 5.5. Figure 6.7 (b) shows the effect of pH on the zeta potential of Fe_2O_3-Al_2O_3 nanocomposite fibers. The isoelectric point (Iep) of mixed nanocomposite fibers is 5.7, so the charge on the particles nears this pH is zero. The surface charge is positive at pH values lower than Iep, neutral at Iep, and negative at pH values higher than it. At higher pH, the reaction solution would be negatively charge. Hence, all the succeeding investigations were performed at pH 6.

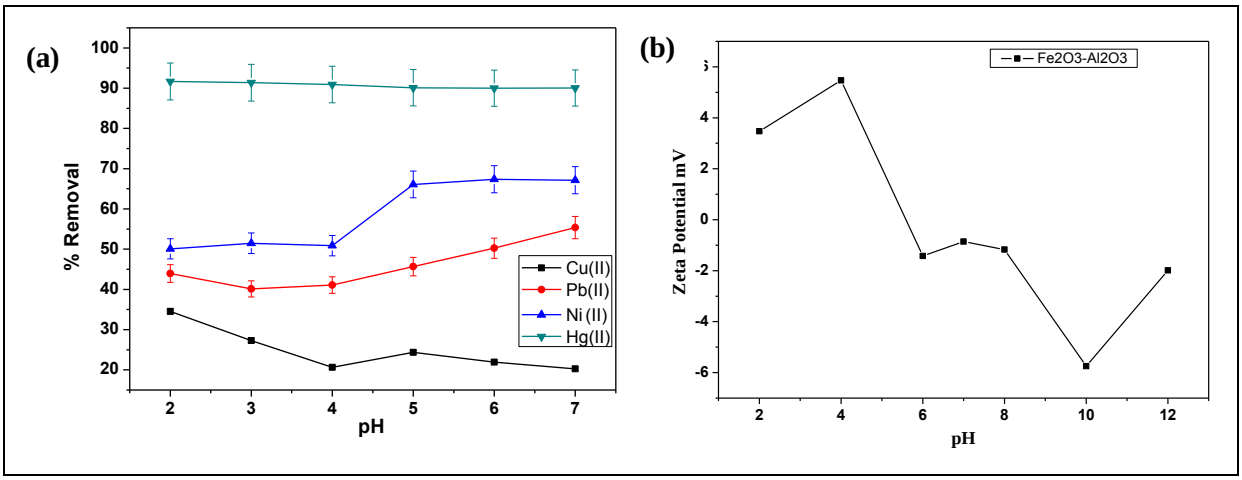

Figure 6.7(a) Percentage removal of metal ions with variation in pH and (b) zeta potential of Fe_2O_3-Al_2O_3 nanocomposites as a function of pH.

6.4.2 Effect of contact time on adsorption study of metal ions

To establish the equilibrium time for maximum adsorption and to know the kinetics of the sorption process, the sorption of Cu(II), Pb(II), Ni(II) and Hg(II) ions by mixed oxide nanoadsorbent was carried out at different contact times from 10 to 160 min. The results obtained are shown in Figure 6.8. It is observed from the figure that, the adsorption efficiency of divalent cations increases gradually with increasing contact times and reaches a plateau afterward. After the adsorbing ions get adsorbed on the surface, the capacity of the adsorbent gets exhausted and the saturation adsorption capacity is reached. Rajurkar et al. (2011) have studied adsorption of Cr (III), Ni (II) and Cu (II) from aqueous solution by activated alumina. The equilibrium attained for effect of contact time was at 50min for Cr (III), 80 min for Ni (II) and 40min for Cu (II). In the present study, it is observed, that the optimum time for maximum adsorption is 60 min for all of the four cations at pH 6.

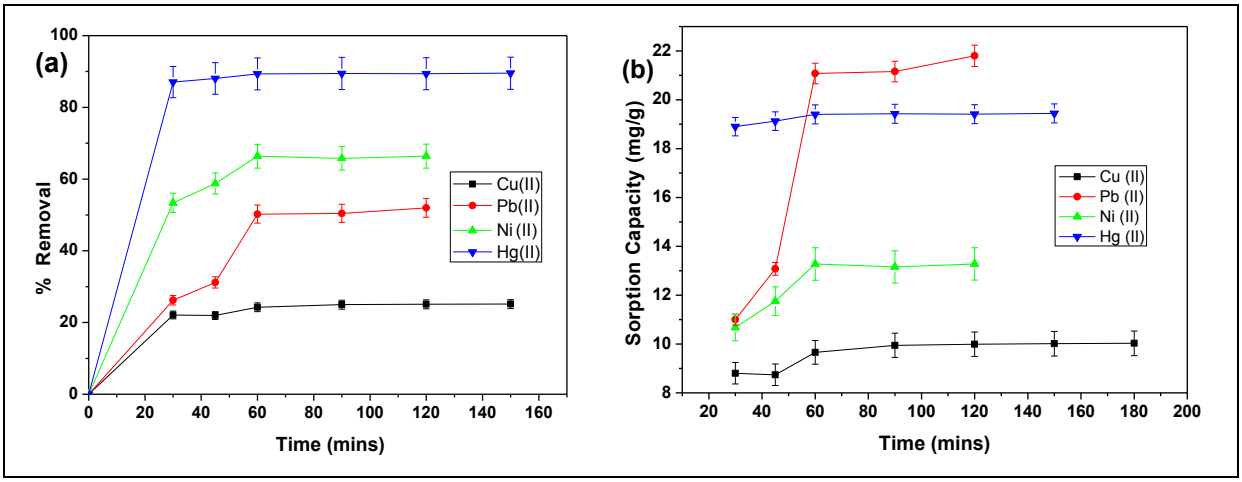

Figure 6.8(a) Percentage removal of metal ions with a function of time (min) and (b) sorption capacity versus variation in time (min).

6.4.3 Effect of initial concentration of adsorbate on adsorption study

The initial concentration of adsorbate is one of the important parameter for determining the adsorption capacity of an adsorbent. In these studies we have varied the initial concentration of the adsorbate from 5 to 50mg/L. The batch experiments were carried out at room temperature by using 20ml of adsorbate solutions and adsorbent dose of 0.05 gm at pH 6. Figure 6.9 shows the effect of initial concentrations on the removal of four metal ions i.e. Cu^{2+}, Ni^{2+}, Pb^{2+} and Hg^{2+}. It is observed from the figure that percentage removal decreases with increase in initial concentration from 5 mg/L to 50 mg/L. This is because at higher concentration, the availability of adsorbent surface site is low, subsequently the adsorption is low. Except, in case of copper ion, percentage removal increases with increase in initial concentration. This is attributed to the increase in the number of metal ions competing for available binding sites on the adsorbent at higher concentration levels. Similar type of result has been reported by Abasi et al. (2011).

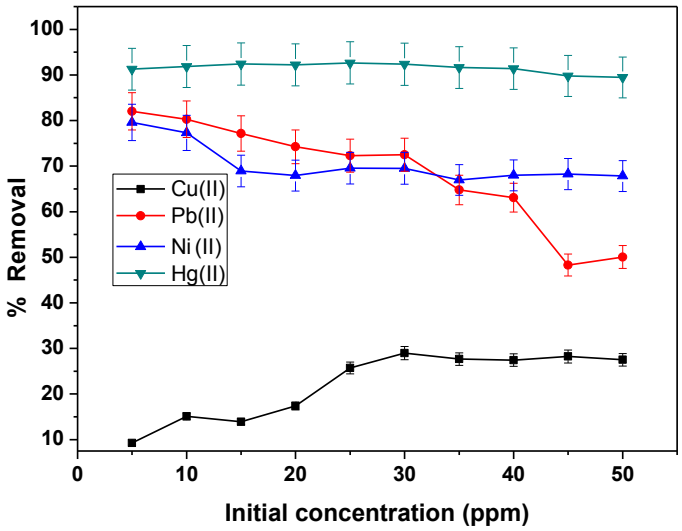

Figure 6.9 Percentage removal of different ions with a function of initial concentration (mg/L).

6.4.4. Adsorption isotherm study of metal ions

The adsorption data were analyzed with the help of linear form of Langmuir isotherm and Freundlich isotherm models, expressed by the Eqn (1) and (2), respectively.

Langmuir isotherm applies to adsorption on completely homogeneous surfaces with negligible interaction between adsorbed molecules. It is represented as:

$$\frac{C_e}{q_e} = \frac{C_e}{q_m} + \frac{1}{bq_m} \qquad (1)$$

where q_e is the equilibrium adsorption capacity of ions on the adsorbent (mg/g), C_e is the equilibrium ions concentration in solution (mg/L), q_m is the maximum capacity of the adsorbent (mg/g) and b is the Langmuir adsorption constant (L/g).

Freundlich isotherm can be applied for heterogeneous surfaces and multilayer sorption. It is expressed as:

$$q_e = K_F C_e^{1/n} \qquad (2)$$

$$\log q_e = \log K_F + \frac{1}{n} C_e \qquad (3)$$

where equilibrium capacity q_e and C_e are defined as above, K_F the Freundlich constant (mg/g) and n is heterogeneity factor (Ge et al., 2012). The linear Freundlich isotherm plot for the sorption of the four cations onto mixed oxide nanocomposite is shown in Figure 6.10. Table 6.1 shows the linear Freundlich sorption isotherm constants and coefficients of determination (R^2). Based on the R^2 values, the linear form of the Freundlich isotherm appears to produce a

reasonable model for sorption in all four systems, with the lead, nickel and mercury isotherms seeming to fit the experimental data better than copper.

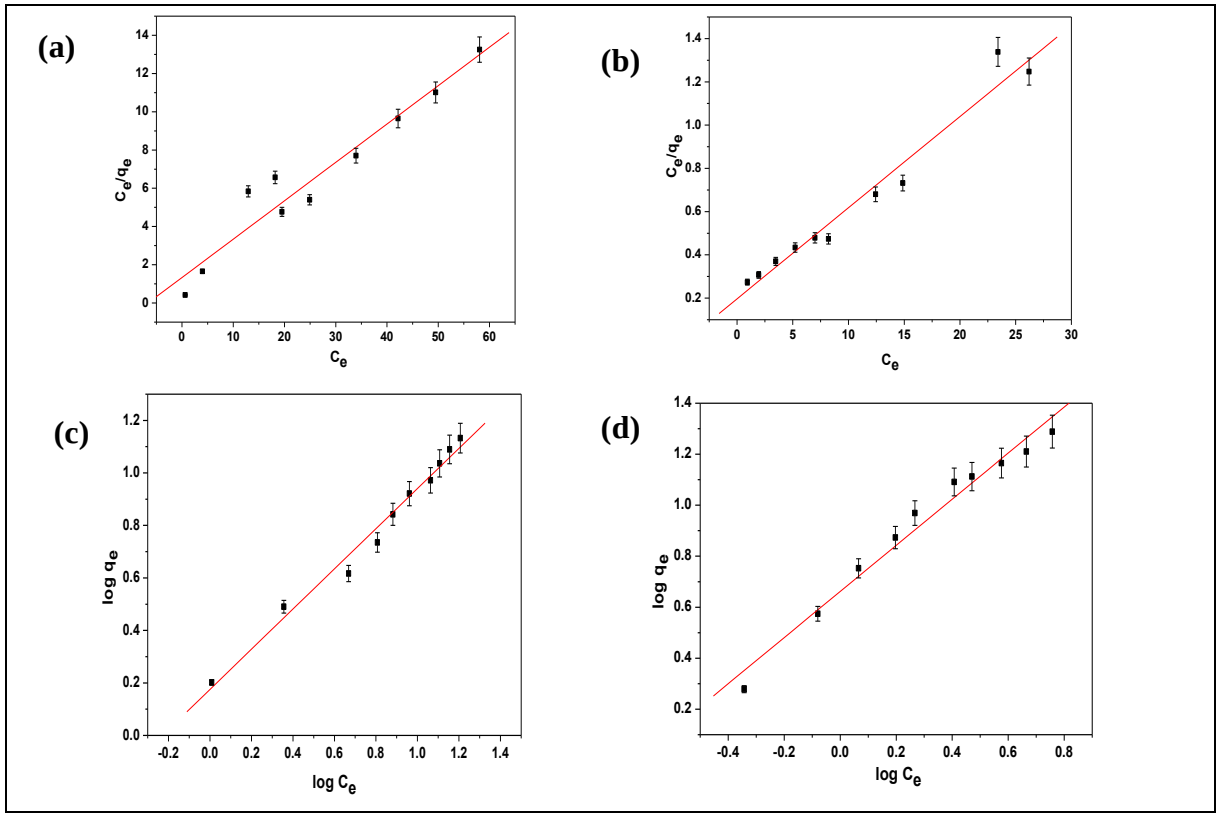

Figure 6.10 Langmuir adsorption isotherm of Fe_2O_3–Al_2O_3 mixed oxide nanocomposite using (a) Cu(II) and (b) Pb(II). Freundlich adsorption isotherm of Fe_2O_3–Al_2O_3 mixed oxide nanocomposite using (c) Ni (II) and (b) Hg (II) at room temperature.

In fact, the adsorption isotherm data for the metal ions were consistently better with Freundlich isotherm as compared to Langmuir isotherms, which were determined by the correlation coefficients (R^2) in Table 6.1. The maximum adsorption capacity (q_m) calculated by Langmuir isotherm has been shown in Table 6.1. The maximum adsorption capacities for Cu (II), Pb (II), Ni(II) and Hg(II) are 4.98, 23.75, 32.36 and 63.69 mg/g, respectively.

Table 6.1 Langmuir and Freundlich parameters for adsorption of cations on mixed oxide nanocomposites.

Cations	Langmuir coefficients			Freundlich coefficients		
	q_m(mg/g)	b(L/g)	R^2	K_f(mg/g)	N (L/g)	R^2
Cu(II)	4.98	0.267	0.937	1.59	3.81	0.823
Pb(II)	23.75	0.008	0.964	4.52	1.91	0.905
Ni(II)	32.36	0.024	0.598	1.49	1.307	0.983
Hg(II)	63.69	0.003	0.641	4.58	1.105	0.974

6.4.5. Adsorption kinetic studies of metal ions

The adsorption kinetics of metal ions with mixed oxide nanocomposite fibers was investigated by two kinetics models: Lagergren pseudo-first-order and pseudo-second- order models, for Eqs (4) and (5), respectively (Reddad et al., 2002).

Pseudo-first-order model is a simple kinetic analysis of adsorption in the form of

$$\ln(q_e - q_t) = ln\, q_e - k_1 t \qquad (4)$$

Pseudo-second-order model:

$$\frac{t}{q_t} = \frac{1}{k_2 q_e^2} + \frac{1}{q_e} t \qquad (5)$$

where q_t (mg/g) is the adsorption at time t (min), q_e (mg/g) is the adsorption capacity at adsorption equilibrium and k_1 (min^{-1}) and k_2 (g mg^{-1} min^{-1}) are the kinetic rate constants for the pseudo-first-order and the pseudo-second-order models, respectively. The kinetic adsorption data were fit to equation (4) and (5), and the calculated results are in Table 6.2 and psuedo-first-order and psuedo-second-order plots are given in Figure 6.11. The correlation coefficients (R^2) for the pseudo-second-order adsorption model were all higher than for the pseudo-first-order model. Therefore, the adsorption data are well obeyed by pseudo-second-order kinetic model. Table 6.2 shows the different parameters of kinetics study, where we observe that the experimental value of adsorption capacity (*Qe*, mg/g) also in agreement with the theoretical pseudo-second order kinetics (*Qe*, mg/g) model.

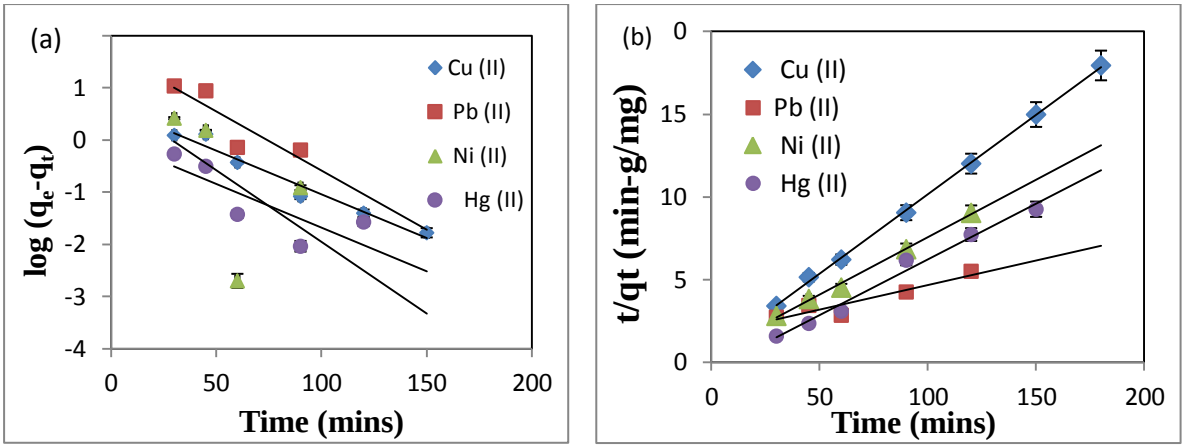

Figure 6.11 Kinetic study of all of the four ions (a) psuedo-first order model and (b) psuedo-second order model.

The kinetics parameters for two kinetic models and correlation coefficients of metal ions were calculated from these plots and are listed in Table 6.2. From Table 6.2 it is observed that R^2 values for the first order kinetics for Cu (II), Pb (II), Ni (II) and Hg (II) vary in the range of 0.24-0.96. Where in case of Ni (II), R^2 value were only 0.24 and also the predicted loading capacities shows wide variations as compared to experimental values. Similarly, in case of pseudo-second order kinetics the R^2 values for all four cations ranges from 0.87 to 0.99. But here it is observed that the Q_e values are comparable with the experimental values suggests the applicability of pseudo-second order model.

Table 6.2 Kinetics parameters for adsorption of various cations on mixed oxide nanocomposites.

Cations	**Experimental**	**Pseudo-first order Reaction**			**Pseudo-second order Reaction**		
	Q_e(mg/g)	Q_e(mg/g)	K_1(min^{-1})	R^2	Q_e(mg/g)	K_2	R^2
Cu(II)	10.2	4.35	0.038	0.964	10.405	0.005	0.999
Pb(II)	21.1	1.05	3.887	0.761	23.52	0.001	0.977
Ni(II)	13.5	6.14	0.062	0.244	14.409	0.002	0.996
Hg(II)	19.4	1.58	0.027	0.672	19.53	0.001	0.999

6.4.6 Desorption studies and reusability study

Desorption of metal ions from adsorbent and re-generation of the adsorbent is an important issue in view of re-usability of the adsorbent. With rising prices of raw materials and wastewater treatment processes, the attractiveness of product recovery processes has increased significantly. The main objective of regeneration process is to restore the adsorption capacity of exhausted adsorbent and to recover valuable components present in the

adsorbed phase. In this paper, for desorption studies, the used adsorbent were first washed with double distil water to remove the un-adsorbed/loosely bound metal ions on adsorbent surface. In order to estimate the recovery of metal ions, desorption experiments were carried out with varying HCl concentration. Highly concentrated HCl is more effective for desorption studies of metal ions. Therefore to determine the optimal HCl concentration for efficient desorption of adsorbed metal ions, 0.05-2 HCl solution were tested. In this case, 0.05 M HCl was chosen for desorption of metal ions. The adsorbent completely disappeared at 2 M H^+ after 3h. Considering the desorption efficiency and the reusability cycles of the adsorbents, the initial concentration of 0.05M was better than others. After adsorption of metal ions the adsorbent was separated by filtration and dried at 60°C. The desorption experiments involved adding of 0.05 g metal ion loaded adsorbents to 50 ml aqueous solution with 0.05 M Hydrochloric acid. The mixture was shaken for 3h to reach desorption equilibrium. The metal ion adsorption capacity of Al_2O_3-Fe_2O_3 mixed nanocomposite remained almost constant for all of the 4 cycles.

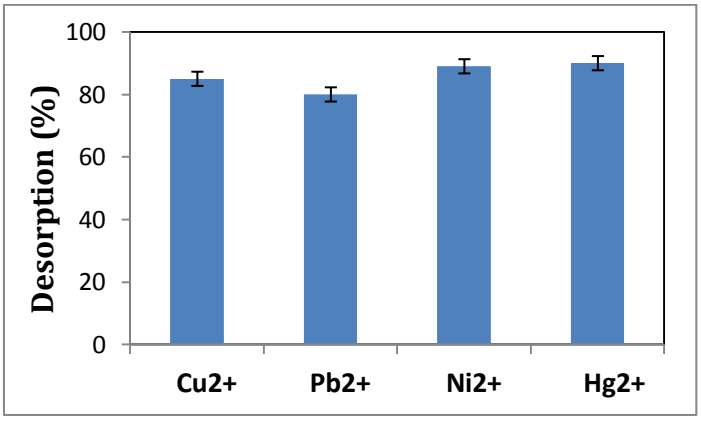

Figure 6.12 Desorption of metal ions (Cu^{2+}, Pb^{2+}, Ni^{2+} and Hg^{2+}) from Al_2O_3-Fe_2O_3 mixed nanocomposite using 0.05 M HCl solution.

From the above graph (Figure 6.12) it is observed that the desorption efficiency of Fe_2O_3-Al_2O_3 mixed nanocomposite was 90% approximately. For regeneration studies, successive adsorption-desorption processes were carried out for four consecutive cycles which is shown in Figure 6.13. Figure 6.13 shows the removal efficiency, (R %) of all the metal ions, during a four cycles of adsorption-desorption-regeneration, from a 20 ml solution of initial metal ion concentration of 50 mg/L at pH 5.5, which indicate that there were no irreversible sites on the surface of the adsorbent. Thus, the Fe_2O_3-Al_2O_3 mixed oxide nanocomposite could retain the original metal removal capacity after four successive adsorption-desorption process.

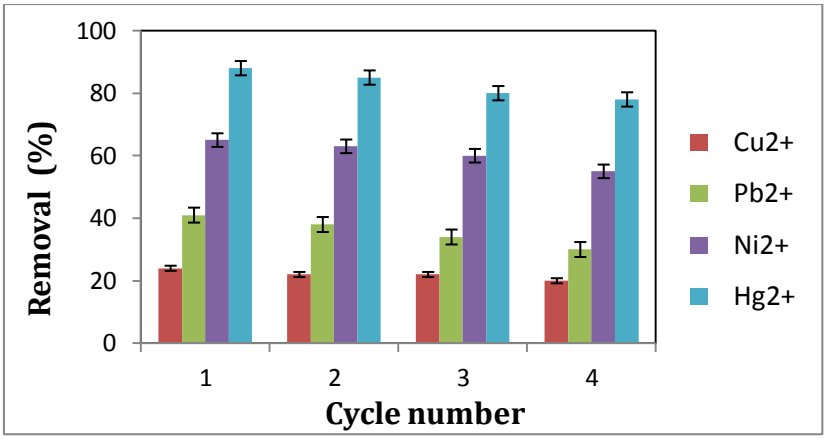

Figure 6.13 Reusability of Al_2O_3-Fe_2O_3 mixed nanocomposite adsorbent for adsorption/desorption of metal ions during four cycles.

6.5 Conclusion

Fe_2O_3-Al_2O_3 mixed oxide nanocomposite fibres was successfully prepared by electrospinning of boehmite impregnated Iron acetylacetonate and PVP polymer solution. The diameters of the fibres are found to be in the range of 200-500 nm by TEM study. XRD analysis of the calcined fibre at 1000°C confirms the formation of mixed oxide nanocomposite fibres. SEM image shows that with increase in sintering temperature the morphology becomes rough but continuous fibre mats were obtained. The EDAX analysis of sintered fibres suggests the presence of Fe, Al and O elements, indicating the formation of mixed nanocomposite nanofibers of Fe_2O_3-Al_2O_3. The BET surface area and pore diameter were found to be 9.6m^2/g and 5.2 nm. The obtained iron oxide-alumina mixed nanocomposite fibres were able to remove Cu (II), Pb (II), Ni (II) and Hg (II) from aqueous solutions. The best isotherm fit for copper and lead was obtained with Langmuir adsorption isotherm while Freundlich was the best option for nickel and mercury. Complete removal of mixed oxide nanocomposite fibres was achieved followed by copper (21%), lead (52%), nickel (67%) and mercury (89%). Finally the metal affinity to the mixed oxide nanocomposite fibres was found to be in the sequence of Cu< Pb <Ni <Hg and the preference of this sorbent for a metal ion may be explained on the basis of electronegativity of the metal ions and on the basis of their cation/anion state. The loaded adsorbent can be efficiently regenerated by diluted HCl and a regeneration efficiency of 90% was achieved using 0.05 mol/L HCl.

CHAPTER 7

SYNTHESIS OF ELECTROSPUN PAN-Ag COMPOSITE NANOFIBER FOR ANTIBACTERIAL APPLICATION

7.1 Introduction

Polymer/inorganic composite nanofiber materials containing metal nanoparticles have attracted a great deal of attention because of their unique optical, electrical, and catalytic properties. The properties of these nanocomposites are strongly dependent on the size, content, dispersivity, and structure of the metal nanoparticles that are incorporated within the polymer matrix (Son et al., 2006). The size and shape-dependent properties of nanocomposites fibers provide a challenge to synthetic chemists for obtaining highly functional advanced materials. Since past several years nanosized metallic particles, especially silver nanoparticles impregnated with polymer matrix have been synthesized successfully by various research groups using various synthetic techniques (Bai et al., 2008, Rujitanaroj et al., 2008, Francis et al., 2010). The polymers can acts as a stabilizer in such system, and its role is to prevent the further growth and aggregation of silver nanoparticles. Silver is particularly attractive among metal nanoparticles because of its significance widespread applications in biology (Chen et al., 2005), antimicrobial properties (Kim et al., 2007), optical properties and oxidative catalysis (Shirashi et al., 2000). There are many research literature reported on the synthesis of silver nanoparticles from Ag^+ ions. Few of them are chemical reduction using aqueous solution of sodium borohydride ($NaBH_4$), hydrazinium hydroxide (N_2H_4OH), dimethyl formamide (DMF), photoreduction by UV irradiation and simple heat treatment. DMF is essentially used as a solvent and is also able to reduce Ag ions to the metallic silver even at room temperature and in the absence of any external reducing agent (Navaladian et al., 2007, Santos et al., 2000, Lee et al., 2005). Recently Lee et al. (2010) have reported an antibacterial activity of silver nanoparticles

prepared by chemical reduction of $AgNO_3$ in water with $NaBH_4$ in presence of SDS as a stabilizer. The prepared silver nanoparticles were spherical in shape having diameters in the range of 10-20 nm and showed good antibacterial activity against *S.aureus* and *E.coli* bacteria. The fundamental mechanism by which silver kills bacteria is by disruption of metabolic processes. Since ancient times, the silver ion has been known to be effective reagent for killing of a broad range of microorganisms (Das et al., 2011, Silver et al., 1996). Similarly, Lanje et al. (2010) has reported on the preparation and antibacterial studies of silver nanoparticle using a simple and low cost chemical route by reducing silver nitrate with glucose in presence of protective agent polyvinylpyrrolidone (PVP). The average particle size of prepared silver nanoparticles were about 15nm, and antimicrobial properties were tested against *S.aureus, E.coli* and *P.aeruginosa* microorganism. Different types of polymers such as Cellulose acetate, PVA, PAN, PVP, PVC, polyurethane etc, have been used as a stabilizers as well as polymer matrix for in-situ formation of polymer-silver composite nanofibers (Lala et al., 2007, Jin et al., 2007). Polyacrylonitrile (PAN) is an important engineering polymer material that has been widely used to produce a variety of synthetic fibers (Lee et al., 2005, Lee et al., 2008) having a unique thermal property (i.e. melting point = 317°C and glass transition temperature = 85°C) and good solvent resistance. Therefore, PAN-Ag nanocomposites are expected to provide a possibility to produce functional fibers with anti-electrostatic, fungicidal and ultraviolet-resisting effects (Feng et al., 1994, Sichani et al., 2010).

Electrospining method was thought to be a simple and user friendly fiber fabrication technique. It uses the electrostatic force to spin fibers from a polymeric solution. Electrospun fibers, however, are often collected in the form of randomly oriented, nonwoven fabrics (Saquing et al., 2009, Zhang et al., 2007). In the recent years electrospinning has been widely used to produce various polymer nanofibers mats functionalized with inorganic nanoparticles. Bai et al. (2007) have synthesized AgCl / PAN composite nanofibers by electrospinning method. The average diameter of the fibers and the number as well as the size of the AgCl particles varies with the change in mole ratio of silver ions to PAN polymer. Dong et al. (2010) have reported on the preparation of uniform Ag nanoparticle–embedded PVA and PVP nanofibers by electrospinning method. The Ag nanoparticles formed on the polymer matrix were in the range of 5-18 nm. Furthermore, the antibacterial study indicates that these Ag nanoparticle–embedded PVP nanofibers can effectively inhibit the propagation and biological activity of yeast cells. Rujitanaroj et al. (2010) have reported on preparation, characterization and antibacterial activity of electrospun PAN fibrous membranes containing

silver nanoparticle. Fiber size was found to be in the range of 180-230 nm and silver nanoparticles were of in the size range 5.3 - 7.8 nm. The authors reported that the antibacterial activity of the membrane against *S.aureus* and *E.coli* bacteria increases with increase in concentration of $AgNO_3$ and UV irradiation time. Zhang et al. (2011) have studied on antimicrobial nanofibrous membrane developed from electrospun polyacylonitrile nanofibers. These PAN nanofibrous membrane were treated with hydroxylamine (NH_2OH) at 70°C to form amidoxime group functionalized nanofibrous membrane. The –(CN) groups on the surface of PAN nanofibers reacted with NH_2OH molecules and led to the formation of $-C(NH_2)=$ N–OH groups, which were used for coordination of Ag^+ ions. Subsequently, the coordinated Ag+ ions were converted into silver nanoparticles. The fibre diameter was found to be ~450 nm. These nanofiber membranes were further used for antimicrobial efficacies against Staphylococcus aures and Escherichia coli. These functionalised espun membrane were found to be highly capable of killing the organisms in 30 min. Recently, Yu et al. (2012) have approached in a modified and new coaxial electrospinning method to synthesize polyacrylonitrile nanofibers coated with silver nanoparticle. The synthesized PAN nanofibers have a diameter of 230 ± 70 nm with the AgNPs uniformly distributed on their surface. The antibacterial experiments were carried out against B.subtilis and E.coli microorganism, the results shows strong antimicrobial activity. Very recently, Chai et al. (2013) have studied on electrospinning preparation of ferrocene/poly (vinly-pyrrolidone) composite nanofibers. The diameter of the obtained composite fibers was found to be 30-200 nm with variation in concentration of ferrocene. Further Fc/PVP composite nanofiber was used for antimicrobial activity using Gram-negative E.coli as model organisms and also can be used as electrochemical sensing applications.

In this present study, we have prepared PAN nanofibers containing $AgNO_3$ by using electrospinning method. The reduction of silver ion into silver metallic nanoparticles could be performed by three different techniques such as chemical reduction using $NaBH_4$, heat treatment and refluxed the PAN/DMF solutions containing $AgNO_3$ at 80°C for 2 h prior to electrospinning. The PAN nanofiber membrane functionalized with Ag nanoparticles (i.e. PAN-Ag nanocomposites) obtained was used to study for antibacterial properties against gram negative *E. coli* and gram positive *S. aureus and B. subtilis* bacteria.

7.2 Experimental procedure

7.2.1 Materials

Polyacrylonitrile (PAN) polymer (av. mol.wt. = 150,000) were purchased from Sigma-Aldrich Co, USA. N, N-dimethylformamide (DMF), and silver nitrate ($AgNO_3$, 99%) were obtained from Merck, India. Ethanol was purchased from Merck, Germany. Beef extract was purchased from Rankem, India. Peptone and NaCl were obtained Loba Chimie Ltd. India. Agar was purchased from Himedia Lab Ltd. Mumbai, India. *Escherichia coli* (NCIM 5051), *Bacillus subtilis* (NCIM 2699) and *Staphylococcus aureus* (NCIM 2654) bacterial stain were obtained from NCIM, Pune, India. Neat and clean glass beaker, conical flasks, funnel (Borosil) and disposable petri-dishes were used to carry out the experiments. Double distilled water was used throughout the experiments. All the chemicals were used without further purifications.

7.2.2 Fabrication of PAN nanofiber containing silver nanoparticle

Polyacrylonitrile (PAN) polymer solution (12 wt %) was prepared by dissolving required amount of PAN polymer in DMF solvent. The mixture was stirred using a magnetic stirrer for 2-3 h at room temperature to form a clear solution. Then 8 wt % (w. r. t PAN polymer) of $AgNO_3$ was added to PAN/DMF transparent solution and was stirred for another 1 h. The above solution was then divided into two parts. One part of the solution was used directly for electrospinning and was loaded into a 3ml plastic syringe fitted with a metallic needle. The PAN solution containing silver ion was pushed to the needle tip using the syringe pump and the feed rate was kept at 0.5 ml/h. Then a positive voltage of 12 kV was applied to the needle tip using high voltage power supply (Glassman Japan) and the negative voltage was connected to the grounded collector covered with aluminium foil which served as counter electrode. The tip to collector distance was maintained 15 cm. All the experiments were conducted at room temperature with a relative humidity (50 - 55 %) condition. Then the as-spun PAN nanofibers containing silver ion could be reduced to metallic silver either by heat treatment or by chemical reduction process. A part of as-spun PAN/$AgNO_3$ composite membrane was sintered at 160°C for 2 h and the other part of the composite membrane was immersed in the 0.1 M $NaBH_4$ aqueous solution for 30 min at room temperature. Then the membrane was washed with distilled water and dried in an oven at 60°C for 2 h to obtain the PAN nanofibers containing Ag nanoparticles.

The other part of the PAN/DMF polymer solution was refluxed at 80°C using water bath for 2h with constant stirring and then used this solution for electrospinning. The previous electrospinning parameters/condition was also maintained same in this case. The PAN nanofibers mats containing Ag nanoparticles in the form of membrane sheet was obtained from the collector and was studied for antibacterial study. Figure 7.1 shows the flow chat of the preparation of Ag nanoparticles functionalized with PAN nanofibers using electrospinning method.

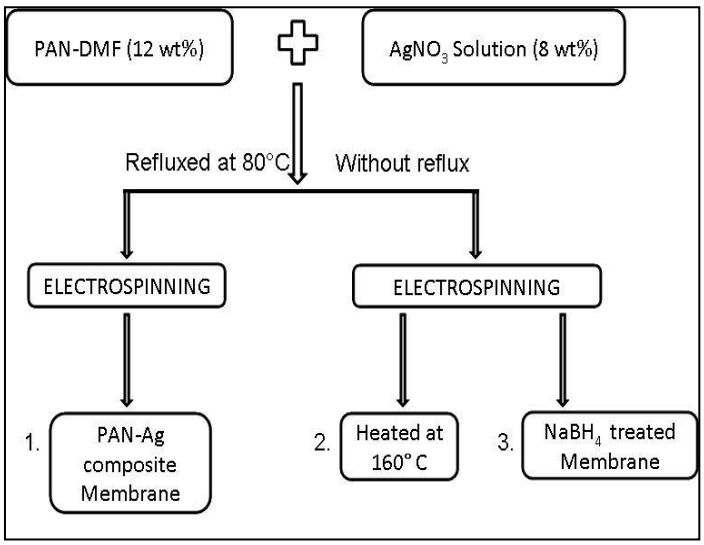

Figure 7.1 Flow chat of the formation PAN-Ag composite nanofibers via electrospinning methods.

7.2.3 Characterization techniques

Surface morphology of electrospun PAN-Ag composite nanofibers were characterized by using Carl-Zeiss FESEM (Carl-Zeiss Supra 55) equipped with Oxford INCA energy dispersive X-ray analyzer system and was operated at 10 kV. Energy dispersive X-ray analysis (EDAX) in SEM was also carried out for the elemental composition analysis of the samples. A Philips TEM (CM-200) was used to observe the Ag nanoparticles on the PAN nanofibers and the size of electrospun composite nanofibers. The composite fibers were collected on a carbon coated Cu grid (300 mesh) and was dried under vacuum for few hours before taking the imaging at 200 kV. IR transmittance spectra in the range of 600–4000 cm^{-1} were measured at room temperature using a Fourier-transform IR spectrometer (Thermo Nicolet, AVATAR 360-FT IR). Absorption spectrum was recorded using a Shimadzu UV-Vis spectrophotometer (UV-2045).

7.2.4. Antimicrobial tests

The antimicrobial activity of nanofiber spun membrane was analyzed by zone inhibition test for which the bactericidal experiment was carried out with gram negative bacteria *Escheria coli* and gram positive bacteria *Bacillus subtilis* and *Staphylococcus aureus.* From stock culture obtained from *NCIM, PUNE,* the microbes were inoculated in 200 ml nutrient media composed of peptone (10g/l), NaCl (5g/l), and beef extract (10g/l) with the pH maintained at 7-7.5 in three separate flasks and were incubated for whole night at 37ºC. Throughout this study, the same nutrient media was used for all strains, unless otherwise specified.

For zone inhibition test, next day, the nutrient agar was prepared with the above mentioned constituents along with solidifying agent agar (20% w/v) followed by sterilization and then pouring into the sterilized disposable petri dishes. The peri plates were kept for solidification. Then from each (flask) bacterial suspension 100 μL volumes were removed and spread uniformly over the agar plates. Small circular pieces of (fixed weight) PAN-Ag composite ultra-fine fiber membranes (test samples) prepared by three different reduction methods were gently placed over the solidify agar gel in different petri dishes. Since there was high chance of discoloration of the membrane disc after zone inhibition test, the petri dishes bearing different groups of sample were properly marked for their identification. Then the petri plates were kept for incubation at 37ºC for whole night. Next day the clear zones surrounding the disc were measured with the help of scale, which depicts the zone of inhibition for that particular bacterium.

7.3 Result and discussion

The entire synthetic procedure of PAN-Ag composite nanofibers using electrospinning mediated synthesis is illustrated in Figure 7.1. The Ag^+ ions present in PAN/Ag^+ as-spun composite nanofiber membrane can be reduced to Ag metallic nanoparticles by three different ways i.e. $NaBH_4$ treated, refluxed with DMF and heat treatment. The mechanism involving the reduction of Ag^+ ions to silver particles in these cases are represented as below.

$$Ag^+ + BH_4^- \rightarrow Ag^0 + \frac{1}{2}H_2 + \frac{1}{2}B_2H_6 \text{ ($NaBH_4$ as reducing agent)}$$

$$HCONMe_2 + 2\ Ag^+ + H_2O \rightarrow 2\ Ag^0 + Me_2NCOOH + H^+ \text{ \{DMF as reducing agent\}}$$

$$Me_2NCOOH \rightarrow Me_2NH + CO_2\uparrow$$

$$2AgNO_3 \xrightarrow{\Delta} 2Ag^0 + O_2\uparrow + 2NO_2\uparrow \text{ (Heat treatment)}$$

DMF has been used as a solvent for electrospinning PAN polymer and besides it can also act as a self reducing agent for reduction of Ag^+ ions (Lee et al., 2005, Rujitanaroj et al., 2010). We have refluxed the PAN and $AgNO_3$ solution in DMF solvent to increase the reaction rate. The formation of a yellow-brown color solution after refluxing confirmed the reduction of Ag^+ ion to silver nanoparticles.

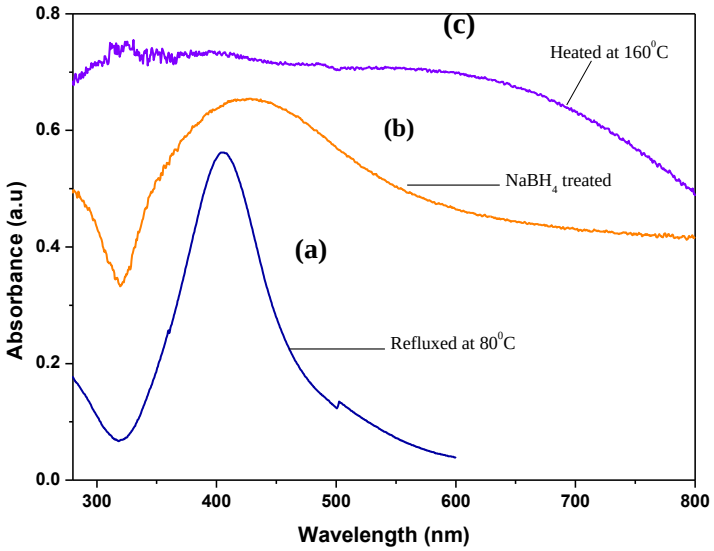

Figure 7.2 UV-Vis spectra of PAN-Ag nanocomposites prepared by (a) refluxed method, (b) $NaBH_4$ reduction method and (c) heat treatment method.

Figure 7.2 shows the UV-Vis spectra of PAN-Ag nanocomposites prepared by three reduction methods. Figure 7.2a represents Ag functionalized PAN polymer prepared by refluxing PAN-$AgNO_3$ (8 wt %) solution in DMF solvent at 80^0C. The surface plasmon absorption band of Ag nanoparticles with size ranges between 2 to 50 nm would be basically observed in the UV-Vis spectrum at a wavelength in the range of 400 to 450 nm (Lee et al., 2005, Lee et al., 2010, Lala et al., 2007). We have observed an absorption maximum peak at 405 nm (Figure 7.2a), which indicates the formation of Ag nanoparticles. We have electrospun this PAN solution containing Ag nanoparticles to obtain the silver nanoparticles embedded on and within PAN nanofibers membrane. Similarly to obtain silver nanoparticles impregnated PAN nanofibers membrane, the Ag^+ ions present in the electrospun PAN nanofiber membrane were reduced to silver nanoparticles using sodium borohydride (Figure 7.2b) and heat treatment (Figure 7.2c) technique. The surface plasmon absorption band between 400-450 nm in the UV-Vis spectra confirmed the formation of Ag nanoparticles.

These silver nanoparticles functionalized PAN nanofibers membrane has been used for antimicrobial applications.

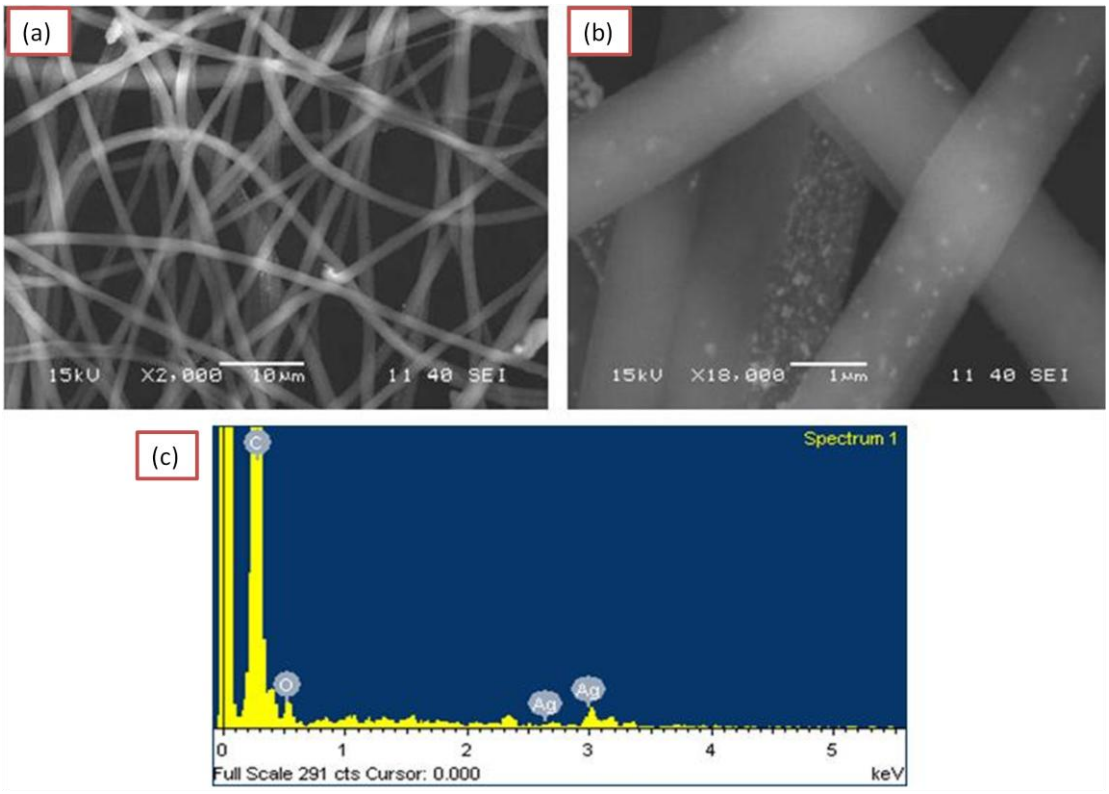

Figure 7.3 SEM images of PAN-Ag nanofiber $NaBH_4$ reduction (a) Lower magnification, (b) Higher magnification and (c) EDAX pattern.

Figure 7.3 shows the SEM images of PAN-Ag composite membrane synthesized by sodium borohydride reduction method. It is observed from the images (Figure 7.3(a, b)) that the obtained fibers are tubular in shape and have a smooth morphology. However, the magnified SEM image (Figure 7.3b) indicates the presence of some aggregated form of the Ag particles on and within the PAN fibers. The sizes of the fibers are found to be in the range of 500 nm to 1 µm. To evaluate the chemical composition of the samples, we have carried out the SEM EDAX analysis of the PAN-Ag composite fibers. Figure 7.3(c) shows the EDAX pattern of the PAN-Ag composite nanofibers prepared by borohydride reduction method. The elemental compositions of the composite fiber were found to be 78.31% of carbon, 12.44% of oxygen, and 8.25 % of Ag, which confirm the formation of PAN-Ag composite fibers.

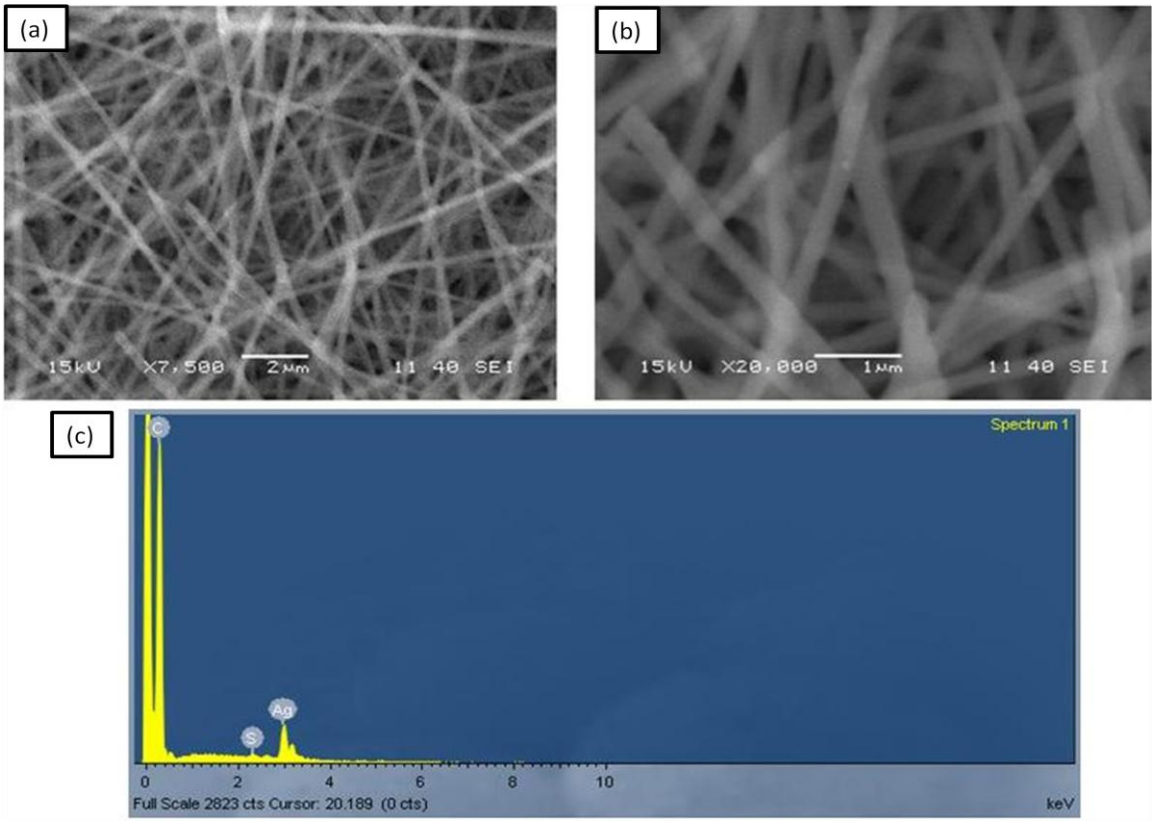

Figure 7.4: SEM images of PAN-Ag composite nanofiber prepared by refluxed method; (a, b) different magnification and (c) EDAX spectrum.

Figure 7.4 provides the SEM images of the PAN-Ag composite membrane synthesized by refluxing with DMF solvent. This image indicates that the fibers are cylindrical shape and have smooth morphology. In this case the fibers obtained are in the range of 200-500 nm in diameter, which is much smaller than that of borohydride reduction method. This might be because of the in situ formation of Ag nanoparticles and presence of $AgNO_3$ in PAN solution that the conductance of the system increases and hence smaller size fibers can be obtained (Jin et al., 2007). As the Ag particles are below 50 nm we haven't observed any Ag nanoparticles in the magnified SEM images. From the chemical analysis EDAX data (figure 7.4(c)), we found that the wt % of carbon is 90.64 and of Ag is 9.04%, with little impurities of S (0.32%) that confirm the formation of PAN-Ag composites.

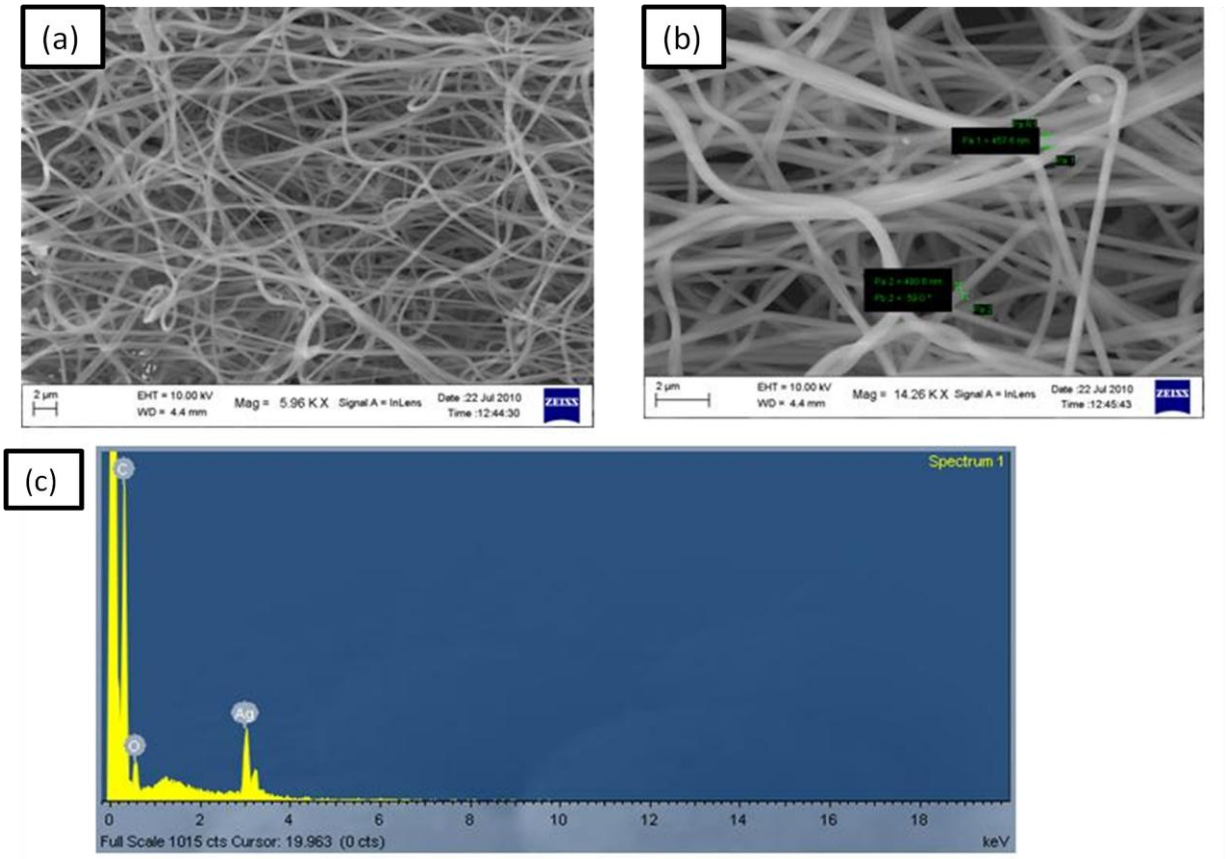

Figure 7.5: SEM images of PAN-Ag composite nanofibers prepared by heat treatment method; (a, b) different magnification and (c) EDAX spectrum.

Similarly, Figure 7.5 indicates the SEM images of the PAN-Ag composite membranes obtained by heating of the PAN/$AgNO_3$ composite membrane above 160°C. These images also suggest the formation of continuous ultrafine fibers having diameter in the range of 200-500 nm. The SEM-EDAX spectra (figure 7.5(c)) suggest the presence of C, Ag, and O atoms, indicating the formation of Ag/ Ag_2O nanoparticles on the surface of PAN fibers.

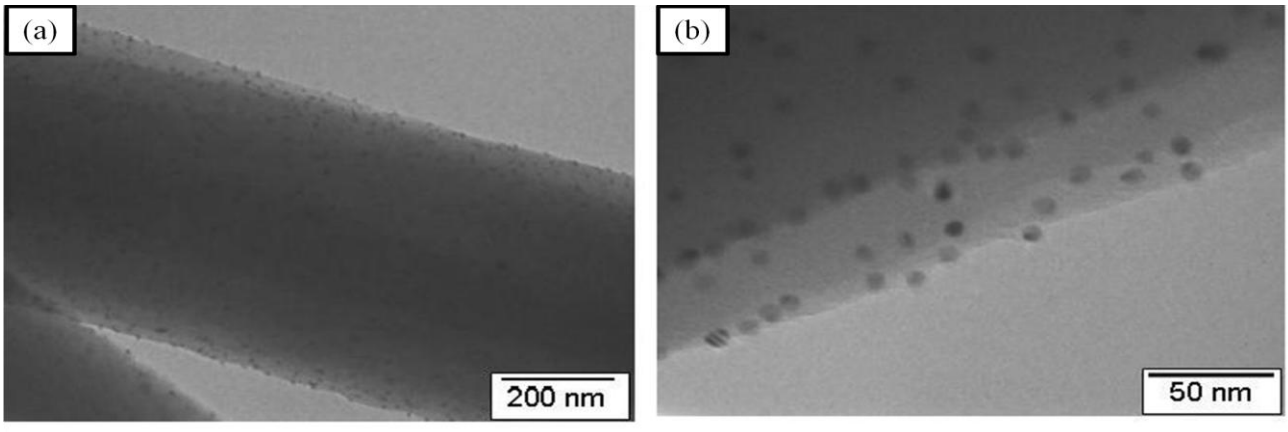

Figure 7.6 TEM images of PAN-Ag composite nanofibers prepared by refluxing method; (a. b) different magnification images.

Figure 7.6 represents the TEM images of the PAN-Ag composite nanofibers, prepared by refluxing $AgNO_3$ in DMF/PAN at 80°C. It is observed that uniform, spherical Ag nanoparticles with a narrow size distribution having diameter in the range of 7–10 nm are formed on and within the fibers. However, the diameters of the PAN fibers are found to be 400 nm, which is consistent with the results obtained from SEM.

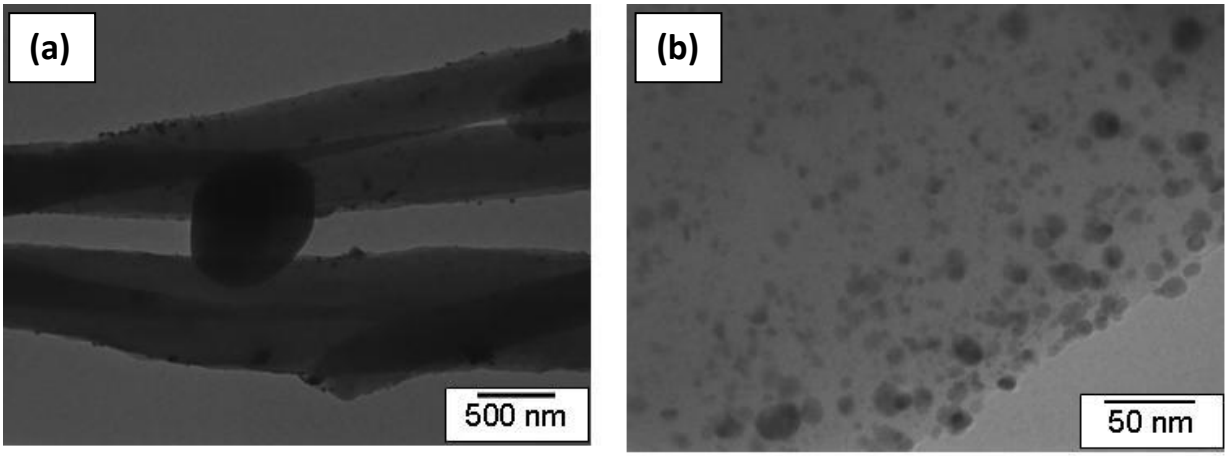

Figure 7.7 TEM images of PAN-Ag composite nanofibers, prepared by $NaBH_4$ reduction; (a, b) different magnification images.

Figure 7.7, shows the TEM images of the PAN-Ag composite membrane prepared by $NaBH_4$ reduction method. In this case also spherical Ag nanoparticles are formed on and within the fiber surface, but they are polydisperse in nature. The size of the Ag nanoparticles as measured from the TEM images is found to be in the range of 5–20 nm.

7.3.1 Antibacterial activity

The antibacterial activity of PAN nanofibers membrane functionalized with the Ag nanoparticles was assessed against bacterial strain *S. aureus, E. coli and B. subtilis*. The length of the inhibition zones of the composite fibers mats were analyzed and are shown in the figure 7.8.

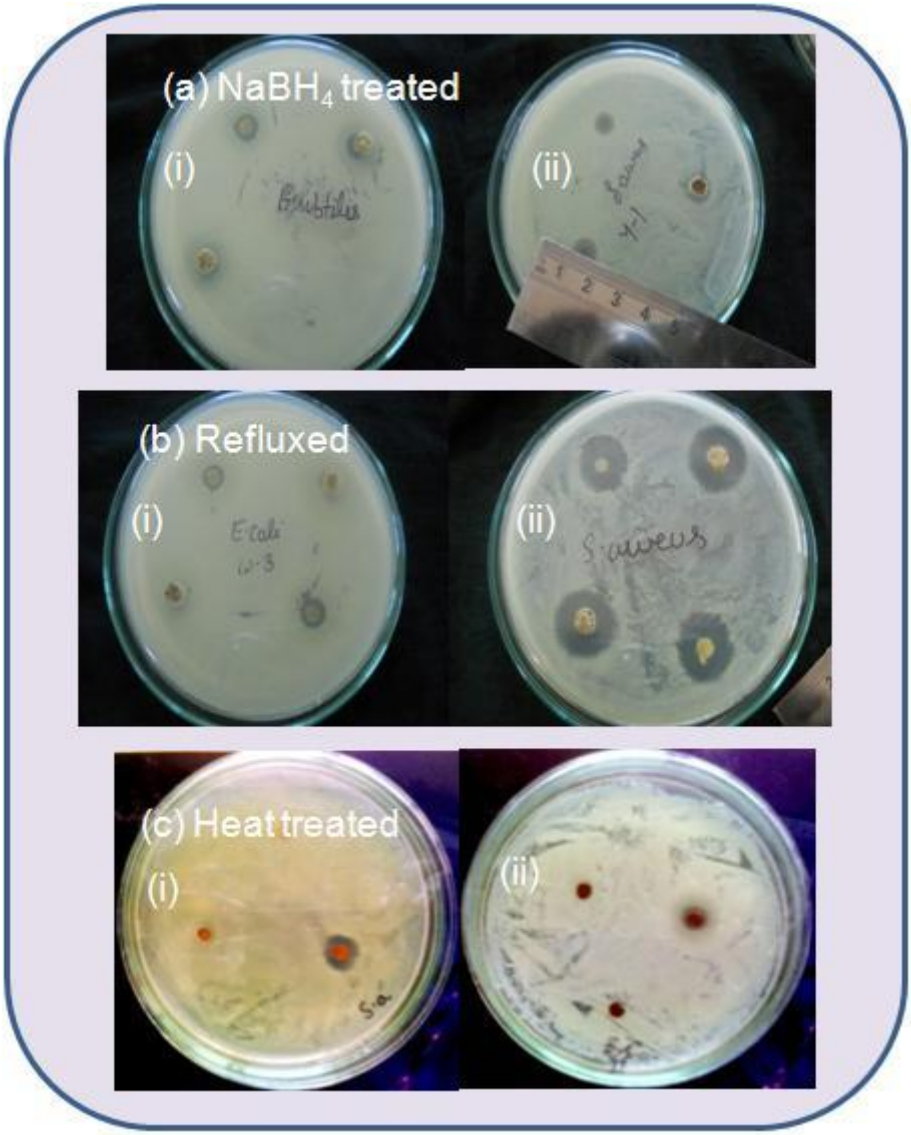

Figure 7.8: Photographs showing zone of inhibition of the PAN-Ag composite membrane prepared by (a) $NaBH_4$ treated (i) *B. Subtilis (ii) S. aureus* (b) Refluxed (i) *E. Coli* (ii) *S. aureus*, and (c) Heat treatment *(i) S. aureus* and (ii) *B. Subtilis*.

It is reported that electrospun pure PAN nanofibers mats shows nonbacterial properties against *S. aureus* and *E coli* bacterial and hence inhibition zone is absent in case of PAN fibers mats (Lala et al., 2007). However, the Ag nanoparticles loaded polymer fibers show strong bactericidal properties (Lala et al., 2007, Rujitanaroj et al., 2010). We have used all three different types of PAN nanofibers mat functionalized with Ag nanoparticles (containing 8 wt % of $AgNO_3$ w.r.t. to PAN) for the antibacterial test against above three mentioned bacterial strain. The length of inhibition zone against the three bacteria is reported in Table 7.1.

Table 7.1 Antibacterial activity of PAN-Ag composite fibers prepared by different synthetic strategies.

Sl.No	Microorganisms	Zone of inhibition in mm		
		Reduction using $NaBH_4$	Heated at 150°C	Refluxed at 80°C
1)	*Bacillus subtilis*	7.5	6	10
2)	*Staphylococcus aureus*	9	10	20
3)	*Escherichiacoli*	Not recognisible	6	9

It is observed from the table that all the three different PAN-Ag composite nanofibers mats prepared by different reduction methods show good antibacterial properties. However, the length of inhibition zone is found to be highest against S.aureus bacteria for the PAN-Ag composite membrane that was prepared by refluxing Ag^+ ions in DMF solvent in the presence of PAN polymer prior to electrospinning. This data showed a very good antibacterial property. This result can be interpreted as in case of PAN-Ag composite fibers prepared by refluxed method where the silver ion present on the surface as well as inside PAN polymer solution get reduced in situ to Ag nanoparticles. The rate of formation of Ag particles is also increase because of refluxing in DMF solvents. However, DMF solvent can also acts as a reducing agent for Ag^+ ions to form Ag nanoparticles, but the rate of reduction is very slow and taes several days for complete reduction of silver ions into silver nanoparticles (Rujitanaroj et al., 2010). Since the Ag nanoparticles dispersed PAN matrix has been electrospun to form PAN-Ag nanocomposites in this refluxed method, there is a greater probability of formation of uniform Ag nanoparticles on and within the surface of the fibers. The nanoparticles formed were also smaller in size (i.e. 7-10 nm) as compared to other two reduction methods. As a result, these nanofiber mats show better antibacterial properties. However, for PAN-Ag composite membrane prepared by $NaBH_4$ and heat treatment method, the Ag nanoparticles formed were comparatively larger in size and perhaps more in numbers embedded inside the polymer matrix and hence less exposure to bacterial cell. Similarly in case of heat treatment nanofiber mat, there might be presence of mixture of Ag and Ag_2O nanoparticles on and inside the fiber surface. Although all the three PAN-Ag composite nanofibers membrane show good antibacterial properties, the composite fibers membrane prepared by refluxing method is best for killing the S. aureus microorganism.

7.4 Conclusion

PAN/$AgNO_3$ composite nanofibers containing 8 wt% of $AgNO_3$ with respect to PAN has been prepared by electrospinning method. The reduction of Ag^+ ions on and inside the fiber surface leads to form PAN-Ag composite ultra-fine fibers. We have performed three different methods such as refluxing in DMF prior to electrospinning, using $NaBH_4$ as reducing agent and on heating at higher temperature (160^0C) to prepare PAN-Ag composite membrane. The obtained PAN-Ag composite fibers were characterized by UV-Vis, SEM, EDAX and TEM analytical techniques. UV-Vis spectra confirmed the formation of Ag nanoparticles. SEM images show that the fibers have a smooth morphology and having diameter in the range of 200-500 nm for refluxed and heat treated fibers. However, an increase in fibers diameter was observed for PAN–Ag composite membrane prepared by borohydride reduction method. The antibacterial activity of PAN-Ag composite fibers prepared by all three methods has been studied against three microorganisms such as *S. aureus, E coli and S. Bacillus*. All the three different PAN-Ag composite fibers membrane shows good antibacterial properties. However, the PAN-Ag fibers prepared by refluxing in DMF were most prominent against *S.aureus* microorganisms. This result might be due to formation of more percentage of Ag nanoparticles on the fibers surface as compared to fibers prepared by other two reduction method.

Conclusions

One dimensional nanosized alumina specifically boehmite phase and iron oxides are important ceramic materials that show promising chemical and physical properties and are used in water treatment applications. In this thesis we have worked on the synthesis of one dimensional aluminium, iron oxide and their mixed nanocomposite materials.

In this present studies, we have successfully synthesized rod, and fiber shaped alumina, iron oxide, and iron oxide-alumina mixed nanocomposite by three different synthetic methods i.e. sol-gel, hydrothermal and electrospinning method. The formation, structure, size, surface morphology, thermal stability, surface area and sorption capacities of the synthesized 1d nanomaterials and mixed oxide nanocomposites have been characterized by using different characterization techniques such as FT-IR, XRD, SEM-EDAX, TEM, TGA-DTA, BET, UV-Vis and AAS. The obtained alumina and iron oxide-alumina mixed nanocomposites were used as adsorbents for removal of both toxic metal ions like Cr (VI), Pb (II), Hg (II), Ni (II), Fluoride ions and organic dyes like Congo red from aqueous solution. It is observed that, the needle shaped boehmite, synthesized by sol-gel method is a very good adsorbent for removal of Congo red (CR) dye. Within a very short contact time of 10 min, 99% of CR removal is observed having a maximum sorption capacity of 198 mg/g. On further sintering at higher temperature, boehmite phase converted to alumina and its adsorption capacity for removal of CR dye decreases. It is because of the absence of oxyhydroxy group in alumina material which plays an important role in the removal of Congo red dye. Alumina nanofibers with diameter in the range of 100-500 nm have been synthesized by electrospinning method. The obtained alumina nanofibers are found to be suitable adsorbents for removal of Cr (VI) and fluoride (F^-) ions. The maximum removal was found to be 70 % for Cr (VI) and 50 % for fluoride ions. Moreover, the adsorption kinetics is governed by pseudo-second-order rate law. The mixed iron oxide-alumina nanocomposites have been synthesized using hydrothermal method and used for removal of Congo red dye. Complete removal (100%) of Congo red dye by mixed iron oxide-alumina nanocomposite was observed within a short contact time of 15 min and the adsorption capacity was found to be 498 mg/g. However, Fe_2O_3-Al_2O_3 nanocomposites synthesized by electrospinning method

are very good adsorbent for removal of toxic ions such as Cr, Pb, Hg and Ni. The metal removal affinity onto the mixed oxide nanocomposite fibers surface was found to be in the sequence of Cu <Pb <Ni <Hg and the preference of this sorbent for a metal ion may be explained on the basis of electronegativity of the metal ions and on the basis of their cation/anion state.

All the above results show that the obtained alumina and iron oxide-alumina composites are excellent nano-adsorbents for decontamination of both heavy metals ions and organic dye pollutants. Furthermore, using electrospinning method we have synthesized PAN-Ag composite polymer nanofibers. These PAN nanofibers functionalized with Ag nanoparticles on the surface. The obtained PAN-Ag composite nanofibers have been used for environmental application especially antibacterial studies. It is observed that the obtained PAN-Ag nanocomposite fibers are promising materials for decontaminating both gram positive and gram negative microbial such as *S. Aureus, E. Coli & S. Bacillus*.

Reference

Abd El-Latif, M. M., Ibrahim, A. M., and El-Kady, M. F., "Adsorption Equilibrium, kinetics and thermodynamics of methylene blue from aqueous solutions using biopolymer oak sawdust composite," J. American Sci., **6**, 267-283 (2010) .

Abdullayev, E., Sakakibara, K., Okamoto, K., Wei, W., Ariga, K., and Lvov, Y., "Natural Tubule Clay Template Synthesis of Silver Nanorods for Antibacterial Composite Coating," Appl. Mater. Inter., **3**, 4040–4046 (2011).

Acemioglu, B., "Adsorption of Congo red from aqueous solution onto calcium-rich fly ash," J. Colloid Interface Sci., **274**, 371–379 (2004).

Afkhami, A., and Moosavi, R., "Adsorptive removal of Congo red, a carcinogenic textile dye, from aqueous solutions by maghemite nanoparticles," J. Hazard. Mater., **174**, 398-403 (2010).

Agarwal, S., Wendorff, J. H.,and Greiner, A., "Use of electrospinning technique for biomedical applications," Polymer **49,** 5603–5621 (2008).

Ahn, B. W., and Kang, T. J., "Preparation and characterization of magnetic nanofibers with iron oxide nanoparticles and Poly (ethylene terephthalate)", J. Appl. Polym. Sci., **125**, 1567- 1575 (2012).

Akbari, B., Tavandashti, M. P., and Zandrahimi, M., "Particle Size Characterization of Nanoparticles – A Practicalapproach," IJMSE **8**, 48-56 (2011).

Al'myasheva, O. V., Korytkova, E. N., Maslov, A. V., and Gusarov, V. V., "Preparation of nanocrystalline alumina under hydrothermal conditions", Inorg. Mater., **41**, 460- 467 (2005).

Allen, S. J., Mckay, G., and Porter, J. F., "Adsorption isotherm models for basic dye adsorption by peat in single and binary component systems," J. Colloid Inter. Sci., **280,** 322-333 (2004).

Almeida, T. P., Fay, M., Zhu, Y., and Brown, P. D., "Process map for the hydrothermal synthesis of α- Fe_2O_3 nanorods", J. Phys. Chem. C, **113**, 18689- 18698 (2009).

Alves, A. K., Berutti, F. A., and Bergmann, C. P., "The effects of pH on the preparation of alumina by sol-gel process," Part. Sci. Tech., **23**, 351-360 (2005).

Arami, H., Mazloumi, M., Khalifehzadh, R., and Sadrnezhaad, S. K., "Bundles of self assembled bohemite nanostrips from a surfactant free hydrothermal route", J. Alloy Comp., **461**, 551- 554 (2008).

Arias, M., Pantojas, V. M., Perales, O., and Otano, W., "Synthesis and characterization of magnetic diphase $ZnFe_2O_4$/ϒ- Fe_2O_3 electrospun fibers", J. Magn. Magn. Mater., **323**, 2109- 2114 (2011).

Aslani, A., and Morsali, A., "Sonochemical synthesis of nano-sized metal-organic lead (II) polymer: A precursor for the preparation of nano-structured lead (II) iodide and lead(II) oxide," Inorganica Chimica Acta., **362**, 5012–5016 (2009)

Asmatulu, R., Ceylan, M., and Nuraje, N., "Study of superhydrophobic electrospun nanocomposite fibers for energy systems," Langmuir., **27**, 504-507 (2010).

Asokan, K., Park, J. Y., Choi, S. W., and Kim, S. S., "Nanocomposite ZnO- SnO2 nanofibers synthesized by electrospinning method", Nanoscale Res. Lett., **5**, 747- 752 (2010).

Asuha, S., Zhao, Y. M., Zhao, S., and Deligeer, W., "Synthesis of mesoporous maghemite with high surface area and its adsorptive properties," Sol. state Sci., **14**, 833-839 (2012).

Azad, A. M., "Fabrication of transparent alumina (Al_2O_3) nanofibers by electrospinning", Mater. Sci. Eng., A, **435- 436**, 468- 473 (2006).

Aziz, M., Abbas, S. S., and Baharom, W. R. W., "Size-controlled synthesis of SnO_2 nanoparticles by sol–gel method," Materials Letters, **91**, 31–34 (2013).

Viswanathan, B., "Nano Materials," Narosa publishing house, 13.1- 13.36 (2009).

Bai, J., Li, Y., Li, M., and Yang, Q., "Electrospinning method for the preparation of silver chloridenanoparticles in PVP nanofiber," Appl. Surf. Sci., **254**, 4520–4523 (2008).

Bai, J., Yang, Q., and Chen, X., "Synthesis of AgCl/PAN composite nanofibres using an electrospinning method," Nanotechnology., **18**, 305601 (2007).

Baji, A., Mai, Y. W., Wong, S. C., Abtahi, M., and Chen, P., "Electrospinning of polymer nanofibers: Effects on oriented morphology, structures and tensile properties", Compos. Sci. Technol., **70**, 703- 718 (2010).

Bang, J. H., and Suslick, K. S., "Sonochemical Synthesis of Nanosized Hollow Hematite," J. Am. Chem. Soc., **129**, 2242-2243 (2007).

Baykal, A., Toprak, M. S., Durmus Z., Senel, M., Sozeri, H., and Demir, A., "Synthesis and Characterization of Dendrimer-Encapsulated Iron and Iron-Oxide Nanoparticles, J Super. Cond. Nov. Magn., **25**,1541–1549 (2012).

Bhardwaj, N., and Kundu, S. C., "Electrospinning: A fascinatingfiber fabrication technique," Biotechnol. Adv., **28**, 325–347 (2010).

Bhattacharjee, C. R., and Nath A., "Chemical Vapour Deposition (CVD) Technique and the Synthesis of Carbon Nanomaterials (CNMs)," J. Chem. Pharm. Res., **4**, 706-713 (2012).

Bhushan, B., "Handbook of Nanotechnology", publisher Springer, 1-5 (2010).

Biswas, A., Park, H., and Sigmund, W. M., "Flexible ceramic nanofibermat electrospun from TiO_2–SiO_2 aqueous sol," Ceram. Internat., **38**, 883–886 (2012).

Bouslama, M., Amamra, M. C., Jia, Z., Amar, M. B., Chhor, K., Brinza, O., Abderrabba, M., Vigens, J.-L., and Kanaev, A., "Nanoparticulate TiO2- Al2O3 photocatalytic media: effect of particle size and polymorphism on photocatalytic activity", ACS Catal., **2**, 1884- 1892 (2012).

Braga, T. P., Vasconcelos, I. F., Sasaki, J. M., Fabris, J. D., deOliveira, D. Q. L., and Valentini, A., "Magnetic composites based on hybrid spheres of aluminium oxide and superparamagnetic nanoparticles of iron oxides," J. Magn. Magn. Mater., **322,** 633–637 (2010).

Bulut, E., Ozacar, M.,˙and Sengil, I. A., "Equilibrium and kinetic data and process design for adsorption of Congo red onto bentonite," J. Hazard. Mater., **154**, 613–622 (2008).

Byrappa, K., Yoshimura, M., "Handbook of Hydrothermal Technology", Pub: William Andrew, (2012).

Cai, W., Hu, Y., Chen, J., Zhang G., and Xia, T., "Synthesis of nanorod-like mesoporous γ-Al_2O_3 with enhanced affinity towards Congo red removal: Effects of anions and structure-directing agents," Cryst. Eng. Comm., **14**, 972-977 (2012).

Cai, W., Yu J., Gu, S., and Jaroniec, M., "Facile Hydrothermal Synthesis of Hierarchical Boehmite: Sulfate-Mediated Transformation from Nanoflakes to Hollow Microspheres," Cryst. Growth & Des., **10**, 3977-3982 (2010).

Cai, W., Yu, J., and Jaroniec, M., "Template-free synthesis of hierarchical spindle-like γ-Al_2O_3 materials and their adsorption affinity towards organic and inorganic pollutants," J. Mater. Chem., **20**, 4587–4594 (2010).

Cannas, C., Musinu, A., Peddis, D., Piccaluga, G., "New synthesis of ferrite-silica nanocomposites by a sol-gel auto-combustion", J. Nanopart. Res., **6**, 223- 232 (2004).

Cao, C. Y., Qu, J., Yan, W. S., Zhu, J. F., Wu, Z. Y., and Song, W. G., "Low-cost synthesis of flowerlike α-Fe_2O_3 nanostructures for heavy metal ion removal: adsorption property and mechanism," Langmuir., **28**, 4573-4579 (2012).

Cao, H. Q., Xu, Z., Sang, H., Sheng, D., and Tie, C. Y., "Template Synthesis and Magnetic Behavior of an Array of Cobalt Nanowires Encapsulated in Polyaniline Nanotubules," Advanced Mater., **13**, 121-123 (2001).

Cao, M., Liu, T., Gao, S., Sun, G., Wu, X., Hu, C., and Wang, Z. L., "Single-crystal dendritic micro- pines of magnetic α-Fe_2O_3: large scale synthesis, formation mechanism, and properties", Angew. Chem. Int. Ed., **44**, 4197- 4201 (2005).

Chae, H.,H., Kim, B-H., Yang, K. S., and Rheed, J. I, "Synthesis and antibacterial performance of size-tunable silver nanoparticles with electrospun nanofiber composites," Synthet. Meta., **161,** 2124–212 (2011).

Chai, J-H., and Wu, Q-S., "Electrospinning preparation and electrical andbiological properties of ferrocene/poly (vinylpyrrolidone) composite nanofibers," Beilstein J. Nanotechnol., **4**, 189–197 (2013).

Chandradass, J., Bae, D. S., and Balasubramanian, M., "Synthesis and characterization of sol-gel alumina fiber by seeding α-alumina through extended ball milling", Mater. Manuf. Processes, **23**, 786- 790 (2008).

Chan, W.C.W. and Nie, S., "Quantom dot bioconjugates for ultrasensitive nonisotopic detection", Science, 281, 2016-2018 (1998).

Chang, C., Zhang, C., Wang, W., and Li, Q., "Preparation and magnetic properties of Fe_2O_3 microtubules prepared by sol-gel template method", Rare Metals, **29**, 501- 504 (2010).

Chang, T. S., Na, J. H., Jung, C.U., and Koo, S. M., "An easy one-pot sunthesis of structurally controlled aluminium hydroxide particles from an aqueous sidium aluminate solution," J. Phys. Cer. Process. Res., **10**, 832-839 (2009).

Chatterjee, S., Lee, D. S., Lee, M. W., and Woo, S. H., "Enhanced adsorption of congo red from aqueous solutions by chitosan hydrogel beads impregnated with cetyl trimethyl ammonium bromide," Bioresources Techno., **100**, 2803–2809 (2009).

Chatterjee, S., Lee, D. S., Lee, M.W., Woo, S. H., "Congo red adsorption from aqueous solutions by using chitosan hydrogel beads impregnated with nonionic or anionic surfactant," Bioresour. Technol., **100**, 3862–3868 (2009).

Chatterjee, S., Lee, M. W., and Woo, S. H., "Adsorption of Congo red by chitosan hydrogel beads impregnated with carbon nanotubes," Bioresour. Technol., **101**, 1800–1806 (2010).

Chattopadhyay, K. K., and Banerjee, A. N., "Introduction to Nanoscience and Nanotechnology", Publisher PHI learnings pvt ltd, Chap 1, 1-5 (2009).

Chaudhari, S., and Srinivasan, M., "1D hollow α-Fe_2O_3electrospun nanofibers as high performance anode material for lithium ion batteries," J. Mater. Chem., **22**, 23049-23056 (2012).

Chaudhury, N. K., Gupta, R., and Gulia, S., "Sol-gel Technology for Sensor Applications", Defence Sci. J., **57**, 241-253 (2007).

Chen, C. H., Garofano, J. K. M., Muoto, C. K., Mercado, A. L., Suib, S. L., Aindow, M., Gell, M., and Jordan, e. H., "A foaming esterification sol- gel route for the synthesis of Magnesia- Yttria nanocomposites", J. Am. Ceram. Soc., **94**, 367- 371 (2011).

Chen, J., Saeki, F., Wiley, B. J., Au, L., Li, X .D., and Xia, Y., "Gold Nanocages: Bioconjugation and Their Potential Use as Optical Imaging Contrast Agents," Nano Lett., **5**, 473-477 (2005).

Chen, Y-H, and Li, F-A, "Kinetic study on removal of copper (II) using goethite and hematite nano-photocatalysts," J. Colloid Interface Sci., **347**, 277–281 (2010).

Cheng, B., Le, Y., Cai, W., and Yu, J., "Synthesis of hierarchical Ni $(OH)_2$ and NiO nanosheets and their adsorption kinetics and isotherms to Congo red in water," J. Hazard. Mater., **185**, 889–897 (2011).

Chiou, M. S., Ho, P. Y., and Li, H. Y., "Adsorption of anionic dyes in acid solutions using chemically cross-linked chitosan beads," Dyes and Pigments., **60**, 69–84 (2004).

Choi, H., Stathatos, E., and Dionysiou, D. D., "Sol–gel preparation of mesoporous photocatalytic TiO_2 films and TiO_2/Al_2O_3 composite membranes for environmental applications," Appl. Catal., B **63**, 60–67 (2006).

Chronakis, I. S., "Novel nanocomposites and nanoceramics based on polymer nanofibers using electrospinning process- A review", J. Mater. Process. Technol., **167**, 283- 293 (2005).

Colleen, M., Janczak, Craig A, Aspinwall, "Composite nanoparticles: the best of two worlds," Anal. Bioanal. Chem., **402**, 83-89 (2012).

Compagnini, G., Scalisi, A. A., and Puglisi, O., "Production of gold nanoparticles by laser ablation in liquid alkanes," J. Appl. Phys. **94**, 7874-7877 (2003).

Cornell, R.M., and Schwertmann, U., "The Iron Oxides: Structure, Properties, Reactions, Occurrences and Uses", Publihers Wiley. 51-52 (2003).

Creighton, J. R., and Ho, P., "Introduction to Chemical Vapor Deposition (CVD)," ASM International. Chemical Vapor Deposition (#06682G) (2001).

Cui, H., Liu, Y., and Ren, W., "Structure switch between α-Fe_2O_3, ϒ-Fe_2O_3 and Fe_3O_4 during the large scale and low temperature sol–gel synthesis of nearly monodispersed iron oxide nanoparticles", Adv. Powder Technol., **24**, 93–97 (2013).

Cullity, B. D., "Elements of X-Ray Diffraction," Addison-Wesley Publishing Company, (1956).

Dablemont, C., Lang, P., Mangeney, C., Piquemal, J-Y., Petkov V., Herbst, F., and Viau, G., "FTIR and XPS Study of Pt Nanoparticle Functionalization and Interaction with Alumina," Langmuir., **24**, 5832-5841 (2008).

Dahl, J. A., Maddux, B. L. S., and Hutchison, J. E., "Toward Greener Nanosynthesis," Chem. Rev. **107**, 2228−2269 (2007).

Dahlan, Marsih, I. N., Makertihartha, I. G. B. N., Praserthdam, P., Panpranot, J., and Ismunandar., "γ-Alumina nanotubes prepared by hydrothermal method as support of iron, cobalt and nickel for Fischer-Tropsch catalysts," Chem. Mater. Res., **2**, 31-38 (2012).

Dai, H., Gong, J., Kim, H., and Lee, D., "A novel method for preparing ultra- fine alumina-borate oxide fibers via electrospinning technique", Nanotechnology, **13**, 674- 677 (2002).

Dai, Y., Liu, W., Formo, E., Sun, Y., and Xia, Y., "Ceramic nanofibers fabricated by electrospinning and their applications in catalysis, environmental science, and energy technology," Polym. Adv. Technol., **22**, 326–338 (2011).

Darzi, S. J., and Mahjoub, A. R., "Investigation of phase transformations and photocatalytic properties of sol–gel prepared nanostructured ZnO/TiO_2 composites," J. Alloys Compds., **486**, 805–808 (2009).

Das, M. R., Sarma, R. K., Saikia, R., Kale,V. S., Shelke, M. V., and Sengupta, P., "Synthesis of silver nanoparticles in an aqueous suspension of graphene oxide sheets and its antimicrobial activity," Colloid.and Surf B., **83**, 16–22 (2011).

Davis, S. R., Brough, A. R., and Atkinson, A., "Formation of silica/epoxy hybrid network polymers," J. Non-Crystalline Solids., **315**, 197-205 (2003).

Dawood, S., and Sen, T. K., "Removal of anionic dye Congo red from aqueous solution by raw pine and acid-treated pine cone powder as adsorbent: Equilibrium, thermodynamic, kinetics, mechanism and process design," Water Res., **46**, 1933-1946 (2012).

Deb, P., Basumallick, A., Chatterjee, P., and Sengupta, S.P., "Preparation of a α-Fe_2O_3 Nanoparticles from a Nonaqueous Precursor Medium," Script Materialia., **45**, 341-346 (2001).

Deng, Y. H., Wang, C. C., Hu, J. H., Yang, W. L., and Fu, S. K., "Investigation of formation of silica-coated magnetite nanoparticles via sol-gel approach", Colloids Surf., A, **262**, 87- 93, (2005).

Deng, Y., Yang, Q., Lu, G., and Hu, W., "Synthesis of Υ-Al_2O_3 nanowires through a bohemite precursor route", Ceram. Int., **36**, 1773- 1777 (2010).

Devan, R. S., Patil, R. A., Lin, J-H, and Ma, Y-R, "One-Dimensional Metal-Oxide Nanostructures: Recent Developments in Synthesis, Characterization, and Applications," Adv. Funct. Mater. **22**, 3326–3370 (2012).

Dia, Y., Lu, X., McKiernan, M., Lee, E. P., Sun, Y., and Xia, Y., "Hierarchical nanostructures of K-birnessite nanoplates on anatase nanofibers and their application for decoloration of dye solution," J. Mater. Chem., **20**, 3157–3162 (2010).

Dong, G., Xiao, X., Liu, X., Qian, B., Ma, Z., Ye, S., Chen, D., and Qiu, J., "Preparation and characterization of Ag nanoparticleembedded polymer electrospun nanofibers," J. Nanopart Res., **12**, 1319–1329 (2010).

Dong, H., Xie, M., Xu, J., Li, M., Peng, L., Gue, X., and Ding, W., "Iron oxide and alumina nanocomposite applied to Fischer-Tropsch synthesis," Chem. Commun., **47**, 4019-4021 (2011).

Dong, M., Lin, Q., Sun, H., Chen, D., Zhang, T., Wu, Q., and Li, S., "Synthesis of Cerium Molybdate Hierarchical Architectures and Their Novel Photocatalytic and Adsorption Performances," Cryst.Growth Des., **11**, 5002-5009 (2011).

Dong, Z., Kennedy, S. J., and Wu, Y., "Electrospinning materials for energy-related applications and devices," J. Power Sources, **196**, 4886–4904 (2011).

Dorigato, A., and Pegoretti, A., "The role of alumina nanoparticles in epoxy adhesives," J. Nanoparticle Res., **13**, 2429-2441 (2011).

Dringen, R., Koehler, Y., Derr, L., Tomba, G., Schmidt, M. M., Treccani, L., Ciacchi, L. C., and Rezwan, K., "Adsorption and reduction of glutathione disulfide on α-Al_2O_3 nanoparticles: experiments and modeling," Langmuir., **27**, 9449-9457 (2011).

Durrani, S. K., Hussain, S. Z., Saeed, K., Khan, Y., Arif, M., and Ahmed, N., "Hydrothermal synthesis and characterization of nanosized transition metal chromite spinels", Turk. J. Chem., **36**, 111- 120, (2012).

Eid, C., Brioude, A., Salles, V., Plenet, J. C., Asmar, R., Monteli, Y., Khoury, A., and Miele, P., "Iron based 1D nanostructures by electrospinning process", Nanotechnology, **21**, 125701- 7 (2010).

Farag, H. K., Zoubi, M. A., and Endres, F., "Sol- gel synthesis of alumina, titania and mixed oxide alumina/titania in the ionic liquid 1-butyl-1-methylpyrrolidinium bis(trifluoromethylsulphonyl) amide", J. Mater. Sci., **44**, 122- 128 (2009).

Fei, J., Cui, Y., J. Zhao, J., Gao, L., Yang, Y., and Li, J., "Large-scale preparation of 3D self-assembled iron hydroxide and oxide hierarchical nanostructures and their applications for water treatment," J.Mater.Chem., **21**, 11742-11746 (2011).

Feng, C., Khulbe, K. C., Matsuura, T., Tabe, S., and Ismail A.F., "Preparation and characterization of electro-spun nanofiber membranes and their possible applications in water treatment," Sep. Purif. Technol., **102**, 118–135 (2013).

Firmansyah, D, A., Sullivan, K., Lee, K-S., Kim, Y. Ho., Zahaf, R., Zachariah, M. R., and Lee, D., "Microstructural Behavior of the Alumina Shell and Aluminum Core Before and After Melting of Aluminum Nanoparticles," J. Phys. Chem. C., **116**, 404–411 (2012).

Formo, E., Yavuz, M.S., Lee, E. P., Lane, L., and Xia, Y., "Functionalization of electrospun ceramic nanofibre membranes with noble-metal nanostructures for catalytic applications," J. Mater. Chem., **19**, 3878–3882 (2009).

Fouda, M.F.R., ElKholy, M. B., Mostafa, S. A., Hussien, A. I., Wahba, M. A., and El-Shahat, M. F., "Characterization and evaluation of nano-sized α-Fe_2O_3 pigments synthesized using three different carboxylic acid", Adv. Mat. Lett., **4**, 347-353 (2013).

Francis, L., Giunco, F., Balakrishnan, A., and Marsano, E., "Synthesis, characterization and mechanical properties of nylon–silver composite nanofibers prepared by electrospinning," Curr.Appl.Phys., **10**, 1005–1008 (2010).

Fung, Y-L E., and Wang, H., "Investigation of reinforcement of porous alumina by nickel aluminate spinel for its use as ceramic membrane," J. Membr. Sci., **444**, 252–258 (2013).

Gangwar, J., Dey, K. K., Komal, Praveen, Tripathi, S. K., and Srivastava, A. K., "Microstructure, phase formations and optical bands in nanostructured alumina," Adv. Mat. Lett., **6**, 402-408 (2011).

Gao-feng, F., Jing, W., and Jian, K., "Influence of AlF_3 and hydrothermal conditions on morphologies of α-Al_2O_3", Trans. Nonferrous Met. Soc. China, **18**, 743- 748 (2008).

Ge, S., Shi, X., Sun, K., Li, C., Uher, C., Baker, J. R. Jr., Holl, M. M. B., and Orr, B. G., "Facile Hydrothermal Synthesis of Iron Oxide Nanoparticles with Tunable Magnetic Properties," J. Phys. Chem. C, **113**, 13593–13599 (2009).

Goergen, S., Yin, C., Yang, M., Lee, B., Lee, S., Wang, C., Wu, P., Boucher, M. B., Kwon, G., Seifert, S., Winans, R. E., Vajda, S., and Flytzani-Stephanopoulos, M., "Structure sensitivity of oxidative dehydrogenation of cyclohexane over FeO_x and Au/Fe_3O_4 nanocrystals," Catalysis., **3**, 529-539 (2013).

Gong, J. L., Wang, B., Zeng, G. M., Yang, C. P., Niu, C. G., Niu, Q. Y., Zhou, W. J., and Liang, Y., "Removal of cationic dyes from aqueous solution using magnetic multi-wall carbon nanotube nanocomposite as adsorbent," J. Hazard. Mater., **164**, 1517–1522 (2009).

Greiner, A., and Wendorff, J. H., "Electrospinning: A Fascinating Method for the preparation of Ultrathin Fibers," Angew. Chem. Int. Ed., **46**, 5670 – 5703 (2007).

Grzmil, B., Kic, B., and Lubkowski, K., "Studies on Obtaining of Zinc Phosphate nanomaterials, Rev.Adv.Mater.Sci., **14**, 46-48 (2007).

Guo, Z., Lei , K., Li, Y., Ng, H. W., S., Prikhodko, Hahn, H. T., "Fabrication and characterization of iron oxide nanoparticles reinforced vinyl-ester resin nanocomposites," Compos. Sci. Technol., **68**, 1513–1520 (2008).

Gupta, V. K., and Suhas, "Application of low-cost adsorbents for dye removal – A review," J. Envion. Manag., **90**, 2313-2342 (2009).

Hassan, M. S., Anna, T., Al- Deyab, S. S., Kim, H. C., Oh, T. H., and Khil, M. S., Toxicity of Ce_2O_3/TiO_2 composite nanofibers against S. aureus and S. typhimurium: A novel electrospun material for disinfection of food pathogens, Colloids and Surf., A, **415**, 268- 273 (2012).

Hayashi, H., and Hakuta, Y., "Hydrothermal Synthesis of Metal Oxide Nanoparticles in Supercritical Water," Materials, **3**, 3794-3817 (2010).

Hayashi, N., Muranaka, S., Yamamoto, S., Takano, M., Zhang, D. F., Sun, L. D., and Yan, C. H., "Microscopic studies of a SnO2/ α-Fe_2O_3 architetectural nanocomposite using Mossbauer spectroscopic and magnetic measurements", J. Solid State Chem., **181**, 3283- 3296 (2008).

He, T., Xiang, L., and Zhu, S., "Hydrothermal preparation of bohemite nanorods by selective adsorption of sulphate", Langmuir, **24**, 8284- 8289 (2008).

Hema, M., Arasi A.Y., and Tamilselvi P., Anbarasan R.,"Titania Nanoparticles Synthesized by Sol-Gel Technique", Chem. Sci. Trans., **2**, 239-245 (2013).

Hornyak, G. L., Tibbals, H. F., Dutta, J., and Moore, J. J., "Introduction to Nanoscience & Nanotechnology", Publisher Taylor & Francis group, Chap 1, 1-54 (2009).

Horzum, N., Shahwan, T., Parlak, O., and Demir, M. M., "Synthesis of amidoximated polyacrylonitrile fibers and its application for sorption of aqueous uranyl ions under continuous flow," Chem. Eng. J., **213**, 41-49 (2012).

Hoskins, C., Min, Y., Gueorguieva, M., McDougall, C., Volovick, A., Prentice, P., Wang, Z., Melzer, A., Cuschieri A., and Wang, L., "Hybrid gold-iron oxide nanoparticles as a multifunctional platform for biomedical application," Hoskins et al. J. Nanobiotechnology., **10**, 27 (2012).

Hu, J., Song, Z., Chen, L., Yang, H., Li, J., and Richards, R., "Adsorption Properties of MgO (111) Nanoplates for the Dye Pollutants from Wastewater," J. Chem. Eng. Data., **55**, 3742-3748 (2010).

Hua, M., Zhang, S., Pan, B., Zhang, W., Lv, L., and Zhang, Q., "Heavy metal removal from water/wastewater by nanosized metal oxides: A review," J. Hazard. Mater., **211-212**, 317-331 (2012).

Huang, P. X., Wu, F., Zhu, B. L., Gao, X. P., Zhu, H. Y., Yan, T. Y., Huang, W. P., Wu, S. H., and Song, D. Y., "CeO_2 Nanorods and Gold Nanocrystals Supported on CeO_2 Nanorods as Catalyst," J. Phys. Chem. B., **109**, 19169-19174 (2005).

Huang, S. H., and Chen, D. H., "Rapid removal of heavy metal cations and anions from aqueous solutions by an amino-functionalized magnetic nano-adsorbent," J. Haz. Mat., **163**, 174-179 (2009).

Huber, D. L., "Synthesis, Properties and Applications of Iron Nanoparticles", Small, **1**, 482-501 (2005).

Hung-Low, F., Peterson, G. R., Davis, M., and Hope-Weeks, L. J., "Rapid preparation of high surface area iron oxide and alumina nanoclustures through a soft templating approach of sol-gel precursors", New J. Chem., 37, 245- 249 (2013).

Hussain, F., Hojjati, M., kamoto, M. O., and Gorga, R. E., "Review article: Polymer-matrix Nanocomposites, Processing, Manufacturing, and Application: An Overview," J. Compos. Mater., **40**, 1511-1559 (2006).

Hwang, K. T., Lee, H. S., Chung, K. C., Park, S. S., and Lee, J. H. J., "Synthesis of aluminium hydrates by a precipitation method andtheir use in coatings for ceramic membranes," European Ceramic Soc., **21**, 375-380 (2001).

Iqbal, M. J., and Asiq, M. N., "Thermodynamics and Kinectics of Adsorption of Dyes from Aqueous Media onto Alumina," J. Chem. Soc. Pak., **32**, 419- 428 (2010).

Iram, M., Guo, C., Guan, Y., Ishfaq, A., and Liu, H., "Adsorption and magnetic removal of neutral red dye from aqueous solution using Fe_3O_4 hollow nanospheres," J. Hazard. Mater., **181**, 1039-1050 (2010).

Isobe, T., Kameshima, Y., Nakajima, A., Okada, K., and Hotta, Y., "Gas permeability and mechanical properties of porous alumina ceramics with unidirectionally aligned pores," J. Eur. Ceram. Soc., **27**, 53–59 (2007).

Iturbe-García, J. L., García-Núñez, M. R., and López-Muñoz, B. E., "Synthesis of the Mg_2Ni Alloy Prepared by Mechanical Alloying Using a High Energy Ball Mill," J. Mex. Chem. Soc., **54**, 46-50 (2010).

Jadhav, A. P., Kim, C. W., Cha, H. G., Pawar, A. U., Jadhav, N. A., Pal, U., and Kang, Y. S., "Effect of Different Surfactants on the Size Control and Optical Properties of Y2O3:Eu^{3+} Nanoparticles Prepared by Coprecipitation Method," J. Phys. Chem. C., **113**, 13600–13604 (2009).

Jain, R., and Sikarwar, S., "Removal of hazardous dye congo red from waste material," J. Hazard.Mater., **152**, 942–948 (2008).

Janardhanan, S. K., Ramasamy, I., and Nair, B. U., "Synthesis of iron oxide nanoparticles using chitosan and starch templates," Transition. Met. Chem., **33**,127–131 (2008).

Janczak, C.M., and Aspinwall, C.A., "Composite nanoparticles: the best of two worlds", Anal. Bioanal. Chem., **402**, 83-89 (2012).

Jayalakshmi, M., and Balasubramanian, K., "Hydrothermal synthesis of CuO-SnO_2 and CuO-SnO_2- Fe_2O_3 mixed oxides and their electrochemical characterization in neutral electrolyte", Int. J. Electrochem. Sci., **4**, 571- 581 (2009).

Jia, C. J., Sun, L. D., Yan, Z. G., Pang, Y. C., You, L. P., and Yan, C. H., "Iron oxide Tube-in-tube Nanostructure," J. Phys. Chem. C., **111**, 13022-13027 (2007).

Jia, C-J, Sun, L-D, Yan, Z-G, You, L-P, Luo, F., Han, X-D, Pang, Y-C, Zhang, Z., and Yanb, C-H, "Single-Crystalline Iron Oxide Nanotubes," Angew. Chem., **117**, 4402–4407 (2005).

Jin, W-J., Jeon, H. J., Kim, J. H., and Youk, J. H., "A study on the preparation of poly(vinyl alcohol) nanofibers containing silver nanoparticles," Synth. Met., **157,** 454–459 (2007).

Jv, Y., Li, B. and Cao, R., "Positively-charged gold nanoparticles as peroxidiase mimic and their application in hydrogen peroxide and glucose detection," Chem. Commun., **46**, 8017–8019 (2010).

Kang, W., Cheng, B., Li, Q., Zhuang, X., and Ren, Y., "A new method for preparing alumina nanofibers by electrospinning technology" Text. Res. J., **81**, 148- 155 (2011).

Karaoglu, M. H., Dogan, M., Alkan, M.,. "Removal of cationic dyes by kaolinite," Micro Meso. Mater., **122**, 20–27 (2009).

Kargi, F., and Ozmihci, S. S., "Biosorption performance of powdered activated sludge for removal of different dyestuffs," Enzy.Microbial Techno., **35**, 267-271 (2004).

Khaleel, A., Shehadi, I., and Al-Shamisi, "Nanostructured chromium-iron mixed oxides: Physicochemical properties and catalytic activity", Colloids Surf., A, **355**, 75- 82 (2010).

Kharlamova, M. V., Sapoletova, N. A., Eliseev, A. A., and Lukashin, A. V., Optical Properties of g-Ferric Oxide Nanoparticles in a Mesoporous Silica Matrix, Tech Phys Lett+., **34**, 288–291 (2008).

Kim, J., Kim, J., Kim, J., and Kim K. H., "Characterization of as-synthesized FeCo magnetic nanoparticles by coprecipitation method," J. Appl. Phys., **113**, 17A313 (2013).

Kim, J.S. Kuk, E., Yu, K. N., Lee, H. J., Jeong, D. H., and Cho, M. H., "Antimicrobial effects of silver nanoparticles," Nano :Nanotech, Bio andMed., **3,** 95– 101 (2007).

Kim, K. D., Kim, S. S., and Kim, H. T., "Formation and characterization of silica-coated magnetic nanoparticles by sol-gel method", J. Ind. Eng. Chem., **11**, 584- 589 (2005).

Kim, T. H., Park, C., Yang, J., and Kim, S., "Comparison of disperse and reactive dye removals by chemical coagulation and Fenton oxidation," J. Hazard. Mater. B., **112**, 95–103 (2004).

Kim, T., Lian, J., Ma, J., Duan, X., and Zheng, W., "Morphology controllable synthesis of ϒ-alumina nanostructures via an ionic liquid- assisted hydrothermal route", Cryst. Growth Des., **10**, 2928- 2933 (2010).

Kim, Y-T, Han, J. H., Hong, B. H., and Kwon, Y-U, "Electrochemical synthesis of Cd-Se quantum-dot arrays on Graphene basal plane using mesoporous silica thin-film templates," Adv. Mater., **22**, 515-518 (2010).

Kritikaki, A., and Tsetsekou, A., "Fabrication of porous alumina ceramics from powder mixtures with sol–gel derived nanometer alumina: Effect of mixing method," J. Eur. Ceram. Soc., **29**, 1603–1611 (2009).

Kulkarni, N. V., Karmakar, S., Asthana, S. N., Nawale, A. B., Sheikh, A., Patole, S. P., Yoo, J. B., Mathe V. L. Das A. K., and Bhoraskar, S. V., "Study on growth of hollow nanoparticles of alumina," J. Mate. Sci., **46**, 2212–2220 (2011).

Lala, N. L., Ramaseshan, R., Bojun, L., Sundarajan, S., Bharate, R. S., Ying-Jun, L., and Ramakrishna, S., "Fabrication of Nanofibers With Antimicrobial Functionality Used as Filters: Protection Against Bacterial Contaminants," Biotech & Bio Engg., **97**, 1357-65 (2007).

Lanje, A. S., Sharma, S. J., and Pode,R. B., "Synthesis of silver nanoparticles: a safer alternative to conventional antimicrobial and antibacterial agents," J. Chem. Pharm. Res., **2**, 478-483 (2010).

Laurent, S., Forge, D., Port, M., Roch, A., Robic, C., Elst, L. V., and Muller, R. N., "Magnetic Iron Oxide Nanoparticles: Synthesis, Stabilization, Vectorization, Physicochemical Characterizations, and Biological Applications," Chem. Rev., **108**, 2064–2110 (2008).

Lee, C. S., Kim, I. D., and Lee, J. H., "Selective and sensitive detection of trimethylamine using ZnO- In_2O_3 composite nanofibers", Sens. Actuators, B, **181**, 463- 470 (2013).

Lee, H. K., Jeong, E. H., Baek, C. K., and Youk, "One-step preparation of ultrafine poly(acrylonitrile) fibers containing silver nanoparticles" J.H. Mater Lett., **59**, 2977 – 2980 (2005).

Lee, S. M., Song, K. C., and Lee, B. S., "Antibacterial activity of silver nanoparticles preparedby a chemical reduction method," Korean J. Chem. Eng., **27**, 688-692 (2010).

Lee, S. S., Bai, H., Liu, Z., and Sun, D. D., "Novel- structured electrospun TiO_2/ CuO composite nanofibers for high efficient photocatalytic cogeneration of clean water and energy from dye waste water", Water Res., **47**, 4059- 4073 (2013).

Li, D., McCann, J. T., and Xia, Y., "Electrospinning: A simple and versatile technique for producing ceramic nanofibers and nanotubes", J. Am. Ceram. Soc., **89**, 1861- 1869 (2006).

Li, G., Liu, Y., Liu, D., Liu, L., and Liu, C., "Synthesis of flower-like Boehmite (AlOOH) via a simple solvothermal process without surfactant," Mater. Res. Bull., **45**, 1487–1491 (2010).

Li, J., and Zhang, J. Z., "Optical properties and applications of hybrid semiconductor nanomaterials," Coor. Chem. Rev., **253,** 3015–3041 (2009).

Li, J., Pan, Y., Xiang, C., Ge, Q., and Guo, J., "Low temperature synthesis of ultrafine α-Al_2O_3 powder by a simple aqueous sol–gel process", Ceram. Int., **32**, 587–591 (2006).

Li, L., Chu, Y., Liu, Y., and Dong, L., "Template- free synthesis and photocatalutic properties of novel Fe_2O_3 hollow spheres" J. Phys. Chem. C, **111**, 2123- 2127 (2007).

Li, N., Xiao, Y., Xu, C., Li, H., and Yang, X., "Facile Preparation of Polyaniline Nanoparticles via Electrodeposition for Supercapacitors," Int. J. Electrochem. Sci., **8**, 1181–1188 (2013).

Li, X., Si, Z., Lei, Y., Li, X., Tang, J., Song, S., and Zhang, H., "Hierarchically structured Fe_3O_4microspheres: morphology control and their application in wastewater treatment," Cryst. Eng. Comm., **13**, 642-648 (2011).

Li, Y., Liu, J., and Jia, Z., "Fabrication of bohemite AlOOH nanofibers by simple hydrothermal process", Mater. Lett., **60**, 3586- 3590 (2006).

Li, Y., Yang, X-Y, Feng, Y., Yuan, Z-Y, and Su, B-L, "One-Dimensional Metal Oxide Nanotubes, Nanowires, Nanoribbons, and Nanorods: Synthesis, Characterizations, Properties and Applications," Crit. Rev. Solid State Mater. Sci., **37**, 1-74 (2012).

Li, Z., Lai, X., Wang, H., Mao, D., Xing, C., and Wang, D., "Direct hydrothermal synthesis of single-crystalline hematite nanorods assisted by 1,2-propanediamine," Nanotechnology., **20**, 245603 (2009).

Lian, L., Guo, L., and Guo, C., "Adsorption of Congo red from aqueous solutions onto Ca-bentonite," J.Hazard.Mater., 161, 126-131 (2009).

Liang, D., Hsiao, B.N S., and Chu, B., "Functional electrospun nanofibrous scaffolds for biomedical applications," Adv. Drug. Deliver. Rev., **59**, 1392–1412 (2007).

Liang, J., Xu, Y., Sui, D., Zhang, L., Huang, Y., Ma, Y., Li, F., and Chen, Y., "Flexible, Magnetic, and Electrically Conductive Graphene/Fe_3O_4 Paper and Its Application for Magnetic-Controlled Switches," J. Phys. Chem. C, **114**, 17465–17471 (2010).

Limousin, G., Gaudet, J. P., Charlet, L., Szenknect, S., Barthe`s, V., and Krimissa, M., "Sorption isotherms: A review on physical bases, modeling and measurement," Appl. Geochem., **22,** 249–275 (2007).

Liu, C., Li, F., Li, X., Zhang, G., and Kuang, Y., "The effect of iron oxides and oxalate on the photodegradation of 2-mercaptobenzothiazole", J. Mol. Catal. A: Chem., **252**, 40- 48 (2006).

Liu, C., Li, J., Liew, K., Zhua, J., and Nordin, M. R., "An environmentally friendly method for the synthesis of nano-alumina with controllable morphologies," RSC Advances, **2**, 8352–8358 (2012).

Liu, R., Ye, H., Xiong, X., and Liu, H., "Fabrication of TiO3/ZnO composite nanofibers by electrospinning and their photocatalytic property, Mater. Chem. Phys., **121**, 432- 439 (2010).

Liu, R., Zhang, B., Mei, D., Zhang, H., and Liu, "Adsorption of methyl violet from aqueous solution by halloysite nanotubes", J., Desalination, **268**, 111-116 (2011).

Liu, X. M., Yin, W. D., Miao, S. B., and Ji, B. M., "Fabrication of CuO/Fe_2O_3, hollow hybrid microspheres", Mater. Chem. Phys., **113**, 518- 522 (2009).

Liu, X., Hu, Q., Fang, Z., Zhang, X., and Zhang, B., "Magnetic chitosan nanocomposites: A useful recyclable tool for heavy metal ion removal," Langmuir., **25,** 3-8 (2009).

Liu, Y., Li, X., Xu, Z., and Hu, Z., "Preparation of flower-like and rod-like bohemite via a hydrothermal route in a buffer solution", J. Phys. Chem. Solids, **71**, 206- 209 (2010).

Liu, Y., Ma, D., Han, X., Bao, X., Frandsen, W., Wang, D., and Su, D., "Hydrothermal synthesis of microscale bohemite and gamma nanoleaves alumina", Mater. Lett., **62**, 1297- 1301 (2008).

Lu, A. H., Salabas, E. L., and Schuth, F., "Magnetic nanoparticles: synthesis, protection, functionalization, and application", Angew. Chem. Int. Ed., **46**, 1222- 1244 (2007).

Lu, C. L., Lv, J. G., Xu, L., Guo, X. F., Hou, W. H., Hu, Y., and Huang H., "Crystalline nanotubes of γ-AlOOH and γ-Al_2O_3: hydrothermal synthesis, formation mechanism and catalytic performance," Nanotechnology, **20**, 215604 (2009).

Lu, X. H., Zheng, D. Z., Gan, J. Y., Liu, Z. Q., Liang, C. L., Liu, P., and Tong, Y. X., "Porous CeO_2 nanowires/nanowire arrays: electrochemical synthesis and application in water treatment," J. Mater. Chem., **20**, 7118-7122 (2010).

Ma, M-G., Zhu, Y-J., and Xu, Z-L, "A new route to synthesis of γ-alumina nanorods," Mater. Lett. **61,** 1812–1815 (2007).

Machala, L., Zboril, R., and Gedanken, A., "Amorphous Iron (III) Oxides- A Review," J. Phys. Chem. B, **111,** 4003-4018 (2007).

Mahmoodi, N. M., and Najafi, F., "Synthesis, amine functionalization and dye removal ability of titania/silica nano-hybrid," Microporous Mesoporous Mater., **156**, 153–160 (2012).

Mahmoud, M. E., Osman, M. M., Hafez, O. F., and Elmelegy, E., "Removal and preconcentration of lead (II), copper (II), chromium (III) and iron (III) from wastewaters by surface developed alumina adsorbents with immobilized 1-nitroso-2-naphthol," J. Hazard. Mater., **173**, 349–357 (2010),

Makovec, D., and Drofenik, M., "Synthesis of plate- like spinel particles and spinel-hexaferrite intergrowth nanocomposite particles using hydrothermal decomposition of Ba- hexaferrite", Cryst. Growth Des., **8**, 2182- 2186 (2008).

Mandal, S., and Muller, A. H. E., "Facile route to the synthesis of porous α-Fe_2O_3 nanorods., Mater. Chem. Phys., 111, 438-443 (2008).

Maneeratana, V., and Sigmund, W. M., "Continuous hollow alumina gel fibers by direct electrospinning of an alkoxide- based precursors", Chem. Eng. J., **137**, 137- 143 (2008).

Mănoiu, V-S., and Aloman, A., "Obtaining Silver Nanoparticles by Sonochemical Methods," U.P.B. Sci. Bull B., **72**, 179-186 (2010).

Mao, Y., Park, T. J., Zhang, F., Zhou, H., and Wong, S. S., "Environmentally friendly methodologies of nanostructure synthesis", small, **3**, 1122- 1139 (2007).

Marszałł, M. P., "Application of Magnetic Nanoparticles in Pharmaceutical Sciences," Pharm Res., **28**,480–483 (2011).

Martinez, A. I., Garcia-Lobato, M. A., and Perry, D. L., "Study of the properties of iron oxide nanostructures," In: Research in Nanotechnology Developments, ISBN: 978-1-60741-028-7, Nova Science Publishers, Inc. (2009).

Masue, Y., Loeppert, R. H., and Kramer, T. A., "Arsenate and Arsenite Adsorption and Desorption Behavior on Co-precipitated Aluminum: Iron Hydroxides," Environ. Sci. Technol., **41**, 837 -842 (2007).

Masue, Y., Loeppert, R. H., and Kramer, T. A., "Arsenate and Arsenite Adsorption and Desorption Behavior on Co-precipitated Aluminum: Iron Hydroxides," Environ. Sci. Technol., **41**, 837 -842 (2007).

Mathiazhagan, A., and Joseph, R., "Nanotechnology-A New Prospective in Organic Coating –Review," Int. J. Chem. Eng. Appl., **2**, 225-237 (2011)

Matsumoto, H., and Tanioka, A., "Functionality in Electrospun Nanofibrous Membranes Based on Fiber's Size, Surface Area, and Molecular Orientation," Membranes, **1**, 249-264 (2011).

Maximous, N. N., Nakhla, G. F., and Wan, W. K., "Removal of heavy metals from wastewater by adsorption and membrane processes: A comparative Study," World academy Sci. Eng. Tech., **40**, 599-604 (2010).

McCann, J. T., Li, D., and Xia, Y., "Electrospinning of nanofibers with core- sheath, hollow or porous structures", J. Mater. Chem., **15**, 735- 738 (2005).

Milanovic, P., Dimitrijevic, M., Heinemann, R. J., Rogan, J., Stojanovic, D. B., Kojovic, A., and Aleksic, R., "Preparation of low cost alumina nanofibers via electrospinnig of aluminium chloride hydroxide/ poly (vinyl alcohol) solution", Ceram. Int., **39**, 2131-2134 (2013).

Milea, C. A., Bogatu, C., and Duta, A., "The influence of parameters in silica sol-gel process", Bulletin of the Transilvania University of Braşov, **4**, 59- 66 (2011).

Mo, C. B., Cha, S. I., Kim, K. T., Lee, K. H., and Hong, S. H., "Fabrication of carbon nanotube reinforced alumina matrix nanocomposite by sol- gel process", Mater. Sci. Eng., A, **395**, 124- 128 (2005).

Moghaddam, A. B., Nazari, T., Badraghi, J., and Kazemzad, M., "Synthesis of ZnO Nanoparticles and Electrodeposition of Polypyrrole/ZnO Nanocomposite Film," Int. J. Electrochem. Sci., **4**, 247– 257 (2009).

Mohammadi, M. R., and Fray, D. J., "Low temperature nanocrystalline TiO_2- mixed oxide by a particulate sol-gel route: physical and sensing characteristics", Physica E, **46**, 43- 51 (2012).

Mohapatra, M. and Anand, S., "Synthesis and applications of nano-structured iron oxides/ hydroxides – a review", International Journal of Engineering, Science and Technology, **2**, 127-146 (2010).

Moon, S. C., and Lee, J., "Electrospun Poly(ethylene oxide)/Hydrated iron oxide/ Sodium alginate composite nanofibers with multi- functional properties", Polym. Eng. Sci., DOI 10.1002/pen.23431, (2012).

Mourad, M. C. D., Byelov, D. V., Petukhov, A. V., Winter, D. A. M., Verkleij, A. J., and Lekkerkerker, H. N. W., "Sol-Gel Transitions and Liquid Crystal Phase Transitions in Concentrated Aqueous Suspensions of Colloidal Gibbsite Platelets", J. Phys. Chem. B, **113**, 11604–11613 (2009).

Mu, L., and Sprando, R. L., "Application of Nanotechnology in Cosmetics," Pharm Res., **27**, 1746–1749 (2010).

Naskar, M. K., "Soft Solution Processing for the Synthesis of Alumina Nanoparticles in the Presence of Glucose," J. Am. Ceram. Soc., **93**, 1260–1263 (2010).

Navaladian, S., Viswanathan, B., Viswanath, R. P., Varadarajan, T. K., "Thermal decomposition as route for silver nanoparticles," Nanoscale Res Lett., **2**, 44–48 (2007).

Nguyen, D. P., Tran, Q. T., Trinh, X. S., Hoang, T. C., Nguyen, H. N. and Nguyen, H. H., "Crystallization and magnetic properties of amorphous iron–chromium oxide nanoparticles synthesized by Sonochemistry," Adv. Nat. Sci.: Nanosci. Nanotechnol. **3**, 015017-21 (2012).

Novoselova, L. Y., "Structure and Properties of Composite Nanomaterials: Products of the Thermal Treatment of Molybdenumand Ironcontaining Powders," Russ. J. Phys. Chem. A, **86**, 1689–1696 (2012).

Panda, P. K., and Ramakrishna, S., "Electrospinning of alumina nanofibers using different precursors", J. Mater. Sci., **42**, 2189- 2193 (2007).

Panigrahi, S. C., Das P. R., Parida B. N., Sharma H. B. K., and Chaudhary R. N. P., "Effect of Gd-substitution on dielectric and transport properties of lead zirconate titanate ceramics," J Mater Sci: Mater Electron, DOI 10.1007/s10854-013-1243-x, (2013).

Parham, H., Zargar, B., and Shiralipour, R., "Fast and efficient removal of mercury from water samples using magnetic iron oxide nanoparticles modified with 2-mercaptobenzothiazole," J. Hazard. Mater., **205-206**, 94-100 (2012).

Park, Y. K., Tadd, E. H., Zubris, M., and Tannenbaum, R., "Size-controlled synthesis of alumina nanoparticles from aluminum alkoxides," Mater. Res. Bull., **40**, 1506–1512 (2005).

Patil, G., Sarode, C., Patil, R., and Gokhale, S., "CVD Synthesisof Highly Graphitized Single-walled Carbon Nanotubes Using Nitrogen-pretreated FeMo/MgO Catalyst," Chem. Lett., **41**, 871873 (2012).

Pavani, T., Chakra, Ch. S., and Venkateswara Rao, K., "A Green approach for the synthesis of nano-sized iron ooxide, by Indian ayurvedic modified bhasmikaran method," Am. J. Biol. Pharm. Sci., **1**, 2328-6814 (2013).

Pérez-Tijerina, E., Gracia Pinilla, M., Mejía-Rosales, S., Ortiz-Méndez, U., Torres, A., and José-Yacamán, M., "Highly size-controlled synthesis of Au/Pd nanoparticles by inert-gas condensation", Faraday Discuss., **138**, 353-362 (2008).

Perkas, N., Koltypin, Y., Palchik, O., Gedanken, A., and Chandrasekaran, S., "Oxidation of cyclohexane with nanostructured amorphous catalysts under mild conditions," Appl. Catal. A, **209**, 125–130 (2001).

Polshettiwar, V., Baruwati, B., and Varma, R.S., "Self-Assembly of Metal Oxides into Three-Dimensional Nanostructures: Synthesis and Application in Catalysis", ACS NANO, **3**, 728-736 (2009).

Pongwan, P., Inceesungvorn, B., Wetchakun, K., Phanichphant, S., and Wetchakun, N., "Highly efficient visible-light-induced photocatalytic activity of Fe-doped TiO_2 nanoparticles," Eng. J., **16**, 143-151 (2012).

Pradhan, G.K., and Parida, K.M., "Fabrication, Growth mechanism, and characterization of α-Fe_2O_3 nanorods", Appl. Mater. Inter., **3**, 317-323 (2011).

Prasad, K., and Jha, A. K., "ZnO nanoparticles: synthesis and adsorption study." Natural sci., **2**, 129-135 (2009).

Predescu, A., and Nicolae, A., "Adsorption of zn, cu and cd from waste waters by means of maghemite nanoparticles," U. P. B. Sci. Bull., series B., **74,** 255-264 (2012).

Prucek, R., Tucek, J., Kilianová, M., Panácek, A., Kvítek, L., Filip, J., Kolár, M., Tománková, K., and Zboril, R., "The targeted antibacterial and antifungal properties of magnetic nanocomposite of iron oxide and silver nanoparticles," Biomaterials, **32**, 4704-4713 (2011).

Prucek, R., Tuček., Kolařík, J., Filip, J., Marušák, Z., Sharma, V. K., and Zbořil, R., "Ferrate(VI)-Induced Arsenite and Arsenate Removal by In Situ Structural Incorporation into Magnetic Iron(III) Oxide Nanoparticles," Environ. Sci. Technol., **47**, 3283−3292 (2013).

Raileanu, M., Crisan, M., Ballo, A., Cosma, C., Petre, J., Stan, C., Predoi, D., Valsangiacom, C. M., Tolea, F., and Secu, C., "The colloida route of the sol-gel process- an alternative to produce Fe_3O_4- SiO_2 nanocmposites", J. Optoelectron. Adv. Mater., **9**, 1399- 1402 (2007).

Ramaseshan, R., Sundarrajan, S., Jose, R., and Ramakrishna, S., "Nanostructured ceramics by electrospinning," J. Appl. Phys., **102**, 111-101 (2007).

Ren, T., He, P., Niu, W., Wu, Y., Ai, L., and Gou, X., "Synthesis of α- Fe_2O_3 nanofibers for applications in removal and recovery of Cr (VI) from wastewater" Environ. Sci. Pollut. Res., **20**, 155- 162 (2013).

Rizov. B., "Phase transformations from goethite to hematite and thermal decomposition in various nickeliferous laterite ores," J. Univ. Chem. Tech. Met., **47**, 207-210 (2012).

Royer, B., Cardoso, N. F., Lima, E. C., Vaghetti, J. C. P., Simon, N. M., Calvete, T., Veses, R. C., "Applications of Brazilian pine-fruit shell in natural and carbonized forms as adsorbents to removal of methylene blue from aqueous solutions—Kinetic and equilibrium study," J. Hazard. Mater., **164**, 1213–1222 (2009).

Rujitanaroj, P., Pimpha, N., and Supaphol, P., "Preparation, Characterization, and Antibacterial Properties of Electrospun Polyacrylonitrile Fibrous Membranes Containing Silver Nanoparticles," J Appl Poly Sci., **116**, 1967–1976 (2010).

Rujitanaroj, P., Pimpha, N., and Supaphol, P., "Wound-dressing materials with antibacterial activity from electrospun gelatin fiber mats containing silver nanoparticles," Polymer., **49**, 4723–4732 (2008).

Saberi., A., "Comparison of Pb removal efficiency by zero valent iron^{2+} nanoparticles and Ni/Fe bimetallic nanoparticles," Iranica J. Energy Env., **3**, 189-196 (2012).

Sadiq, M., Chowdhury, B., Chandrasekaran, N., and Mukherjee, A., "Antimicrobial sensitivity of Escherichia coli to alumina nanoparticles," Nanomed Nanotech Biol Med., **5**, 282-286 (2009).

Sahoo, S. K., Parveen, S., and Panda, J. J., "The present and future of nanotechnology in human health care," Nanomed. Nanotech. Biol Med., **3**, 20– 31 (2007).

Salehia, R., Aramia, M., Mahmoodib, N. M., Bahramia, H., and Khorramfara, S., "Novel biocompatible composite (Chitosan–zinc oxide nanoparticle): Preparation, characterization and dye adsorption properties," Colloids Surf., B Biointerfaces., **80**, 86–93 (2010).

Santos, I. P., Rodriguez, C. S., and Liz-Marzan, L. M., "Self-Assembly of Silver Particle Monolayers on Glass from AgC Solutions in DMF," J. Colloid Interf Sci., **221**, 236–241 (2000).

Saquing, C. D., Manasco, J. L., and Khan, S. A., "Electrospun Nanoparticle–Nanofiber Composites via a One-Step Synthesis" Small., **5**, 944-51 (2009).

Shafi, K. V. P. M., Ulman, A., Yan, X., Yang, N-L., Estourne`s, C., White, H., and Rafailovich, M., "Sonochemical Synthesis of Functionalized Amorphous Iron Oxide Nanoparticles," Langmuir, **17**, 5093-5097 (2001).

Shah, M.A., and Ahmad, T., "Principles of Nanoscience and Nanotechnology", Narosa Publishing House, 32-65 (**2010)**.

Shao, H., Min, C., Issadore, D., Liong, M., Yoon, T-J., Weissleder, R., and Lee, H., "Magnetic Nanoparticles and microNMR for Diagnostic Applications," Theranostics, **2(1)**, 55-65 (2012).

Shao, H., Zhang, X., Liu, S., Chen, F., Xu, J., and Feng, Y., Preparation of pure iron nanofibers via electrospinning", Mater. Lett., **65**, 1775- 1777 (2011).

Sharma, V. K., Yngard, R. A., and Lin, Y., "Silver nanoparticles: Green synthesis and their antimicrobial activities," Adv. Colloid Interface Sci., **145**, 83–96 (2009).

Sharma, Y. C., Srivastava, V., and Mukherjee, A. K., "Synthesis and application of nano-Al_2O_3 powder for the reclamation of hexavalent chromium from aqueous solutions" J. Chem. Eng. Data, **55**, 2390- 2398 (2010).

Sharma, Y. C., Srivastava, V., Upadhyay, S. N., and Weng, C. H., "Alumina nanoparticles for the removal of Ni(II) from aqueous solutions", Ind. Eng. Chem. Res., **47**, 8095-8100 (2008).

Sheets, W. C., Mugnier, E., Barnabe, A., Marks, T. J., and Poeppelmeier, K. R., "Hydrothermal synthesis of Delafossite- type oxides", Chem. Mater., **18**, 7- 20 (2006).

Shen, S. C., Ng, W. K., Zhong, Z. Y., Dong, Y. C., Chia L., and Tan, R. B. H., "Solid- based hydrothermal synthesis and characterization of alumina nanofibers with controllable aspect ratios", J. Am. Ceram. Soc., **92**, 1311- 1316 (2009).

Shen, X., Liu, M., Song, F., and Meng, X., "Structural evolution and magnetic properties of $SrFe_{12}O_{19}$ nanofibers by electrospinning", J. Sol-Gel Sci. Technol., **53**, 448- 453 (2010).

Shirashi, Y., and Toshima, N., "Oxidation of ethylene catalyzed by colloidal dispersions of poly (sodium acrylate)-protected silver nanoclusters," Colloid Surf A., **169**, 59–66 (2000).

Shojaie-Bahaabad, M., and Taheri-Nassal, E., "Economical synthesis of nano alumina powder using an aqueous sol-gel method", Mater. Lett., **62**, 3364- 3366 (2008).

Shu-Hua, M., Shi-Li Z., Hong-Bin, Xu., and Yi, Z., "Spectra of sodium aluminate solutions," Trans. Nonferrous Met. Soc. China., **17**, 853-857 (2007).

Sichani, G.N., Morshed, M., Amirnasr, M., and Abedi, D., "In Situ Preparation, Electrospinning, and Characterization of Polyacrylonitrile Nanofibers Containing Silver Nanoparticles," J Appl Poly Sci., **116**, 1021–1029 (2010).

Sigmund, W., Yuh, J., Park, H., Maneeratana, V., Pyrgiotakis, G., Daga, A., Taylor, J., and Nino, J. C., "Processing and Structure Relationships in Electrospinning of Ceramic Fiber Systems," J. Am. Ceram. Soc., **89**, 395–407 (2006).

Sill, T. J., Recum, H. A. and von, "Electrospinning: Applications in drug delivery and tissue engineering," Biomaterials, **29**, 1989-2006 (2008).

Silver, S., and Phung, L. T., "Bacterial Heavy Metal Resistance: New Surprises," Annu. Rev. Microbiol., **50**, 753-8 (1996).

Singh, B. P., Menchavez, R., Takai, C., Fuji, M., and Takahashi, M., "Stability of dispersions of colloidal alumina particles," J. Colloid. Inter. Sci., **291**, 181–186 (2005).

Son, W. K., Youk, J. H., and Park,W. H., "Antimicrobial cellulose acetate nanofibers containing silver nanoparticles Carbohydrate," Polymers., **65**, 430–434 (2006).

Soultanidis, N., Zhou, W., Kiely, C. J., and Wong, M. S., "Solvothermal Synthesis of Ultrasmall Tungsten Oxide Nanoparticles," Langmuir, **28**, 17771−17777 (2012).

Srivastava, V., Weng, C. H., Singh, V. K., and Sharma, Y. C., "Adsorption of nickel ions from aqueous solutions by nano alumina: kinetic, mass transfer, and equilibrium studies", J. Chem. Eng. Data, **56**, 1414–1422 (2011).

Starbova, K., Petrov, D., Starbov, N., and Lovchinov, V., "Synthesis of supported fibrous nanoceramics via electrospinning," Ceram. Int., **38**, 4645–4651 (2012).

Suber, L., Imperatori, P., Ausanio, G., Fabbri, F., and Hofmeister, H., "Synthesis, Morphology, and Magnetic Characterization of Iron Oxide Nanowires and Nanotubes", J. Phys. Chem. B, **109**, 7103-7109 (2005).

Suchanek, W. L., Garces, J. M., Fulvio, P. F., and Jaroniec, M., "Hydrothermal Synthesis and Surface Characteristics of Novel Alpha Alumina Nanosheets with Controlled Chemical Composition," Chem. Mater. **22**, 6564–6574 (2010).

Sun, Y-P., Li, X-Q., Cao, J., Zhang, W-X., and Wang, H. P., "Characterization of zero-valent iron nanoparticles," Adv. Colloid Interface Sci., **120**, 47–56 (2006).

Tadic, M., Markovic, D., Spasojevic, V., Kusigerski, V., Remskar, M., Pirnat, J., and Jaglicic, Z., "Synthesis and magnetic properties of concentrated α- Fe_2O_3 in a silica matrix", J. Alloys Compd., **44**, 291- 296 (2007).

Tadjarodi, A., Kerdari H., and Imani. M., "Synthesis, Characterization and Adsorption Capability of CdO Microstructure for Congo Red from Aqueous Solution, JNS **2**, 9-17 (2012).

Tang, B., G, J., Zhuo, L., Wang, G., Niu, J., Shi, Z., and Dong, Y., "A facile and controllable synthesis of ϒ- Al_2O_3 nanostructures without a surfactant", Eur. J. Inorg. Chem., **2005**, 4366- 4369 (2005).

Teo, W. E., and Ramakrishna, S., "Electrospun nanofibers as a platform for multifunctional, hierarchically organized nanpcomposite", Compos. Sci. Technol., **69**, 1804- 1817 (2009).

Teo, W-E, and Ramakrishn, S., "Electrospun nanofibers as a platform for multifunctional, hierarchically organized nanocomposite," Compos. Sci. Technol., **69**, 1804–1817 (2009).

Teoh, G. L., Liew, K. Y., and Mahmood, W. A. K., "Synthesis and characterization of sol-gel alumina nanofibers", J. Sol-Gel Technol., **44**, 177- 186 (2007).

Thavasi, V., Singh, G., and Ramakrishna, S., "Electrospun nanofibers in energy and environmental applications," Energy Environ. Sci., **1**, 205–221 (2008).

Titrici, M. M., Antonietti, M., and Thomas, A., "A generalized synthesis of metal oxide hollow spheres using a hydrothermal approach", Chem. Mater., **18**, 3808- 3812 (2006).

Tiwari, J. N., Tiwari, R. N., and Kim, K. S., "Zero-dimensional, one-dimensional, two-dimensional and three-dimensional nanostructured materials for advanced electrochemical energy devices," Prog. Mat. Sci., **57**, 724–803 (2012).

Tomar, L. J., and Chakrabarty, B. S., "Synthesis, structural and optical properties of TiO_2-ZrO_2 nanocomposite by hydrothermal method", Adv. Mat. Lett., **4**, 64- 67 (2013).

Vaseashtaa, A., Vaclavikovac, M., Vaseashtaa, S., Galliosd, G., Royb, P., and Pummakarnchana, O., "Nanostructures in environmental pollution detection, monitoring, and remediation," Sci.Technol. Adv. Mater. **8**, 47–59 (2007).

Vincent, T., Gross, M., Dotan, H., and Rothschild, A., "Thermally oxidized iron oxide nanoarchitectures for hydrogen production by solar-induced water splitting", International Journal of hydrogen energy **37,** 8102-8109 (2012).

Violante, A., Ricciardella, M., and Pigna, M., "Adsorption of heavy metals on mixed Fe-Al oxides in the absence or presence of organic ligands", Water, Air and Soil Pollution, **145**, 289-230 (2003).

Viratyaporn, W., Lehman, R. L., "Spectroscopic analysis of poly (methyl methacrylate)/alumina polymer nanocomposites prepared by in situ (bulk) polymerization," J. Mater. Sci., **45**, 5967–5972 (2010).

Wakihara, T., Hirasaki, T., Shinoda, M., Meguro, T., Tatami, J., Komeya, K., Inagaki, S., and Kubota, Y., "A New Method for the Synthesis of Alumina Nanotubes from Polymer Composite Materials," Cryst. Growth Desgn., **9,** 1260-1263 (2009).

Wang, B., Wu, H., Yu, Le., Xu, Rong., Lim, T. T., and Lou, X. W., "Template- free formation of uniform urchin- like α- FeOOH hollow spheres with superior capability for water treatment", Adv. Mater., **24**, 1111- 1116 (2012).

Wang, C., Feng, C., Gao, Y., Ma, X., Wu, Q., and Wang, Z., "Preparation of a graphene-based magnetic nanocomposite for the removal of an organic dye from aqueous solution," Chem. Eng. J., **173**, 92– 97 (2011).

Wang, H., Xu X., Zhang, J., and Li, C., "A Cost-Effective Co-precipitation Method for Synthesizing Indium Tin Oxide Nanoparticles without Chlorine Contamination," J. Mater. Sci. Technol., **26**, 1037-1040 (2010).

Wang, J., Lin, M., Yan, Y., Wang, Z., Ho, P. C., and Loh, K. P., "CdSe/AsS Core-Shell Quantum Dots: Preparation and Two-Photon Fluorescence," J. Am. Chem. Soc., **131**, 11300-11301 (2009).

Wang, J., Wang, Y., Qiao, M., Xie, S., and Fan, K., "A novel sol-gel synthetic route to alumina nanofibers via aluminium nitrate and hexamethylenetetramine", Mater. Lett., **61**, 5074- 5077 (2007).

Wang, L., and Wang, A., "Removal of Congo red from aqueous solution using a chitosan/ organomontmorillonite nanocomposite," J. Chem. Technol. Biotechnol., **82**, 711–720 (2007).

Wang, P., and Lo, I. M. C., "Synthesis of mesoporous magnetic γ-$Fe_2O_3$and its application to Cr(VI) removal from contaminated water," Water Res., **43**, 3727-3734 (2009).

Wang, S., Boyjoo, Y., Choueib, A., and Zhu, Z. H., "Removal of dyes from aqueous solution using fly ash and red mud,"Water Res., **39**, 129–138 (2005).

Wang, X., Kong, X., Yu, Yi., and Zhang, H., "Synthesis and Characterization of Water-Soluble and Bifunctional ZnO-Au Nanocomposites," J. Phys. Chem. C., **111**, 3836-3841 (2007).

Wang, Y., and Qin, Q-Z, "A Nanocrystalline NiO Thin-Film Electrode Prepared by Pulsed Laser Ablation for Li-Ion Batteries," J. Electrochem. Soc. 149(7), A873-A87 (2002).

Wang, Y., Cao, J., Wang, S., Guo, X., Zhang, J., Xia, H., Zhang, J., and Wu, S., "Synthesis of porousr α-Fe_2O_3nanorods and their application in ethanol sensors," J. Phys. Chem. C., **112**, 17804-17808 (2008).

Wang, Y., Li, B., Zhang, L., Li, P., Wang, L., and Zhang, J., "Multifunctional magnetic mesoporous silica nanocomposites with improved sensing performance and effective removal ability toward Hg(II)," Langmuir., **28**, 1657-1662 (2012).

Wang, Z., Huang, B., Dai, Y., Qin, X., Zhang, X., Wang, P., Liu, H., and Yu J., "Highly Photocatalytic ZnO/In_2O_3 Heteronanostructures Synthesized by a Co-precipitation Method," J. Phys. Chem. C, **113**, 4612–4617 (2009).

Wen, X., Wang, S., Ding, Y., Wang, Z. L., and Yang, S., "Controlled Growth of Large-Area, Uniform, Vertically Aligned Arrays of α-Fe_2O_3 Nanobelts and nanowires," J. Phys. Chem. B, **109,** 215-220 (2005).

Willis, A. L., Turro, N. J., and'Brien, S. O., "Spectroscopic Characterization of the Surface of Iron Oxide Nanocrystals," Chem. Mater., **17**, 5970-5975(2005).

Woo, B. K., Lee, H. J., Ahn, J-P., and Park, Y.S., Sol-gel mediated synthesis of Fe_2O_3 nanorods, Adv. Mater., **15**, 1761-1764 (2003).

Woo, K., and Lee, H. J., "Synthesis and magnetism of hematite and maghemite nanoparticles", J. Magn. Magn. Mater., **272–276**, e1155–e1156 (2004).

Wu, H., Pan, W., Lin, D., and Li, H., "Electrospinning of ceramic nanofibers: Fabrication, assembly and applications," J. Adv. Ceram., **1**, 2-23 (2012).

Wu, K., Liu, T., Xue, W., and Wang, X., "Arsenic (III) oxidation/adsorption behaviors on a new bimetal adsorbent of Mn-oxide-doped Al oxide," Chem. Eng. J., **192**, 343–349 (2012).

Wu, R., Qu, J., and Chen, Y., "Magnetic powder MnO-Fe_2O_3 composite-a novel materials for the removal of azo-dye from water", Water Res., **39**, 630–638 (2005).

Wu, R., Qu, J., and Chen, Y., "Magnetic powder MnO–Fe2O3 composite—a novel material for the removal of azo-dye from water," Water Research., **39**, 630–638 (2005).

Wu, W., Xiao, X., Zhang, S., Zhou, J., Fan, L., Ren, F., and Jiang, C., "Large-scale and controlled synthesis of iron oxide magnetic short nanotubes: Shape evolution, Growth mechanism and Magnetic Properties,"J. Phys. Chem.C, **114**, 16092-16103 (2010).

Wu,Y., He, Y., Wu, T., Chen, T., Weng, W., and Wan, H., "Influence of some parameters on the synthesis of nanosized NiO material by modified sol–gel method", Materials Letters **61,** 3174–3178 (2007).

Xia, W., Wang, P., Sun, Y., Wu, Y., Mayers, B., Gates, B., Yin, Y., Kim, F., and Yan, H., "One-dimensional Nanostructures: synthesis, Characterization, and Applications," Adv. Mater., **15**, 353-389 (2003).

Xiao, S. Shen, M., Guo, R., Huang, Q., Wang, S., and Shi, X., "Fabrication of multiwalled carbon nanotube-reinforced electrospun polymer nanofibers containing zero-valent iron nanoparticles for environmental applications," J. Mater. Chem., **20**, 5700-5708 (2010).

Yang, D. J., Zheng, Z. F., Zhu, H. Y., Liu, H. W., and Gao, X. P., "Titanate nanofibers as intelligent absorbents for the removal of radioactive ions from water," Adv. Mat., **20**, 2777-2781 (2008).

Yang, D., Paul, B., Xu, W., Yuan, Y., Liu, E., Ke, X., Wellard, R. M., Guo, C., Xu, Y., Sun, Y., and Zhu, H., "Alumina nanofibers grafted with functional groups: A new design in efficient sorbents for removal of toxic contaminants from water," **44**, 741-750 (2010).

Yang, L., and Watts, D. J., "Particle surface characteristics may play an important role in phytotoxicity of alumina nanoparticles," Toxicol. Lett., **158,** 122–132 (2005).

Yang, Q., "Synthesis of ϒ-Al_2O_3 nanowires through a bohemite precursor route", Bull. Mater. Sci., **34**, 239- 244 (2011).

Yang, Q., Liang J., and Han, H., "Probing the Interaction of Magnetic Iron Oxide Nanoparticles with Bovine Serum Albumin by Spectroscopic Techniques," J. Phys. Chem. B., **113**, 10454–10458 (2009).

Yang, X., Shao, C., and Liu, Y., "Fabrication of Cr_2O_3/Al_2O_3 composite nanofibers by electrospinning", J. Mater. Sci., **42**, 8470- 8472 (2007).

Ye, J., Zhang, H., Yang, R., Li, X., and Qi, Q., "Morphology-controlled synthesis of SnO_2 nanotubes by using 1D silica mesostructures as sacrificial templates and their applications in lithium-ion batteries," Nanotubes., **6**, 296-306 (2010).

Yin, W., Chen, X., cao, M., Hu, C., and Wei, B., "α-Fe_2O_3 nanocrystals: controllable SSA-assisted hydrothermal synthesis, growth, mechanism and magnetic properties", J. Phys. Chem. C, 113, 15897- 15903 (2009).

Yu, C., Dong, X., Guo, L., Li, J., Qin, F., Zhang, L., Shi, J., and Yan, D., "Template-free preparation of mesoporous $Fe_2O_3$and Its application as absorbents," J. Phys. Chem. C., **112**, 13378-13382 (2008).

Yu, D-G., Zhou, J., Chatterton, N. P., Li, Y., Huang, J., Wang, X., "Polyacrylonitrile nanofibers coated with silver nanoparticles using a modified coaxial electrospinning process," Int. J. Nanomedicine., **7**, 5725–5732 (2012).

Yu, H., Guo, J., Zhu, S., Li, Y., Zhang, Q., and Zhu, M., "Preparation of continuous alumina nanofibers via electrospinning of PAN/DMF solution", Mater. Lett., **74**, 247- 249 (2012).

Zhan, S., Chen, D., Jiao, X., and Liu, S., "Facile fabrication of long α-Fe_2O_3, α-Fe, ϒ- Fe_2O_3 hollow fibers using sol- gel combined co- electrospinning technology", J. Colloid Interface Sci., **308**, 265- 270 (2007).

Zhang G., and Wang D., "Fabrication of Heterogeneous Binary Arrays of Nanoparticles via Colloidal Lithography," J. Am. Chem. Soc., **130**, 5616–5617 (2008).

Zhang, F., and Wang, C. C., "Fabrication of one-dimensional iron oxide/silica nanostructures with high magnetic sensitivity by dipole-directed self-assembly," J. Phys. Chem. C., **112**, 15151-15156 (2008).

Zhang, J., Wei, S., Lin, J., Luo, J., liu, S., Song, H., Elawad, E., Ding, X., Gao, J., Qi, S., and Tang, C., "Template- free preparation of bunches of aligned Bohemite nanowires", J. Phys. Chem. B, **110**, 21680- 21683 (2006).

Zhang, L., and Fang, M., "Nanomaterials in pollution trace detection and environmental improvement," Nano Today, **5**, 128-142 (2010).

Zhang, Q., Wang, W., Goeb, J.S, and Yin, Y., "Self-templated synthesis of hollow nanostructures," Nano Today, **4**, 494-507 (2009).

Zhang, S., Boyd, J., Delaney, K., and Murphy, T. H., "Rapid Reversible Changes in Dendritic Spine Structure In Vivo Gated by the Degree of Ischemia," The Journal of Neuroscience, **25**, 5333–5338 (2005).

Zhang, W. X., Wang,Y. Z., and Sun, C. F., "Characterization on oxidative stabilization of polyacrylonitrile nanofibers prepared by electrospinning," J. Polym Res., **14**, 467–474 (2007).

Zhanga, L., Luob, J., Menkhausc, T. J., Varadarajuc, H., Sunb, Y., and Fonga, H., "Antimicrobial nano-fibrous membranes developed from electrospun polyacrylonitrile nanofibers," J. Membr. Sci. **369,** 499–505 (2011).

Zhao, Z., Frost, R. L., Martens, W. N., and Zhu, H. Y., "Growth and surface properties of bohemite nanofibers and nanotubes at low temperatures using a hydrothermal synthesis route", Langmuir, **23**, 9850- 9859 (2007).

Zhao. B., Wang, Y., Guo, H., Wang, J., He, Y., Jiao, Z, and Wu, M., "Iron oxide(III) nanoparticles fabricated by electron beam irradiation method," Mater. Sci. Poland., **25**, 1143–1148 (2007).

Zheng, W., Li, Z., Zhang, H., Wang, W., Wang, Y., and Wang, C., "Electrospinning route for α-Fe_2O_3 ceramic nanofibers and their gas sensing properties", Mater. Res. Bull., **44**, 1432- 1436 (2009).

Zhong, L. S., Hu, J. S., Cao, A. M., Liu, Q., Song, W. G., and Wan, L. J.,"3D Flowerlike Ceria Micro/Nanocomposite Structure and Its Application for Water Treatment and CO Removal", Chem. Mater.,**19**, 1648–1655 (2007).

Zhou, L., Gao, C., and Xu, W., "Magnetic Dendritic Materials for Highly Efficient Adsorption of Dyes and Drugs," Appl. Mater. Inter., **2**, 1483-1491 (2010).

Zhou, M., Gao, X., Hu, Y., Chen, J., and Hu, X., "Uniform hamburger-like mesoporous carbon-incorporated ZnO nanoarchitectures: One-pot solvothermal synthesis, high adsorption and visible-light photocatalytic decolorization of dyes," Appl. Catal., B., **138-139**, 1–8 (2013).

Zhou, W., Cheng, C., Liu, J., Tay, Y. Y., Jiang, J., Jia, X., Zhang, J., Gong, H., Hng, H. H., Yu, T., and Fan, H. J., "Epitaxial growth of branched α- Fe_2O_3/ SnO_2 nano-heterostructures with improved lithium-ion battery performance", Adv. Funct. Mater., **21**, 1439- 2445 (2011).

Zhou, W., Liu, H., Boughton, R. I., Du, G., Lin, J., Wang, J., and Liu, D., "One-dimensional single-crystalline Ti–O based nanostructures: properties, synthesis, modifications and applications, J. Mater. Chem., **20**, 5993–6008 (2010).

Zhu, H.Y., Fua, Y.Q., Jiang, R., Jiang, J.H., Xiao, L., Zeng, G.M., Zhaod, S.L., and Wang, Y., "Adsorption removal of congo red onto magnetic cellulose/Fe3O4/activated carbon composite: Equilibrium, kinetics and thermodynamic studies", Chem. Eng. J., **173**, 494–502 (2011).

Zhu, J., Wei, S., Rutman, D., Haldolaarachchige, N., Young D.P., and Guo, Z., "Magnetic polyacrylonitrile-Fe@FeO nanocompositefibers - Electrospinning, stabilization and carbonization," Polymer., **52**, 2947-2955 (2011).

Zhu, T., Chen, J.S., and Lou, X .W. D, "Highly Efficient Removal of Organic Dyes from Waste Water Using Hierarchical NiO Spheres with High Surface Area," J. Phys. Chem. C., **116**, 6873-6878 (2012).

Zhu, Y., Zhang, J. C., Zhai, j., and Jiang, L., "Preparation of superhydrophilic α-Fe_2O_3 nanofibers with tunable magnetic properties", Thin Solid Films, **510**, 271- 274 (2006).

Zhua, H. Y., Fu, Y. Q., Jiang, R., Jiang, J. H., Xiao, L., Zeng, G. M., Zhao, S. L., and Wang, Y., "Adsorption removal of Congo red onto magnetic cellulose/Fe_3O_4/activated carbon composite: Equilibrium, kinetic and thermodynamic studies," Chem. Eng. J., **173**, 494– 502 (2011).

Zhuang, X., Jia, K., Cheng, B., Guan, K., Kang, W., and Ren, Y., "Preparation of Polyacrylonitrile Nanofibers by Solution Blowing Process," J. Eng. Fiber Fabr., **8**, 88-93 (2013).

Ziylan, A., Koltypin, Y., Gedanken, A., and Ince, N. H., "More on sonolytic and sonocatalytic decomposition of Diclofenac using zero-valent iron," Ultrason Sonochem., **20**, 580–586 (2013).

BIODATA

Name	**:**	Abhipsa Mahapatra
Date of Birth	**:**	Nov 15, 1985
Father's Name	**:**	K.S. Mahapatra
Mother's Name	**:**	Sabita Mahapatra
Husband's Name	**:**	Er. Subodh K.Panigrahi
Permanent Address	**:**	Pradhanpada, Budharaja Ainthapali, Sambalpur-768004.
Present Address	**:**	Qtr No.B/129, Belpahar Integrated Township, Po:Bandhababahal, Dist:Jharsuguda Pin-768211
Marital Status	**:**	Married

Education Qualification:

- M.Sc in Chemistry from NIT Roukela (2008), with an aggregate of 8.03 CGPA
- B.Sc in Chemistry from G.M College, Sambalpur, Sambalpur University (2006) with an aggregate of 60%.
- XII from Kendriya Vidyalaya, Sambalpur, CBSE (2003) with an aggregate of 62%.
- X from Kendriya Vidyalaya, Sambalpur, CBSE (2001) with an aggregate of 72%.

LIST OF PUBLICATIONS

Refereed Journals

1. A. Mahapatra, B. G. Mishra, G. Hota**, "S**ynthesis of ultra fine α-alumina fibers via electrospinning method" *Ceramic International*, 37, 2329, **2011**,
2. A Mahapatra, N. Garg, B.P.Nayak, B.G. Mishra and G. Hota, "Studies on the synthesis of electrospun PAN-Ag composite fibers for antibacterial application" *J. Appl. Pol. Sci*., 124, 1178, **2012**.
3. A. Mahapatra, B. G. Mishra, G. Hota**,** Adsorptive removal of Congo red dye from wastewater by mixed Iron oxide-Alumina Nanocomposites, *Ceramic International*, 39, 5443, **2013**.

4. A. Mahapatra, B. G. Mishra, G. Hota, **"**Studies on electrospun Alumina nanofibers for removal of Cr (VI) & Fluoride toxic ions from aqueous system" *Ind. Eng. Chem. Res*., 52, 1554, **2013.**
5. A. Mahapatra, B. G. Mishra, G. Hota, **"**Electrospun Fe_2O_3-Al_2O_3 nanocomposite fibers as efficient adsorbent for removal of heavy metal ions from aqueous solution", *J. Hazard. Mater.*, 258-259, 116-123, **2013**.
6. A. Mahapatra, B. G. Mishra, G. Hota, **"**Sol-Gel Mediated Synthesis of Boehmite (AlOOH) Nanomaterials for removal of Congo red (CR) dye from aqueous solutions", (To be communicated).
7. A. Mahapatra, B. G. Mishra, G. Hota, **"**Electrospun Iron oxide nanofibers for removal of Arsenic ions from aqueous solution", (To be communicated).

Conference Proceedings

1. Abhipsa Mahapatra, B. G. Mishra & G. Hota*, 'Sol-Gel Mediated Synthesis of Boehmite (AlOOH) Nanomaterials for Environmental Applications' 23rd annual conference of Orissa Chemical Society & National seminar on recent trends in chemical sciences and Technology (RTCST) 2009, Dec 19-20, NIT Rourkela, Orissa.
2. A. Mahapatra, N. Garg, B.P. Nayak, B.G. Mishra, & G. Hota, "Fabrication and characterization of electrospun PAN-Ag composite nanofibers for antibacterial application" 13th CRSI & 5th RSC National Symposium in Chemistry at NISER , Bhubaneswar, February 4-6th, 2011.(**Best Poster Awarded**).
3. A Mahapatra, B.G Mishra & G. Hota, "Electrospun mediated synthesis of α-alumina using different organometallic precursors" International Conference on Recent Advances in Chemical Engineering and Technology (RACET 2011), March 10-12, 2011, Cochin, India.
4. A. Mahapatra, B.G. Mishra and G. Hota, "Synthesis and characterization of Fe_2O_3-Al_2O_3 mixed nanocomposite using Electrospinning method" International conference on Nanomaterials & Nanotechnology (ICNANO 2011), Dec 18-21, 2011, University of Delhi, India.
5. A. Mahapatra, B. G. Mishra and G. Hota "Synthesis and characterization of Al_2O_3-CeO_2 nanocpmposite for removal of Congo red Dye molecules" OCS conference and National seminar on molecules, at Sambalpur University, Dec 24-26, 2011.